University Library

Loughborough University

Author/Filing Title ...... JAIN, A. ....

....

Class Mark ...... T ....

Please note that fines are charged on ALL overdue items.

THE EVALUATION OF BONE STRENGTH

By

Atul Jain

A Doctoral Thesis

Submitted in partial fulfilment of the requirements for the award of
The Degree of Doctor of Philosophy of Loughborough University

October 2008

ABSTRACT

Bone drilling is a major part of orthopaedic surgery performed during the internal fixation of fractured bones. At present, information related to drilling force, drilling torque, rate of drill bit penetration and drill bit rotational speed is not available to orthopaedic surgeons, clinicians and researchers as bone drilling is performed manually. This research demonstrates that bone drilling force data if recorded in-vivo, during the repair of bone fractures, can provide information about the strength/quality of the bone. Drilling force does not give a direct measure of bone strength; therefore it has been correlated with the shear strength and screw pullout strength to determine the efficacy in estimating the bone strength. Various synthetic bone material densities and animal bones have been tested to demonstrate the use of drilling force data. A novel automated experimental test rig, which enables drilling tests, screw insertion and screw pullout tests to be carried out in a controlled environment, has been developed. Both drilling and screw pullout tests have been carried out in a single setting of the specimen to reduce the experimental errors and increase repeatability of the results. A significantly high value of correlation ($r^2 > 0.99$) between drilling force & shear strength and also between drilling force & normalised screw pullout strength in synthetic bone material was found. Furthermore, a high value of correlation ($r^2 = 0.958$ for pig bones and $r^2 = 0.901$ for lamb bones) between maximum drilling force & normalised screw pullout strength was also found. The result shows that drilling data can be used to predict material strength.

Bone screws are extensively used during the internal fixation of fractured bones. The amount of screw been tightened is one of the main factor which affects the bone-screw fixation quality. Over tightening of screw can result into the loss of bone-screw fixation strength, whereas under tightening can result in the screw loosening. Therefore, optimum tightening of the screw is important to achieve the maximum bone-screw fixation strength. At present, optimum tightening of the screw is entirely dependent upon the skill and judgment of the surgeon, which is predominantly based on the feel of the screw tightening torque. Various studies have been reported in the literature to develop an algorithm to set an optimum tightening torque value to be used in surgery. A method which is based on the use of rotation angle of the screw while tightening, rather than using screw insertion/tightening torque, to optimise the bone-screw fixation strength is proposed in this research. The effectiveness of the proposed method has been successfully demonstrated on the synthetic bone material using the designed test rig. The optimum angle for the tested screw was found to be 120° which is equivalent to 33% of the screw pitch.

Keywords: *Bone drilling, bone mineral density, screw pullout strength, screw insertion torque, screw tightening torque, bone quality, bone ultrasound, bone densitometry, Singh Index, screw fixation, direct testing of bone, indirect testing of bone, animal testing, bone strength, dynamostratigraphy and bone .*

ACKNOWLEDGEMENTS

DEDICATION

To My Parents and Wife:

Thank you for all your patience, understanding and support.

CONTENTS

CHAPTER 3

CHAPTER 7

CHAPTER 8

LIST OF FIGURES

LIST OF TABLES

NOMENCLATURE

A	Centre of femoral head with 1cm diameter
AP	Mechanical bone property measured along the anterior posterior direction
$_{app}BMD$	Dry apparent bone mineral density (g/cm^3)
A_s	Thread shear area (mm^2)
B	Greatest possible extra-cortical area of the femoral head
b	Width of chisel edge cutting element (mm)
b_1	Width of lip region cutting elements (mm)
Bi-cort.	Bi-cortical bone specimen
BMC	Bone mineral content (mg), measured using DXA
BMD	Bone mineral density (g/cm^3)
BMD_V	Normalized bone mineral density (mg/cm^3) with respect to the bone thickness, measured using either DXA or DPA
BS	Breaking stress (N/mm^2)
BUA	Broadband ultrasound attenuation (dB/MHz)
C	Centre of femoral neck
CC	Mechanical bone property measured along the cephalo caudal direction (head-tail)
C_c	Constant that depends on the values chosen for α and β
Canc.	Cancellous bone specimen
CDA	Collodiaphysis angle
C_d	Distance from the centroid of the specimen to the surface (mm)
Comp.	Compression testing
Corr. Coeff.	Correlation coefficient between the property of the specimen measured using the mechanical testing and indirect testing
Cort.	Cortical bone specimen

c/sA	Cross sectional area of the bone specimen (mm^2)
CSMI	*Cross sectional moment of inertia of the bone specimen (mm4)*
D	Greatest possible extra-cortical area of the femoral neck
D_d	Drill bit diameter (mm)
DEXA	Dual energy X-ray absorptiometry
d_i	Minor diameter of thread (mm)
d_m	Mean diameter of the screw head bearing surface (mm)
d_n	Nominal diameter of the screw (mm)
D_o	Major diameter of thread (mm)
DPA	Dual photon absorptiometry
DXA	Dual energy X-ray absorptiometry
d'	Web thickness of the drill bit (mm)
E	Modulus of elasticity or Young's Modulus (N/mm^2)
E_e	Margin of error
En_{Lead}	Encoder mounted on the lead screw
En_{Shaft}	Encoder coupled to the end of drilling motor shaft
$E_{Pullout}$	Error between theoretical and experimental screw pullout force (N)
F	Failure load (N)
F_c	Clamping load in the screw joint (N)
F_d	Drilling force (N)
F_{davg}	Average drilling force (N)
F_{dmax}	Maximum drilling force (N)
f_{Drill}	Drill feed rate (mm/min)
f'_{Drill}	Drill feed rate (mm/rev)
FEM	Finite element modelling
$^{exp}F_{Pullout}$	Experimental screw pullout force (N)
$^{th}F_{Pullout}$	Theoretical screw pullout force (N)

F_{exp}	Drilling force measured experimentally (N)
F_f	Friction force due to drill chip flow (N)
F_h	Force acting on the cutting edges which produces the drilling torque (N)
f_{Hz}	Frequency supplied to the control board (Hz)
F_L	Force per unit length (N/mm)
F_{NSPF}	Normalised screw pullout force w.r.t the specimen thickness (N/mm)
F_{opt}	Optimum clamping load (N)
F_{PC}	Axial pullout force in the case of a coarse pitch screw (N)
F_{PF}	Axial pullout force in the case of a fine pitch screw (N)
$f_{Pullout}$	Screw pullout rate (mm/min)
F_{RC}	Radial component of the reaction force in the case of a coarse pitch screw (N)
F_{RF}	Radial component of the reaction force in the case of a fine pitch screw (N)
F_{SPF}	Screw pullout force (N)
F.S.	Fall simulation
F_v	Resultant drilling force of resistance to cutting at each point of the lip of a drill bit (N)
F_z	Force acting on both lips of a drill bit (N)
F_{z1}	Drilling force for zone 1 (N)
F_{z2}	Drilling force for zone 2 (N)
F_1	Force acting upwards which impedes the penetration of the drill into the work (N)
F_2	Force acting on the chisel edge along the drill axis (N)
G	Shear modulus of elasticity (N/mm^2)
G'	Geometric parameter, defined by equation 5.35,
G_p	This indicates that tissue effect was simulated by using plexi glass sheet during densitometry measurements
gr	Total reduction in speed or total gear ratio

H	In-vivo densitometry measurements taken on the human cadaver without removing any tissues or muscles
h	Depth of drill bit indentation (mm)
H_B	Brinell hardness of the material
HC	Point of contact of screw head with the specimen or washer
I	Area moment of inertia (mm^4)
J	Polar moment of inertia (mm^4)
k	Total energy required to cut per unit volume (Joules/mm^3 or N/mm^2)
k_L	Specific energy based on Langella's model (N/mm^2)
L	Length of the bone specimen (mm)
LA	Lever arm of the bending forces (mm) (distance from the middle of the femoral head to the femoral shaft)
$L_{Ball\_Sc.}$	Lead of ball screw (mm/rotation)
L_c	Length of chisel edge (mm)
LC_{Drill}	Load cell used to measure drilling force
$LC_{Pullout}$	Load cell used to measure screw pullout force
L_d	Contact length (mm)
L_{es}	Distance between end supports (mm)
L_{th}	Length of thread engagement (mm)
Meth.	Method of indirect measurement used i.e., in-vitro or in-vivo
ML	Mechanical bone property measured along the medial lateral direction
n	Number of samples
N	Number of oblique cutting elements
NC	No correlation found
ncf	Number of cycles to failure
ND	Femoral neck diameter (mm)
NL	Femoral neck length (mm)
Non-convn.	Bone density was determined using the standard method, i.e., by measuring weight and volume of the bone specimen;

n_{pmin}	Minimum number of pulses which can be recorded
P	Statistical significance of the correlational study
p	Thread pitch (mm)
p_d	Pressure exerted by the drill bit (N/mm^2)
PMMA	Polymethylmethacrylate
pQCT	Peripheral quantitative computer tomography
Prop. Msrd.	Property measured
prox.	Proximal
QCT	Quantitative computer tomography
R	Radius of drill bit (mm)
R_a	Distance from the centre of the drill to the transition point A or radius of zone 1 (mm)
R_C	Reaction force acting on the coarse thread (N)
R_{Ci}	Distance from the centre of the drill bit to the centre of each element for i = 1 to 5 (mm)
R_F	Reaction force acting on the fine thread (N)
r	Correlation coefficient between the mechanical property of the specimen and the specimen property measured using the indirect method
r_a	Correlation coefficient under the alternative hypothesis.
R_o	Half length of chisel edge (mm)
r_o	Outer radius of the bone specimen (mm)
ROI	Region of interest
r_n	Correlation coefficient under the null hypothesis
$(rpm)_{Ball\_Sc.}$	Rotational speed of the ball screw (rev/min)
$(rpm)_{shaft}$	Rotational speed of the main shaft (rev/min)
$(rpm)_{SM_{Feed}}$	Rotational speed of the feed stepper motor shaft (rev/min)
$(rpm)_{SM_{Sc\_Ins}}$	Rotational speed of the screw insertion stepper motor (rev/min)

s	This indicates that tissue effect was simulated by using saline water bath during densitometry measurements
Sc.Ins.Tor	Screw insertion torque test
Sc.P.out	Screw pullout test
SE-QCT	Single energy quantitative computer tomography
SI	Singh Index
SM_{Feed}	Feed stepper motor, part of feed mechanism assembly, which provides drill feed rate and screw pullout rate
SM_{Sc_Ins}	Stepper motor used for screw insertion and screw tightening
SM_{Step}	Number of steps per revolution of stepper motor shaft (steps/rev)
SOS	Speed of sound (m/s)
SPA	Single photon absorptiometry
T	Applied torsional load (N.m)
T_{bs}	Torque at the ball screw (N.m)
T_d	Drilling torque (N.m)
T.E.	Method used to simulate the effect of soft tissues present around the bone specimen during the indirect testing
Tech.	Indirect testing technique used in the presented study
T_i	Screw insertion torque (N.m)
T_{max}	Maximum screw insertion torque at the start of thread stripping (N.m)
T_{opt}	Optimum screw insertion torque (N.m)
TPI	Tooth per inch
T_r	Recommended screw tightening torque value (N.m)
T_s	Total torque applied at the screw (N.m)
TSF	Thread shape factor (dimensionless)
T_{Shaft}	Torque at the main shaft (N.m)
$T_{SM_{Feed}}$	Torque at the feed stepper motor (SM_{Feed}) shaft (N.m)

$T_{SM_{Sc\_Ins}}$	Torque at the screw insertion stepper motor shaft (N.m)
t_t	Total thickness of the bone specimen (mm)
U.L	Ulna length (mm)
US	Ultimate compressive strength (MPa)
$_vBMC$	Bone mineral content (mg)
$_vBMD$	Volumetric bone mineral density (mg/cm^3)
$_vBMC_L$	Bone mineral content (mg/cm), as measured using QCT
W	This indicates that tissue effect was simulated by using water bath during densitometry measurements
w_1	Half web thickness of the drill bit (mm)
Whole-bone	Indicates the undamaged or entire bone specimen of a skeletal location without taking any part out of it or making any cuts to the bone sample, therefore, it gives the combined cortical and cancellous bone density/mechanical strength.
x	Linear displacement of the ball screw (mm)
x_{min}	Minimum drill bit displacement which can be measured (mm)
Z	Number of teeth on the spur gear
Z_9	Spur gear with 9 teeth
Z_{20}	Spur gear with 20 teeth
Z_{32}	Spur gear with 32 teeth
Z_{70}	Spur gear with 70 teeth
Z_{80}	Spur gear with 80 teeth
$z_{\alpha/2}$	Upper $\alpha/2$ critical value of the standard normal distribution which is found in the table of the standard normal distribution
$Z_{(1-\beta)}$	Upper $(1-\beta)$ critical value of the standard normal distribution which is found in the table of the standard normal distribution
3-pbt	Three-Point bending test
%area	Contacting area of chisel edge
τ_{max}	Maximum shear stress (N/mm^2)
σ	Standard deviation of the data

σ_s	Shear strength (N/mm^2),
σ_{sy}	Yield shear stress of the material (N/mm^2)
α	Probability of detecting a false effect
α_c	Angle calculated using equation 5.15 (radians)
α_n	Oblique rake angle (radians)
α_p	Drill bit cutting edge angle (radians)
2ψ	Drill bit point angle (radians)
ψ_d	Inclination angle (radians)
ρ	Material density (g/cm^3)
β	Probability of detecting a true effect (or power of the experiment)
β_d	Angel calculated using equation 4.19
θ	Included thread angle (Degree)
θ_C	Half thread angle of the coarse pitch screw (Degree)
θ_F	Half thread angle of the fine pitch screw (Degree)
θ_f	Screw thread flank angle (Degree)
θ_h	Helix angle of the screw thread (Degree)
θ_{min}	Minimum screw rotation angle which can be measured (Degree)
θ_r	Screw rotation angle (Degree)
$\theta_{SM_{Feed}}$	rotational displacement of stepper motor (SM$_{Feed}$) shaft (radians)
δ	Linear deformation in the joint (mm)
δ_a	Helix angle of the drill bit (radians)
ϕ	Angular twist of the fixed end of bone specimen with respect to the rotating end (radians)
ϕ_s	Orthogonal shear angle of metal cutting (radians)
ε	Angle as shown in figure 5.4 (B) (radians)
φ	Chisel edge angle (degree)
γ	Orthogonal rake angle (radians)
γ_d	Dynamic rake angle (radians)
Δ	The deformation of specimen at the point of load application measured as actuator displacement (mm)

η_{bs}	Efficiency of ball screw
η_{gb}	Efficiency of reduction gear box
η_{sg}	Efficiency of spur gear
$\times$	Indicates that the effect of bone tissue for the indirect testing was not simulated in the study
-	Indicates that no information was given in the referred paper
μ_h	Friction between the screw head and either the bone plate or washer or bone (Dimensionless)
μ_t	Friction between the screw thread and bone thread (Dimensionless)

CHAPTER 1

RESEARCH AIMS AND OBJECTIVES

This chapter identifies the general problems related to orthopaedic surgery, and defines the research aims and objectives. An overview of the thesis is also presented.

1.1 IDENTIFICATION OF THE PROBLEMS IN ORTHOPAEDIC SURGERY

The patient's bone strength is useful information for the surgeon, especially if the bone is affected by low density or diseases such as, osteoporosis. The problems that are identified in estimating the bone strength of a patient along with other problems, which are related to bone fracture treatment surgery, are listed below. This helps to identify the impetus to carry out this research.

1. In the case of a trauma patient undergoing a bone fracture repair surgery, with no quantitative information of the patient's bone strength, the surgeon's evaluation of *bone strength is subjective. Such evaluation is deduced from the patient's age,* gender, fracture history and feel of the bone drilling force that is experienced by the surgeon while doing initial preparations for the bone fracture fixation [1]. This subjective information does not give a quantitative measure of the bone strength and can only be used as supporting information to the surgeon [2]. Moreover, an interpretation of the subjective information will vary from surgeon to surgeon. This shows that there is a need for an inter-operative bone strength measurement technique.

2. In the same scenario as presented above, the surgeon may be able to use the patient's quantitative bone strength measurement taken before the surgery rather than relying on subjective information to predict the patient's bone strength. This is possible in two ways; (i) by measuring bone mineral density of the patient (as bone mineral density gives an indirect measure of the bone strength) using an indirect method, as described in chapter 2, or (ii) by using already available bone mineral density information for the patient, if any prior record of the patient's bone mineral density measurement is kept.

However, for case (i), bone mineral density measurement after bone fracture cannot be taken at the patient's fracture site, as it would give an incorrect measurement because of the crack in the bone. Instead, bone strength at the fractured site is estimated by taking a bone mineral density measurement at some other skeletal location. This is known as non-site specific bone mineral density measurement. However, it has been established through research and investigations (which are presented in chapter 3) that non-site specific bone mineral density measurements give a less accurate prediction of bone strength, as compared to site specific bone mineral density measurements [3-9]. Moreover, in emergency or trauma cases where fractures follow an accident there is less time or resources to implement conventional techniques to detect osteoporosis or to get an estimation of the patient's bone strength.

In the latter case (ii), a record of bone mineral density measurement is generally maintained for patients who are over 40 years or have any bone disease [7]. However, this is not always the case because it is very expensive to carry out bone mineral density measurements for the entire population over the age of 40. Moreover, it is not feasible to have a record of bone mineral density history of all the skeletal bones in the body. Therefore, in these cases, bone mineral density measurement history available for any other skeletal site can be used to predict bone strength of the bone skeletal site of interest. However, this would again lead to non-site specific bone mineral density predictions, which are not very accurate as stated above.

3. Presently only indirect methods, which estimate bone mineral density, are used in clinics to estimate bone strength, as explained in chapter 2. However, bone mineral density is only one of the determinants of bone strength [1, 10, 11] and does not take into consideration bone quality (i.e. bone structure, material property and turn over), as indicated in figure 2.1. Another disadvantage of using bone mineral density measurements to predict bone strength is that there are many inherent measurement errors associated with the commercially available measurement techniques, which could lead to a wrong prediction of the bone strength [12-15]. These inherent bone mineral density measurement errors are related to the size of the area or region of the bone being scanned, the thickness of the bone and presence of soft tissue. Hence, estimating bone strength using indirect methods could lead to a less accurate prediction of a patient's bone strength, especially in the case of osteoporotic patients [16]. In addition, bone mineral density measurement techniques are expensive and expose the human body to harmful radiation. Thus, bone mineral density is not an accurate and effective method of predicting bone strength, which leads to a need for another more accurate, easy, cheap and effective in-vivo bone strength prediction technique.

4. At present in orthopaedic surgery, bone drilling is performed at a preset drilling speed which is designed by the manufacturer of the drilling tool. If the drilling speed can be controlled based on the strength of the bone, then it could produce better drilling results and avoid necrosis [17]. This is not possible with the standard available surgical drills in the market.

5. Advancement of the drill bit (feed rate) during bone drilling is manually controlled by surgeons and it would vary with different surgeons [18]. A strong surgeon will generally apply more force and will have a higher feed rate as compared to a weaker surgeon. On the other hand, an optimum drill bit feed rate set in accordance to the bone strength, would give a better drilling result with less chances of bone necrosis [19, 20].

6. The selection of the screw type and its size by the surgeon for bone fracture fixation is subjective in nature. It is either based on experience or on the recommendations made by the screw and drill manufacturing companies. This might result in a

selection of an oversized or undersized screw. To select the correct size of the screw, accurate information of the patient's bone strength is required. Information on bone strength could determine the optimum size and type of screw for a good fracture fixation.

7. Holding strength of bone screw fixation depends critically on the screw tightening torque. At present, a surgeon limits the tightening of the screw based on their feel or experience, which may result in either over tightening or under tightening of the screws. Over tightening can cause damage to the threads on the bone, whereas under tightening could result in the loosening of the bone screw fixation [21]. Hence, bone fixation quality can be improved if surgeons know the optimum screw tightening torque required for the particular bone strength of the patient and can monitor or control screw insertion torque during the process of screw insertion.

8. During bone drilling, the drill bit may break through the bone and may result in damage to the ligaments or other vital organs that are adjacent to the bone. To prevent drill bit breakthrough surgeons reply upon the feel of the drilling force which is subjective in nature.

1.2 PROPOSED SOLUTIONS TO THE ABOVE IDENTIFIED PROBLEMS

1.2.1 Estimation of Bone Strength Using Drilling Data

In orthopaedic surgery, bone drilling is extensively carried out during the fixation procedure of fractured bones. Over 230,000 fractures, due to osteoporosis, are treated every year in the UK (www.nhs.uk). At present, drilling is performed manually, hence information on bone drilling is not available to orthopaedic surgeons and clinicians. This is because; there are no means of acquiring the drilling data (drilling force, torque, speed, feed and temperature) using currently available medical drilling equipment. This research proposes the measurement and the use of drilling data.

Bone drilling data could be used for bone strength prediction and automation of the bone drilling process. This can be supported by the investigation done by Chagneau and Levasseur [22]. They developed a technique called Dynamostratigraphy, which measures drilling forces while advancing a drill bit at a constant rate. Continuous changes in drilling forces in human femoral heads were found using this technique. The drilling forces measured by Dynamostratigraphy showed clear changes across the femoral head for different drilling trajectories. Similar results were also found in a research conducted at Loughborough University by Ong and Bouazza-Marouf [23]. Therefore, it is proposed to extract quantitative in-vivo information on bone quality using the bone drilling data. The main objective of this research is to investigate the efficacy of bone drilling data in predicting bone strength. The results from this investigation will be extremely beneficial when implemented in the design and development of a drilling tool for mechatronic/robotic assisted orthopaedic surgery. This drilling tool can be used routinely during orthopaedic surgical procedures to automatically get bone strength along a drilled hole.

Taking into account that bone drilling is part of most orthopaedic procedures, hence valuable site-specific information on bone strength could be obtained for all patients undergoing any orthopaedic surgical procedure that involves drilling. Additionally, the drilling data would give a higher accuracy and resolution in comparison to bone densitometry, which only provides an average value of bone strength in the region of interest.

An electromechanical test rig is designed and built to establish the validity of the proposed method of using drilling data to predict bone strength.

1.2.2 Using Screw Pullout Testing to Validate the Use of Drilling Data to Estimate Bone Strength

Bone drilling data does not give a direct measure of the bone strength, as it does not give directly any information on the mechanical properties of the bone. Therefore, preliminary correlation of the drilling data with an established direct method of bone strength measurement has to be investigated to evaluate the effectiveness of using

drilling data in bone strength prediction. A brief introduction to the various direct methods of bone strength measurement is presented in chapter 2 to facilitate the selection of a direct method for this research. Apart from the screw pullout test, the accuracy of other direct test methods is limited by the size of the bone specimen and requires a large number of samples to be prepared. Moreover, the screw pullout test not only measures bone mechanical property but it also gives; (i) a direct estimation of the screw bone fixation quality, which is a very useful information for optimisation of the bone-screw joint fixation quality, (ii) the same test setup can be used to conduct screw tightening tests, which are required to conduct the optimisation study of screw tightening using screw rotation angle, and (iii) additional information on the screw insertion torque can also be extracted during the testing, which is used presently in clinics to optimise screw tightening. Due to the above mentioned advantages, screw pullout testing is used in this research to validate the use of bone drilling data in predicting bone strength.

1.2.3   Improving Screw Tightening Quality

As mentioned above, screw insertion torque is presently used to optimise the screw tightening quality. To investigate this, many studies are presented in the literature review in chapter 6. Screw insertion torque measurements can be erroneous and could lead to a completely wrong estimation of the optimum value of the screw tightening torque (as discussed in chapter 6). The use of screw rotation angle is proposed in this research. To establish the use of screw rotation angle, screw tightening tests (as described in chapter 6) are conducted in this research. These tests correlate the screw rotation angle with the screw pullout strength. The main advantage of the screw tightening test is that it can be done with the designed test rig without having to use any additional test setup or instruments.

1.2.4   The Development of a Handheld Mechatronic Drill

Based on the outcome of this research, a handheld mechatronic drill can be designed and used in surgery instead of a surgical drilling tool used in clinics at present as proposed by Bouazza-Marouf [24]. The proposed mechatronic drill is not designed and developed as a part of this research but it addresses all the identified problems in orthopaedic surgery. The mechatronic drill will have the following features,

1. Prediction of bone strength by analysing bone drilling data,

2. A range of bone drilling speeds should be available, which could be set or adjusted based on the measured bone strength,

3. Drilling at a constant feed rate irrespective of the force applied by the surgeon on the drilling tool,

4. Screw insertion at a controlled speed by maintaining a constant pressure on the screw head,

5. Measurement and control of screw rotation angle to optimise screw tightening,

6. Safety enhancement feature of drill bit breakthrough prevention,

Based on the aforementioned problems and solutions in sections 1.1 and 1.2, the research aims and objectives of this research are defined below.

1.3   RESEARCH AIMS

The main aims of this research are:

1. To investigate the use of bone drilling force data to estimate bone strength by using a specifically designed instrumented electromechanical rig to conduct experiments on synthetic and animal bones.

2. To study the use of screw rotation angle to optimise screw tightening torque by conducting experiments on synthetic bone, using the designed electromechanical test rig.

1.4   RESEARCH OBJECTIVES

From the aims, a number of objectives for the research have been established. These are given as:

1. To critically review the efficacy of using indirect methods to estimate bone strength in clinics and identify the limitations and errors involved in the estimations.

2. To investigate the advantages and limitations of using the screw pullout test against the available direct methods of bone strength measurement. This will support the use of screw pullout testing in this research to validate the use of bone drilling data for bone strength prediction.

3. To review the screw pullout test method and to identify the parameters affecting screw pullout strength. Also to identify the range of various screw pullout test parameters used in the literature. This helps in setting up the design specifications of the test rig.

4. To study and review the use of screw insertion torque, screw tightening torque and screw rotation angle in optimising screw tightening torque.

5. To study and review the current progress of bone drilling. Also to identify the range and effect of various drilling parameters. This helps in setting up the design specification of the test rig.

6. To design and develop an electromechanical test rig which can cater for bone drilling, screw insertion, screw removal, screw pullout and screw tightening tests. This development involves also interfacing of the rig with a personal computer and software programming for the control of the tests and data acquisition.

7. To demonstrate a correlation between the drilling force and screw pullout strength by using the data acquired during the drilling and screw pullout testing of synthetic bone material and animal bone. This is to verify the use of drilling data in predicting bone strength.

8. To investigate the relationship between the screw rotation angle and screw pullout strength of foam in order to investigate the use of screw rotation angle in optimising the strength of bone-screw fixation.

1.5   THESIS OVERVIEW

Chapter 1 has presented the aims and objectives of this research. This includes a list of problems which are identified in orthopaedic surgery. Solutions to the identified problems are presented and based on the solutions, aims and objectives of this research are defined. This chapter proposes to use the bone drilling data to estimate bone strength. Use of screw rotation angle instead of screw insertion torque, to optimise the quality of bone-screw fixation is also proposed in this research.

Chapter 2 of this thesis presents the definition of bone strength and the importance of its measurement. Bone strength depends upon various factors which have also been presented in this chapter. Finally various bone strength measurement methods which include direct and indirect, have also been discussed.

To support the use of drilling data as a means to predict bone strength, a literature review of the presently employed indirect bone strength measurement methods is presented in chapter 3. As indirect methods do not give a measurement of bone strength directly, a comprehensive review of the correlational studies conducted between the indirect and direct methods of bone strength measurement is presented. This chapter identifies drawbacks, limitations and errors associated with various indirect methods. This review concludes that there is a need for another method of bone strength estimation, which can be used in clinics. Therefore, this justifies the reason for investigating drilling data to be used as an additional mean of bone strength estimation in this research.

This research proposes to use drilling data for bone strength evaluation, hence, a background study of bone drilling process and various parameters which affect drilling force are discussed in chapter 4, which also presents the literature review on the use of bone drilling data in orthopaedic surgery.

To use drilling data as a means of bone strength prediction, first an investigation has to be carried out to establish if drilling data can be used to estimate bone strength. This will be done by correlating drilling data with a known method of bone strength measurement. Bone strength measured by screw pullout testing is used for such correlational studies in this research. Chapter 5 presents the literature review and background study of the screw pullout testing and the reason for selecting screw pullout testing to validate the use of drilling data.

Screw insertion torque or screw tightening torque can be recorded or controlled during bone fracture fixation surgery. Therefore, many studies have investigated the use of screw insertion torque and screw tightening torque, as a controlling parameter to optimise the bone-screw fixation strength. Such studies correlated the bone-screw fixation strength (determined using the screw pullout testing) and screw insertion torque and have been presented in chapter 6. This research proposes to use screw rotation angle as a controlling parameter instead of screw insertion torque or screw tightening torque, for optimising the bone-screw fixation quality. To justify this, various limitations of using screw insertion torque or screw tightening torque are discussed and it is shown how they can be overcome by using screw rotation angle. A background study on the

use of screw rotation angle to optimise bone-screw fixation quality is also presented in this chapter.

To verify the proposed method of using drilling data for bone strength evaluation, an electromechanical test rig has been designed and appropriately set up in order to gather relevant measurement data for analysis. This is presented in chapter 7.

To investigate the efficacy of drilling data to estimate bone strength and use of screw rotation angle to optimise bone-screw fixation strength, initial experiments are conducted on foam material. Chapter 8 presents the experimental results and discussions of the experiments conducted.

Further experiments on animal bones are conducted and are presented in Chapter 9.

Chapter 10 summarises the major conclusions of this thesis and outlines potential areas of future work.

The appendices of the thesis present a general introduction of bone, information regarding the design of the test rig and assembly drawings of the designed test rig.

1.6   CONCLUDING REMARKS

Various shortcomings in the current orthopaedic surgical procedures and bone strength evolution in clinics have been presented in this chapter. It is identified in this chapter that the indirect methods which are used in clinics to estimate bone strength have various limitations, errors and are expensive. Therefore, a need for another intra-operative method of bone strength evaluation is identified. This is the main aim of this research, which is to use the bone drilling data to predict bone strength. Another aim which is defined in this chapter is to use screw rotation angle to optimise screw tightening rather than using screw insertion torque which is used by many researchers at present. Based on the identified research aims, various objectives of this research have been presented in this chapter. The next chapter presents an introduction to the bone strength and various bone strength measurement techniques.

CHAPTER 2

INTRODUCTION

2.1   BONE STRENGTH – DEFINITION

In general, strength can be defined as an inherent property of a material to resist an externally applied force without breaking or yielding. The internal resistance offered by the material to an externally applied force is called stress [25]. According to this definition, any property of a material which can give a measurement of its induced stress will give a direct measurement of the material strength. Mechanical properties of the material give such a measurement of induced stresses. In the case of metals, these mechanical properties include tensile, compressive, shear and bending strength, stiffness, elasticity, plasticity, ductility, brittleness, malleability, toughness, resilience, creep and hardness.

Bone strength and its measurement have been a matter of debate for several years. Based on the above definition of strength, bone strength can be defined as the force required to produce a mechanical failure of bone under a specified loading condition. Bone strength is used as a means to evaluate the risk of bone fracture [26, 27]. Bones fracture when internal stresses (concentration of loading forces) exceed the local capacity of the material to withstand them [28]. Therefore, any mechanical property of the bone, which gives the measurement of its internal stresses produced due to loading (like in metals), will give a measure of bone strength [1, 26, 27, 29-32]. In addition, any factor that contributes to the fracture risk of the bone, such as bone geometry and bone turn over rate will also contribute towards the bone strength. This shows that there is no single property that is adequate to describe bone strength. Broadly, the factors most

likely to influence the fracture risk of bone are summarised in figure 2.1; they includes [33]: (i) the overall composition of bone (i.e., proportion of mineral, collagen, water and matrix proteins); (ii) the physical and biochemical characteristics of these components (i.e., nature of the collagen, type of collagen cross-linking, size and structure of hydroxyapatite crystals and degree of mineralization); (iii) the morphology and architecture of bone (i.e., bone size, cortical cross-sectional geometry, porosity, osteon size and density and trabecular micro-architecture); and (iv) the amount and nature of pre-existing micro-damage present in the bone (i.e., crack length and its location). Based on the above factors, the parameters on which the bone strength depends on can be divided into two main categories, [1, 10, 11, 34-36] (i) bone quality and (ii) bone quantity. Bone quality includes bone structure (which includes bone geometry and architecture), material properties (which includes matrix deposition, mineralization, mechanical properties, micro damage, location and connectivity of trabeculae), and bone turnover. Bone quantity includes bone mineral density (BMD) and bone size. BMD is measured using bone densitometry techniques.
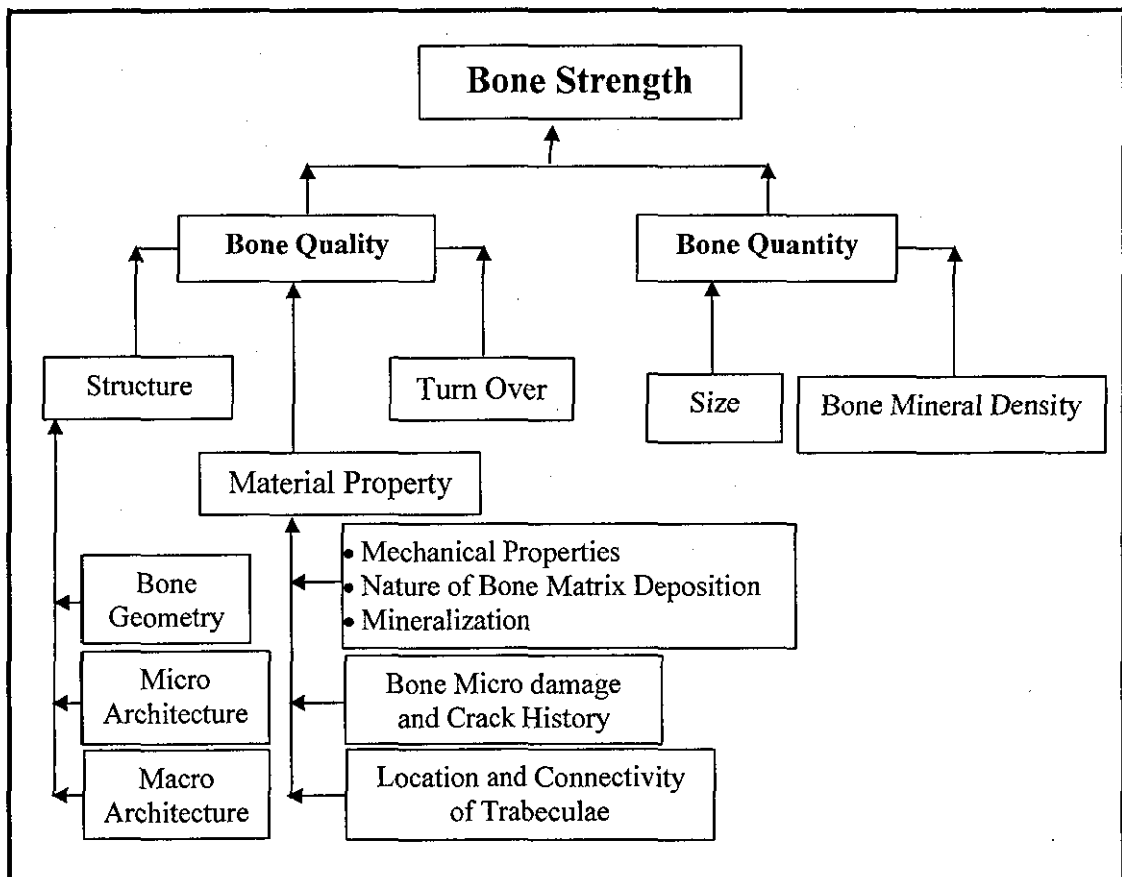
Figure 2.1   Parameters Contributing to the Bone Strength.

The main benefits of measuring (or estimating) bone strength [37] are: (i) in the prediction of the fracture risk and taking preventive actions; (ii) in deciding the type of fixation that could be used, as well as in deciding post fixation precautions that should be taken for a successful bone fracture fixation [35]; and (iii) in the development of finite element modelling (FEM) and optimisation of implants.

The main objective of this research is to investigate the use of bone drilling data, which can be recorded intra-operative, to evaluate bone strength. Drilling data does not give a direct measurement of bone strength, therefore an investigation is conducted in this research to evaluate how effective drilling data can correlate to a known test method of bone strength measurement. In order to ascertain which test method should be used in this investigation, various methods of bone strength evaluation are studied and are discussed within this chapter. This helps in understanding of the various bone strength measurement methods used in clinics and in justifying, in subsequent chapters, the use of drilling data to evaluate bone strength.

2.2   BONE STRENGTH MEASUREMENT TECHNIQUES

During normal daily activities, the skeletal system is subjected to a complex system of loading exerted by the forces of gravity and the muscles attached to the bones. Such loading modes include tensile, compressive, bending, and torsional forces. Therefore, in evaluating the tolerance limits of bones, it is important to determine the bone strength under all of these loading conditions. Various bone strength measurement techniques are discussed in this section.

Bone strength is affected by diseases such as osteoporosis and osteoarthritis. Osteoporosis, which is defined by decreased bone mass and alteration of bone micro architecture, is a common disease, the effect of which is a reduction of bone strength and thus an increase in the risk of bone fracture [38]. A large proportion of the population is affected by osteoporosis and therefore timely and accurate diagnosis and treatment are very important. Anti-osteoporotic treatment aims to improve either, or both, bone quality and/or bone quantity which would result in an improvement of bone strength. Different indirect non-invasive methods, such as bone densitometry, the Singh Index and ultrasound methods, have been used to estimate bone strength. At present,

bone densitometry is the most common indirect method used [1, 27, 39, 40]. However, the indirect methods merely measure (or estimates) bone quantity, or bone mass, which is only one of the determinants of bone strength [1, 10, 11, 41-43], without taking into consideration the bone quality, as indicated in figure 2.1. Hence, the indirect methods do not give a direct measurement of bone mechanical properties; therefore various correlational studies between direct and indirect methods have been carried out in order to evaluate the efficacy of the indirect methods in predicting bone strength. These correlational studies are presented in subsequent chapters as part of the literature review of this research. The direct methods, which are performed in-vitro, measure bone mechanical properties through tensile, compressive, bending, torsion and hardness tests as well as simulating real life bone fracture conditions or screw pullout tests [26, 29-32].

2.2.1   Direct Methods of Bone Strength Evaluation

Mechanical properties of bone give a direct measurement of bone strength and are evaluated using destructive mechanical testing methods [26, 29-31]. Although, bone is a living viscoelastic and anisotropic composite material, its mechanical properties are determined by the same methods that are used for metals, wood and other composites. An introduction to bone, its classification, composition and functioning is given in Annexure 1. Figure 2.2 presents the mechanical properties of bone (enclosed in the single dotted line rectangle), which can be obtained by using various mechanical tests, such as tensile, compressive, and bending tests (to determine modulus of elasticity or Young's modulus), torsion and screw pullout tests (to determine the shear modulus) and hardness tests. Real life simulation tests are also used to predict failure, e.g., a vertical fall is simulated by impacting the femur or radius vertically, falls which induce a side force on the femur are simulated by applying a side impact, and the double support phase of gait is simulated by applying vertical loading on the femur. These mechanical test methods of bone strength measurement are presented in figure 2.2 (enclosed in the double dotted line rectangle).
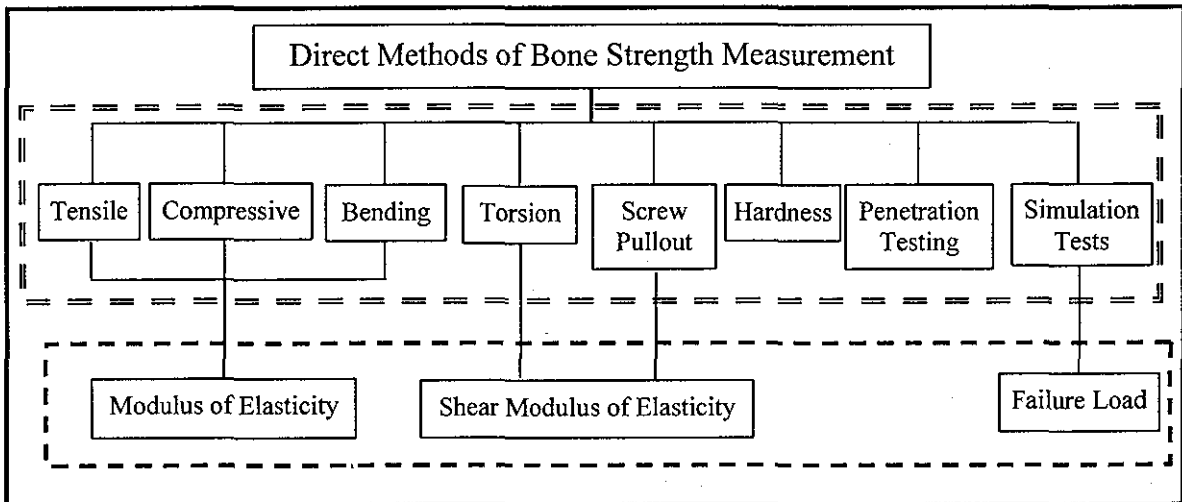
Figure 2.2 Direct Methods of Bone Strength Measurement (Listed inside a Double Dotted Line rectangle) and the Mechanical Properties (Listed Inside a Dotted Line Rectangle) which can be Measured Using These Direct Methods.

Direct test methods involve a specimen of bone sample taken out from the parent bone. Hence, the method of preservation, preparation and mechanical fixation while testing the bone specimen must be considered for reliable test results.

Mechanical properties of the bone specimen can be greatly influenced by the method of bone preservation before conducting any mechanical tests. Water accounts for approximately 6% of the total weight of bone. Thus, any change in the water content has a significant effect on the bone mechanical property. Any treatment of bone like, drying, freezing, storage in saline or alcohol solution, etc. would also change the nature or relative composition of the bone and can influence its mechanical property. This is evident from the outcome of an investigation were it was found that after drying the tensile and compressive strength characteristics, the modulus of elasticity and the hardness of bone tested increased as compared to bone tested without drying [29].

A bone should be frozen and kept as moist and hydrated as possible for long term storage, because there is no significant change in the mechanical properties of the bone when frozen and stored at -20°C [29, 44]. To minimise the freeze drying of bone samples, the surrounding musculature should be left intact. A plastic wrap or a bag should be used to cover the musculature to minimise freeze drying and freeze burns. If

musculature and surrounding tissues were removed before freezing, the bone sample should be wrapped in gauze, soaked in normal saline and placed in a sealed airtight plastic bag. It should be stored at $-20^{\circ}C$ and must be placed in a freezer within one hour of harvesting.

Various direct methods of bone testing which are shown in figure 2.2 are discussed below.

A. Tensile and Compression Testing of Bone

A bone specimen, or a sample, needs to be prepared for both tensile and compression testing. This is because it is very difficult to conduct tensile or compression testing on the whole-bone[1], as whole-bone specimens have the added difficulty of attachment to the testing machine. Whole-bone mechanical test specimens do not have a nice prismatic or symmetrical shape like machined (or prepared) test specimens, thus special fixtures and casting procedures would be required. In this thesis, the whole-bone specimen testing is not discussed, only the tensile and compression testing of machined bone specimen is explained. Before testing, the bone specimen has to be prepared by machining. The method used for the specimen preparation is described below.

Specimen Preparation

The preparation of the bone specimen involves cutting and machining of the bone. Initial rough cuts are made to cut bone into the required thickness using either a hacksaw or a band saw or a jig saw. Figure 2.3 (A) shows an example of the rough cuts (shown as dashed lines) made on a bone specimen. Figure 2.3 (B) shows a slice of bone specimen after making rough cuts. These initial cuts can cause overheating of the bone upto a depth of 1 mm or 2 mm from the cut. The affected area is normally removed either by using a wet sand paper or by making finer cuts. After rough cuts, the bone slices are cored using a tabletop drill press. C-clamps are used to secure the bone to the machining platform to prevent the effect of vibration. An example of a cored bone specimen is shown in figure 2.3 (C). Coring is done using a diamond coring tool and

---

[1] Whole-bone in this thesis refers to the undamaged or entire bone specimen of a skeletal location without taking any part out of it or making any cuts to the bone sample

both tool and specimen are completely immersed in a water or saline bath during the coring process [30]. After coring, the bone specimen is examined microscopically or using a densitometry technique to detect cracks and other defects, as shown in figure 2.3 (D), and discard the defected specimens. After the initial rough cuts and coring, the bone specimen is generally potted in cement PMMA (Polymethylmethacrylate) to get a good grip of the specimen with the testing apparatus, as shown in figure 2.3 (E). Plotting is done with the help of a customised alignment jig, which is shown in figure 2.3 (F). The bone marrow and fat are removed before potting the bone specimen into the cement to get an adequate grip or bonding. After potting, the bone specimen is machined using a lathe or milling machine to obtain a desired geometry of the specimen, as shown in figure 2.3 (G). Grinding or polishing is often used to adjust uneven cut surfaces. The most common specimen geometry used in testing is either a cube (of 6 to 8mm side length) or a cylinder with a diameter from 6 to 8 mm and a length/diameter ratio varying between 1 to 2. The size of the specimen used in testing is very critical, as it should be small enough to satisfy a continuum scale assumption and at the same time it should be large enough to ensure that the specimen is homogeneous.
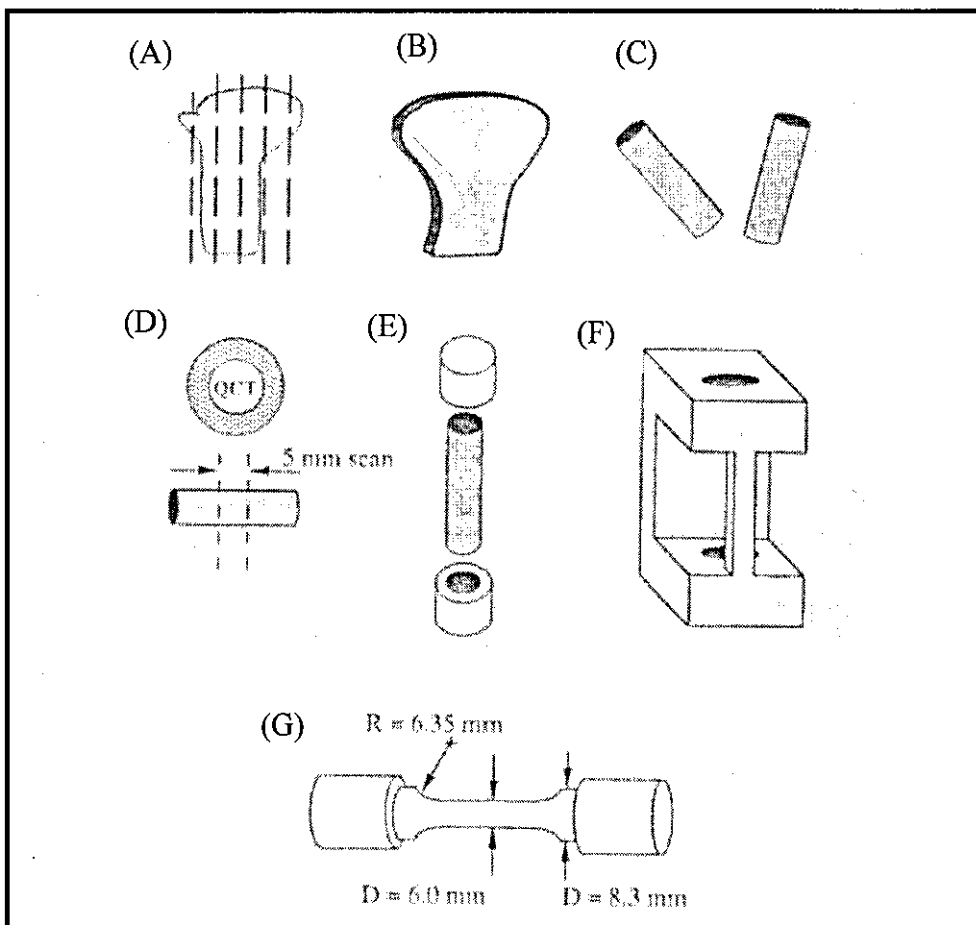
Figure 2.3 Specimen Preparation for Compression or Tensile Testing [45]

Tensile and Compression Testing of Bone

The tensile and compression testing of the bone is done in a similar way as that of metal testing. A load is applied on the test specimen and the corresponding strain is measured at the gauge region of the bone specimen using usually, a clip extensometer, as shown in figure 2.4.
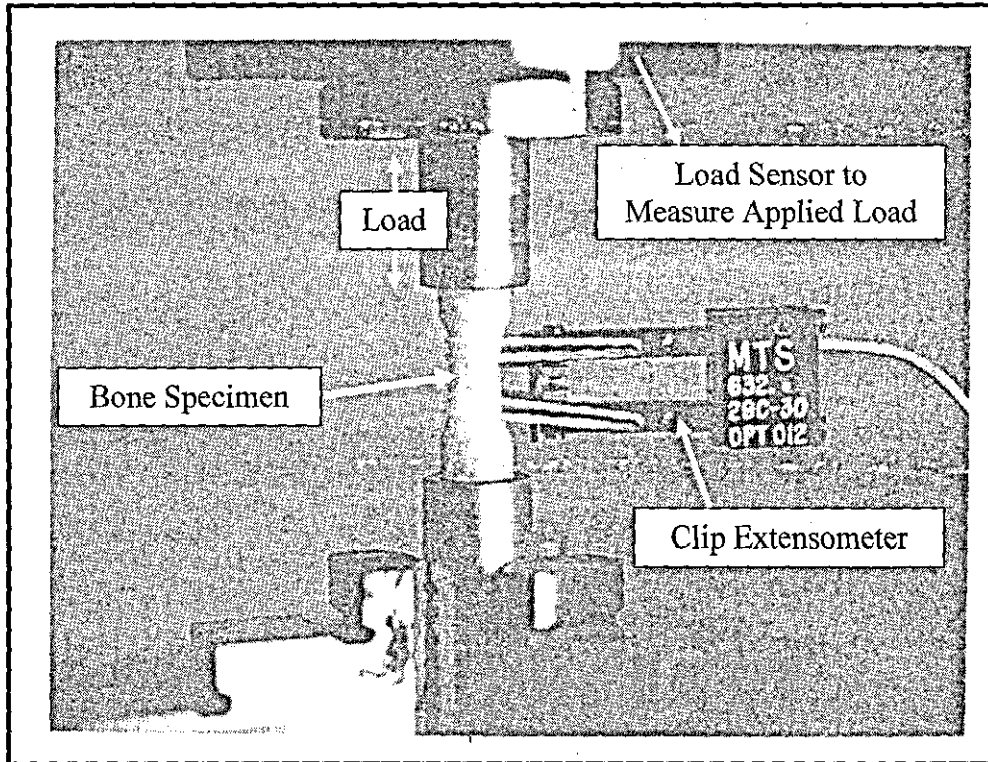
Figure 2.4 Test Set up of Compression Testing [45]

Stress is calculated as the applied force divided by the cross-sectional area of the mid section of the bone. To calculate the modulus of elasticity or Young's modulus of the bone specimen, a stress-strain curve is plotted. A typical stress-strain curve is shown in figure 2.5. The elastic portion of the stress-strain curve is characterized by a straight line (Hooke's law) and the slope of this line, or the ratio of stress-strain within the elastic range, is defined as the modulus of elasticity. As the stress is increased further, a yield point is reached beyond which stress is no longer proportional to the strain. Beyond the yield point the specimen enters into its plastic region. Further increase in the load will cause the specimen to reach its point of failure and the stress corresponding to the failure load is called ultimate stress.
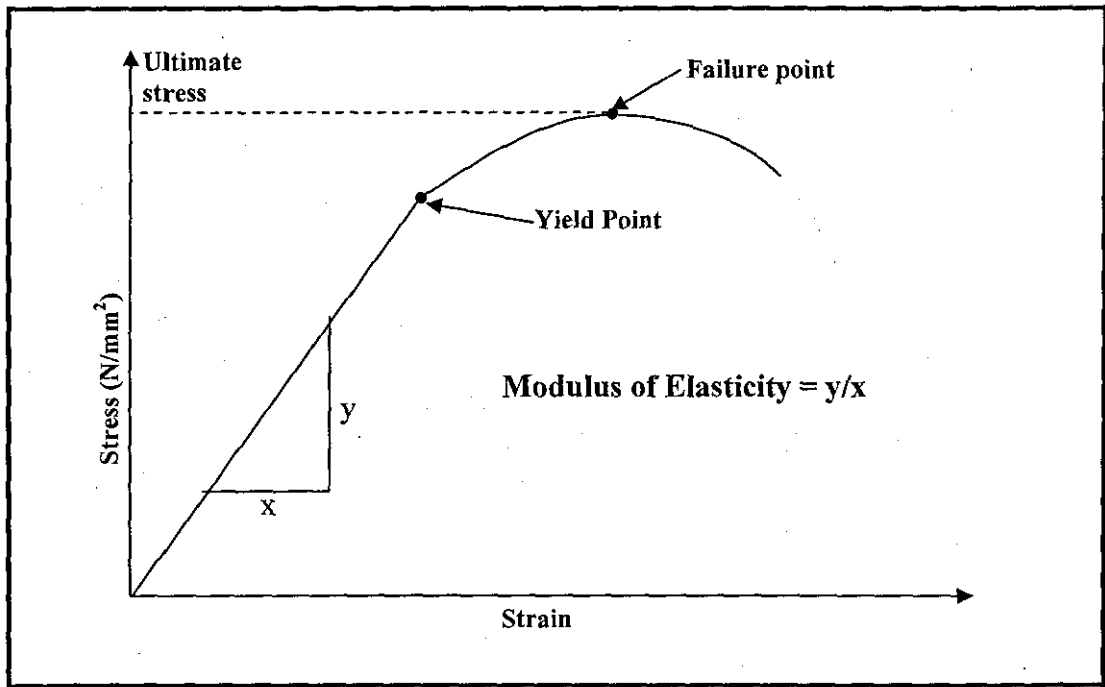
Figure 2.5 **Typical Stress-Strain Curve for Tensile or Compression Testing of a Bone Specimen**

The main advantage of compression over tensile testing is that a relatively small test specimen can be tested. This is because no special fixture or clamp is required to apply load in compression testing. Cortical bone specimens can have a comparatively smaller size relative to the cancellous bone specimens because the former has a relatively homogeneous structure. Therefore, compression testing is more suitable for testing cortical bones. Another advantage of compression testing is that the specimen preparation is simple, as the test does not require clamping the specimen. However, compression testing is less accurate than tensile testing. This is mainly because of; (i) the error caused due to the friction between the surface which apply load and bone; and (ii) the compression-platen misalignment which causes parallelism problems. The friction problem could be minimised by using polished and lubricated straight steel platen with controlled surface roughness. Whereas, to minimize the parallelism problem the spherical socket type of loading surface plate should be used.

B.   Bending Testing of Bone

The bending test is quite useful to determine the combined strength of the bone and its fixation device together. The bending test of bone determines strength of the bone when load is applied in a manner that causes it to bend about an axis. During the test, the bone is subjected to a combination of tension and compression loads acting on the two sides of the neutral axis, as shown in figure 2.6 (A) and (C). These tensile and compression loads induce stress in the bone whose magnitude is proportional to their distance from the neutral axis. Due to an asymmetry of the bone, the maximum tensile and compressive stresses may not be equal. Since the bone is weak in tension, fracture propagates from the tensile surface to the compressive surface of the bone. There are two types of bending tests which are generally performed on bones, namely; (i) three-point bending, and (ii) four-point bending tests. A general loading configuration along with the bending moments acting about the neutral axis of the bone specimen for both three and four-point bending test is shown in figure 2.6 (A) and (C), respectively. In these figures, the bending moment diagram is also given for both three and four-point bending tests. Another example of a three-point bending test set up on a rat tibia is also shown in figure 2.6 (B). Four-point bending test is advantageous for testing where one might be uncertain about the strongest or weakest point and does not wish to influence the test by locating the maximum bending moment at a specific place like in the three-point bending test. However, the most commonly used bone testing method is three-point bending. In a three-point bending test, no special machining is required for the specimen preparation, however, all soft tissues should be removed from the bone to avoid introduction of any error. A single point actuator is used for loading in three-point bending tests and the support used for holding the bone specimen should be strong enough to withstand the applied forces, wide enough to support the bone width, and of sufficient length for the area of interest to be contained within the support span. The end supports should be smooth, flat, and perpendicular to the horizontal axis of the bone. The applied load on the bone and its deflection is recorded for bending strength calculations.
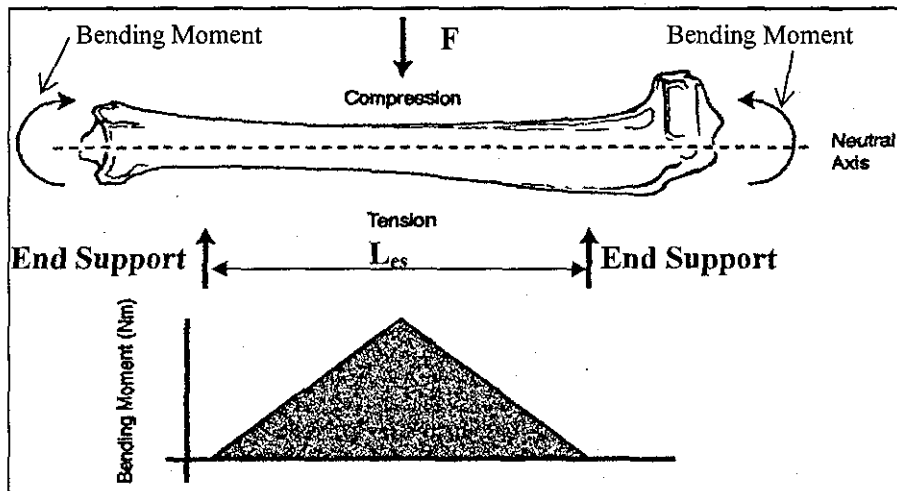
(A) Three-Point Bending Test with Loading and its General Bending Moment Diagram [30]
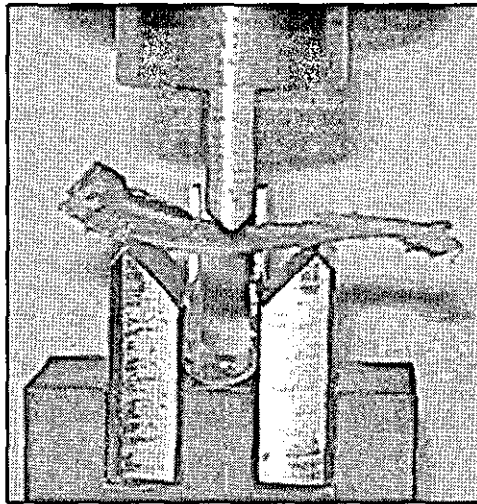
(B) Three-Point Bending Test on a Rat Tibia [46]
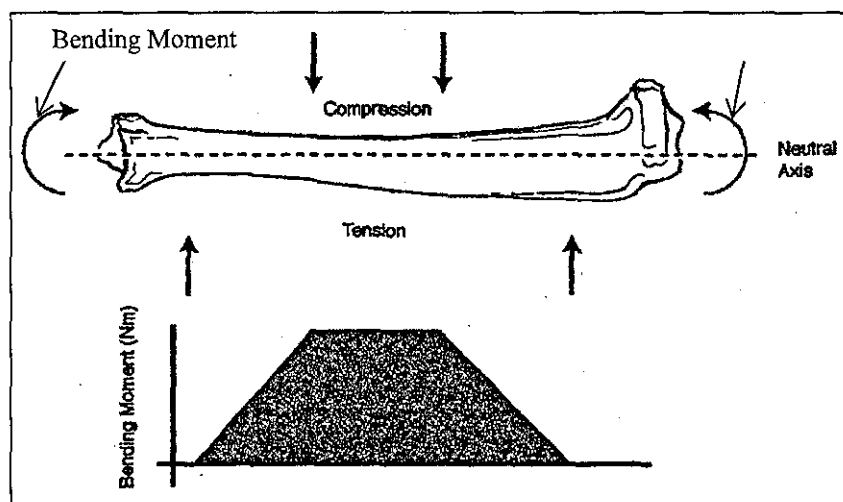
(C) Four-Point Bending Test with Loading and its General Bending Moment Diagram [30]

Figure 2.6 Tensile and Compression Loading with respect to the Neutral Axis in Three and Four Point Bending Test

Most equations to calculate the structural and material properties of bone in bending are based on the assumption that bones are long prismatic beams where the beam is initially straight, the cross section of the beam does not vary along its length, and the beam is made of an isotropic, homogeneous, linearly elastic material. Bone does not conform to many of these assumptions, but calculations based on these equations provide a means for comparison between studies. Bone properties which are commonly calculated for three-point bending includes breaking strength, and modulus of elasticity. Breaking stress (BS, N/mm^2) can be calculated using the formula [30]:

$$BS\left(\frac{N}{mm^2}\right) = \frac{F \times L_{es} \times C_d}{4 \times I} \tag{2.1}$$

where,   F = failure load (N),

L$_{es}$ = distance between end supports (mm),

C_d = distance from the centroid of the specimen to the surface (mm) and

I = area moment of inertia (mm^4).

The modulus of elasticity (E, N/mm^2) for a bone in three-point bending is calculated using the formula [30]:

$$E\left(\frac{N}{mm^2}\right) = \frac{F \times L_{es}^3}{48 \times I \times \Delta} \tag{2.2}$$

where,   F = failure load (N),

L$_{es}$ = distance between end supports (mm),

I = area moment of inertia (mm^4) and

Δ = the deformation of specimen at the point of load application measured as actuator displacement (mm).

Bending tests are preferred over compression or tensile tests because;

- They do not require any special specimen preparation.

- Varied size of bones can be tested, as no special fixture is required to hold the bone.

- It is not required to harvest a portion of the bone. Hence, whole-bone can be tested.

C.   Torsion Testing of Bone

Many of the long bones and the spine are subjected to a significant amount of torsional load. Adaptation of trabecular bone to in-vivo compressive and tensile loads involves alignment of the trabeculae along the main loading axis. Loads due to trauma are not aligned along this axis and, therefore, cause shear stress fractures. Torsion tests provide information on mechanical parameters such as shear modulus and shear stress to failure. Only limited information is available in the literature on the mechanical behaviour of bones under torsion loading. This is because torsion testing requires a specially designed test set up, such as a biaxial servo-hydraulic mechanical testing system, which is not commonly available in most of the university engineering departments or industrial testing labs. In this test, one end of the test specimen is fixed and the torsional load is applied to the other end. A very simple (and very old) setup of torsion testing is shown in figure 2.7. The test setup consists of a fixed jaw and a rotating jaw. The test specimen is gripped in these two jaws and the rotating jaw is rotated with a wheel or a pulley. A known torsional force is applied by placing weights in a pan which is suspended by a thread wrapped around the rim of the wheel, or the pulley, with graduated marks to indicate the angle of twist. At present, servo-hydraulic control torsional testing machines are normally used. In these machines, the torsional load can be controlled automatically using a computerised controller, however these machines are costly.

The equations, given below, to calculate the structural and material properties of bone in torsion are based on the assumption that (i) bone specimen used is perfectly cylindrical in form, i.e., without any variation in the cross section along its length, and (ii) the bone specimen is made of an isotropic, homogeneous, and linearly elastic material.

Bone properties which are commonly calculated for torsion testing include maximum shear stress and shear modulus of elasticity. Maximum shear stress (τ_{max}, N/mm^2) can be calculated using the formula [30]:

$$\tau_{max}\left(\frac{N}{mm^2}\right) = \frac{T \times r_o}{J} \qquad (2.3)$$

where,   T = applied torsional load (mN.m),

r_o = outer radius of the bone specimen (mm) and

J = polar moment of inertia (mm^4).

Shear modulus of elasticity (G, N/mm^2) of bone specimen can be calculated using the formula [30]:

$$G\left(\frac{N}{mm^2}\right) = \frac{T \times L}{J \times \phi} \qquad (2.4)$$

where,   T = applied torsional load (mN.m),

L = length of the bone specimen (mm),

J = polar moment of inertia (mm^4) and

ϕ = angular twist of the fixed end of bone specimen with respect to the rotating end (radians).

Wheel or Pulley

Bone Specimen

Rotating Jaw

Fixed Jaw

Pan to Put Weights for Applying Torsional Load
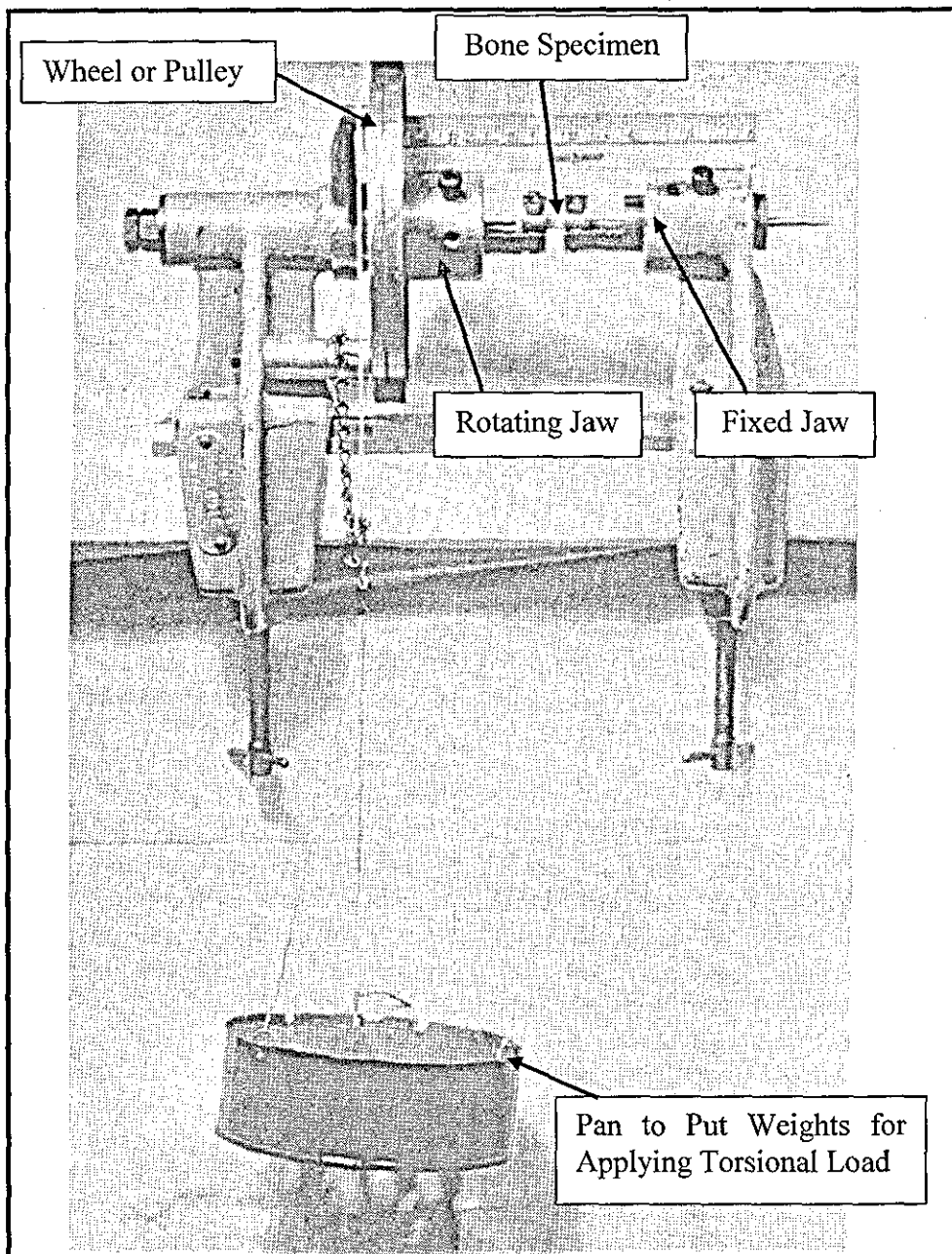
Figure 2.7 Torsion Testing of Bone [29]

As stated above the bones are not normally perfectly cylindrical in form, and the equations given above can only give a rough approximations of the behaviour observed in real bones. A closer approximation can be obtained from computed mechanical models using actual mechanical test data, especially when examining localized behaviours within a complex formation. An example of such a detailed analysis can be found in the work of Levenston *et al* [47]. Another assumption made is that the bone specimen is free from any cut, split, or hole along the entire or part of the length of bone

specimen. Such a split is usually referred to as an opening in the structure, which causes stress concentration around the split and considerably reduces the torsional rigidity of the bone specimen. In such cases, the failure load of the bone specimen should be used as a measurement of its torsional strength. This is extremely useful information to find the bone strength of a specimen with screws or pinholes.

D.   <u>Screw Pullout Testing of Bone</u>

Bone-screw fixation is a commonly used technique for treating trauma patients. Mechanical strength of the bone-screw fixation is an important factor to obtain a rigid fixation and is determined by the screw pullout test. Screw pullout testing refers to the measurement of the force required to pull out a screw inserted in a bone specimen. The analysis of the test gives a direct measurement of bone shear strength and also determines the optimum screw size, insertion technique, angle of penetration and optimum screw hole preparation method. All these parameters are very useful to have a successful bone screw fixation. A schematic diagram of a screw pullout test setup is shown in figure 2.8 (A). It consists of a test block (bone specimen under testing) clamp and base. The base is fixed to the base of the load frame. Prior to the pullout, a screw is inserted into a predrilled hole in the test block. Drill bushing, which is fixed to the load frame, is used to maintain the alignment of the screw axis with the direction of applied load during the pullout. A suitable load fixture is used to apply tensile pullout load on the bone screw. The tensile force which is transferred through the head of the screw should be aligned with the screw's longitudinal axis. The tensile load should be applied to the test specimen at a fixed feed rate until the bone threads fail and the screw releases from the test block. The maximum load recorded is known as screw pullout force (F_{SPF}), and is used to calculate the shear stress of the bone specimen using the equation given below [48, 49]:

$$F_{SPF} = \sigma_s \times A_s = \sigma_s \times \pi \times D_o \times L_{th} \times TSF \qquad (2.5)$$

where, F_{SPF} = screw pullout force (N),

σ_s = shear stress of thread material (N/mm^2),

A_s = thread shear area (mm^2),

D_o = maximum diameter of the external thread (mm),

L_{th} = length of thread engagement (mm) and

TSF = thread shape factor (dimensionless)

The thread shaper factor (TSF) used in equation 2.5 is defined as,

$$TSF = \left[0.5 + \left(\frac{D_o - d_i}{2 \times p} \right) \times \tan \frac{\theta}{2} \right] \qquad (2.6)$$

where, d_i = minimum diameter of the internal thread (mm),

p = thread pitch (mm) and

θ = included thread angle (degree)

The above equation is used for metals, which are homogenous and non-porous in nature unlike bone material. The above equation can also be applied for bones to calculate their material property, by assuming that bone is homogeneous and non-porous in nature. The main advantage of the screw pullout test is that it can be performed on any shape or size of bone specimen without any prior specimen preparation. An example of screw pullout testing of a bone shaft, conducted by Stromsoe *et al* [50], is shown in figure 2.8 (B). The main shortcomings of the screw pullout testing are that it does not take into account the shearing or cycling loading of screws, and deformation of screw threads; also, the direction of pullout force should be maintained in line with the screw axis to have consistent results. In addition, surgical screws, surgical drill bits and surgical taps used for testing are significantly expensive.
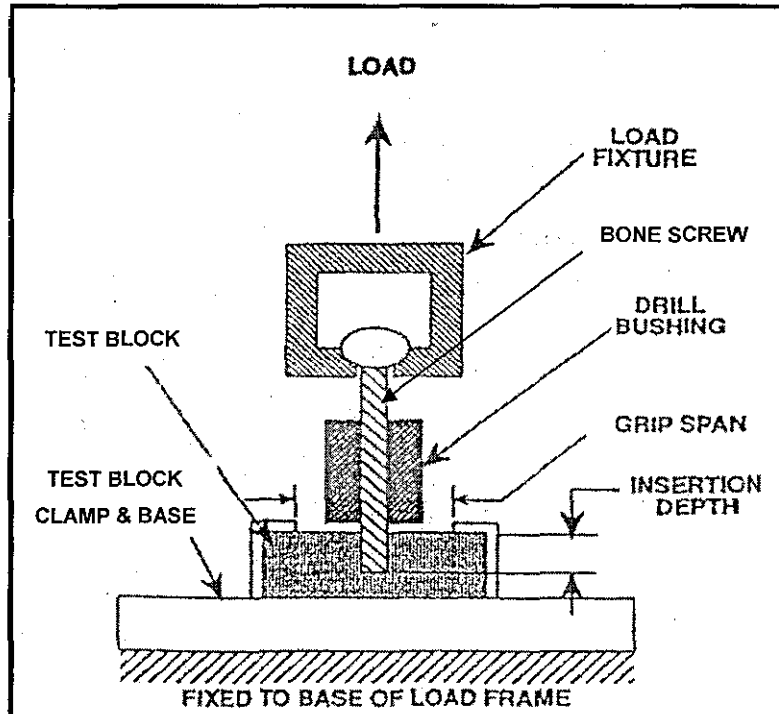
(A) Schematic Diagram of Screw Pullout Test Setup [ASTM F1691-96] [51]
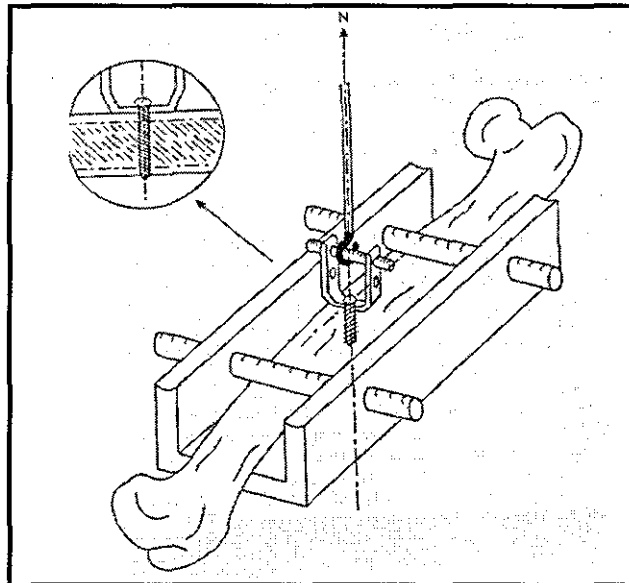
(B) Screw Pullout Testing Setup of the Bone Shaft [50]

Figure 2.8 Screw Pullout Testing

E.   Hardness Testing of Bone

The hardness of a solid material is defined as its resistance to penetration by another solid body. Hardness or indentation tests measure hardness of bone by driving an indenter of a specific geometry into the bone surface. There are various hardness tests which are categorised based on the geometry or size of the indenter. Based on the geometry of the indenter, various hardness tests are Brinell, Rockwell, Vickers, and Knoop. Indentation testing can be done at different hierarchical levels based on the size of the indenter, such as, macro-structural level (cortical or cancellous bone), micro-structural level (haversian system or osteon), and nano-structural level (fibillar collagen and lamella). Hardness testing does not give a direct measure of any mechanical property of the bone; however, it correlates quite closely to some important properties of bone, e.g., modulus of elasticity.

F.   Penetration Testing of Bone

Penetration testing is another indirect method to predict bone strength. It is done using an Osteopenetrometer, which penetrates a probe through the bone. The force required to penetrate the probe is used as a predictor of bone strength [52-56]. Penetration testing is similar to the hardness testing of bone, which uses a different indenter and measures the hardness of bone at the macro structural level. Like hardness testing, penetration testing also does not give a direct measure of any mechanical property of the bone, however, it correlates quite closely to some important properties of bone [52, 54]. The idea of the Osteopenetrometer has evolved to have a tool which can measure bone strength intra-operatively, therefore, it has to be small to facilitate a handheld operation and should be able to withstand repeated exposure to high pressure and high temperature during sterilisation. Penetration force can be exerted manually by an operator or by using hydraulic, pneumatic or electrical force input. A typical handheld and hydraulic (or pneumatic) Osteopenetrometer is shown in figure 2.9. The main advantage of penetration testing is that it gives an overall strength of the cancellous bone along the penetration trajectory of the probe into the bone. It also considers the variation in the bone structure and density along the penetration trajectory unlike compression testing, which gives the localised strength of the bone specimen without taking into

consideration of the effect of the adjacent bone structure from where the bone specimen was taken. However, penetration testing can only estimate the strength of the cancellous bone as the outer cortical layer of the bone has to be removed before testing.
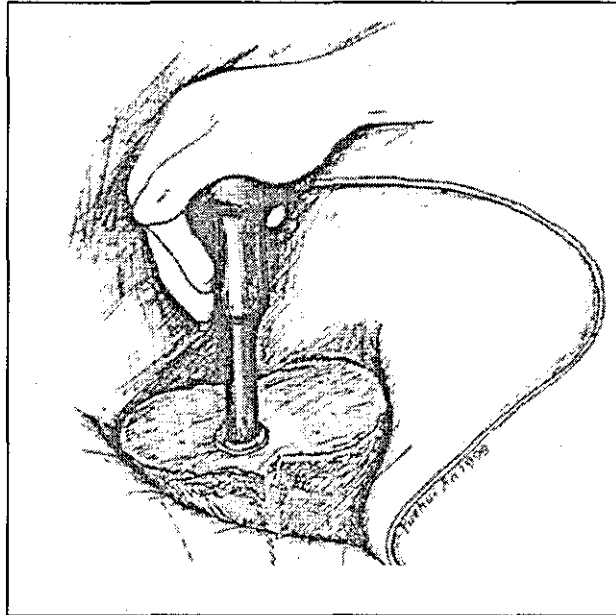
(A) Penetration Testing Using Handheld Osteopenetrometer
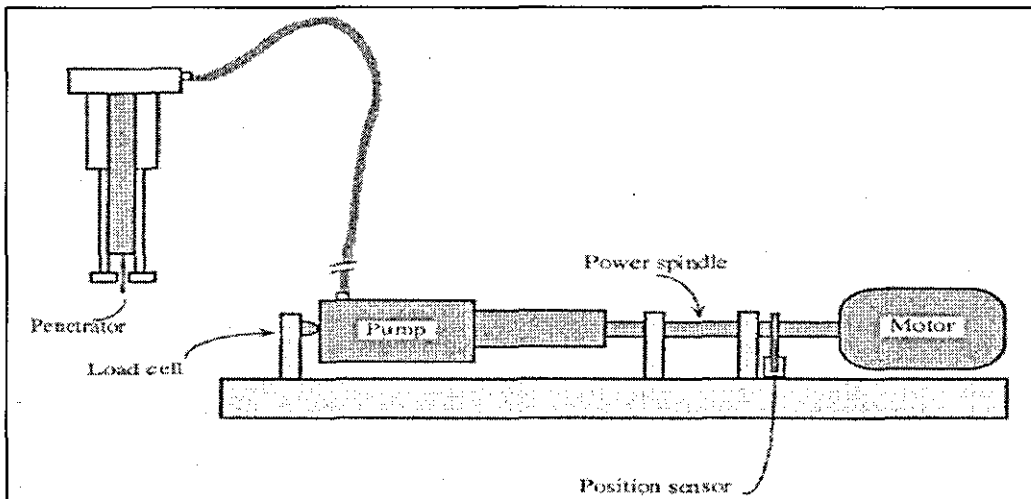
(B) Pneumatic or Hydraulic Osteopenetrometer

Figure 2.9 Penetration Testing of Bone Using an Osteopenetrometer [30]

G.   Simulation Testing of Bone

A real life loading condition of bone is simulated in these tests. The failure load is recorded to predict the failure of bone or bone implant. An example of simulation testing is shown in figure 2.10, in which a side impact fall is simulated on a proximal femur.
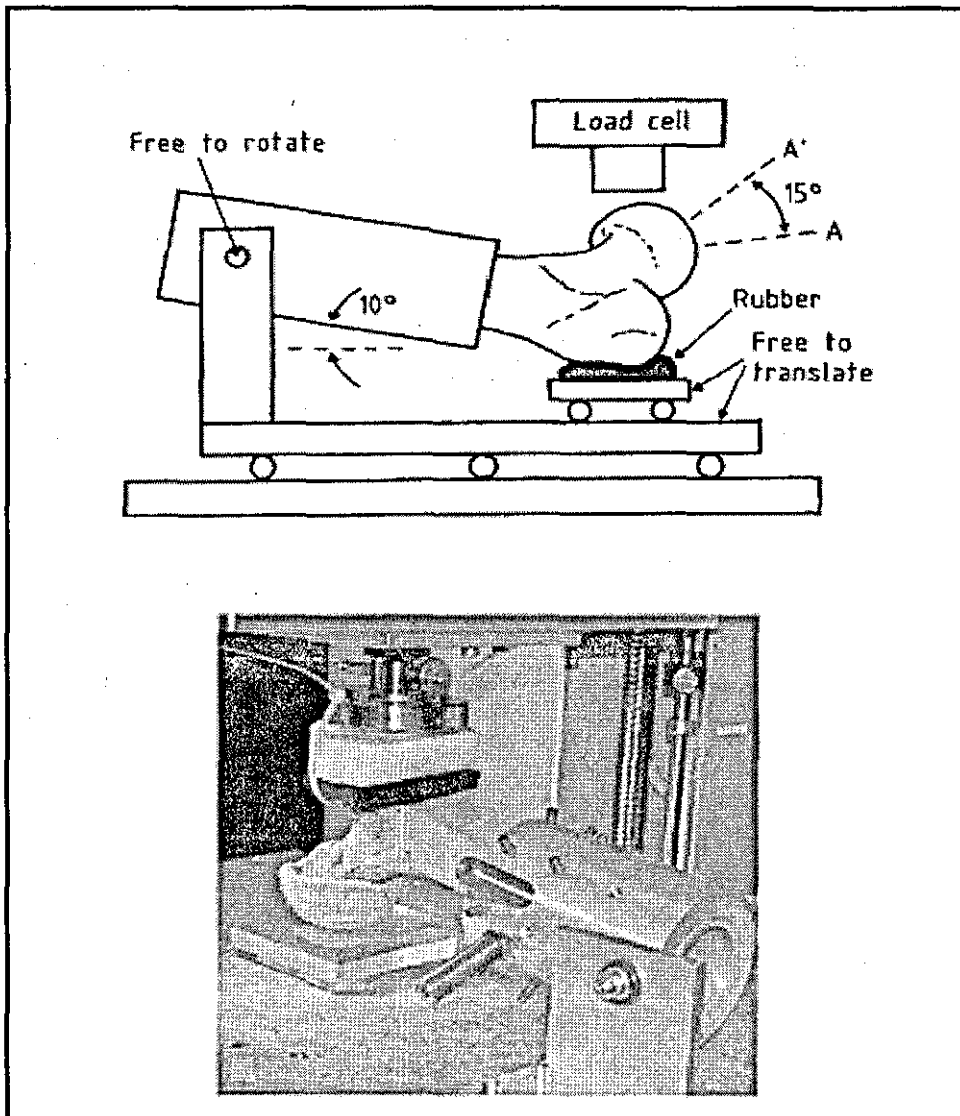
Figure 2.10   Schematic and Actual Test Set Up for Mechanical Testing of Proximal Femur Under Simulated Side Impact Fall Test [57]

Out of the various direct methods discussed above, tensile/compression, bending and simulations tests are the most commonly used methods to evaluate bone strength. Hence, a comparison between these methods is presented below in table 2.1.

Table 2.1 Comparison of Commonly Used Mechanical Tests

Parameters for comparison	Three-point Bending Test	Compression Test	Simulation Test
Type of bone that can be tested	Whole-bone	Either cortical or cancellous	Whole-bone
Effect of adjacent trabeculae	Considered	Not Considered	Considered
Fixture for holding bone	No special fixture is required	No special fixture is required	Special fixture is required
Specimen shape	Any shape of the bone specimen can be tested	Only regular specimen shape can be tested, like, cylindrical or cubic	Any shape of bone specimen can be tested
Limitation on the Specimen size	Large size of bone specimen is required	Very small size of specimen can be tested	Large size of bone specimen is required
Application	It can only measure mechanical strength at the shaft of long bones, not at the proximal or distal end of the bone.	It can measure the bone strength at any skeletal location.	Testing of only radius and proximal femur bone has been reported in the literature.

2.2.2   Indirect Methods of Bone Strength Evaluation

Bone strength is usually measured using indirect methods, which are based on the photo-densitometry analysis of X-ray images, or on the analysis of ultrasonic frequency waves. Indirect methods include; bone densitometry, the Singh Index and bone ultrasound, as shown in figure 2.11. Bone densitometry, which is based on X-ray absorption, measures the amount of bone mineral (calcium hydroxyapatite) per unit volume of bone tissue and is also used as a measurement of osteoporosis [1, 10, 40]. As shown in figure 2.11, there are four methods of measuring bone densitometry; these are single photon absorptiometry (SPA), dual photon absorptiometry (DPA), dual energy X-ray absorptiometry (DXA or DEXA) and quantitative computer tomography (QCT). Another technique called peripheral quantitative computer tomography (pQCT) which is based on QCT technique is also used for bone density measurement of peripheral

bones like radius. The most common scanning method is DXA. However, ultrasound methods are generally used for *initial screening tests on patients*, despite the fact that they are less accurate than densitometry methods. This is because they are faster, easily available, cheaper and require comparatively less skill. If results from an ultrasound test indicate that the bone density is low, *other indirect techniques are recommended for the* confirmation of the results. Broadband ultrasound attenuation (BUA) and the speed of sound (SOS) are the two main types of ultrasound techniques which are used commercially. The Singh Index (SI), *which is based on the analysis of proximal femur* trabecular patterns using X-ray images, is also used as an additional scanning method. The Singh Index is generally used for a quick analysis of the bone when other indirect methods are not available.
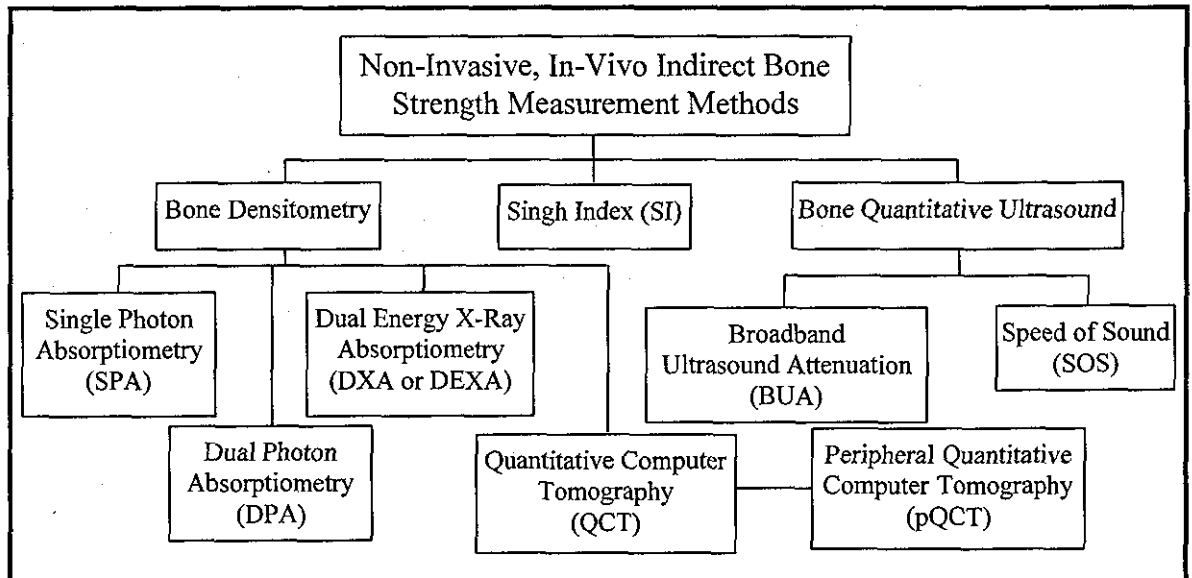
Figure 2.11 Various Indirect, Non-Invasive Bone Strength Measurement Methods

However, while indirect methods of estimating bone strength are widely used to predict bone fracture risk, these methods do not give a direct measurement of bone mechanical properties. Therefore, various correlational studies between the direct and indirect methods have been carried out in order to evaluate the efficacy of the indirect methods. A review of these studies is presented in chapter 3.

A. Bone Densitometry

The main components of a general densitometry system for bone mineral density measurement are shown in figure 2.12. It consists of an X-ray source which produces the radiations. These radiations, after passing through the human body whose density is to be measured, are received by a receiver or detector. The attenuation in the intensity of the radiation after passing through the body is recorded and is used as a measurement of the bone density. The most commonly used non-invasive densitometry methods, shown in figure 2.11, are discussed below.
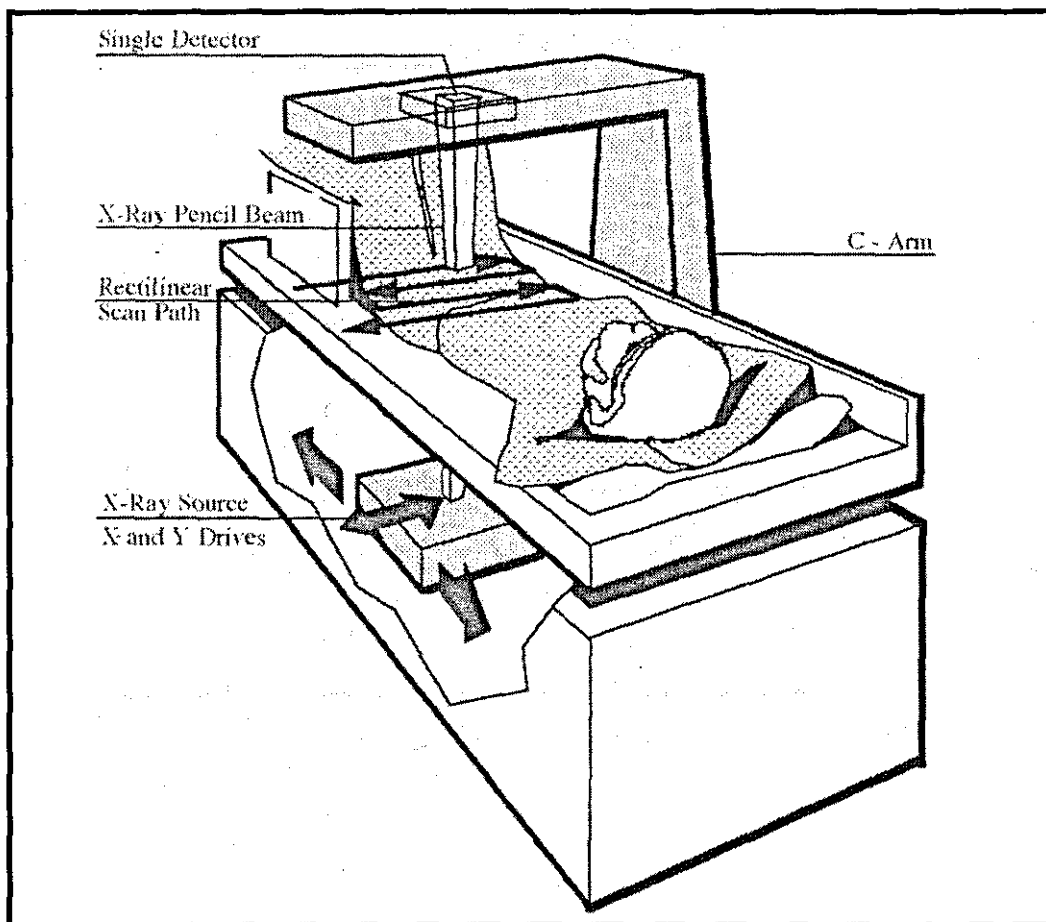
Figure 2.12 Main Components of a Densitometry System [58]

Single Photon Absorptiometry (SPA)

This method is specially used to diagnose osteoporosis and to measure bone mineralisation in infants as it uses low energy radiations. It uses a narrow beam of mono-energy radiations, emitted from a low energy radio-nuclide source commonly ^{125}I or ^{241}Am, to measure bone density. Lower energy sources are optimal to measure bone density of smaller bones (like radius, ulna, metacarpals, etc.) where tissue cover is minimal. Usually a NaI (Tl) scintillation detector is used to monitor the radiation beam. The source and detector are coupled on a yoke and move together over the body part that is being examined, thereby creating an image. Measurements are restricted to the appendicular skeleton, usually the forearm, since the bone must be encased in a constant thickness of soft tissue or its equivalent. Single line or rectilinear scanning is performed over the bone. The difference in the attenuation count rate between the bone and the soft tissue region allows calculation of the bone mineral content in the scan path. This method cannot separate cancellous and cortical bone components. The accuracy and precision error of this method is around $\pm$ 2-4% [59] and 1-2% [58, 59], respectively.

Dual Photon Absorptiometry (DPA)

Dual photo absorptiometry uses a dual-energy radio-nuclide as radiation source. The most commonly used radio-nuclide is ^{153}Gd. Photons of different energy are attenuated differently by bone and soft tissues. Bone density can be calculated by measuring the percentage of each transmitted beam absorbed by bone and soft tissue and then applying simple simultaneous equations. DPA eliminates the need for a constant soft tissue thickness across the scan path and it can be used effectively in the spine and femur regions. The accuracy and precision error of DPA is around 1-4% [59] and 1-2% [59], respectively.

Dual X-Ray Absorptiometry (DXA)

DXA technique uses X-ray tube as a source to emit radiations rather than using radioisotope energy source as used in DPA. Other than this, DXA technique is similar to DPA, however, DXA overcomes many disadvantages of DPA which are:

- Scan time for high precision spine and hip measurement is very large (20-40 min) [58] with limited resolution (4-8mm) for DPA [58]. Whereas, DXA uses higher photon flux of X-ray tube which reduces scanning time to almost six times as compared to DPA with a resolution and precision of 1% or less [58].

- Decrease of the radiation source strength with time requires complicated corrections to be made in DPA.

- The availability of the radioisotope, used in DPA, is limited and its use is strictly regulated.

Quantitative Computer Tomography (QCT)

Like DXA, QCT also uses x-ray tubes as a radiation source. However in QCT, a three-dimensional image of a body structure is constructed by a computer from a series of plane cross-sectional images made along an axis. An advantage of QCT is that it can separately measure the cortical and cancellous bone mineral density. However, QCT exposes the patient to very high levels of radiations in comparison to other techniques. Hence, it should not be used to make frequently repeated measurements in the same patient.

Peripheral Quantitative Computer Tomography (pQCT)

pQCT is a type of QCT but can only be used to measure the bone density of peripheral bone skeletal sites, like radius.

A comparison of the commonly used densitometry techniques is given in table 2.2.

Table 2.2   **Comparison of Various Densitometry Methods**

Parameters for comparison	SPA	DPA	DXA	QCT
Radiation Source	Low mono-energy radiation from ^{125}I or ^{241}Am	Dual-energy radiation from ^{153}Gd	X-Ray Tube	X-Ray Tube
Application	At peripheral skeleton, where the tissue cover is minimal or has constant thickness	At spine, hip or whole body.	At spine, hip or whole body.	Whole skeleton. Cannot be repeated frequently as it exposes the body to high radiations.
Precision	1-2% [1, 39, 59, 60]	2-5% [1, 39, 59, 60]	1-3% [1, 39, 60-62]	2-6% [1, 39, 61, 62]
Accuracy	±2-4% [1, 39, 59, 60]	±5-10% [1, 39, 59, 60]	±4-8% [1, 39, 60]	3-7% [1, 39, 59]
Distinguish cortical and cancellous bone	No	No	No	Yes
Effect of tissue thickness	Tissue thickness has to be constant	Can distinguish between bone and tissue.	Can distinguish between bone and tissue.	Can distinguish between bone and tissue.

B.   The Singh Index (SI)

The Singh Index (SI) is another method which has been used to estimate the degree of osteoporosis using ordinary X-ray radiographs [63]. In the Singh Index, the degree of osteoporosis is graded by the radiographic evaluation of the trabecular pattern of the proximal femur from one to six, with grade one being severe osteoporosis and grade six being normal, as shown in figure 2.13. The main advantages of using the Singh Index are that it is inexpensive, fast, less harmful and easy to use. However, the Singh Index is subjective in nature and, therefore, should only be used as a rough estimation of bone quality, provided that readings are taken by experienced clinicians. Also, the Singh Index has only been developed for the proximal femur, thus it cannot be used to predict bone strength at other bone skeletal sites except the proximal femur.

(a) Grade six: All normal, trabecular groups are visible, cancellous bone seems to occupy completely the upper end of the femur.

(b) Grade five: Structure of principal tensile and principal compressive trabeculae is accentuated. Ward's triangle appears prominent.

(c) Grade four: Principal tensile trabeculae are markedly reduced but can still be traced from the lateral cortex to the upper part of the femoral neck.

(d) Grade three: Continuity of the principal tensile trabeculae is broken opposite the greater trochanter.

(e) Grade two: All trabeculae except the prominent principal compressive trabeculae are nearly resorbed.

(f) Grade one: Even the principal compressive trabeculae are markedly reduced and no longer prominent

Figure 2.13 The Singh Index for Estimating Osteoporosis in Proximal Femur [64]

C.   Bone Quantitative Ultrasound

In bone quantitative ultrasound testing, two ultrasound transducers, one transmitting and one receiving, are placed opposite to one another in a water bath. Bone specimen, usually from peripheral skeleton sites like calcaneus, is placed between the transducers. Ultrasound wave is transmitted, and the attenuation or the change in speed of the wave caused because of the bone specimen is measured. Compared to osteoporotic bone, normal bone demonstrates higher attenuation of the ultrasound waves and is associated with a greater velocity of the wave passing through bone. Broadband ultrasound attenuation (BUA) and speed of sound (SOS) are the two main types of ultrasound techniques used commercially. The ultrasound technique is rapid, painless and does not use potentially harmful radiation. It can also be used to measure geometric properties of the bones. One disadvantage of using an ultrasound technique is its inability to predict the density of the bones which are most likely to fracture because of osteoporosis, like hip and spine.

2.3   CONCLUDING REMARKS

This chapter has presented the definition of bone strength and various parameters which contribute to the bone strength. As this thesis investigates the evaluation of bone strength, the reasons for bone strength measurement have also been presented. Bone strength can be estimated either through direct or indirect testing methods and a detailed discussion of various direct and indirect testing methods have been presented. Following the discussion on various bone strength measurement methods, the structure of the thesis is outlined. The next chapter presents the literature review of the various indirect methods and the limitations associated with them.

CHAPTER 3

USE OF INDIRECT METHODS FOR BONE STRENGTH PREDICTION

The indirect methods do not give a direct measurement of the bone mechanical properties; therefore various correlational studies between direct and indirect methods have been carried out in order to evaluate the efficacy of the indirect methods in predicting bone strength. A review of these studies are presented in the following sections and are subdivided into three sections, (i) densitometry methods, (ii) Singh Index, and (iii) ultrasound methods.

For every correlational review study, a table is given as a summary and all tables have similar style and format. Therefore, only the style and format of table 3.1 is fully explained. The main objective of this chapter is to identify the limitations and shortcomings of the indirect methods; hence, these have been discussed at the end of each review study. It should be noted that in some correlational studies presented below, the statistical significant value 'P' is missing and also the coefficient of correlation is stated as r instead of r^2, as per the information available in the respective publications.

3.1 BONE DENSITOMETRY METHODS OF BONE STRENGTH EVALUATION

Among the various indirect methods, bone densitometry is the most commonly used and reported as the most accurate method [30]. Densitometry methods measure bone density to get an estimate of the bone strength. Bone density can be determined either by using the standard method of measuring density of material, which measures the bone weight and volume of the water displaced by the bone when it is immersed in the water, or by using commercially available densitometry techniques (as shown in figure 2.11 in

chapter 2). This method is referred to as "standard method" in this paper. The standard method is more accurate than the commercial densitometry methods, as the latter have inherent measurement errors due to limitations of the measurement techniques (e.g., the presence of more than two layers of fat tissue around the bone would result in an erroneous measurement) and the variability of the results obtained from different densitometry machines (e.g., accuracy and precision of densitometry machines vary for different manufactures) [13-15, 60, 65, 66]. In order to establish how well bone density can be used to estimate the bone strength, a review of the studies correlating bone density, as measured by the standard method, with the bone mechanical properties is presented first. This is followed by the review of various commercially available densitometry methods. Out of the various methods, quantitative computer tomography (QCT), peripheral quantitative computer tomography (pQCT) and dual energy X-ray absorptiometry (DXA or DEXA) are reviewed in this paper, as they are commonly used, with DXA being the most commonly used. Therefore, the various limitations and drawbacks of DXA are discussed in detail. Ideally a clinician or a surgeon should know which densitometry method should be used to obtain accurate results, rather than simply using what is available to him/her locally (in the hospital). Hence, various parameters which should be considered before the selection of a densitometry technique for the measurement of the bone density are discussed. The effect of other factors on the use of bone density measurements for bone strength prediction is also presented. These factors include, bone geometry, non-site specific bone density measurements and anisotropic property of bone.

3.1.1 Prediction of Bone Strength Using the Standard Method of Bone Density Measurements

Review of the Correlational Studies Presented in Table 3.1

McCalden *et al* [67] found a high correlation ($r^2 = 0.942$; P<0.001) between ultimate compressive strength (US, MPa) and dry apparent bone mineral density ($_{app}$BMD, mg/cm^3) of the human cadaver cancellous distal femur. The $_{app}$BMD is the dry weight of the bone after removing all of the fat and marrow per unit volume. Another study on the human cadaver lumbar vertebrae, femoral metaphyses and femoral diaphyses revealed

the same range of correlation coefficient ($r^2 = 0.969$) between the ultimate compressive strength and $_{app}$BMD [68]. However, a comparatively lower correlation between the $_{app}$BMD and ultimate compressive strength ($r^2 = 0.88$) was found for the bovine femur cancellous bone [69]. Rice *et al* [70] pooled data from a number of studies for statistical analysis and found a square relationship between the $_{app}$BMD and both Young's modulus and ultimate bone strength. A detailed tabular summary of the various correlational studies conducted between the dry apparent bone mineral density, measured using the standard method, and the bone strength, measured using direct methods, are presented in table 3.1.

Discussions

From the presented studies it can be concluded that bone density can be used to predict bone strength as $_{app}$BMD showed a high correlation with bone strength. However, $_{app}$BMD measurements were performed in-vitro after removing the fat and bone marrow. This in-vitro method cannot be used in actual patients; non-invasive methods are used instead. Hence, many correlational studies have been conducted to investigate the accuracy of non-invasive densitometry methods to predict bone strength. These are presented in the next section.

Table 3.1 **Summary of Various Correlational Studies Conducted which Validates the Use of Bone Density, As Measured By the Standard Method, In Predicting Bone Strength**

Column 1		Column 2					Column 3						Column 4	
		Mechanical Testing (In-vitro)					Indirect Testing						Corr. Coeff.	
	Bone Specimen Source	Bone Specimen		Test Specification			Bone Specimen		Measurement Conditions					
Author		Site	Type	Test	n	Prop. Msrd.	Site	Type	Tech.	T.E.	Meth.	Prop. Msrd.	r^2	P
Mc Calden et al 1997 [67]	Human cadaver	Distal femur	Canc.	Comp.	255	US (MPa)	Distal femur	Canc.	Non-convn.	×	In-Vitro	BMD (mg/cm³)	0.94	<0.001
Keller et al 1994 [68]	Human cadaver	Vertebrae and femoral metaphyses and diaphyses	Whole-bone	Comp.	496	US (MPa)	Vertebrae and femoral metaphyses and diaphyses	Whole-bone	Non-convn.	×	In-Vitro	BMD (mg/cm³)	0.96	-
						E (MPa)							0.96	-
Brear et al 1988 [69]	Bovine cadaver	Prox. femur	Canc.	Comp.	62	US (MPa)	Prox. femur	Canc.	Non-convn.	×	In-Vitro	BMD (mg/cm³)	0.88	-
						E (MPa)							0.80	-

List of symbols and abbreviations used in the table

$_{app}$BMD = apparent bone mineral density (mg/cm³), measured as dry weight of the bone per unit volume; Canc. = cancellous bone specimen; Comp. = compression testing; Corr. Coeff. = correlation coefficient between the property of the specimen measured using the mechanical testing and indirect testing; E = Young's Modulus (MPa); Meth. = Method of indirect measurement used i.e., in-vitro or in-vivo; n = number of samples tested; Non-convn. = bone density was determined using the standard method, i.e., by measuring weight and volume of the bone specimen; P = statistical significance of the correlational study; Prop. Msrd. = property measured; prox. = proximal; r^2 = correlation coefficient between the mechanical property of the specimen and the specimen property measured using the indirect method; Tech. = indirect testing technique used in the presented study; T.E. = method used to simulate the effect of soft tissues present around the bone specimen during the indirect testing; US = ultimate strength of the specimen (MPa); Whole-bone = indicates that combined cortical and cancellous bone density/mechanical strength was measured; × = indicates that the effect of bone tissue for the indirect testing was not simulated in the study; - = indicates that no information was given in the referred paper.

Description of the style and format of the table

Column 1: This column provides the reference (i.e., name of the authors and year of publication) of the referred correlational study. It also gives information about the source from where the bone specimen was taken for testing in the referred study.

Column 2: The information about the mechanical testing, by direct method, that was conducted on the bone specimen is provided in this column. It gives the bone site from where the specimen was taken for the testing, as well as information on the type of bone which was used in the study (i.e., cancellous or cortical or Whole-bone) and the type of test that was conducted on the bone specimen (i.e., tensile or compression or bending or simulation); and finally, the number of samples which were tested and the measured mechanical property (for the correlation).

Column 3: This column gives the information about the indirect testing method (e.g, QCT or DXA or BUA, etc.) which was used in the referred study. It gives the information of the bone site and the type of bone that was used for the indirect testing. It also provides the information on: (a) the method that was used to simulate the effect of soft tissues during the measurement, (b) wether the referred study was conducted in-vivo or in-vitro and (c) the bone property that was measured using the indirect method.

Column 4: This column provides the correlation cofficient between the mechanical property of the bone specimen which was measured by mechnical testing of the specimen and the bone property measured using the indirect method. It also gives the statistical significance of the presented correlational study.

3.1.2 Prediction of Bone Strength Using the Conventional QCT Densitometry Method

Review of the Correlational Studies Presented in Table 3.2

The use of cancellous bone density measured using QCT technique for bone strength prediction was investigated in-vitro on the human cadaver tibia cancellous bone by Bentzen et al [53]. QCT volumetric bone mineral density (vBMD, mg/cm^3) data from the proximal tibia epi- and metaphysis of six human cadaver knees were correlated with the bone properties determined by compression testing. vBMD correlated better with ultimate strength (r = 0.84) and yield strength (r = 0.85) in a power function relationship as compared to the linear relationship (straight line). In another similar study, bovine cadaver tibia cancellous bone exhibited elastic behaviour at low strains and a good linear correlation (r^2 = 0.84; P<0.001) was also found between the Young's modulus determined by compression testing and vBMD [45]. In contrast, in a study conducted on the human cadaver vertebrae cancellous bone, a poorer correlation between vBMD and both ultimate compression bone strength (r = 0.72; P<0.001) and Young's modulus (r = 0.574; P<0.001) was found, as compared to other studies [71]. Moreover, the variance of the presented data was also very high [71].

The effectiveness of cortical bone density as measured by QCT to predict bone strength was investigated by Snyder and Schneider [37]. A moderate correlation was found between in-vitro vBMD and three-point bending bone properties of the cortical mid diaphysis human cadaver tibia (r = 0.55 for Young's modulus and r = 0.50 for ultimate strength). In another study, a human femoral mid-diaphysis cortical bone was extracted from patients undergoing total hip replacement and vBMD of the cortical bone specimen was correlated with uniaxial compression ultimate strength and Young's modulus with a coefficient of r = 0.64; P<0.005 and r = 0.69; P<0.005, respectively [72]. No information was given on simulating the soft tissue effect during the in-vitro QCT measurements.

Discussions

A detailed tabular summary of the various studies conducted which evaluated the use of QCT to predict both cortical and cancellous bone strength are given in table 3.2. The following observations can be made from the presented table:

(i)   Lower values of correlation were found for the QCT as compared to the standard method.

(ii) QCT is not a good predictor of the cortical bone strength as compared to the cancellous bone strength. This is evident, as the value of correlational coefficients found for the cortical bone (r^2 ranging from 0.48 to 0.25) was far less as compared to that found for the cancellous bone (r^2 ranging from 0.87 to 0.33).

(iii) The strength of skeletal sites which can be best predicted by QCT cancellous bone density are the proximal femur [73, 74] followed by the tibia [45, 53] and vertebrae [71].

(iv) In-vitro QCT bone density measurement of cadavers were conducted in all the presented studies. This does not represent a real clinical condition. In the case of cadaver bone samples, after the bone specimens were removed from the body they were frozen and stored for further testing after defatting and removing the bone marrow. This process of freezing, defatting and removing the bone marrow from bone specimens, results in the change of bone mechanical properties [44, 75-78]. Therefore, the correlational results which were found in the various cadaver studies might not be the same as it would be for the living human bones.

(v)   A lower correlational value was found when the bone sample was taken from the patient undergoing surgery [72] as compared to the studies conducted on cadavers. This avoids an approximate 10% change which occurs in the mechanical property of the bone, during the life to death transition period [44]. This shows that QCT bone density is a less accurate predictor of the bone strength in the case of living humans as compared to the bone strength of cadavers.

Table 3.2 Summary of Various Correlational Studies Conducted to Evaluate the Use of QCT in Predicting Bone Strength

Column 1		Column 2					Column 3						Column 4	
		Mechanical Testing (In-vitro)					Indirect Testing						Corr. Coeff.	
	Bone Specimen Source	Bone Specimen		Test Specification			Bone Specimen		Measurement Conditions					
Author		Site	Type	Test	n	Prop. Msrd.	Site	Type	Tech.	T.E.	Meth.	Prop. Msrd.	r^2	P
Wachter et al 2002 [72]	Human patients undergoing hip replacement	Femoral mid diaphysis	Cort.	Comp.	23	US (MPa) / E (MPa)	Femoral mid diaphysis	Cort.	QCT	-	In-vitro	$_v$BMD (mg/cm^3)	0.40* / 0.48*	<0.005
Snyder et al 1991 [37]	Human cadaver	Tibia mid diaphysis	Cort.	3-pbt	45	US (MPa) / E (MPa)	Tibia mid diaphysis	Cort.	QCT	W	In-vitro	$_v$BMD (mg/cm^3)	0.25* / 0.3*	-
Lang et al 1997 [73]	Human cadaver	Prox. femur	Whole-bone	Side F.S.	26	Failure Load (KN)	Prox. femur	Canc.	QCT	W	In-Vitro	$_v$BMD (mg/cm^3)	0.87	<0.01
Keaveny et al 1994 [45]	Bovine cadaver	Tibia	Canc.	Comp.	29	E (MPa)	Tibia	Canc.	QCT	x	In-Vitro	$_v$BMD (mg/cm^3)	0.84	<0.001
Lotz and Hayes 1990 [74]	Human cadaver	Prox. femur	Whole-bone	Side F.S.	12	Failure Load (KN)	Prox. femur	Canc.	QCT	s	In-Vitro	$_v$BMD (mg/cm^3)	0.87	<0.001
Lang et al 1988 [71]	Human cadaver	Vertebrae	Canc.	Comp.	41 / 34	US (MPa) / E (MPa)	Vertebrae	Canc.	QCT	x	In-Vitro	$_v$BMD (mg/cm^3)	0.51* / 0.33*	<0.001
Bentzen et al 1987 [53]	Human cadaver	Prox. tibia	Canc.	Comp.	165	US (MPa) / E (MPa)	Prox. tibia	Canc.	QCT	x	In-Vitro	$_v$BMD (mg/cm^3)	0.71* / 0.72*	-

Note: Symbols and abbreviations used in the previous tables presented in this chapter are not repeated here.

* = indicates that the coefficient of correlation 'r' (as given in the referred paper), has been converted to r^2 in this table for consistency; Cort. = cortical bone specimen; F.S. = fall simulation; prox. = proximal; s = this indicates that tissue effect was simulated by using saline water bath during densitometry measurements; $_v$BMD = Volumetric bone mineral density (mg/cm^3); W = this indicates that tissue effect was simulated by using water bath during densitometry measurements; 3-pbt = three-Point bending test.

The main advantage of using QCT is that it can independently measure the density of the cortical and cancellous portions of the bone [1, 39]. Its main disadvantage is that it is expensive and exposes the human body to more harmful radiations for a longer period as compared to any other densitometry technique [1, 7, 39, 58, 59]. This makes it non-feasible for predicting bone strength in infants and cannot be used frequently. Hence, DXA scanning is more commonly available and used [7, 39, 60]. In the next section, use of pQCT technique, is reviewed.

3.1.3 Use of Peripheral QCT Technique (pQCT) to Predict Bone Strength

Review of the Correlational Studies Presented in Table 3.3

The effectiveness of using pQCT technique to predict four-point bending stiffness $(N.mm^2)$ was investigated by Martin et al [79]. They used rabbit humeri for this investigation and calculated bone bending stiffness in two different ways; (i) by recording pQCT bone density measurements and substituting them in an existing relationship, established by Carter and Hayes [80, 81], between the bone density and Young's modulus, and (ii) by carrying out four-point bending mechanical tests. A very high correlation ($r^2 = 0.96$) was found between the bone bending stiffnesses calculated using the aforementioned two methods, but their study did not cover the entire range of bone density, since they used the rabbit humeral specimens of similar density and size from a single gender. In another study by Jamsa et al [82], $_v$BMD measurements of femur and tibia bone of mice, using the pQCT technique, were correlated with three-point bending failure load. The coefficients of correlation, r = 0.79; P<0.0001 and 0.78; P<0.0001, were obtained for the femur and tibia respectively. Lill et al [83], investigated the use of pQCT measurements to estimate human cadaver distal radius bone strength determined by simulating a fall on the outstretched hand (test configuration is shown in figure 3.4 (C)) and recording the failure load. It was found that the failure load correlated higher with the cortical area (r = 0.7; P<0.05) and cancellous $_v$BMD (r = 0.6; P<0.05), as compared to the cortical $_v$BMD (r = 0.43) and cancellous area (r = 0.40; P<0.05).

Discussion

The studies conducted to investigate the use of pQCT to predict bone strength are presented in table 3.3. The following observations can be made from the presented table:

(i)   Lower values of correlation were found for the pQCT as compared to the standard method.

(ii) Geometric properties of the bone are a better predictor of bone strength as compared to the bone density [82, 83].

(iii) Moderate to low correlation coefficients were found for both, bone density (r^2 ranging from 0.62 to 0.19) and geometric properties (r^2 ranging from 0.88 to 0.49).

pQCT technique exposes the patient to a smaller radiation dose as compared to the QCT technique. It is more accurate for the skeletal sites where the distribution of soft tissues and fat are minimal and homogenous, i.e., at the peripheral skeletal sites. Hence, non-site specific pQCT bone density measurements of the peripheral skeletal sites, like radius bone, have to be used to predict the bone density at the proximal femur or spine where the soft tissues are thick and non-homogeneous. However, non-site specific bone density measurements taken at the radius bone were found not to be a good predictor of the femur or spine bone strength as compared to site specific measurements [4]. Review of DXA technique is presented next.

Table 3.3   Summary of Various Correlational Studies Conducted to Evaluate the Use of pQCT in Predicting Bone Strength

Column 1		Column 2					Column 3						Column 4	
		Mechanical Testing (In-vitro)					Indirect Testing						Corr. Coeff.	
Author	Bone Specimen Source	Bone Specimen		Test Specification			Bone Specimen		Measurement Conditions					
		Site	Type	Test	n	Prop. Msrd.	Site	Type	Tech.	T.E.	Meth.	Prop. Msrd.	r^2	P
Lill et al 2003 [83]	Humna cadaver	Distal radius	Whole-bone	F.S.	118	Failure Load (KN)	Distal radius	Cort.	pQCT	-	In-vitro	vBMD (mg/cm^3)	0.19*	<0.05
								Cort.				Area (mm^2)	0.49*	
								Canc.				vBMD (mg/cm^3)	0.36*	
Jamsa et al 1998 [82]	Mouse	Femur mid-shaft	Cort.	3-pbt	20	Failure Load (KN)	Femur mid-shaft	Cort.	pQCT	-	In-vitro	vBMD (mg/cm^3)	0.62*	<0.0001
												CSMI (mm^4)	0.74*	
												c/sA (mm^2)	0.69*	
		Tibia mid-shaft			20		Tibia mid-shaft					vBMD (mg/cm^3)	0.6*	
												CSMI (mm^4)	0.74*	
												c/sA (mm^2)	0.88*	

Note: Symbols and abbreviations used in the previous tables presented in this chapter are not repeated here.

c/sA = cross sectional area of the bone specimen (mm^2); CSMI = cross sectional moment of inertia of the bone specimen (mm^4).

3.1.4   Use of DXA Technique to Predict Bone Strength

Review of the Correlational Studies Presented in Table 3.4

The use of densitometry technique, DXA, which was also compared with QCT, to predict bone strength using the human cadaver proximal femur bone was investigated by Cheng et al [57]. In the study, the femur bone strength was determined by simulating a side fall on the greater trochanter (as shown in figure 2.10) and recording the failure loads. It was found that trochanteric bone mineral density measured by DXA (BMD, mg/cm^2) correlated better with the failure load (KN) of the femur ($r^2 = 0.88$; P<0.001) as compared to cancellous trochanteric vBMD (mg/cm^3) ($r^2 = 0.69$; P<0.001) measured using the QCT technique. Of the QCT measurements, trochanteric cortical area (mm^2) gave the best correlation with the femur failure load ($r^2 = 0.83$; P<0.001). It was

concluded that both DXA and QCT have a similar ability to predict femoral strength in-vitro, with trochanteric BMD and the trochanteric cortical area being the best parameters for DXA and QCT, respectively. Similar studies were conducted by other researchers [84, 85] who found a similar range of correlation coefficient values (presented in table 3.4) between the bone density and the failure load data. In the above referred studies, correlations found between the mechanical bone strength and (i) the bone geometry measured using DXA, or (ii) the ultrasound measurements, are also presented in the table 3.4.

Discussions

The studies conducted to investigate the use of DXA to predict bone strength are presented in table 3.4. The following observations can be made from the presented table:

(i)   Lower values of correlation were found for the QCT as compared to the standard method.

(ii) High to moderate correlations (r^2 ranging from 0.92 to 0.59) can be observed. These are comparatively higher than both QCT and pQCT.

(iii) DXA has a better ability to predict proximal femur bone strength as compared to QCT [57].

(iv) DXA is a better predictor of bone strength as compared to ultrasound methods [84].

(v) All studies presented in table 3.4 have simulated side fall on the proximal femur to determine the bone strength. The main disadvantage with simulation testing is that the exact region of failure is not known and cannot be controlled. Therefore, it is difficult to predict the exact region of the bone density scan for the site specific measurements which make the results more erroneous.

In all the studies presented, the bone density measurements were done in-vitro by simulating the effect of soft tissues; thus, neglecting various errors and limitations of the DXA technique when performed in-vivo.

Table 3.4 Summary of Various Correlational Studies Conducted to Evaluate the Use of DXA in Predicting Bone Strength

Column 1		Column 2					Column 3						Column 4	
		Mechanical Testing (In-vitro)					Indirect Testing						Corr. Coeff.	
Author	Bone Specimen Source	Bone Specimen		Test Specification			Bone Specimen		Measurement Conditions					
		Site	Type	Test	n	Prop. Msrd.	Site	Type	Tech.	T.E.	Meth.	Prop. Msrd.	r^2	P
Cheng et al 1997 [57]	Human cadaver	Prox. femur	Whole-bone	Side F.S.	64	Failure Load (KN)	Femoral neck	Cort.	QCT	-	In-Vitro	vBMD (mg/cm³)	0.07	<0.05
							Trochanter						0.28	
							Trochanter	Canc.					0.69	<0.001
							Femur neck	Cort.				Area (mm²)	0.66	
							Trochanter						0.83	
							Femoral neck		DXA	Gp	In-Vitro	BMD (mg/cm²)	0.71	
							Trochanter	Whole-bone					0.88	<0.001
							Inter trochanter						0.69	
							Ward's triangle						0.59	
Bouxsein et al 1995 [84]	Human cadaver	Prox. femur	Whole-bone	Side F.S.	16	Failure Load (KN)	Femoral neck	Whole-bone	DXA	s	In-Vitro	BMD (mg/cm²)	0.79	<0.001
							Trochanteric		DXA			BMD (mg/cm²)	0.81	<0.001
							Calcaneus		DXA			BMD (mg/cm²)	0.63	<0.001
							Calcaneus		BUA			BUA (dB/MHz)	0.51	<0.002
							Calcaneus		SOS			SOS (m/s)	0.40	<0.008
							Femoral neck length		DXA			Length (mm)	0.27	<0.04
Courtney et al 1995 [85]	Human cadaver	Prox. femur	Whole-bone	Side F.S.	17	Failure Load (KN)	Femoral neck	Whole-bone	DXA	s	In-Vitro	BMD (mg/cm²)	0.92	<0.001
							Trochanteric						0.73	-
							Femoral neck					Area (mm²)	0.79	-

Note: Symbols and abbreviations used in the previous tables presented in this chapter are not repeated here.

BMC = bone mineral content (mg), measured using DXA; BMD = bone mineral density (mg/cm²), measured using DXA; BUA = broadband ultrasound attenuation (dB/MHz); G_p = this indicates that tissue effect was simulated by using plexi glass sheet during densitometry measurements; SOS = speed of Sound (m/s).

The main source of inherent inaccuracies in the DXA in-vivo bone density measurement is due to its inability to distinguish more than two absorptiometrically distinguishable components in the scan region of interest (the "two component DXA limitation") [13-15, 58]. Therefore, accurate DXA bone density measurements are restricted to the bone sites that have homogeneous soft tissues over the entire scanning region. The two-component DXA requirement cannot be satisfied for in-vivo bone scans; because all of the skeletal sites contain non homogeneous distribution of several absorptiometrically distinguishable soft tissues such as fat and lean muscles tissue and yellow/red marrow mix in intra osseous region. Most of the correlational studies presented in the literature, measured bone density in-vitro by removing extra and intra osseous soft tissues [3, 52, 57, 86, 87], thus, neglecting the effect of extra osseous fat and lean muscle tissues and intra osseous yellow/red marrow mix. However, in some in-vitro studies [4, 5, 37, 73, 88-90], bone density measurements were performed by simulating both extra and intra osseous soft tissues as one homogeneous medium, thus neglecting the effect of the presence of different absorptiometry soft tissues. In some studies (table 3.7), in-vivo bone density measurements were used for bone strength prediction, but these were done on the peripheral skeleton bone sites, which have almost homogenous soft tissues [4, 5]. Moreover, the correlations found with in-vivo investigations were far lower as compared to the investigations with in-vitro measurements. Thus, DXA when used in-vivo on patients will give a less accurate prediction of bone strength.

The impact of the soft tissues on the accuracy of in-vivo bone mineral density measurements of the human spine and hip by DXA, also the forearm by single photon absorptiometry (SPA) was assessed on 14 human cadavers by Svendsen et al [65]. In this study, three sets of DXA and SPA measurements were performed. Firstly, bone mineral density measurements were performed in-vivo followed by in-vitro measurements after carefully removing the soft tissues with the help of scissors and scalpels (vitro-1), and finally removing the remaining extra and intra osseous soft tissues with the help of chemicals (vitro-2). The calculated accuracy error between in-vivo and vitro-1 measurements were found in the range of 5.2-12.2% at the spine and 3.4-11.1% at the proximal femur for DXA measurements, and 2.9% at the forearm for SPA measurements. Between in-vivo and vitro-2 measurements, the calculated accuracy errors were found in the range of 5.3-9.7% at the spine and 2.6-13.2% at the proximal

femur for DXA measurements, and 4.8% at the forearm for SPA measurements. In another study, accuracy errors of less than 9% in the total femur, but errors of 8-22% for regional analyses of the femur and the lumbar spine were found due to soft tissues [66]. The above studies show that soft tissues can introduce an error in measurement which can be up to 22%.

Furthermore, an extensive series of quantitative simulation studies, replicating the ideal in-vivo DXA bone density measurements of a typical lumbar vertebral and proximal femur have been carried out to quantitatively assess the extent of inherent systematic inaccuracies in the DXA measurements [12-15]. It was found that the clinical in-vivo DXA bone density measurement inaccuracies may exceed $\pm 20\%$ or more, particularly in the cases of osteopenic or osteoporotic bone, post menopausal women, and in elderly patients.

Watts [91] found that, as a result of human error, common pitfalls like, errors in entering demographic information of the patient into the bone density analysis software, improper patient positioning, incorrect scan analysis and other interpretation mistakes lead to erroneous results in DXA measurements. This can have serious consequences.

It can be concluded from the above discussion that the DXA bone density measurements when performed in-vivo could lead to an inaccurate or wrong prediction of the bone strength. Hence, the use of bone drilling data is proposed in this research to estimate bone strength, which will overcome the above discussed disadvantages of using QCT, pQCT and DXA.

The use of three most commonly used densitometry techniques, i.e., QCT, pQCT and DXA to predict bone strength are reviewed above. However, a surgeon or clinician should know which densitometry technique among the three should be used to get the most accurate estimate of the bone strength. The factors on which the selection criteria of a technique should depend upon are discussed in the next section. However, QCT and pQCT use the same technique with the only difference that pQCT can only be used at the peripheral skeletal sites; therefore, only the selection between QCT and DXA is discussed.

3.1.5 Selection of Appropriate Bone Density Measurement Technique, DXA vs QCT

Depending upon the skeletal site being measured, 50% to 100% of the bone mineral content is contained in the cortical bone; yet it is the cancellous bone that, (i) provides weight bearing capacity, (ii) gets affected during osteoporotic treatment and (iii) gets affected because of change in the bone metabolism [92, 93]. For example, at the lumbar spine, 50% to 75% of the bone mineral is contained in the cortical bone. Thus, when the lumbar spine density is measured using DXA, which gives the combined bone density of cortical and cancellous bone, 50% to 75% of the signal will be generated from the cortical bone alone. However, it is the cancellous bone of the vertebral body that predominantly responds to antiresorptive therapy. Thus, a 10% change in the cancellous bone of the spine will appear only as 2.5% to 5% change in the spinal bone density measurements taken by DXA [40]. The above reasoning can be supported by the study conducted by Cefalu [10] and Faulkner [40] looking on at the pharmacological treatment of osteoporosis using medicines, like alendronate, risedronate and raloxifene. They found that a 4-5% increase in bone mineral density was associated with a 40-50% reduction in fracture risk. Thus, DXA may underestimate the change in bone fracture risk during osteoporotic treatment. QCT can measure cancellous bone density without considering the cortical bone density. This makes QCT a better predictor of fracture risk than DXA with regards to osteoporotic treatment. However, the disadvantage of using QCT in the case of osteoporotic patients is that it exposes the human body to more harmful radiations for a longer length of time. Also, unlike DXA, QCT cannot be used effectively to predict bone screw fixation strength as it does not give a combined measurement of cortical and cancellous bone, since the holding strength of bone screws depends on both the cortical and cancellous bone. This can be supported by the studies conducted by Snyder *et al* 1995 [94], Stromsoe *et al* 1993 [50] and Hirano *et al* 1997 [95]. They estimated the bone screw fixation strength using the bone density measurements done by DXA and QCT. A tabular summary of the correlational results are presented in the table 3.5. They all found that the screw pullout strength correlated by higher values with the DXA bone density in comparison to the QCT bone density. Furthermore, Heller *et al* [96] and Harnroongroj *et al* [97] found no correlation of QCT bone density with the bone screw fixation strength.

Therefore, different bone density measurement techniques are required to predict bone strength in different cases and at different skeletal sites. It is not economical to have both QCT and DXA scanning facilities in every hospital. Furthermore, densitometers from different companies can yield different bone density values, even when the same skeletal site is measured [40, 98]. This makes it more challenging for surgeons or clinicians to compare the bone density results of the same patient if taken using machines from different manufacturers. Hence, the need for a common bone strength prediction technique which can be used in-vivo in clinics at all skeletal sites is warranted.

In addition to bone density, bone strength also depends upon the bone geometry (as shown in figure 2.1); therefore, an investigation which has been conducted to study the effect of bone geometry on the bone strength and also on the bone density is presented in the next section. The relationship of the bone geometry with bone strength and density also highlights another disadvantage of using bone density measurement as a means to diagnose osteoporosis or to monitor the progress of an osteoporotic patient undergoing the treatment.

Table 3.5   Summary of Various Correlational Studies Conducted to Compare the Use of QCT and DXA in Predicting the Bone Screw Fixation Strength

Column 1		Column 2					Column 3						Column 4	
		Mechanical Testing (In-vitro)					Indirect Testing							
Author	Bone Specimen Source	Bone Specimen		Test Specification			Bone Specimen		Measurement Conditions				Corr. Coeff.	
		Site	Type	Test	n	Prop. Msrd.	Site	Type	Tech.	T.E.	Meth.	Prop. Msrd.	r^2	P
Snyder et al 1995 [94]	Two week old calf	Lumbar vertebrae	Whole-bone	Sc.P.out	24	T_i (N.m)	Lumbar vertebrae	Whole-bone	DXA	W	In-vivo	BMD (mg/cm^2)	0.47	<0.05
								Canc.	QCT			vBMD (mg/cm^3)	0.21	
Stromsoe et al 1993 [50]	Human cadaver	Femur shaft	Whole-bone	Sc.P.out	14	F_{SPF} (N)	Femur shaft	Whole-bone	DXA	x	In-vitro	BMD (mg/cm^2)	0.61[#]	-
								Cort.	QCT			vBMD (mg/cm^3)	0.25[#]	
Hirano et al 1997 [95]	Human cadaver	Lumbar vertebrae	Whole-bone	Sc.P.out	43	Bone stiffness (N/m)	Lumbar vertebrae	Canc.	DXA	-	In-vitro	BMD (mg/cm^2)	0.72	<0.0001
								Canc.	pQCT	-	In-vitro	vBMD (mg/cm^3)	0.49	

Note: Symbols and abbreviations used in the previous tables presented in this chapter are not repeated here.

T_i = screw insertion torque (N.m); F_{SPF} = screw pullout force (N); Sc.P.out = screw pullout test

3.1.6 Effect of Bone Geometry on Bone Strength and Its Relationship with Bone Mineral Density

Review of the Correlational Studies Presented in Table 3.6

In the study conducted on human cadaver proximal femur by Bonnaire *et al* [99], conventional X-rays were performed on bone specimens. Various geometric parameters of the bone specimen (as shown in table 3.6), e.g., collodiaphysis angle, diameter of neck, etc. were measured on the radiographs. After the x-ray imaging, single energy quantitative computer tomography (SE-QCT) was performed in six different regions of interest (ROI) (as shown in figure 3.1 (B)), namely, (i) centre of the femoral head (labelled as region A), (ii) greatest possible extra-cortical area of the femoral head (labelled as region B), (iii) centre of femoral neck (labelled as region C), (iv) greatest possible extra-cortical area of the femoral neck (labelled as region D), (v) centre of trochanteric area (labelled as region E), and (vi) greatest possible extra-cortical area in the trochanteric area (labelled as region F). $_V$BMD was measured using SE-QCT in a slice of 1 cm thickness, along the axis of the femoral neck. Mechanical testing of the proximal femur specimens were performed by simulating the peak load direction during the double support phase of gait and failure loads were recorded. The mechanical test setup is shown in figure 3.1 (A). From all the measured geometric data, the diameter of the femoral neck was best correlated with the failure load (r = 0.53, P<0.01). The collodiaphysis angle showed a lower correlation (r = 0.37; P<0.01), followed by the lever arm (mm) of the bending forces (distance from the middle of the femoral head to the femoral shaft) (r = 0.31, P<0.05). However, the femoral neck length showed no significant relationship with the failure load.

Bonnaire *et al* [99] also correlated bone density measurements taken at different regions with the failure load and found that bone density is a better predictor of bone strength than bone geometric parameters. Bone density at the femoral head (region B) was found to be the best predictor of the femur failure load (r = 0.73; P<0.01), followed by the centre of femoral head (region A) (r = 0.59; P<0.01), and lastly the femoral neck (region D) (r = 0.46; P<0.01). A low or insignificant correlation with the failure load

was found at other regions of the femur. A summary of the correlation values found in the above study are presented in table 3.6.

A → centre of femoral head with 1cm diameter
B → greatest possible extracortical area of head
C → centre of femoral neck
D → greatest possible extracortical area of neck
E → centre of trochanteric area
F → greatest possible extracortical area of trochanter
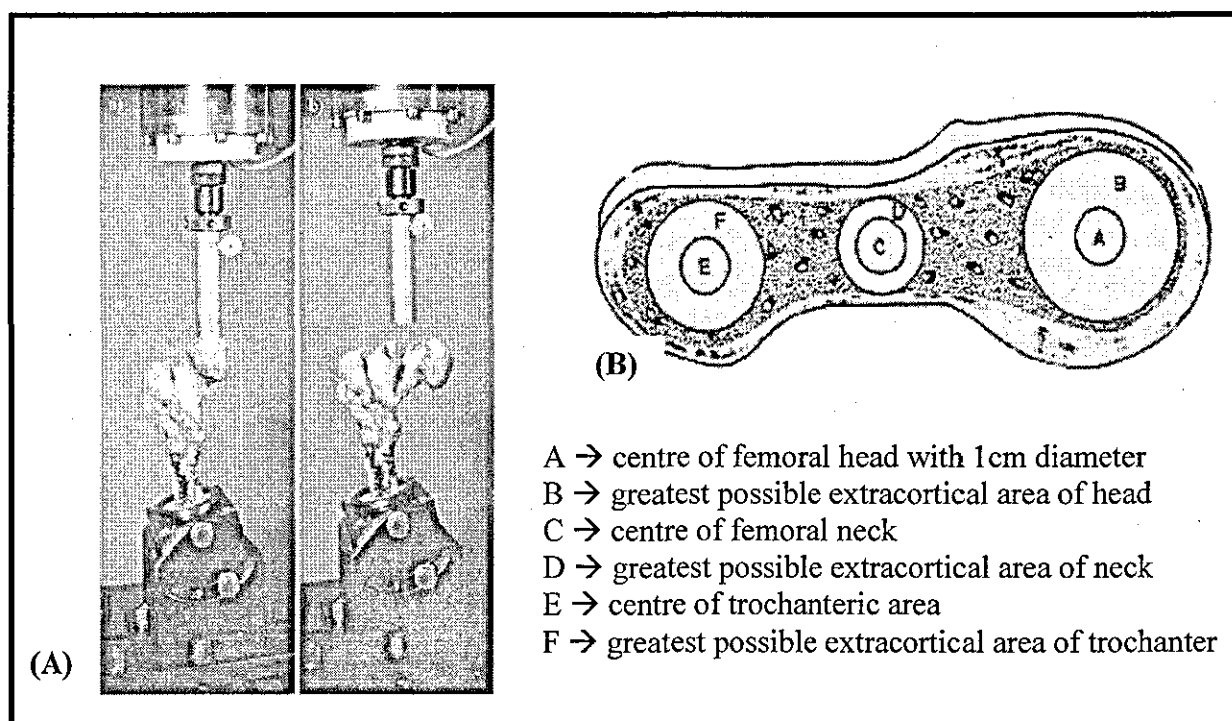
Figure 3.1 (A) Testing of proximal Femur by Simulating the Double Support Phase of Gait and (B) Region of Interest (ROI) of Volumetric Bone Mineral Density Measurements Conducted by SE-QCT [99]

Bonnaire *et al* [99] also evaluated relationships between the geometric parameters and the bone density. The Collodiaphysis angle was best correlated to the density of the femoral neck (regions C and D) and to the trochanteric area (region F). The length of the femoral neck had a negative correlation to the density of the femoral neck (regions C and D). Bone density at all the six regions of interest showed no significant correlation with both diameter of the neck and lever arm of the bending forces. It can be observed from this study that only one geometric parameter (collodiaphysis angle) had a meaningful correlation with the bone density at only one site (bone density at the femoral neck), but with a very low coefficient of correlation (r = 0.35; P<0.01) as compared to the correlation of other measured geometric parameters to the failure load.

Table 3.6 Summary of the Correlational Study Conducted to Evaluate the Effect of Bone Geometry on Bone Strength

Column 1		Column 2					Column 3						Column 4	
		Mechanical Testing (In-vitro)					Indirect Testing						Corr. Coeff.	
Author	Bone Specimen Source	Bone Specimen		Test Specification			Bone Specimen		Measurement Conditions					
		Site	Type	Test	n	Prop. Msrd.	Site	Type	Tech.	T.E.	Meth.	Prop. Msrd.	r^2	P
Bonnaire et al 2002 [99]	Human cadaver	Prox. Femur	Whole -bone	Simulation of the peak load direction during double support phase of gait	46	Failure Load (KN)	A	Whole-bone	SE-QCT	-	In-Vitro	vBMD (mg/cm³)	0.35#	<0.01
							B						0.55#	
							C						0.20#	
							D						0.26#	
							E						0.09#	<0.05
							F						0.14#	-
							CDA		SE-QCT	-	In-Vitro	Geometric parameters	0.14#	<0.01
							ND						0.28#	
							NL						0.006#	-
							LA						0.09#	<0.05

Note: Symbols and abbreviations used in the previous tables presented in this chapter are not repeated here.

A = centre of femoral head with 1cm diameter; B = greatest possible extra-cortical area of the femoral head; C = centre of femoral neck; CDA = Collodiaphysis angle; D = greatest possible extra-cortical area of the femoral neck; E = centre of trochanteric area; F = greatest possible extra-cortical area in the trochanteric area; LA = lever arm of the bending forces (mm) (distance from the middle of the femoral head to the femoral shaft); ND = femoral neck diameter (mm); NL = femoral neck length (mm); SE-QCT = single energy quantitative computer tomography

Discussions

The following findings can be made from table 3.6:

(i)   there is a correlation between; (a) bone strength and bone geometric parameters and (b) bone strength and bone density;

(ii)   bone density is a better predictor of bone strength than bone geometric parameters; and

(iii)   there is no or a very weak correlation between geometric parameters and bone density as compared to the correlation between geometric parameters and failure load.

The above finding shows that a change in the bone geometric parameter will affect the bone strength or fracture risk but would have a comparatively low effect on the bone density. Thus, the medicines (used for osteoporotic treatment) which change the geometry or architecture of the bone will increase or reduce the bone strength or fracture risk without resulting in a noticeable change in the bone density [34, 100]. This shows that the bone density measurements if used as a mean to predict bone strength or to monitor the progress of osteoporotic treatment could be misleading, especially in the case of patients taking medicines. The above conclusion can be supported by the investigation by Cefalu [10] and Faulkner [40]. They found that the treatment of osteoporosis using medicines, like alendronate, risedronate and raloxifene, showed very little increase in the bone mineral density for a considerable reduction in bone fracture risk.

All the reviews presented above on QCT, pQCT, DXA and bone geometry used site specific bone density measurements to estimate bone strength. However, it is the non-site specific bone density measurements which are commonly used to predict bone strength (as stated in chapter 1). The studies presented next evaluate the effectiveness of using non-site specific measurements as compared to the site specific measurements.

3.1.7 Use of Non-Site Specific Bone Mineral Density Measurements to Predict Bone Strength

Review of the Correlational Studies Presented in Table 3.7

The use of non-site specific bone density measurements to predict bone strength was investigated by Cheng et al [3]. In-vitro DXA BMD (mg/cm^2) measurements at the vertebral body, proximal femur and calcaneus of human cadaver were recorded under a plexi glass sheet to simulate the effect of soft tissues. All vertebral and proximal femoral specimens were mechanically tested to determine their bone strength. The failure load of third lumbar vertebra was determined by a uniaxial compression testing whereas the configuration of the femoral test was designed to simulate a fall on the greater trochanter (side fall simulation, as shown in figure 2.10). The failure load of the vertebrae correlated better with the site specific bone density measurements taken at the vertebrae ($r^2=0.64$; $P<0.01$), as compared to the non-site specific bone density measurements taken at the proximal femur ($r^2=0.50$; $P<0.01$) and the calcaneus

(r^2=0.18; P<0.01). Similarly, the proximal femur failure load showed a better correlation with the site specific femoral bone density ($r^2 = 0.88$; P<0.01) as compared to the non-site specific bone density measurements taken at the vertebra ($r^2 = 0.50$; P<0.01) and the calcaneus ($r^2 = 0.54$, P<0.01).

In another study by Lochmuller *et al* [4] on human cadaver, bone density at the various skeletal locations of the femur, tibia and distal radius bone were measured using the pQCT technique. A detailed diagrammatic description of all the measurement sites is shown in figure 3.2. At the proximal femur, in-vitro bone density measurements were taken after removing the soft tissues from the bone samples and submerging them into a water bath to simulate the effect of soft tissues. In-vivo bone density measurements were taken at the distal radius and tibia. Failure load of the femur was determined by simulating vertical loading (as shown in figure 3.3) and side impact fall condition (as shown in figure 2.10). Failure load correlated better ($r^2 = 0.4$-0.49) with the in-vitro site specific pQCT bone mineral content ($_v$BMC) (mg) of the proximal femur bone as compared to the non-site specific in-vivo $_v$BMC measurements taken at the femur shaft, distal femur, tibia and distal radius (ranged from $r^2 = 0.26$ to 0.44). A complete summary of all the correlation coefficients found in the study are given in table 3.7.

Since, QCT, pQCT and DXA are the most commonly used techniques in clinics to measure bone density, therefore, Lochmuller *et al* [5] performed bone density measurements using all three techniques, i.e., QCT, pQCT and DXA in a single study. They investigated and compared the ability of both site-specific and non site-specific bone density measurements taken using QCT, pQCT and DXA to predict the mechanical strength of the distal radius in different loading configurations. DXA measurements of the distal forearm, spine, femur, total body and pQCT measurements of the distal radius were obtained in-vivo in human cadavers. Spinal QCT and calcaneal quantitative ultrasound (QUS) were performed in-vitro on bone samples after submerging them in an aqueous solution. To determine the bone strength, left radius was mechanical tested for three-point bending and axial compression, whereas, right forearm was tested for a fall simulation. Test setup of the mechanical testing is shown in figure 3.4. Site specific DXA bone density of the radius bone was correlated with a coefficient of r = 0.89, 0.84 and 0.7 with the failure load of the three-point bending, axial compression and the fall simulation tests, respectively.
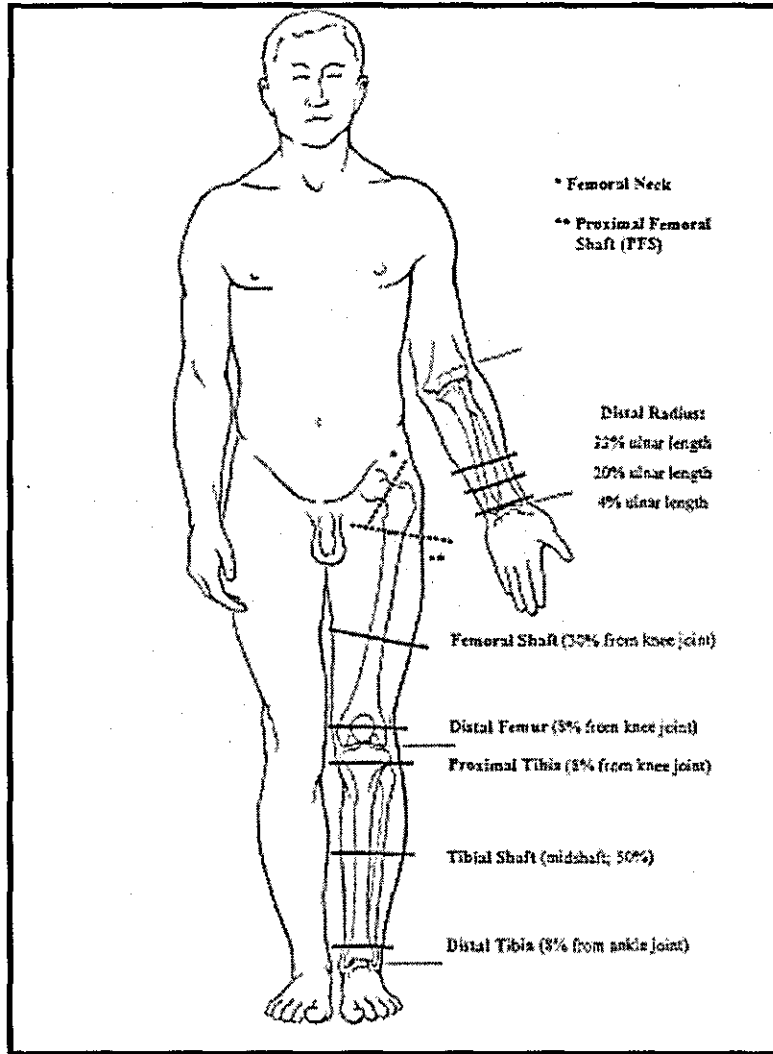
Figure 3.2 In-Vitro Measurement Sites at the Proximal Femur (Dotted Lines) and the In-vivo Measurement Sites at the Distal Radius and Lower Extremity (Solid Lines) [4]
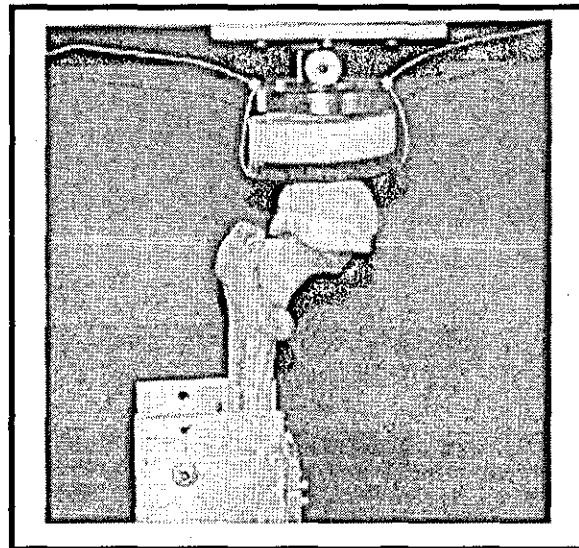
Figure 3.3 Mechanical Test Set Up to Simulate Vertical Loading Condition on the Proximal Femur [4]

A → 3-point bending (left radius)
B → Axial compression (Left Radius)
C → Fall Simulation (Right Forearm)
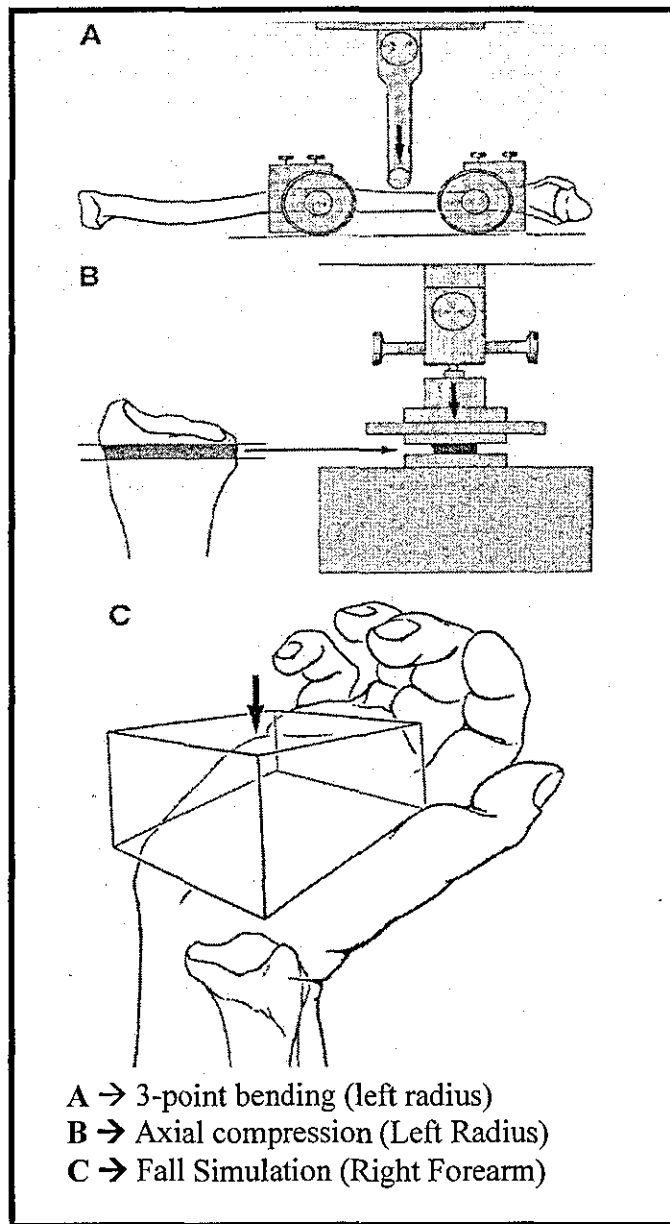
Figure 3.4   Mechanical Tests Conducted on Left Radius and Right Forearm [5]

The site specific DXA and pQCT bone density measurements correlated better than the non-site specific DXA, QCT and QUA bone density measurements, for all the three types of mechanical tests. Furthermore, pQCT was found not to be superior to DXA in estimating the mechanical strength of the distal radius bone, even under in-vivo conditions. This could be because there are generally fewer soft tissues at the distal radius, which would have reduced the DXA measurement errors which are usually incurred due to the soft tissue thickness. It was also found that the calcaneal QUS measurements displayed significantly lower correlation coefficient with the failure loads

in all loading configurations as compared to the site specific densitometry measurements. Additionally, correlation coefficients for both site specific and non-site specific bone density measurements were found to be generally higher for the three-point bending test, followed by the axial compression test and eventually by the fall simulation test. In another study, the prediction of bone strength using site-specific DXA measurements in human infants and children was investigated with the help of a swine piglet model [6]. DXA measurements were taken from sedated swine piglets and afterwards were killed and tested for three-point bending. Correlation between the DXA measurements and the bending strength was found to be different for the left and right femur and tibia bone. This shows that the bone density and strength vary at different skeletal locations and therefore only site-specific bone density measurements should be used to predict the bone strength.

Discussions

The studies conducted to investigate the use of non-site specific bone density measurements to predict bone strength are presented in table 3.7. The following observations can be made from the presented table:

(i) Bone strength correlated better with the site specific bone density measurements as compared to the non-site specific bone density measurements. The bone sites investigated for using site specific bone density to predict bone strength in different studies were vertebrae [3] (compared using DXA), proximal femur [3] (compared using DXA and pQCT) and radius (compared using DXA, QCT, pQCT and QUA).

(ii) In a single study, Lochmuller *et al* [5] performed bone density measurements using all three techniques, i.e., DXA, QCT and pQCT to predict bone strength which was determined using three different mechanical tests, i.e., compression, fall simulation and three point bending, of radius bone through site specific and non-site specific bone density measurements. As expected they found that site specific bone density is a better predictor of bone strength.

It is generally the non-site specific bone density measurements which are used on patients to predict their bone strength. Therefore, errors due to non-site specific

measurements would also add up to the other measurement errors discussed in the previous sections. The effect of bone anisotropic on the bone strength and bone strength estimation using bone density is presented in the next section.

Table 3.7   Summary of the Correlational Studies Conducted to Evaluate the Use of Non-Site Specific Bone Density to Estimate the Bone Strength

Column 1		*Column 2*					*Column 3*						*Column 4*	
		Mechanical Testing (In-vitro)					Indirect Testing						Corr. Coeff.	
Author	Bone Specimen Source	Bone Specimen		Test Specification			Bone Specimen		Measurement Conditions					
		Site	Type	Test	n	Prop. Msrd.	Site	Type	Tech.	T.E.	Meth.	Prop. Msrd.	r^2	P
Lochmuller et al 2002 [5]	Human cadaver	Radius	Whole-bone	3-pbt	119	Failure Load (KN)	Distal radius 33%U.L	Whole-bone	DXA	H	In-vivo	BMC (mg)	0.8[*1]	<0.01
			Cort.	Comp.	124								0.70[*1]	
			Whole-bone	F.S.	102								0.49[*1]	
		Radius	Whole-bone	3-pbt	119	Failure Load (KN)	Distal radius 20%U.L	Whole-bone	pQCT	H	In-vivo	$vBMC_L$ (mg/cm)	0.82[*1]	<0.01
			Cort.	Comp.	124								0.62[*1]	
			Whole-bone	F.S.	102								0.42[*1]	
		Radius	Whole-bone	3-pbt	119	Failure Load (KN)	Spine, femur and total body	Whole-bone	DXA	H	In-vivo	BMC (mg)	0.60[*2a]	<0.01
			Cort.	Comp.	124								0.50[*2a]	
			Whole-bone	F.S.	102								0.30[*2a]	<0.05
		Radius	Whole-bone	3-pbt	119	Failure Load (KN)	Spine	Cort.	QCT	W	In-vitro	$vBMC_L$ (mg/cm)	0.37[*2b]	<0.01
			Cort.	Comp.	124								0.32[*2b]	
			Whole-bone	F.S.	102								0.30[*2b]	
		Radius	Whole-bone	3-pbt	119	Failure Load (KN)	Calcaneus	Whole-bone	QUA	W	In-vitro	BUA (dB/MHz)	0.30[*2c]	<0.01
			Cort.	Comp.	124								0.36[*2c]	
			Whole-bone	F.S.	102								0.22[*2c]	

Note: Symbols and abbreviations used in the previous tables presented in this chapter are not repeated here.

[1] = site-specific correlations; [2] = non site-specific correlations; [a] = in the study, correlations for spine, femur and total body DXA bone density measurements were determined, however the correlation of only total body measurement is presented in the table as it was higher than that of the spine and femur; [b] = in the study, correlations for both cortical and cancellous QCT bone density measurements were determined, however the correlation of only cortical bone density measurement is presented in the table as it was higher than that of the cancellous bone; [c] = in the study, correlations for both SOS and BUA measurements were determined, however the correlation of only BUA measurement is presented in the table as it was higher than that of SOS; $vBMC_L$ = Bone mineral content (mg/cm), as measured using QCT; U.L = ulna length

Table 3.7   Summary of the Correlational Studies Conducted to Evaluate the Use of Non-Site Specific Bone Density to Estimate the Bone Strength (continued)

Column 1		Column 2					Column 3						Column 4	
		Mechanical Testing (In-vitro)					Indirect Testing						Corr. Coeff.	
Author	Bone Specimen Source	Bone Specimen		Test Specification			Bone Specimen		Measurement Conditions					
		Site	Type	Test	n	Prop. Msrd.	Site	Type	Tech.	T.E.	Meth.	Prop. Msrd.	r^2	P
Cheng et al 1998 [3]	Human cadaver	3rd lumbar vertebral	Whole-bone	Comp.	70	Failure Load (KN)	3rd lumbar vertebral	Whole-bone	DXA	G	In-Vitro	BMD (mg/cm^2)	0.64[1]	<0.01
							Femur neck						0.34[2]	
							Trochanter						0.36[2]	
							Calcaneus						0.18[2]	
		Prox. femur	Whole-bone	Side F.S.		Failure Load (KN)	3rd lumbar vertebral						0.50[2]	
							Femur neck						0.71[1]	
							Trochanter						0.88[1]	
							Calcaneus						0.54[2]	
Lochmuller et al 2002 [4]	Human cadaver	Prox. femur	Whole-bone	Vertical F.S.	105	Failure load (KN)	Femur Neck	Canc.	pQCT	W	In-vitro	vBMC (mg)	0.4[1]	<0.01
							Prox. Femur Shaft						0.45[1]	
							Femoral Shaft	Cort.	pQCT	H	In-vivo	vBMC (mg)	0.35[2]	<0.01
							Distal Femur						0.26[2]	
							Prox. Tibia						0.44[2]	
							Tibia Shaft						0.36[2]	
							Distal Tibia						0.38[2]	
							Radius 4%U.L						0.33[2]	
							Radius 20%U.L						0.33[2]	
							Radius 33%U.L						0.30[2]	
		Prox. femur	Whole-bone	Side F.S.	105	Failure load (KN)	Femur Neck	Canc.	pQCT	W	In-vitro	vBMC (mg)	0.42[1]	<0.01
							Prox. Femur Shaft						0.49[1]	
							Femoral Shaft	Cort.	pQCT	H	In-vivo	vBMC (mg)	0.42[2]	<0.01
							Distal Femur						0.33[2]	
							Prox. Tibia						0.40[2]	
							Tibia Shaft						0.40[2]	
							Distal Tibia						0.40[2]	
							Radius 4%U.L						0.27[2]	
							Radius 20%U.L						0.41[2]	
							Radius 33%U.L						0.34[2]	

Note: Symbols and abbreviations used in the previous tables presented in this chapter are not repeated here.

vBMC = Bone mineral content (mg); H = in-vivo densitometry measurements taken on the human cadaver without removing any tissues or muscles.

3.1.8 Effect of Bone Anisotropy on the Prediction of Bone Strength Using Bone Mineral Density

Review of the Correlational Study Presented in Table 3.8

Bone anisotropy has a major effect on bone mechanical properties and is characterised by the organisation and orientation of the bone architecture in the direction of loading [90, 101-105]. Augat *et al* [90] investigated the effect of anisotropy on human cadaver cancellous bone samples. Calcaneus, proximal femur, distal femur and the spine bone samples were compression tested multi directionally, along the cephalo caudal (CC), anterior posterior (AP) and medial lateral (ML) directions. Various body planes and the testing directions are shown in figure 3.5. It was found that not only the mechanical properties themselves, but also their relationship to the bone density ($_v$BMD), measured in-vitro by the QCT, showed large variations as a function of anatomic location and loading direction. Superior mechanical properties of the bone samples were found in their principle load bearing direction. The mechanical properties correlated better with $_v$BMD at the spine ($r^2 = 0.73$) and the proximal femur ($r^2 = 0.52$) along the CC direction as compared to the other perpendicular directions, i.e., AP and ML, while higher correlations were found for calcaneus ($r^2 = 0.84$) and distal femur ($r^2 = 0.56$) along the AP direction as compared to the other perpendicular directions, i.e., CC and ML. A summary of the above correlational study is presented in table 3.8.

Discussions

Bone is an anisotropic material [101-104, 106] and its mechanical properties take into account the directional dependency of the bone properties, whereas bone density being a scalar entity cannot, i.e., bone density measured at a location gives only an average mineral density over a region of interest (ROI), regardless of the trabecular orientation and density variation within. Hence, bone strength of the locations where anisotropy is rather uniform or less pronounced can be better predicted by bone mineral density [90]. Moreover, mechanical strength of the bone differed at different anatomic sites, thus supporting the use of site specific bone density measurements for a more accurate estimation of bone strength. On the other hand, drilling data would take into

consideration the effect of bone anisotropy would make it a better estimator of bone strength than bone density.

Anterior-Posterior (AP) Axis

Medial-Lateral (ML) Axis

Cephalo-Caudal (CC) Axis

Sagittal Plane

Coronal Plane

Transverse Plane

Body Planes

Coronal Plane (Frontal Plane): A vertical plane running from side to side; divides the body or any of its parts into anterior and posterior portions

Sagittal Plane (Lateral Plane): A vertical plane running from front to back; divides the body or any of its parts into right and left sides.

Traverse Plane (Axial Plane): A horizontal plane; divides the body or any of its parts into upper and lower parts.

Figure 3.5   Planes of the Body and Testing Directions used by Augat *et al* [90]

Table 3.8   Effect of Bone Anisotropy on Bone Strength Prediction

Column 1		Column 2					Column 3						Column 4	
		Mechanical Testing (In-vitro)					Indirect Testing						Corr. Coeff.	
Author	Bone Specimen Source	Bone Specimen		Test Specification			Bone Specimen		Measurement Conditions					
		Site	Type	Test	n	Prop. Msrd.	Site	Type	Tech.	T.E.	Meth.	Prop. Msrd.	r²	P
Augat et al 1998 [90]	Human cadaver	Spine	Canc.	Comp.	28	Compressive Stiffness (MPa)	Spine	Canc.	QCT	W	In-Vitro	vBMD (mg/cm³)	0.73 (CC) 0.53 (AP) 0.33 (ML)	-
		Distal femur			33		Distal femur						0.56 (CC) 0.26 (AP) 0.18 (ML)	
		Prox. femur			29		Prox. femur						0.22 (CC) 0.56 (AP) 0.34 (ML)	
		Calcaneus			7		Calcaneus						0.84 (AP)	

Note: Symbols and abbreviations used in the previous tables presented in this chapter are not repeated here.

AP = mechanical bone property measured along the anterior posterior direction; CC = mechanical bone property measured along the cephalo caudal direction (head-tail); ML = mechanical bone property measured along the medial lateral direction

3.2 USE OF THE SINGH INDEX TO PREDICT BONE STRENGTH AND ITS COMPARISON WITH BONE DENSITY MEASUREMENT TECHNIQUES

Review of the Correlational Studies Presented in Table 3.9

The use of Singh Index to predict the mechanical strength of the cancellous portion of the human proximal femur was investigated by Krischak et al [64] and Wachter et al [107]. They also compared Singh Index with the in-vitro vBMD QCT measurements to investigate which technique is a better predictor of the bone strength. In these studies, proximal femoral bone specimens were harvested from the patients who were

undergoing hip joint replacement surgery and were immediately stored at $-20^{\circ}C$. Krischak *et al* [64] conducted compression tests on proximal femur cancellous bone slice samples of 8 mm thickness, taken at an angle of 45° to the femoral shaft axis and at the centre of femoral head, by indenting a $\phi 4$ mm stainless steel cylinder in the bone specimen at a constant strain rate. Whereas, Wachter *et al* [107] carried out destructive uniaxial compression tests to assess the mechanical property of the proximal femur cancellous bone specimens. As the Singh Index is subjective in nature [64, 107, 108], its mean value as observed by two independent observers was taken for the correlations. $_V$BMD correlated better with the ultimate bone strength ($r = 0.86$; $P<0.0001$ [64] and $r = 0.82$; $P<0.0001$ [107]) as compared to the Singh Index ($r = 0.70$; $P<0.0001$[64] and $r = 0.73$; $P<0.0001$ [107]). Krischak *et al* [64] found higher correlation values as compared to Wachter *et al* [107]. A summary of the above studies is presented in table 3.9.

Discussions

Singh Index is another indirect method of in-vivo bone strength prediction. The following observations can be made from the presented studies in table 3.9:

(i) Average to low correlations were found between the Singh Index and the bone strength [64, 107].

(ii) Proximal femoral bone specimens were harvested from the patients who were undergoing hip joint replacement surgery. This avoids any change in the bone property during the life to death transition phase [44], thus giving more realistic results.

(iii) Bone density was found be a better predictor of bone strength in comparison to the Singh Index [64, 107].

(iv) Krischak *et al* [64] found higher correlation values in contrast to Wachter *et al* [107], this could be because Krischak *et al* [64] used the bone slice as a specimen for mechanical testing, in comparison to Wachter *et al* [107] who harvested a portion of the bone from its parent bone. Using a bone slice confines the neighbouring trabeculae, hence, improving the accuracy of measuring mechanical properties of the bone specimen, thus resulting in a better correlation.

The main advantages of using the Singh Index are that it is inexpensive, quick, less harmful and easy to use. In the studies presented in table 3.9, the Singh Index was determined by two independent observers and the mean value of Singh Index as read by the two observers was used for the correlations [64, 107]. However, information on the inter-observer and intra-observer variability was not given in the study. The inter-observer and intra-observer variability in the Singh Index measurement was investigated using six different observers who independently assessed the radiograph of the fractured proximal femur of patients undergoing treatment [108]. It was observed that the inter-observer variation was large; with only 3 out of 72 radiographs were given the same classification by all six observers and the kappa values ranged from 0.15 to 0.54. The intra-observer variation showed substantial strength of agreement with kappa values ranging from 0.63 to 0.88. As the inter-observer variations are more important than the intra-observer, it was concluded that the Singh Index prediction was highly subjective as it varies largely from observer to observer [64, 107, 108]. In addition, no correlation was found between the Singh Index observed on patients before the fracture treatment, and in-vivo DXA measurements (which is the most commonly used in-vivo method of bone strength prediction in clinics) performed on the patients after the first week of operative treatment, and it was concluded that the Singh Index has no value in assessing the grade of osteoporosis [108].

Therefore, the Singh Index is subjective [64, 107, 108] and should only be used for a rough or first estimation of the mechanical bone strength, provided that the evaluation is performed by an experienced clinician. Furthermore, the Singh Index has been developed only for the proximal femur and it cannot be used for any other anatomic sites.

Table 3.9　**Summary of Various Correlational Studies Conducted to Evaluate the Use of Singh Index in Predicting Bone Strength**

Column 1		Column 2					Column 3						Column 4	
		Mechanical Testing					Indirect Testing						Corr. Coeff.	
	Bone Specimen Source	Bone Specimen		Test Specification			Bone Specimen		Measurement Conditions					
Author		Site	Type	Test	n	Prop. Msrd.	Site	Type	Tech.	T.E.	Meth.	Prop. Msrd.	r^2	P
Krischak et al 1999 [64]	Human patient undergoing hip replacement	Proxi. Femur	Canc.	Indentation destructive compression test	689	US (MPa)	Proxi. Femur	Canc.	QCT	×	In-Vitro	vBMD (mg/cm³)	0.74*	<0.0001
						E (MPa)							0.46*	
					28	US (MPa)	Proxi. Femur	Canc.	Singh Index	-	In-Vivo	Grades 1 to 6	0.49*	
						E (MPa)							0.27*	
		Correlation between QCT (vBMD) and Singh Index (n=28)											0.50*	
Wachter et al 2001 [107]	Human patient undergoing hip replacement	Proxi. Femur	Canc.	Comp.	29	US (MPa)	Proxi. Femur	Canc.	QCT	-	In-Vitro	vBMD (mg/cm³)	0.68*	<0.0001
						E (MPa)							0.54*	
					29	US (MPa)	Proxi. Femur	Canc.	Singh Index	-	In-Vivo	Grades 1 to 6	0.54*	
						E (MPa)							0.44*	<0.0001
		Correlation between QCT (vBMD) and Singh Index (n = 31)											0.53*	

Note: Symbols and abbreviations used in the previous tables presented in this chapter are not repeated here.

3.3　USE OF ULTRASOUND METHODS TO PREDICT BONE STRENGTH AND ITS COMPARISON WITH BONE DENSITY MEASUREMENT TECHNIQUES

Review of the Correlational Studies Presented in Table 3.10

To evaluate the efficacy of ultrasound methods (SOS and BUA), both bone strength and bone density were correlated with the ultrasound measurements in the studies presented below. Lee et al [89] investigated the use of SOS to estimate the bone strength. In-vivo SOS measurements were performed on the human cadaver tibia cortical bone and afterwards a cylinder of cortical bone was removed from the tibia at the site of the SOS scanning. The cylinder specimen was scanned using the pQCT, and was also tested

mechanically under tension. Both SOS ($r^2 = 0.84$; P<0.0001) and pQCT bone density ($r^2 = 0.89$; P<0.0001) correlated well with the Young's modulus. SOS measurements were also correlated with the pQCT bone density ($r^2 = 0.74$; P<0.0001).

The use of ultrasound was further investigated to predict the compressive strength of the bovine femur and tibia bone samples by Toyras *et al* [86, 87]. In these studies, ultrasound in-vitro measurements were also compared with the DXA in-vitro bone density measurements. Correlation coefficients that were found in the investigation are presented in table 3.10. It can be observed from table 3.10 that the ultimate strength of the bone was best predicted by the DXA bone mineral density measurements [86, 87]. These results were also supported by another study conducted on the human cadaver proximal femur and calcaneus bones by Nicholson *et al* [88]. In this study, femoral bone strength was determined by simulating a fall condition onto the greater trochanter and recording the failure loads. Bone strength correlated better with the in-vitro proximal femur neck DXA bone density measurements ($r^2 = 0.88$; P<0.01) as compared to the calcaneal ultrasound measurements (SOS: $r^2 = 0.46$; P<0.01 and BUA: $r^2 = 0.47$; P<0.01).

Toyras *et al* [87] also found that BUA showed no correlation with either Young's modulus, ultimate strength, or in-vitro DXA measurements of the bovine bone samples, but it showed a positive correlation with the human calcaneal in-vivo DXA measurements. The poor correlation of the BUA in bovine bone samples was due to the high bone density (low porosity) of the bovine bones, as compared to the human bones. High density bovine bone samples make a continuous material for the ultrasound propagations which results in the poor performance of the BUA due to the ineffective internal scattering of the ultrasound waves, as suggested by Serpe and Rho [109]. Therefore, BUA is more suitable for quantitative analysis of low density cancellous bones. The effect of bone density or porosity on BUA measurements was further investigated by Toyras *et al* [86] and the relationship found between them is shown in figure 3.6.
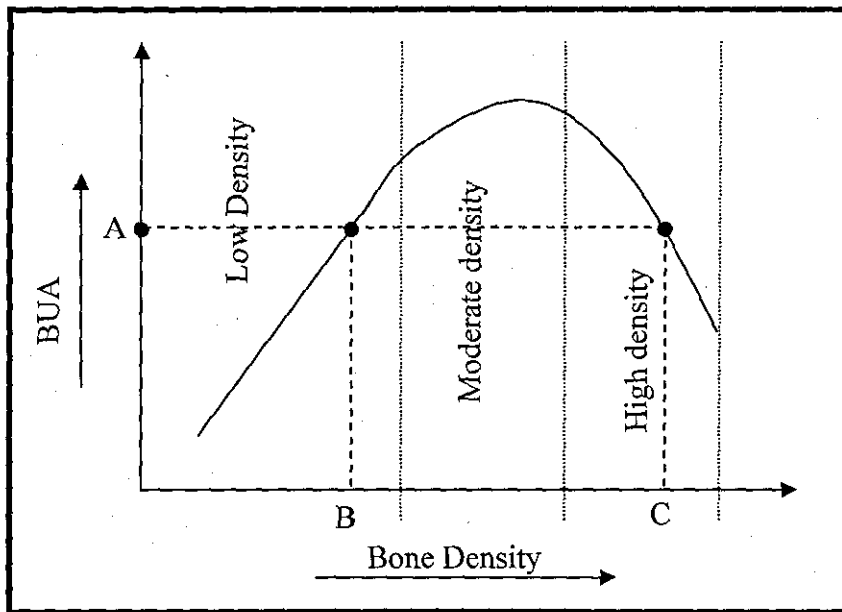
Figure 3.6 Relationship Between BUA and Bone Mineral Density

In addition to the above results Toyras *et al* [87] also found a positive linear correlation of bovine bone thickness with the in-vitro DXA bone density measurements (r = 0.98) and the SOS (r = 0.98) measurements. On the other hand, BUA showed a linear relationship with the bovine bone thickness, only for the thickness of less than 25 mm. For the bone thickness of greater than 25 mm, BUA showed a non-linear relationship and subsequently reached at a constant value for the higher values of the bone thickness. In-vivo results of BUA in human calcaneus were found independent of the heel width, whereas SOS showed a weak and negative correlation. This could be because the BUA value is relatively constant for bone thicknesses greater than 25 mm, and the typical thickness of calcaneus (24-35mm) and heel (>30mm) is above 25 mm.

Chapter 3: Use of Indirect Methods for Bone Strength Prediction

Table 3.10 Summary of Various Correlational Studies Conducted to Evaluate the Use of Ultrasound Methods in Predicting Bone Strength

Column 1		Column 2					Column 3						Column 4	
		Mechanical Testing					Indirect Testing						Corr. Coeff.	
Author	Bone Specimen Source	Bone Specimen		Test Specification			Bone Specimen		Measurement Conditions					
		Site	Type	Test	n	Prop. Msrd.	Site	Type	Tech.	T.E.	Meth.	Prop. Msrd.	r^2	P
Toyras et al 2002 [86]	Bovine cadaver	Femur and tibia	Canc.	Comp.	37	US (MPa)	Femur and tibia	Canc.	DXA	-	In-vitro	BMD_V (mg/cm³)	0.83*	<0.05
						US (MPa)			SOS	-	In-vitro	SOS (m/s)	0.67*	
						US (MPa)			BUA	-	In-vitro	BUA (dB/MHz)	-0.3*	
	Bovine cadaver	Correlation between SOS and DXA (BMD_V) (In-vitro measurements) of bovine femur and tibia (n = 29)											0.79*	<0.05
		Correlation between BUA and DXA (BMD_V) (In-vitro measurements) of bovine femur and tibia (n = 29)											-0.29*	
	Human calcaneal	Correlation between BUA and DXA (BMD) (In-Vivo, low density measurements) (n = 32)											0.72*	<0.01
		Correlation between BUA and DXA (BMD) (In-Vivo, both low and high density measurements) (n = 408)											Non linear	
Lee et al 1997 [89]	Human cadaver	Mid tibia	Cort.	Tensile	11	US (MPa)	Mid tibia	Cort.	SOS	H	In-vivo	SOS (m/s)	0.75	<0.0001
						E (MPa)							0.84	
						US (MPa)			pQCT	W	In-vitro	$_VBMD$ (mg/cm³)	0.80	
						E (MPa)							0.89	
		Correlation between SOS vs pQCT ($_VBMD$) (In-vitro measurements) (n = 24)											0.74	

Note: Symbols and abbreviations used in the previous tables presented in this chapter are not repeated here.

BMD_V = Normalized bone mineral density (mg/cm³) with respect to the bone thickness, measured using either DXA or DPA

- 75 -

Table 3.10 **Summary of Various Correlational Studies Conducted to Evaluate the Use of Ultrasound Methods in Predicting Bone Strength (continued)**

Column 1		Column 2					Column 3						Column 4	
		Mechanical Testing					Indirect Testing						Corr. Coeff.	
Author	Bone Specimen Source	Bone Specimen		Test Specification			Bone Specimen		Measurement Conditions					
		Site	Type	Test	N	Prop. Msrd.	Site	Type	Tech.	T.E.	Meth.	Prop. Msrd.	r²	P
Nicholson et al 1997 [88]	Human cadaver	Prox. femur	Whole-bone	F.S.	64	Failure Load (KN)	Femoral neck	Whole-bone	DXA	G	In-vitro	BMD (mg/cm²)	0.71	<0.01
							Trochanter						0.88	
							Calcaneus	Whole-bone	SOS	W	In-vitro	SOS (m/s)	0.46	
									BUA			BUA (dB/MHz)	0.47	
Toyras et al 1999 [87]	Bovine cadaver	Femur and tibia	Canc.	Comp.	56	US (MPa)	Femur and tibia	Canc.	DXA	-	In-vitro	BMD$_V$ (mg/cm³)	0.73*	<0.05
												BMD (mg/cm²)	0.66*	<0.01
						E (MPa)						BMD$_V$ (mg/cm³)	0.43*	<0.05
												BMD (mg/cm²)	0.34*	<0.05
						US (MPa)	Femur and tibia	Canc.	SOS	-	In-vitro	SOS (m/s)	0.48*	<0.01
						E (MPa)							0.52*	-
						US, E	Femur and tibia	Canc.	BUA	-	In-vitro	BUA (dB/MHz)	No correlation	
	Bovine cadaver	Correlation between SOS and DXA (BMD) (In-vitro measurements) for bovine femur and tibia (n = 47)											0.26*	-
		Correlation between BUA and DXA (BMD) (In-vitro measurements) bovine femur and tibia (n = 47)											No correlation	
	Human calcaneal	Correlation between SOS and DXA (BMD) (In-Vivo measurements) (n = 34)											0.38*	-
		Correlation between BUA and DXA (BMD) (In-Vivo measurements) (n = 34)											0.45*	-

Note: Symbols and abbreviations used in the previous tables presented in this chapter are not repeated here.

Discussions

The following observations can be made from the correlations presented in table 3.10:

(i) SOS showed a moderate correlation (r^2 ranged from 0.46 to 0.84) with the bone strength and bone density (r^2 ranged from 0.79 to 0.26) [86-89].

(ii) Bone strength correlated better with the bone density measurements as compared to the ultrasound measurements (both SOS and BUA) [86-89].

(iii) BUA showed no or poor correlation with the site specific bone strength [86, 87]. On the other hand Nicholson *et al* [88] found a moderate correlation of BUA with the non-site specific bone strength (in this case proximal femur with respect calcaneus); no correlations were determined for the site-specific bone strength measurements.

(iv) When BUA was related to the bone density, it was found that BUA showed a positive linear correlation with lower bone density, non-linear correlation with moderate bone density and negative linear correlation with higher bone density [86]. The relationship of BUA with bone density is plotted in figure 3.6.

The main advantages of using ultrasound techniques are: quick measurement, inexpensive, painless and does not use any potentially harmful radiations [1, 30, 89]. Ultrasound techniques are usually performed at the peripheral bone sites, such as the heel or tibia, where the presence of tissues around the bone is minimal, so as to minimise measurement errors. Ultrasound methods cannot be used accurately to estimate bone strength at the sites which are most likely to fracture due to osteoporosis, i.e., hip and spine because of the presence of a large amount of non homogeneous tissues around the bone. SOS can be used as a predictor of bone strength, but it is not a superior predictor as compared to other densitometry methods [87-89]. BUA showed a non-linear relationship with bone mineral density, as shown in figure 3.6, and no or poor correlation with the bone strength. It can be seen from figure 3.6 that a single value of BUA (e.g., A) could correspond to two different values of bone density (B & C), one low (B) and the other high (C). This could therefore lead to a false prediction of the bone density and bone strength using BUA. However, an aged person suffering from

osteoporosis will always have a low bone mineral density, therefore, a BUA value corresponding to the low bone density can be used to predict its bone strength by neglecting the higher bone density value. Similarly, young people tend to always have a high density value. However, in cases of low bone density in young people, BUA would lead to a completely wrong prediction of bone strength. The use of BUA to predict bone strength was not recommended [86]. Moreover, ultrasound measurements were more accurate only for a bone thickness of less than 25 mm and their accuracy also depends upon the amount of soft tissues present around the bone site [86, 87]. Ultrasound is mostly conducted on human calcaneal because of the small bone specimen thickness and the reduced amounts of soft tissues around it. However, these measurements cannot be effectively used to predict bone strength of other non-specific sites, like femur or spine which are more prone to fracture, as bone strength is site specific.

3.4   CONCLUDING REMARKS

A critical evaluation of the various indirect in-vivo methods and their application to predict bone strength has been presented. The main findings are that bone density could predict bone strength when determined using the standard method of measuring density of material, which measures the bone weight and volume of the water displaced by the bone when it is immersed in the water; however, such method cannot be used in-vivo to measure bone density. Commercially available densitometry techniques on the other hand give a less accurate prediction of bone strength. QCT, pQCT and DXA are the most commonly commercially available densitometry techniques. QCT gives a good prediction of the cancellous bone strength but its use is limited because it is expensive and exposes patients to high radiation. Moreover, all the reported correlational studies, to evaluate the use of QCT, performed only in-vitro measurement of the bone density. Therefore, more studies should be carried out to evaluate the accuracy of QCT when used under in-vivo clinical conditions. pQCT has a limited use as it can only be used at the peripheral bone sites; and DXA bone density measurements when performed in-vivo could lead to an inaccurate or wrong prediction of the bone strength.

It has been found that the variation in bone geometry, use of non-site specific bone density measurement, and bone anisotropy affect the bone strength prediction using the indirect methods. Bone densitometry methods were found to be better predictors of

bone strength as compared to the Singh Index and ultrasound methods. The Singh Index is subjective and its use to predict bone strength was not recommended. Among ultrasound measurements, SOS can be used to predict bone strength, and the use of BUA is not recommended as it can lead to a wrong prediction of bone strength. Moreover, the use of ultrasound methods is limited to the peripheral sites.

Overall, a wide range of correlation coefficient values can be seen for the correlational studies conducted between direct and indirect methods. This is because the distribution of strength and density in the bone varies according to the anatomic location [68, 110-113] and because different methods of sample preservation [29, 44, 76], preparation [75, 77, 111], sample geometry [114, 115], fixation and testing temperature [69] have been adopted. This makes it difficult to compare the results from different studies.

It can be concluded that the various commercial indirect methods which have been evaluated in this chapter are not very accurate, effective and reliable methods for in-vivo bone strength prediction. Furthermore, densitometers from different companies can yield different bone density values, even when the same skeletal site is measured [40, 98]. This makes it more challenging for surgeons or clinicians to compare the bone density results of the same patient if taken using machines from different manufacturers. An ideal method of in-vivo bone strength prediction should be cheap, accurate, easy to use and easy to interpret. This justifies the use of bone drilling data as another method to predict the bone strength, which is proposed in this research. The next chapter presents the background study conducted on bone drilling process.

CHAPTER 4

DRILLING OF BONE

In orthopaedic surgery, the drilling of bone is extensively carried out for the fixation of fractured bones using implants and screws. However, at present no information on bone drilling data like, drilling force, rate of drill bit penetration and rotation speed, etc. is available to surgeons, as drilling is performed manually. In this research, the use of drilling force data to evaluate the strength of bone is investigated. This chapter presents a brief overview of the progress in the area of bone drilling. The overview is divided into four main areas of investigation, (i) an introduction to the drilling process, (ii) bone drilling performance, (iii) prediction of bone drilling force and (iv) the automation of the drilling process.

4.1   INTRODUCTION TO THE DRILLING PROCESS

Drilling is a machining method to produce a hole using drilling bits. There are many different types of drill bits which are used in metal machining, such as spade drills, core drills, split point drills, etc. The most commonly used drill bit is the twist drill. Most surgical drill bits use the general geometry of twist drills. The general specifications of a twist drill bit are detailed in figure 4.1. The point angle is the angle at the tip of the drill bit. Most surgical drill bits have a point angle of 90° and industrial drill bits have a point angle of approximately 118°. There are two main cutting edges joined by a straight edge called the chisel edge. The thickness between the two cutting edges is termed as the web thickness. The helix angle gives a measure of the flutes twist.
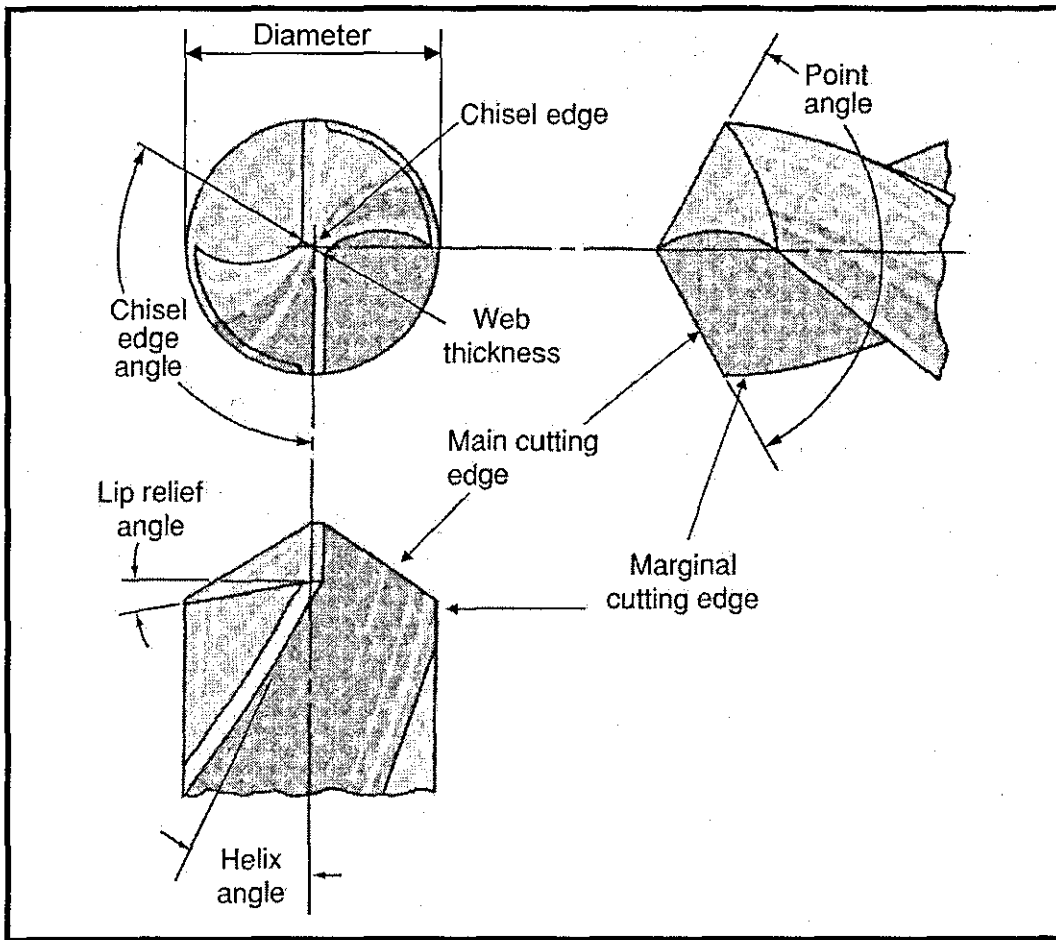
Figure 4.1 General Twist Drill Specifications [116]

Although most of the literature describes the process of drilling in metals, the basic function can be expanded to any material. Cutting is performed by the straight edges (lips) of the drill bit and the chisel edge at the tip. Chips produced by the cutting process travel along the flutes of the drill bit. The cutting edges are curved and the cutting mechanics are known to change dramatically along the cutting edge. The tip of the drill bit (the chisel edge) does not cut but rather indents and pushes the material out to the cutting edges [117-119]. The web thickness is necessary to protect the drill bit point and stiffen the drill bit [120]. The action of the chisel edge can be considered much like a hardness test and is responsible for a large portion of the drilling force [117, 121]. Shaw and Oxford (1957) [121] found that up to 77% of the total drilling force was due to the web thickness (based on a ratio of chisel length over diameter of 0.36 which is similar to those seen in the surgical and industrial twist drill bits). Williams (1974) [118] also found that the chisel edge contributes towards 60% of the total drilling force. It has even been shown to be responsible for up to 70% of the drilling force in bones

[119]. Therefore, this shows that the chisel edge is of a significant importance when calculating drilling forces. The complexity of drill bit geometry comes from the fact that the rake angle (the angle between the cutting edge and the material) changes along the radius of the drill bit. A positive rake angle promotes easy chip removal. Whereas a negative rake angle pushes the chip back into the material, inhibiting chip flow. Therefore, due to the complex drill bit geometry and cutting mechanism, deriving an equation to predict drilling force is very complicated. Most models to predict drilling force have been developed empirically and apply only to the drill bits and materials used in the experiment used to develop the model.

4.2 BONE DRILLING PERFORMANCE

Various studies have been carried out to study and optimise the bone drilling performance based on measurable parameters such as, drilling force, drilling torque, rotational speed, feed rate, temperature and accuracy of the drilled hole. Based on these parameters different drill bit shapes and drilling conditions were investigated in order to provide recommendations for the drill bit design and drilling instrument.

Jacob and Berry (1976) [19] studied drill bits of seven different shapes and geometries to investigate the effect of drilling speed on drilling force and drilling torque for a constant feed rate. The study was carried out on a mature bovine tibia mid-shaft under constant lubrication. Out of the seven drill bits investigated, five were standard available surgical drill bits (Q, O, X, T, Y type) and two were non-standard drill bits (M and F type), as shown in figure 4.2. The following observations were made in the study:

- Both drilling force and drilling torque decrease with an increase in the cutting speed,
- Q-type drill bit (point angle 110° and helix angle of 24°) was found to be the best drill bit and produced the lowest cutting force and cutting torque,
- Q-type drill bit showed a significantly lower thermal effect, while O-type bit suffered severe heating effect which was indicated by boiling of the coolant used,
- It was also recommended that a surgical drill bit should have a rake angle ranging from 25° to 30°.
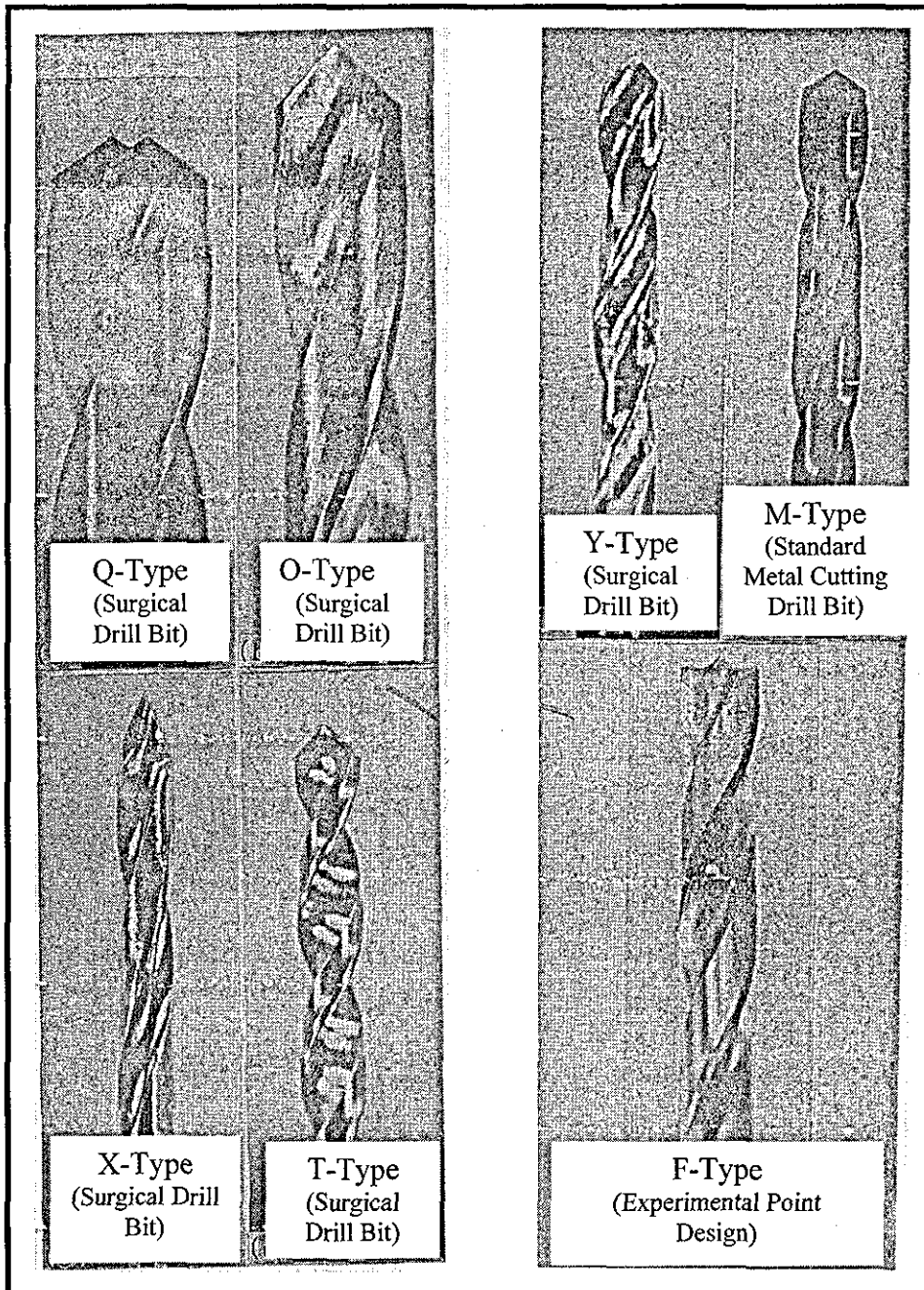
Figure 4.2 Drill Bits Used For Comparison [122]

In another study by Wiggins and Malkin (1976) [20], drilling performance was evaluated by measuring feed rate, drilling torque and specific energy at a constant drilling force. The experiments were carried out on a human cadaveric male femur using three different types of drill bit. The following observations were made in the study:

- At higher feed rates, less energy is required to drill, thus less thermal damage should occur at higher feed rates as the temperature generated is directly related to the energy expended,

- The flutes of twist drill bits may tend to clog when the depth of the drilled hole becomes appreciable compared to its diameter, thus leading to a substantial increase in torque and specific cutting energy,

- The drilling performance under constant drilling force was found to be independent of the rotational speed, implying that the performance depended primarily on the drill bit geometry.

In the above two studies by Jacob & Berry and Wiggins & Malkin, either the feed rate [19] or drilling force [20] was kept constant to study the effect of other drilling parameters on the performance of bone drilling. However, none of the two conditions represent the actual clinical condition were drilling is performed manually. Hobkirk and Rusiniak (1977) [18] conducted experiments which represented actual clinical conditions. In the study, the drilling force exerted by surgeons during manual drilling (feed rate not constant) of bone was investigated. Twenty operators (dentists experienced in surgical preparation) used six different drill bits at high and low speeds to prepare standardized holes and slots in the angle of bovine mandible. Each operator drilled a hole (10mm deep) and cut a slot (6mm deep and 6mm long) with each drill bit or bur at two cutting speeds. Three categories of operator were found. The A operator, varied the drilling force rapidly while preparing the bone; operator B, maintained a relatively constant drilling force for a somewhat longer period and operator C, exerted relatively higher drilling forces for short periods.

Saha and Albright (1982) [119] optimised the design of drill bit for the effective removal of bone chips and to minimize the drilling force and temperature. The performance optimised drill bit was compared with other surgical drill bits for drilling into bovine bones. It was found that the new design decreased the drilling force by 45% and peak temperature rise by 41%. The walking on the bone was eliminated and dimensional tolerance of the size of drilled hole was also improved. Overall the

proposed design reduced the tissue damage and surgery time. They also found that the chisel edge was the main contributor to the drilling force.

The accuracy and quality of the hole drilled into the bone is important for a good fracture fixation using screws. Robinson *et al* (1992) [123] investigated the effect of drill bit guide length and drilling method on accuracy of the diameter of drilled holes. They drilled 225 holes in fresh porcine mandibles and drill diameter was measured with a micrometer (accuracy of 0.005mm). Holes were drilled using long guides, short guides and without any guides, with a drill press, a pneumatic drilling machine and a manual drilling machine. A drill bit of 2 mm diameter was used in the study and it was changed after drilling 15 holes. The drill press was found to be the most accurate method of drilling followed by the pneumatic drill and then manual drill. In the case of using drill bit guides, drilling without using any drill bit guide was found to be the most accurate method followed by using the short length drill bit guide and then the long length drill guide. However, they did not consider the drill bit length during their investigation for example, they used short drill bits when using no guide.

4.3 PREDICTION OF BONE DRILLING FORCE

Metal is homogeneous in nature; therefore drilling force models that have been established for metals are presented initially in this section. These are followed by models developed for bone drilling.

4.3.1 Drilling Force Estimation Models - For Metals

The thrust force required to drill a material is generally derived by close examination of the mechanics of drilling. The various forces acting on a drill bit during drilling are shown in figure 4.3 and are defined as [117]:

F_v = the resultant force of resistance to cutting at each point of the lip which can be resolved into three components, F_1, F_z and F_h acting in a direction mutually perpendicular to each other,

F_z = force acting on both lips which counterbalances each other,

F_1 = force acting in the vertically upward direction which impedes the penetration of drill bit into the specimen,

F_h = force acting on cutting edges which produces the drilling torque and

F_2 = force acting on the chisel edge along the drill axis.

In addition to the above forces, there are frictional forces (F_f) due to the chip flow.
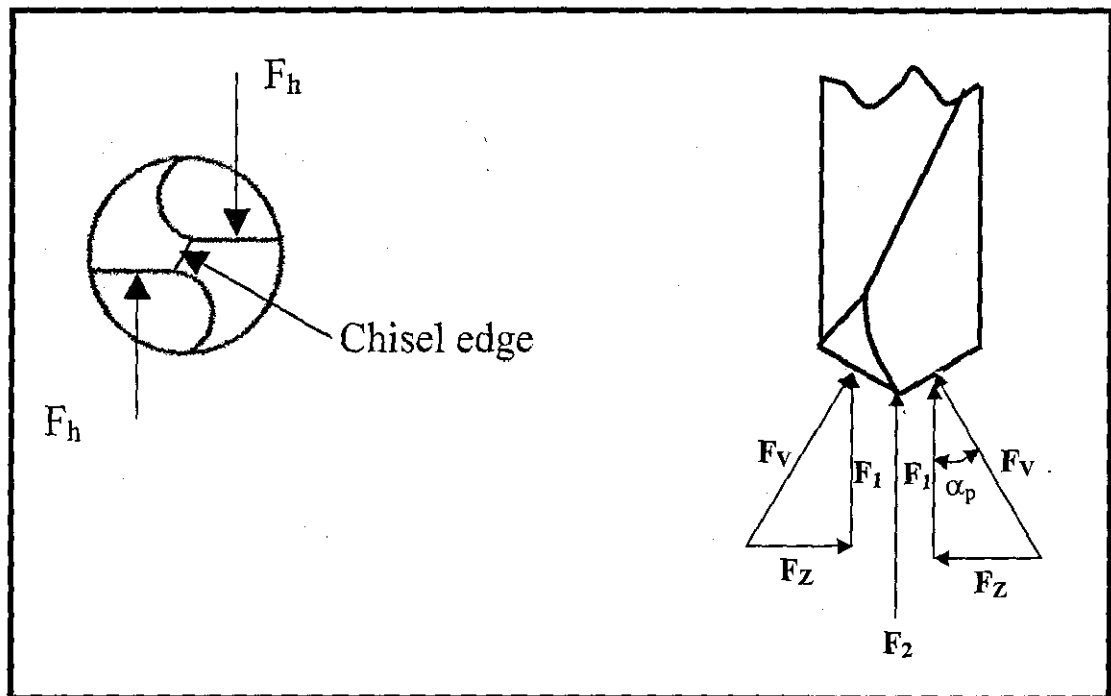
Figure 4.3 Forces Acting on a Drill Bit during Drilling [117]

In order for the drill bit to penetrate into the specimen, the drilling force (F_d) applied to the drill bit must overcome the sum of the resistance forces acting along the drill axis. Thus,

$$F_d = 2F_1 + F_2 + F_f \qquad (4.1)$$

It was found experimentally that the force F_1 developed on the lips is approximately 40 percent of the total drilling force (F_d), the force F_2 developed on the chisel edge is

approximately about 57 percent and the friction force F_f is about 3 percent approximately. This shows that the contribution of the friction force to the total drilling force is very small and therefore can be ignored to simplify equation 4.1. Hence,

$$F_d \cong 2F_1 + F_2 \text{ (ignoring the effect of friction)} \qquad (4.2)$$

In order to calculate the drilling force, an expression for F_1 and F_2 should be known. Early work in metal by Cook (1966) [117] provided the equations to calculate F_1 and F_2 as:

$$2F_1 = 2k \times \left(\frac{D_d}{2}\right) \times \left(\frac{f'_{Drill}}{2}\right) \times \frac{F_v}{F_h} \times \cos\alpha_p \qquad (4.3)$$

$$F_2 = (\%area)\frac{\pi(d')^2}{4} H_B \qquad (4.4)$$

where, α_p = angle of cutting edge (degree),

   D_d = drill bit diameter (mm),

   f'_{Drill} = drilling feed rate (mm/rev),

   d' = web thickness (mm),

   H_B = Brinell hardness of the material (N/mm^2),

   %area = percentage contacting area of the chisel edge,

   k = total energy required to cut per unit volume (Joules/mm^3 or N/mm^2)

The cutting edge angle (α_p) can be calculated as,

$$\alpha_p = 90 - \psi \qquad (4.5)$$

where, 2ψ = drill bit point angle

Taking into consideration the change of rake angle over the diameter, F_v/F_h is typically between 10 and 20 percent [117]. It is difficult to calculate the exact value of F_2 because it is not easy to estimate the portion of the chisel edge zone that is actually in contact with the metal. This portion will vary when the ratio of feed to cutting speed varies. Roughly the percentage area contacting the chisel edge is between 10 and 20 percent of

the area of a circle of diameter equal to the web thickness inscribed within the drill bit web [117].

In the drilling force prediction model presented by Cook (1966) [117] in equations 4.3 and 4.4, there remains one main parameter that is difficult to determine and yet it is critical for the prediction of drilling force. That parameter is the energy required to remove one unit volume of material, known as the specific energy (k).

Shaw and Oxford (1957) [121] state that the specific cutting energy is very much like the Brinell Hardness measure. In fact the specific cutting energy and the Brinell hardness are proportional to one another over a small range in metals [121]. They have also listed a set of guidelines to be used in estimating the specific energy. These are:

- The material strength and structure are of primary importance,
- Increasing the rake angle causes a decrease in k,
- Cutting speed (rotational speed of the drill bit), depth of cut and clearance angles have a negligible effect on k,
- A decrease in friction between the chip and tool will decrease k,
- Dulling of the tool will increase k.

Specific cutting energy is measured in pressure or stress units (N/mm^2). Shaw and Oxford (1957) [121] also presented equations to estimate k, but they contain constants that were experimentally determined for metals only. Another way to estimate the specific cutting energy is to calculate it from the torque on drill bit using equation 5.6 given below:

$$k = \frac{8\,T_d}{f'_{Drill}\,D_d^2}$$

(4.6)

where, T_d = drilling torque (N.mm),

The drilling torque can be measured by either monitoring the current output of the DC drilling motor or by using a strain gauge sensor.

The above equations 4.3 and 4.4 present the general relationship for the drilling force. Further work was carried out by other researchers by developing equations that take into

consideration the rake angle and its changes along the cutting edge, one such model was presented by Mauch and Lauderbaugh (1990) [124]. In their model, the drill bit was divided into three different zones with three different metal cutting models. The drilling process has two motions; feed and rotation, which complicates the absolute motion that the drill bit experiences at any point along its cutting edge. At the outer edge of the drill bit, the effect of feed is negligible when compared with the rotation component. However, at the centre of the drill, feed is the primary component. For this reason the model of drill bit was separated into three distinct zones which are shown in figure 4.4. Zone 1 was defined as the part of chisel edge of the drill that is between the centre of the edge and the transition point A (as shown in figure 4.4 (A)). As stated above, for this part of the drill, the feed becomes the prominent motion. Therefore, zone 1 was modelled as an indentation of a rigid wedge (as shown in figure 4.4 (B)). The drilling force for the zone 1 (F_{z1}) was found using the equation below:

$$F_{z1} = 2\ F_L\ R_a \tag{4.7}$$

where, F_L = force per unit length (N/mm), was calculated using equation 4.8 and

R_a = distance from the centre of the drill to the transition point A or radius of zone 1, given by equation 4.12.

$$F_L = 2\ p_d\ L_d\ \sin(\psi) \tag{4.8}$$

where, p_d = pressure exerted by the drill bit (N/mm^2), found using equation 4.9

L_d = contact length as shown in figure 4.4 (B), calculated using equation 4.10.

2ψ = drill bit point angle (radians)

$$p_d = 2\ \sigma_{sy}\ (1 + \varepsilon) \tag{4.9}$$

where, σ_{sy} = yield shear stress of the material (N/mm^2) and

ε = angle (radians) as shown in figure 4.4 (B), which can be calculated using equation 4.11.

Contact length L_d can be found by:

$$L_d = \frac{h}{[\cos\psi - \sin(\psi - \varepsilon)]} \tag{4.10}$$

where,   h = depth of drill bit indentation (mm)

The angle ε was calculated using the equation given below,

$$2\psi = \varepsilon + \cos^{-1}\left[\tan\left(\frac{\pi}{4} - \frac{\varepsilon}{2}\right)\right]$$

(4.11)

The radius of zone 1 (R_a) was calculated using the equation given below,

$$\tan\alpha_p = \frac{f'_{Drill}}{2R_a}$$

(4.12)

where, α_p = cutting edge angle (radians)

f'_{Drill} = feed rate of the drill bit (mm/rev)

Zone 2, as shown in figure 4.4(A), was defined as the chisel edge region that is between the transition point A and the outer edge of the chisel region. This portion of the chisel edge was modelled with orthogonal cutting theory. The orthogonal rake angle (γ)was found from the equation given below:

$$\gamma = -1 \times \left[\tan^{-1}\left[\tan(\psi)\cos(\pi - \varphi)\right]\right]$$

(4.13)

where, γ = orthogonal rake angle (radians)

φ = chisel edge angle (radians)

The rake angle γ is constant for the chisel edge. However, clearance angle α_c varies depending upon the angle between the chisel edge and work piece. In order to calculate forces acting along this portion of the chisel edge, the zone 2 was divided into five elements. The angle α_c was found for the centre of each element and the dynamic rake angle (γ_d) was calculated based on α_c and was held constant over the element.

$$\gamma_{di} = \gamma + \alpha_{ci}$$

(4.14)

where, α_{ci} = clearance angle (in radians) calculated using equation 4.15.

Zone 3: Lip Region of the Drill

Chisel Edge

Zone 1: Chisel Edge Region From Centre of the Chisel Edge to the Transition Point A

Transition Point A: Point Dividing Zone 1 and Zone 2

Zone 3: Lip Region of the Drill

Zone 2: Chisel Edge Region between the Transition Point A and the Outer Edge of the Chisel Region
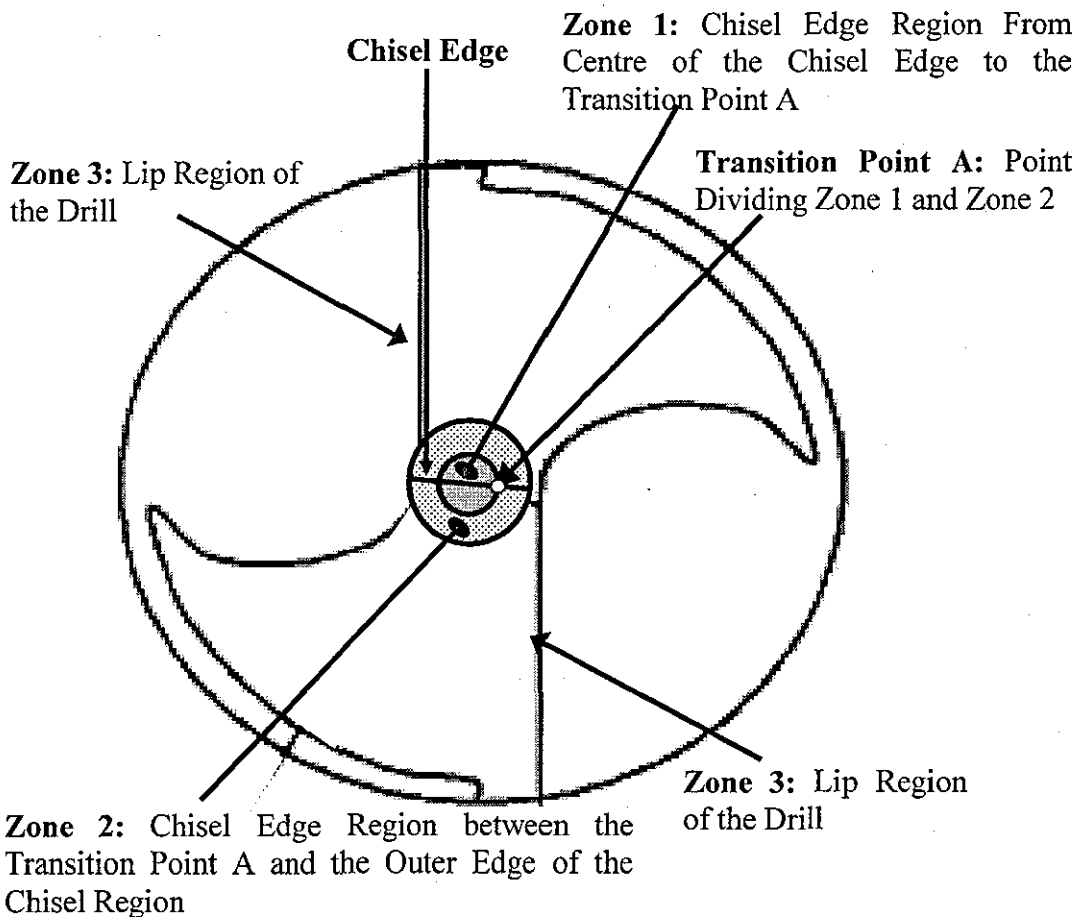
(A)   Model of Drill Bit Showing Three Distinct Zones in Drilling Model of Metal Cutting

Drill Bit

$AB = AC = L_d =$ **Contact Length**

2ψ

A

C

h

B

Specimen

ε
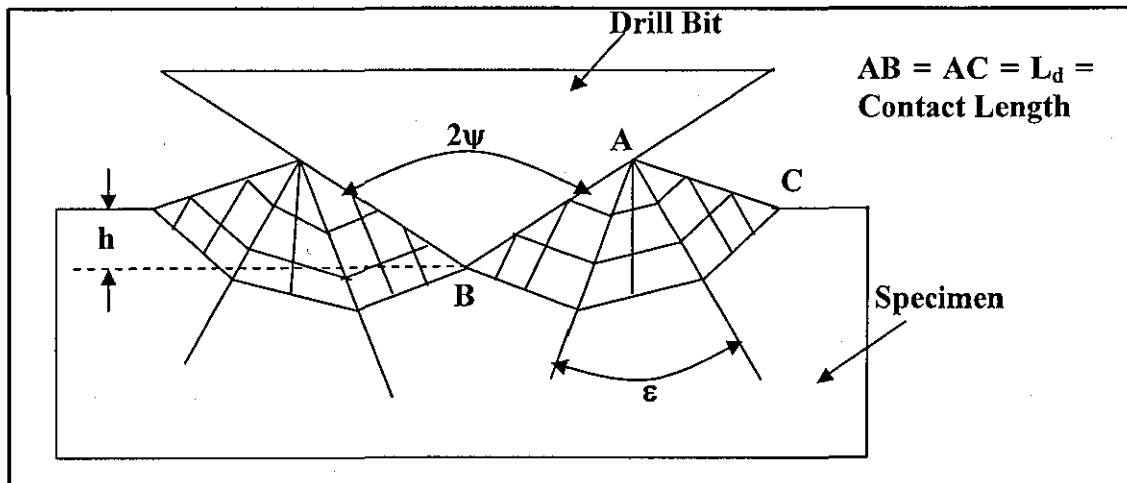
(B)   Indentation Model in Zone 1 of the Drilling Model

Figure 4.4   Schematic of the Tip of a Drill Bit Showing Three Zones of Metal Cutting in the Drilling Model [124]

$$\alpha_{ci} = \tan^{-1}\left[\frac{f_{Drill}}{2\pi R_{Ci}}\right] \tag{4.15}$$

where, R_{Ci} = distance (in mm) from the centre of the drill bit to the centre of each element for i = 1 to 5

$$R_{Ci} = R_a + b * i \qquad \text{(for i = 1 to 5)} \tag{4.16}$$

where   b = width of chisel edge cutting element (mm)

$$b = \frac{1}{5}\left(\frac{L_c}{2} - R_a\right) \tag{4.17}$$

where, L_c = length of chisel edge (mm)

From the Merchant's formula [125], the shear angle (ϕ_s) for metal cutting can be written as:

$$\phi_{si} = \pi/4 - (\beta_d - \gamma_{di}) / 2 \tag{4.18}$$

where $\beta_d = \tan^{-1}\mu \tag{4.19}$

μ = coefficient of friction between the drill bit and metal.

The drilling force for each element in zone 2 was given as:

$$F_{z2i} = \frac{f_{Drill}\, b\, \sigma_{sy}\, \sin(\beta_d - \gamma_{di})}{2 \times \sin(\phi_{si})\cos(\phi_{si} + \beta_d - \gamma_{di})} \tag{4.20}$$

The total drilling force in zone 2 was given as:

$$F_{z2} = \sum_{i=1}^{5} F_{z2i} \tag{4.21}$$

Zone 3 was defined as the lip region of the drill. The modelling of this region is complicated because three-dimensional geometric analysis is required to calculate the cutting rake angle. Two-dimensional oblique metal cutting theory was applied by dividing the region into N oblique cutting elements. The total drilling force in zone 3 was given by:

$$F_{z3} = \sum_{i=1}^{N} \frac{\sigma_{sy} b_1 t_{lip}}{\sin\phi_{ni} \cos(\psi_d)} \left[\frac{\sin(\beta_{ni} - \alpha_{ni})}{\left\{ \cos^2(\phi_{ni} + \beta_{ni} - \alpha_{ni}) + \tan^2(\eta_{ci}) \sin^2(\beta_{ni}) \right\}^{1/2}} \right] \qquad (4.22)$$

The expressions for all the symbols used in equation 4.22 are given below:

b_1 is the width of the lip region cutting elements and is given by

$$b_1 = \frac{\left[(R^2 - w_I^2)^{\frac{1}{2}} - (R_o^2 - w_I^2)^{\frac{1}{2}} \right]}{N \sin\psi} \qquad (4.23)$$

where R = radius of drill bit (mm)

               w_1 = half web thickness (mm)

               N = number of oblique cutting elements and

               R_o = half length of chisel edge (mm)

$$t_{lip} = \frac{f'_{Drill} \times \sin\alpha_p}{2} \qquad (4.24)$$

The oblique rake angle (α_{ni}) was calculated from,

$$\tan\alpha_{ni} = \frac{\tan\delta_{di}}{\sin\psi} \left[\cos(w_i) + \sin(w_i)\tan(w_i)\cos^2(\psi) \right] - \tan(w_i)\cos(\psi) \qquad (4.25)$$

$$\delta_{di} = 2\pi r(i) / L_h \quad (i = 1 \text{ to } N) \qquad (4.26)$$

$$L_h = \pi D_d / \tan(\delta_a) \qquad (4.27)$$

where δ_a is the helix angle of the drill bit.

$$w_i = \sin^{-1}\left(\frac{w_1}{r(i)}\right) \tag{4.28}$$

$$\sin\psi_d = \sin(\beta_d)\sin\psi \tag{4.29}$$

$$\tan\eta_{ci} = \tan(\psi_d)\cos(\alpha_{ni}) \tag{4.30}$$

$$\beta_{ni} = \tan^{-1}\{\tan(\beta_d)\cos(\eta_{ci})\} \tag{4.31}$$

$$\phi_{ni} = \tan^{-1}\left[\frac{1}{1-\tan\alpha_{ni}}\right] - \beta_{ni} \tag{4.32}$$

$$r(i) = \left\{\left[\left(R^2 - w_1^2\right)^{\frac{1}{2}} - \left(R_o^2 - w_1^2\right)^{\frac{1}{2}}\left(\frac{i-\frac{1}{2}}{N}\right)\right]^2 + w_1^2\right\}^{\frac{1}{2}} \tag{4.33}$$

The total drilling force is the addition of drilling forces in zone 1, 2 and 3, given by equations 4.7, 4.21 and 4.22, respectively.

Chandrasekharan et al (1995) [126] and Langella et al (2005) [127] presented another mode to predict the drilling force by applying oblique cutting theories and considering the change in rake angle along the cutting edge and the chisel edge. The model by Chandrasekharan et al (1995) [126] showed good drilling force predictability but required five tests with a conical drill point to be done in order to calibrate the model. This model was improved by Langella et al (2005) [127] who simplified the calibration to two tests. Langella et al (2005) [127] model is presented in equations 4.34 and 4.35.

$$F_{exp} = k_L \cdot 2\left(\frac{f'_{Drill}}{2}\right)G' \tag{4.34}$$

where F_{exp} = drilling force measured experimentally (N),

            k_L = specific energy based on Langella's model (N/mm^2),

            G' = geometric parameter (mm), defined by equation 4.35,

$$G' = \frac{\sin(\psi)(1-\tau)\left(2\tau R^2 - w_1^2 \sin(\psi)\right)}{2\tau R} \qquad (4.35)$$

where $\quad \tau = \dfrac{w_1}{R \sin\varphi}$,

Another formulation for the estimation of the drilling force was presented by Somerton (1959) [128]. In an investigation of sandstone, concrete and shale, he developed a general parameter to explain differences in the drillability of a specific material. He plotted two dimensionless groups $\dfrac{f_{Drill}}{\omega \cdot D}$ and $\dfrac{F_d}{D_d^2 \sigma_s}$ on a log-log graph for each material, where f_{Drill} is the feed rate (in mm/min), ω is the rpm of the drill, D_d is the diameter of the drill bit, F_d is the drilling force and σ_s is the strength of the material. Each material (i.e., concrete, sandstone, etc.) had a separate but parallel line (Figure 4.5 (A)). A value was added to the σ_s to force the line through zero, thus creating a set of coincident lines (Figure 4.5(B)). The value required to make the shift was termed drilling strength (σ_D) and defined as the ratio of energy input to volume of material broken.

In summary, all the models developed for metals require a value for either the specific energy or the Brinell hardness or friction coefficient that will need to be determined experimentally for bone when applying these equations in bone drilling.
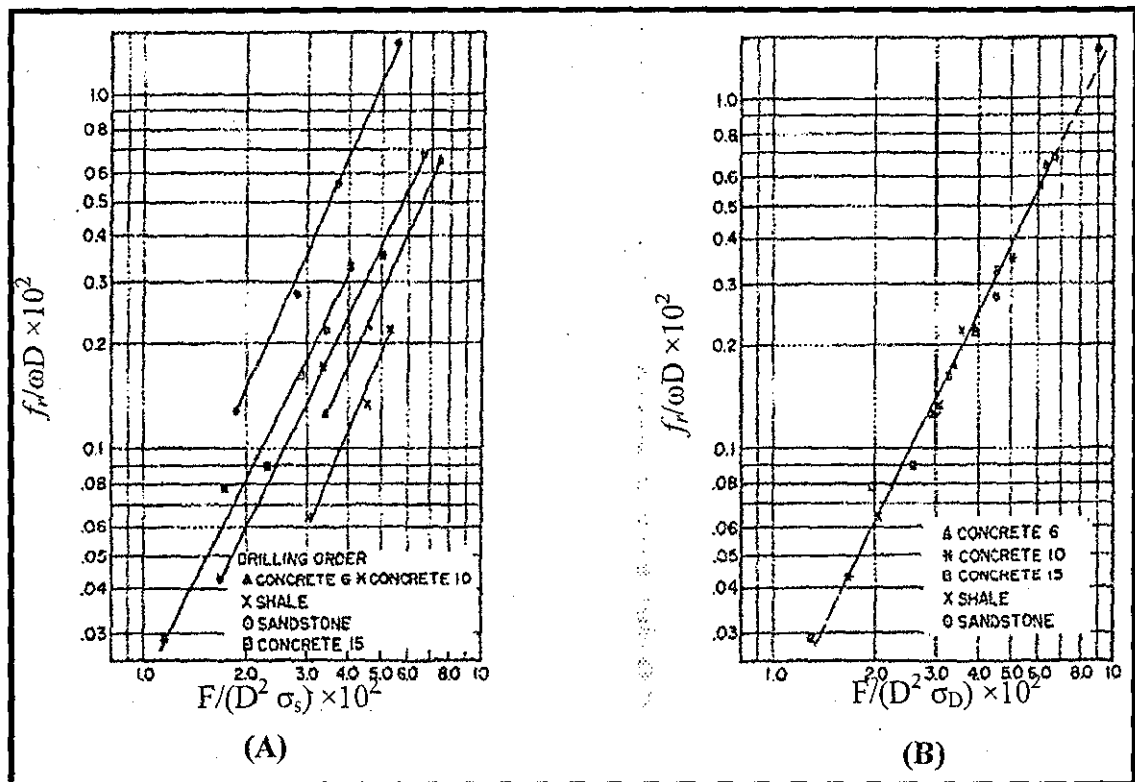
Figure 4.5 Calculating Drilling Strength For Concrete, Shale And Sandstone, (A) Parallel Lines for Each Material, (B) Using σ_D to Force Each Line Through Zero (Somerton, 1959) [128]

4.3.2 Drilling Force Estimation Models - For Bones

The drilling models developed for metals have been applied to bone drilling to estimate the bone drilling force. In order to apply machining theory of metals to bone, an assumption was made that bone behaves like metal when it is machined. This assumption can be supported based on the findings of Jacob *et al* [19] and Wiggins *et al* [20] who found that the chips, when observed microscopically, were formed because of the shearing of the bone material during drilling, which resembles the chip formation in metal drilling.

Significantly less is known about bone in comparison to metals. In 1976, two separate researchers published the initial work on bone drilling. Jacob *et al* (1976) [19] investigated drilling force and drilling torque versus drill bit rotational speed on samples from the mid-diaphysis of bovine tibia. Using equations presented by Cook (1966) [117] for a single edge cutting of metals, Jacob *et al* presented a theoretical analysis of

the drilling force and compared it with experimental data. The theoretical analysis was based on equation 4.36 given below,

$$F_d = k \times \left(\frac{D_d}{2}\right) \times \left(\frac{f'_{Drill}}{2}\right) \qquad (4.36)$$

where $k = 1.5 \times strain \times \sigma_s$ (4.37)

Equation 4.36 calculates the drill bit cutting force which is the same formulation that was derived for metals by Cook (1966) [117] (as given in equation 4.3). In the cutting force equation 4.36, the effect of the chisel edge has been ignored. The shear stress value was obtained from the earlier work in orthogonal cutting (conducted by Jacobs *et al* (1974) [122]). They were unable to obtain a good correlation between the theoretical and experimental drilling force data. The main reason for the poor correlation was because they ignored the effect of chisel edge which is the main contributor (up to 70%) to the drilling force [118, 119, 127]. In general, in bone drilling literature the effect of the chisel edge has largely been ignored.

Wiggins and Malkin (1976) [20] extend their own work done on orthogonal machining of bone to drilling. Using several different drill bit geometries, they measured feed rate, drilling force and drilling torque, while drilling through compact bones of the human femur. The experimental data was plotted and regression analysis was performed for the variables involved in drilling.

Allotta *et al* (1996) [129] proposed a model given below for calculating the drilling force;

$$F_d = k \, f'_{Drill} \, \frac{D_d}{2} \sin \psi \qquad (4.38)$$

where F_d is the drilling force (N), k is the specific energy (N/mm^2), f_{Drill} is the drill feed rate (mm/rev), D_d is the diameter of the drill bit (mm) and 2ψ is the point angle of the drill bit (degree). To estimate k, Allotta *et al* (1996) [129] stated that it is equivalent to five times the ultimate tensile load, which is not supported in the literature. In addition, the above equation neglects drilling force due to the chisel edge, which have been reported to be around 70% of the total drilling force [119]. In summary, they present

only preliminary research and additional information is required to implement the proposed equations.

Karalis and Galanos (1982) [130] applied the theory of rock mechanics and formulation of Somerton (1959) [128] in bone drilling, which resulted in equation 4.39.

$$\frac{f_{Drill}}{\omega \cdot C \cdot D_d} = \left(\frac{F_d}{D_d^2 \sigma_D} \right)^2 \qquad (4.39)$$

Where f_{Drill} is the feed rate (mm/min), ω is the rotational speed of the drill bit (rev/min), C is a material constant and σ_D is the drilling strength (N/mm^2). An experimental study of the bone drilling was conducted to investigate the interrelationship between drilling rates, drilling strength (defined as the ratio of energy input to volume of bone broken), triaxial strength and hardness of the bone. Human cadaver cancellous bone of the femur head and cortical bone of the tibia shaft were used to carry out drilling experiments. The drill bits used were the Q-type recommended by Jacob and Berry [19], with drilling speeds in the range of 1200-1380 rpm at a constant applied force. The regression coefficients found were very low ($r^2 = 0.23$), so the validity of the formulation is not entirely convincing.

Chagneau and Levasseur (1992) [22] proposed a technique called dynamostratigraphy for the mechanical testing of bone. In this technique, the drilling force and the drilling torque is continuously measured along the drill depth at constant rotational speed and feed rate, as shown in figure 4.6. A continuous measurement is useful in finding the density variation, change of structure and property of bone along the drilling length. It is suitable for the study of laminated materials or heterogeneous materials like, cancellous bone. They applied dynamostratigraphy to study the morphology of bone structure and mechanical resistance of head of human cadaver femur bone using a 4.0 mm diameter three-lipped drill bit. The mechanical resistance of bone depends on the density, state of hydration, structure, material property and mineral content of the bone. To compare the mechanical resistance of bone, the hardness testing of the right side femoral head was conducted and the left side was used for dynamostratigraphy. The drill bit rotational speed and the feed rate were fixed at 350 rpm and 10 mm/min, respectively. The results

from dynamostratigraphy showed clear changes in the resistance of the cancellous bone across the femoral head at different drilling trajectories. When compared to results from drilling test, higher forces were obtained by punching. Correlation between punching and drilling forces and a theoretical model to estimate the drilling force was not presented.
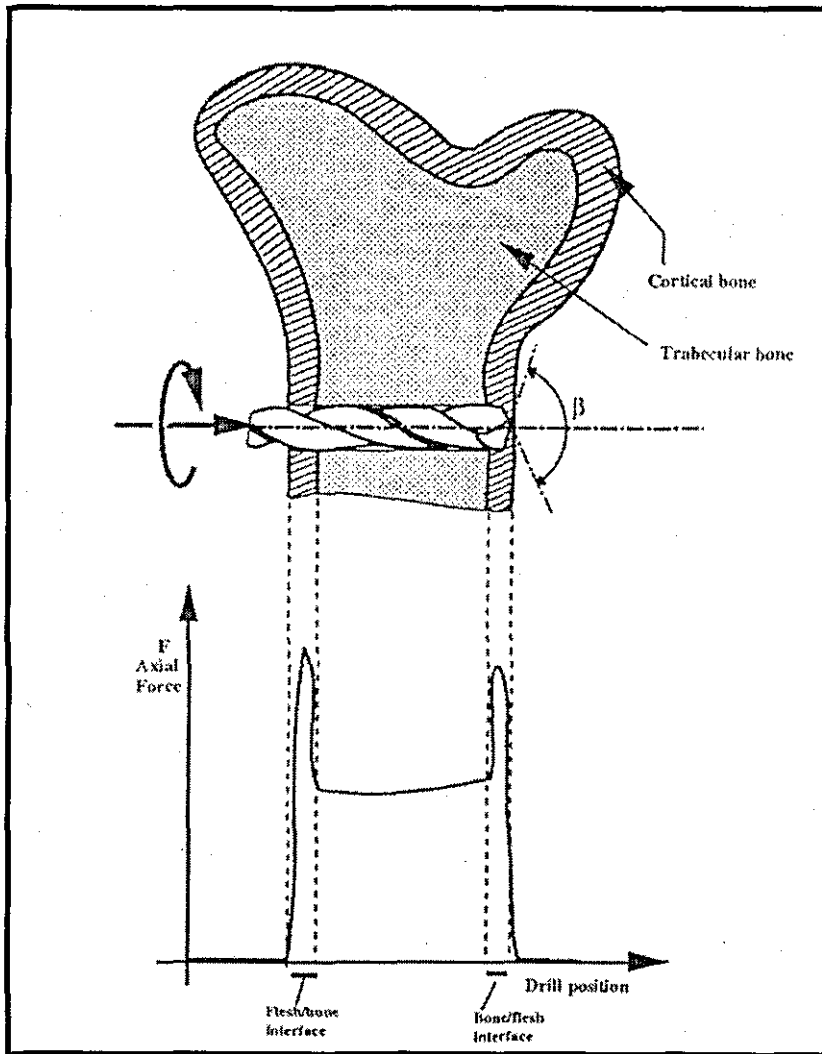
Figure 4.6   Testing of Bone Using Dynamostratigraphy [129]

Ong and Bouazza-Marouf (2000) [23] investigated the relationship between the drilling force and bone mineral density in porcine femurs. Their purpose was to determine if drilling force measurements could be used to estimate the strength of bone. Bone mineral density was obtained by dual X-ray absorptiometry (DXA), which provided an average bone mineral density value over the thickness of the object, in a specified two-

dimensional grid. Drilling was done parallel to the DXA scanning direction in the greater trochanter and the femoral head regions and perpendicular to the DXA scan along the cervical axis (figure 4.7). They found a good correlation ($r^2 = 0.85$) in the greater trochanter region but only an average correlation ($r^2 = 0.51$) in the femoral head region in the holes that were aligned with the DXA scanning direction. However, when the drill holes were perpendicular to the scanning direction, the correlations found were not as good. This could be due to the fact that they used a two dimensional measurement, essentially collecting a bone mineral density for the entire cross section of the bone. However, the drilling trajectory only goes through a small portion of that cross section and thus there is a bone mineral content that is averaged into the bone mineral density that has no effect on the drilling force. Using a three-dimensional bone mineral density measurement such as those from quantitative computed tomography (QCT), would enable better matching between the drilling force and the bone mineral density of the drilled bone. They further stated that the analysis of bone drilling forces had the potential to provide useful information about the strength of bone.
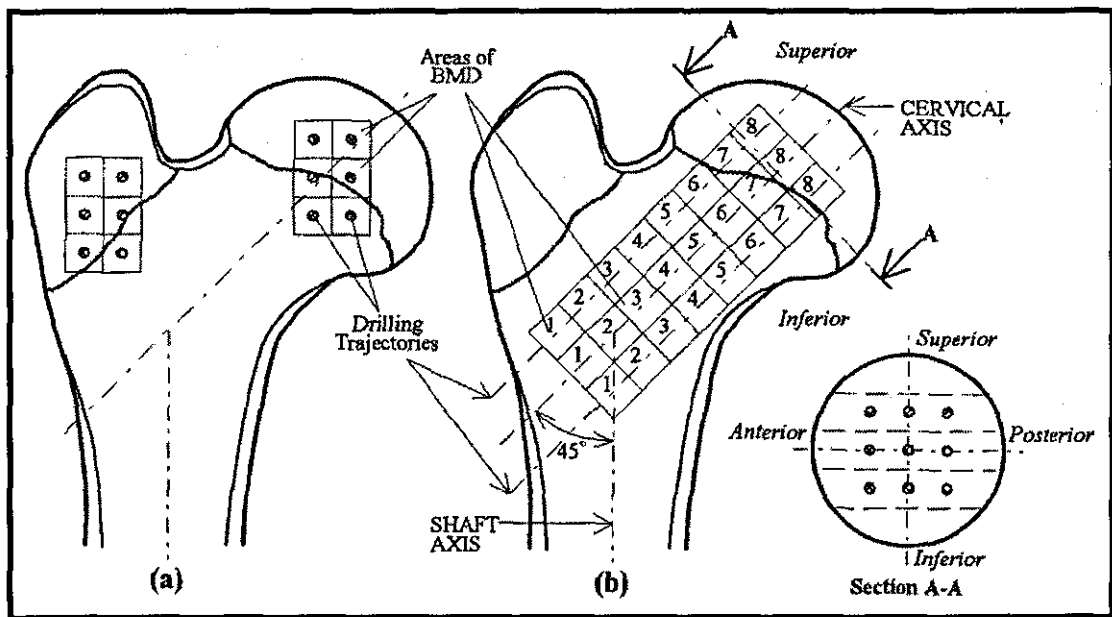
Figure 4.7 **Drilling Trajectories and Corresponding DXA Measurements [23]: a) in the Greater Trochanter and Femoral Head and (b) Parallel to the Cervical Axis**

4.4 AUTOMATION OF THE DRILLING PROCESS

The advantages of automation of the bone drilling process are: (i) steady motion, (ii) high precision and (iii) rapid reaction to sensory data. With the automation of the drilling process, data such as drilling force, drilling torque, drill bit displacement and rotational speed, etc. can be automatically collected during the drilling process and can be further used for analysis. This analysis of data could be used in implementing a control algorithm for safety enhancement and/or predicting bone strength.

Brett *et al* (1995) [131] investigated the technique for controlling the drill breakthrough during low-speed micro drilling of stapes (tiny flexible bone element in the middle ear) during stapedotomy (method of producing a small hole in the staples footplate to recover the loss of hearing). They used cadaver specimens for the experiments. An automated system was presented to determine the thickness and compliance of the bone, to detect the onset of the drill bit breakthrough and to control drill protrusion beyond the medial surface. Drill bit protrusion was achieved within 0.02 mm of accuracy. At the start of drilling both force and torque increases because of the compliance in the system. At the point of drill bit breakthrough, the force falls to zero and there is a rapid decrease in the torque. This characteristic of force and torque was present for all experiments, but only their magnitude varied with the stiffness of stapes, drill bit quality and drill feed rate. This condition was used to detect the starting of the drill bit breakthrough and at this point the drill rotation was stopped and the drill bit was retracted. At this point, the stapes footplate returns to the original position. The stiffness of the stapes footplate was determined from the reduction in force and corresponding deflection of the stapes. After that a second advancement of the drill bit is initiated to achieve a fully formed hole. The peak force at the second time was lower while the peak torque was higher due to a decrease in deflection of the stapes footplate. However, this technique was only accurate and precise if the specimen and drill are held steady. Hence, the system should be fixed relative to the patient to achieve the best results. Further, improvements in the device were also stated such as, hygiene, safety, user interface and compatibility with the operating theatre before clinical application.

Allotta *et al* (1996) [129] developed and validated experimentally a model for the detection of drill bit breakthrough during the penetration of a twist drill into long bones. A force-based real time breakthrough detection technique was devised and tested using a swine femur. Standard industrial drill bit of 3.5 mm diameter, 120° point angle and 25° helix angle was used. The drilling force and drilling torque was measured at feed rates of 50, 75, 100 mm/min and rotational speeds of 1500, 1800, 2000 rpm. The results of drilling force and torque indicated two prominent peaks at the two cortical walls, as a result of sharp changes on entry and exit of the walls, as shown in figure 4.6. Using the force derivative algorithm and second order linear filter, these sharp changes were detected with appropriate lower and upper thresholds to identify the onset of drill bit breakthrough.

Colla *et al* (1998) [132] investigated a method of detecting drill bit breakthrough in bone drilling by means of wavelet based controller. The penetration velocity was generated on the basis of the wavelet analysis of the drilling force signal. They calculated a parameter which was independent from the feed rate, thus reflecting only the strength of the bone portion being cut. The wavelet transform of this normalised parameter was done to obtain the drill bit breakthrough detection. The trials were carried out at feed rates of 50, 75 and 100 mm/min and cutting speeds of 1500, 1800 and 2000 rpm.

Ong and Bouazza-Marouf (1999) [133] proposed a reliable and repeatable method of drill bit breakthrough detection based on a modified Kalman filter, when drilling into long bones. They applied the modified Kalman filter to the force difference between successive samples (FDSS) obtained by drilling fresh porcine femoral shafts. It was found that the imminent drill bit breakthrough can be detected using different threshold levels of Kalman filtered FDSS (K-FDSS), in the presence of system compliance and inherent drilling force fluctuations. This method can be applied to different drill bit types over a range of drilling conditions.

4.5   CONCLUDING REMARKS

A brief description of the drilling process and the studies conducted to improve the drilling performance, by optimising the drill bit design, feed rate value and drilling speed, have been presented. The total drilling force is composed of, (i) the shearing or cutting of the material by the cutting edge of the drill bit (approximately 40% of the total drilling force), (ii) the indentation of the chisel edge of the drill bit into the material (approximately 57% of the total drilling force) and (iii) the friction force due to the chip flow (approximately 3% of the total drilling force). Various theoretical models developed to calculate the drilling force in metals have been presented. Previous studies have assumed that the cutting mechanism in bone behaves in a similar fashion as that of metals, and as thus the drilling force equations developed for metals were adopted to calculate the drilling force in bones. The two main models presented in the literature to calculate the drilling force in bones ignored the effect of chisel edge, which might lead to a wrong calculation as the contribution of the chisel edge to the total drilling force is comparatively high. All the drilling force prediction models used for bones require a value for the specific energy and/or the Brinell hardness and/or the friction coefficient which would need to be determined experimentally. However, it was seen in all the models presented, that the drilling force depends linearly on the shear strength of the material. Hence, the relationship between the drilling force and shear strength of synthetic bone material was explored in this research, to establish if the drilling force can be used as a predictor of material shear strength, the results are presented in chapter 8

A technique, known as dynamostratigraphy, which measures the drilling force and torque continuously along the drill bit depth at constant speed and feed rate, has been presented. Drilling force recorded using this technique can be used to provide information about the bone quality and it can also be used towards the automation of the drilling process by preventing breakthrough of the drill bit. The same technique is used in this research to predict the quality of bone. The following chapter presents the background study conducted on the screw pullout testing.

CHAPTER 5

SCREW PULLOUT TESTING

Various parameters affecting the screw pullout strength are discussed in this chapter. Based on these parameters a theoretical model of screw pullout force is presented and the application of the presented model in case of bone screw is discussed. The main objective of this research is to evaluate the quality of bone by analyzing bone drilling data. Bone drilling data does not give a direct measure of the bone strength; hence it has to be validated against a known method of bone strength measurement. From the direct methods of bone testing which are presented in chapter 2, section 2.2.1, screw pullout testing is selected for the validation of bone drilling data in this research. The reasons for selecting the screw pullout test, from the various direct methods of bone testing, are presented at the end of this chapter.

5.1 PARAMETERS AFFECTING THE SCREW PULLOUT STRENGTH

Mechanical strength at the bone screw interface (screw fixation strength) is an important factor in fracture treatment so as to obtain a rigid fixation. Fixation strength is described in terms of pullout strength of the screw, which is determined by the screw pullout test. The screw pullout test also gives the shear property of the tested material [134-136]; thus providing information on the bone quality. Screw pullout testing is also used in this research for the validation of drilling data; therefore it is crucial to identify the main factors that affect the screw pullout strength. These are discussed below.

5.1.1   Maximum Diameter of the External thread (D_o)

When a screw is pulled out, it shears a cylinder from the material in which it is inserted, as shown in figure 5.1. The area of the cylinder pulled out is directly proportional to the screw pullout force. The diameter of the shear cylinder is equal to the major diameter of the external threads, which is equal to the major diameter of the screw; therefore, screws with a larger major diameter result in higher screw pullout strength [137-140]. This is the reason of using larger diameter screws for the fracture treatment of cancellous and osteoporotic bones.
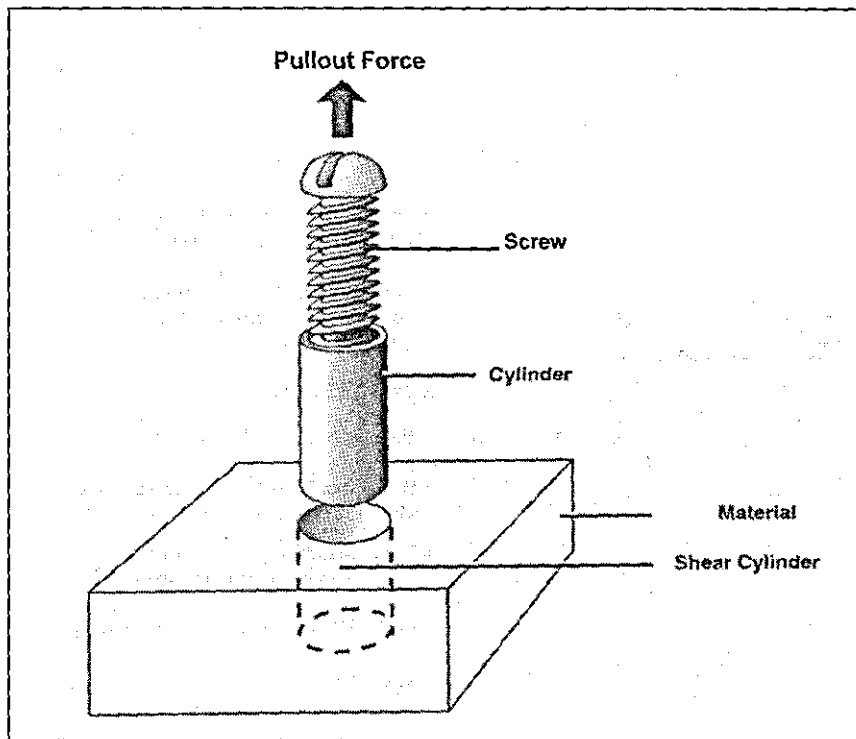
Figure 5.1   Screw Pullout Testing [30]

5.1.2   Length of Thread Engagement (L_{th})

The area of the cylinder sheared also depends upon the length of the screw thread engagement into the material, as shown in figure 5.1. Thus, increasing the length of thread engagement will increase the screw pullout strength [134, 135, 137].

5.1.3   Strength of the Material (σ_s)

The screw pullout strength is highly dependent on the shear strength of the bone and it increases with an increase in the strength.

5.1.4   Pitch of Screw Threads (p)

Screws with fine pitch threads result in a higher pullout strength as compared to the screws with coarse pitch threads, for the same density material [137, 138]. Figure 5.2 shows the free body diagram of a single thread of fine and coarse pitch screws.

Case 1: Fine Pitch   Case 2: Coarse Pitch

F_{PF} = axial pullout force in the case of a fine pitch screw; F_{PC} = axial pullout force in the case of a coarse pitch screw; F_{RF} = radial component of the reaction force in the case of a fine pitch screw; F_{RC} = radial component of the reaction force in the case of a coarse pitch screw; R_F = reaction force acting on fine thread; R_C = reaction force acting on coarse thread; θ_F = half thread angle of the fine pitch screw; θ_C = half thread angle of the coarse pitch screw.

Figure 5.2   Forces Acting on Coarse and Fine Screw Threads

From the free body diagram, the radial force (F_{RF}) acting on the thread with the fine pitch can be written as,

$$F_{RF} = R_F \sin\theta_F \qquad\qquad (5.1)$$

where, F_{RF} = component of the reaction force in the case of a fine pitch screw (N)

R_F = reaction force acting on the fine thread (N)

θ_F = half thread angle of the fine pitch screw (degree)

Similarly, the radial force acting on the thread with a coarse pitch can be written as,

$$F_{RC} = R_C \sin\theta_C \qquad\qquad (5.2)$$

where, F_{RC} = radial component of the reaction force in the case of a coarse pitch screw

R_C = reaction force acting on the coarse thread

θ_C = half thread angle of the coarse pitch screw

Fine pitch threads will always have a smaller thread angle as compared to the coarse pitch threads, i.e., $\theta_F < \theta_C$. From equation 5.1 and 5.2, it can be seen that if $\theta_F < \theta_C$, then $F_{RF} < F_{RC}$ when the same axial pullout force is applied on both the fine and coarse threads. The radial force creates the outward stress and reduces the effective shear area of threads by causing bone displacement, which in turn reduces the screw pullout force required to shear the material. The reduction in shear area of the bone due to wedging action of the threads is known as nut dilation and because of this the finer pitch screws have higher screw pullout force as compared to the coarser pitch screws. In clinics, the screw size (i.e., outer diameter of the screw) is limited by the size and strength of bone, whereas the pitch of the screw is not and can be easily varied for the same screw diameter. This makes the screw pitch a critical parameter in screw design.

5.1.5   Thread Depth ($(D_o-d_i)/2$)

Depth of sheared thread is defined as the difference between the maximum diameter of the external threads (D_o) and minimum diameter of the internal thread (d_i). The screw pullout strength increases with the thread depth [134, 135, 137]. However, the effect of thread depth is more significant in less dense material.

5.1.6   Material Density (ρ)

A denser material has higher screw pullout strength [134, 135, 137]. Shear strength (σ_s) is related to the bone density (ρ) with the following relationship:

$$\sigma_s = 21.6 \times \rho^{1.65} \text{ (for bovine bone) [134, 135]} \tag{5.3}$$

$$\sigma_s = 23.9 \times \rho^{1.54} \text{ (for polyurethane foam) [134, 135]} \tag{5.4}$$

Based on the above identified parameters affecting the screw pullout force (F_{SPF}), screw pullout force can be written as a function of following parameters:

$$F_{SPF} = f(D_o, L_{th}, \sigma_s, p, d_i, \rho) \tag{5.5}$$

Based on the above parameters, an empirical relationship to calculate the screw pullout force was developed in metals and is given in equation 2.5, in chapter 2. Equation 2.5 is based on the homogenous geometry of a unified standard thread. The basic shape of the unified standard thread is shown in figure 5.3.

The formula given in equation 2.5 for metals was applied on foam material by Chapman *et al* [135]. They experimentally determined the screw pullout force of twelve commercially available bone screws and calculated the shear strength of foam material of three different densities, using equation 2.5. A strong correlation ($r^2 = 0.947$) was found between the calculated shear strength and the actual shear strength (determined experimentally) of the foam material.
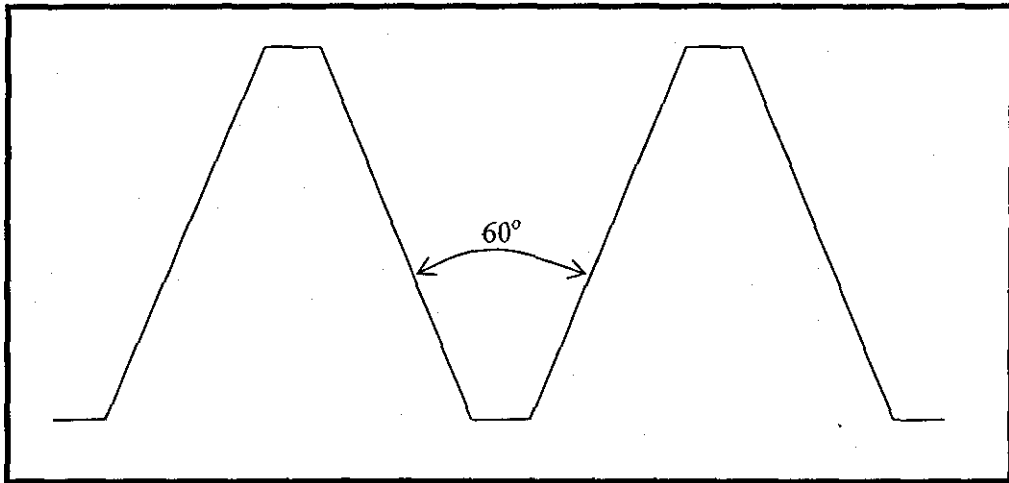
Figure 5.3 Homogeneous Geometrical Shape of the Unified Standard Thread

Asnis *et al* [134] also used equation 2.5, to calculate the shear strength of the foam material. They used screws of symmetrical thread geometry (V-shaped, like unified standard threads) of 25 degree thread angle. Two different densities of the foam material were tested.

The following shortcomings are identified in the above two studies conducted by Chapman *et al* and Asnis *et al*;

- In the study conducted by Chapman *et al* [135], bone screws were used which have non-homogeneous geometry, as shown in figure 5.4. Equation 2.5 is based on the calculation of the shear area of symmetric threads which will be different in case of the bone screws. Hence, equation 2.5 can lead to the wrong calculations of the material shear strength when applied to bone screws.

- In both of the studies, a 30 degree half thread angle value was used (which is for unified standard threads, as shown in figure 5.3). However, Chapman *et al* [135] used twelve commercially available bone screws and it is difficult to calculate the half thread angle in the case of bone screws as their geometry in not homogeneous. Asnis *et al* [134] used screws of symmetrical shape threads with a half thread angle of 12.5 degrees; however they did not use this value in their calculations.

- In both of the studies, diameters of the pilot holes were not equal to the minor diameter of the screws used. However, they used the minor diameter of the screws to calculate the thread depth instead of using the minor diameter of the internal threads cut on the foam material. The minor diameter of the internal threads on the foam material would depend on the diameter of the pilot hole.
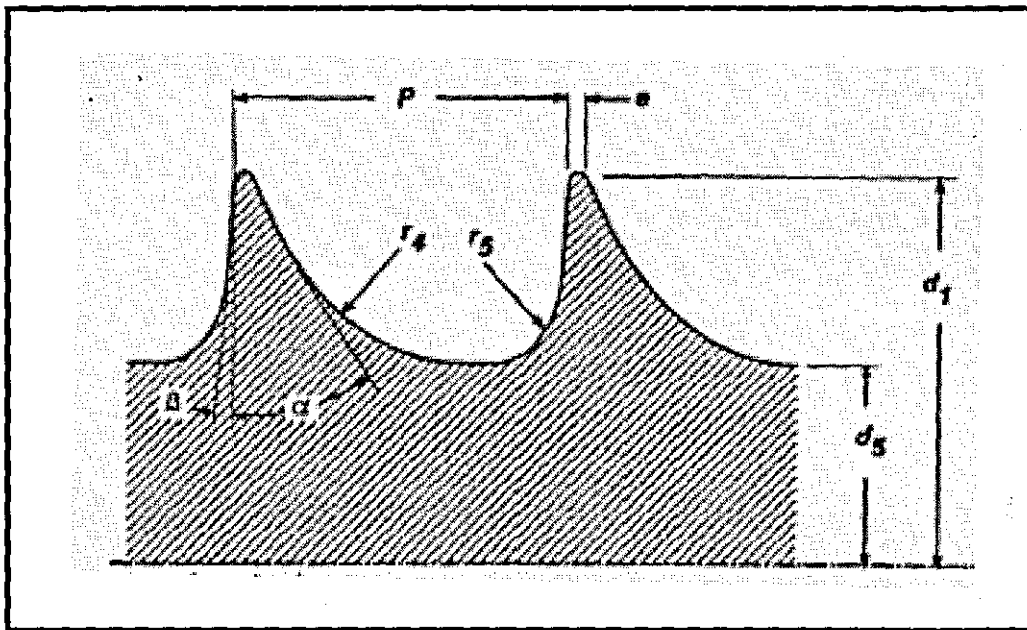
Figure 5.4 Geometry of a Surgical Bone Screw [141]

There is no study which has correctly applied equation 2.5 and validated its use for bone screws. Therefore, in this research the screw pullout force will be experimentally determined and correlated with the shear strength of the foam material to investigate if it can give a prediction of the material shear strength.

5.2   REASONS FOR SELECTING SCREW PULLOUT TESTING TO VALIDATE DRILLING DATA

Screw pullout testing is selected in this research to validate drilling data because of the following reasons:

- In screw pullout testing, any shape and size of the bone specimen can be tested. There are other direct methods of bone testing, such as bending and simulation tests, which can also test bone specimens of any shape and size. However, in both of these tests, the location of failure or the region of interest cannot be controlled and moreover, only the shaft portion of the long bones can be tested using bending tests.

- There are no special fixtures which are required for the specimen clamping.

- In screw pullout testing, the screw which is pulled out can be inserted into both the cortical and cancellous areas of the bone, thus the combined strength of the cortical and cancellous portion of the bone can be evaluated.

- The screw pullout testing simulates the actual or practical condition of the bone-screw fixation failure.

- The main disadvantages of other direct methods of bone testing over screw pullout testing are: a large number of bone samples are required, a meticulous specimen preparation is needed and generally the specimen is removed from its parent bone and hence, tests are carried out under non-physiologic boundary conditions.

- To conduct screw pullout testing, a screw has to be inserted into the bone. During screw insertion, the torque applied on the screw can be recorded and is known as the screw insertion torque. Screw insertion torque can also be recorded under in-vivo conditions, as part of the bone fracture treatment procedure in clinics. The screw insertion torque data which can be obtained as a

part of screw pullout testing can also be used as a supportive information to the surgeons.

- Screw pullout strength data could also be used in the future to optimise the parameters which affect the bone-screw fixation quality, e.g., bone screw design.

5.3   CONCLUDING REMARKS

Various factors on which screw pullout force depends upon are discussed and an empirical formula which can be used to calculated screw pullout force is presented. To validate the use of drilling data in predicting the bone quality, screw pullout testing is used in this research and the reasons for such a selection have been presented. Next chapter presents the background information on bone-screw fixation quality.

CHAPTER 6

BONE-SCREW FIXATION QUALITY

Bone-screw fixation is designed to provide an immediate stability and rigid immobilization of the fractured bone. The information on the bone quality can support the orthopaedic surgeon in taking decisions to improve the quality of a fracture treatment, like; (i) if supplementary augmentation is needed, (ii) if any precautions are to be taken by the patient, (iii) the frequency of post operation check ups and (iv) the need of extra screw fixations. The strength of bone-screw fixation mainly depends upon three parameters and these are:

1. **The quality of the bone:** As proposed in this research, the information on this can be obtained from the drilling data.

2. **The size and design of the screw used for fixation:** The effect of screw size and design on the bone-screw fixation strength can be estimated through screw pullout testing. Screw pullout testing is destructive in nature, therefore indirect in-vivo methods are used for such estimation. The effectiveness of such indirect methods, bone density measurement and screw insertion torque, is evaluated in this chapter by reviewing the correlational studies conducted between the aforementioned indirect methods and screw pullout strength. As drilling data is also correlated in this research with the screw pullout strength, therefore such review would also help to compare the use of drilling force with the indirect methods to predict the screw pullout strength.

3. **How well the screw is tightened into the bone to avoid loosening:** The use of screw tightening torque was proposed and explored by many researchers to optimise the screw tightening. Such studies are reviewed in this chapter. Another method based on controlling the screw rotation angle was proposed at the outset in this research to optimise the screw tightening. Hence, a background study on the use of screw rotation angle is presented in this chapter.

6.1   PREDICTION OF SCREW PULLOUT STRENGTH USING INDIRECT METHODS

Screws are used in orthopaedic surgery to provide stability and carry load at the fracture site while healing. The bone-screw system will often be under considerable stress as it shields the fracture site from loads. Bone fractures are often due to the poor quality of bone tissues, caused by, for example, osteoporosis. The most common method of measuring bone strength in clinics is by indirectly measuring the bone mineral density and screw insertion torque. Many correlational studies, which are presented in this section, have also been conducted to investigate the use of bone mineral density and screw insertion torque in predicting the screw pullout strength.

6.1.1   Use of Densitometry Methods to Predict Screw Pullout Strength

The review of various commercially available densitometry methods to predict the screw pullout strength is presented below in table 6.1. As QCT and DXA are the two most commonly used methods in clinics; consequently, investigations done to evaluate which technique out of QCT and DXA is a better predictor of the screw pullout strength are presented in table 3.5 (in chapter 3). The following observations can be made from the correlational studies presented in tables 3.5 and 6.1:

(i)   DPA bone mineral density was found to be a good predictor of screw pullout strength [142]. Conversely, no relationship was found between the DPA bone mineral density measurements and bone-screw fixation quality by Zdeblick *et al* [16], however they used the number of cycles to specimen failure to find the correlations, rather than using the screw pullout force.

(ii)   DXA bone mineral density measurements were found to be a better predictor of the screw pullout strength as compared to the QCT bone mineral density measurements [61, 95, 96].

(iii)   QCT bone density measurements showed no or average correlation with the screw pullout strength; hence, the use of QCT method to predict the bone-screw fixation quality was not recommended [96, 143, 144].

Screw pullout strength is due to the combined strength of the cortical and cancellous bone, which can be measured using DXA. This is the reason why higher values of correlation were found for the DXA bone mineral density measurements in comparison to the QCT bone mineral density measurements. However, before drawing any conclusions from the presented literature review, their shortcomings and drawbacks should be considered; these are highlighted below:

- **Effect of soft tissues:** All the studies which are presented in tables 3.5 and 6.1 were conducted in-vitro, thus neglecting the inaccuracies which would arise in the DXA measurements due to the presence of soft tissues (as discussed in chapter 3). Therefore, in-vivo DXA measurements might result in a less accurate prediction of the screw pullout strength.

- **Use of site-specific bone density measurements:** Stromsoe *et al* [50] found that the site-specific bone mineral density measurements conducted using both QCT and DXA at the femoral shaft were correlated best with the screw pullout strength as compared to other non-site specific bone density measurements. However, practically in clinics it is not possible to take site specific bone density measurements at the fracture site. Thus, using the non-site specific bone density measurements would lead to a less accurate prediction of the bone strength.

Table 6.1   Summary of the Various Correlational Studies Conducted to Evaluate the Use of Densitometry Methods in Predicting the Screw Pullout Strength

Column 1		Column 2					Column 3						Column 4	
		Mechanical Testing (In-vitro)					Indirect Testing						Corr. Coeff.	
	Bone Specimen Source	Bone Specimen		Test Specification			Bone Specimen		Measurement Conditions					
Author		Site	Type	Test	n	Prop. Msrd.	Site	Type	Tech.	T.E.	Meth.	Prop. Msrd.	r^2	P
Halvorson et al 1994 [142]	Human cadaver	Lumber vertebrae	Whole-bone	Sc.P.out	32	F_{SPF} (N)	Lumber vertebrae	Whole-bone	DPA	-	In-vitro	BMD (mg/cm²)	0.85	-
Zdeblick et al 1993 [16]	Human cadaver	Lumber vertebrae	Whole-bone	Sc.P.out (cyclic test)	6	ncf	Lumber vertebrae	Whole-bone	DPA	-	In-vitro	BMD (mg/cm²)	No relationship was found	
Heller et al 1999 [96]	Human cadaver	Spine T1 Spine T2 Spine T3 Spine T4	Whole-bone	Sc.P.out	71	F_{SPF} (N)	Spine T1 Spine T2 Spine T3 Spine T4	Canc.	QCT	×	In-vitro	vBMD (mg/cm³)	NC[1] NC[1] >0.6*[1] >0.5*[1]	<0.05
Heller et al 1996 [143]	Human cadaver	Cervical spine	Whole-bone	Sc.P.out	136	F_{SPF} (N)	Cervical spine	Canc.	QCT	-	In-vitro	vBMD (mg/cm³)	No correlation was found	
Okuyama et al 1993 [62]	Human cadaver	Lumber vertebrae	Whole-bone	Sc.P.out	15	F_{SPF} (N)	Lumber vertebrae	Whole-bone	QCT	W	In-vitro	vBMD (mg/cm³)	0.54*	<0.01
Reitman et al 2004 [145]	Human cadaver	Cervical spines	Whole-bone	Sc.P.out	54	F_{SPF} (N)	Cervical spines	Whole-bone	DXA	-	In-vitro	BMD (mg/cm²)	0.71	-
Ryken et al 1995 [146]	Human cadaver	Cervical spine	Whole-bone	Sc.P.out	99	F_{SPF} (N)	Cervical spine	Whole-bone	DXA	-	In-vitro	BMD (mg/cm²)	0.29*	<0.0001

List of symbols and abbreviations used in the table

BMD = bone mineral density (mg/cm²), measured using DXA or DPA; Canc. = cancellous bone specimen; Corr. Coeff. = correlation coefficient between the property of the specimen measured using the mechanical testing and indirect testing; Meth. = Method of indirect measurement used i.e., in-vitro or in-vivo; n = number of samples tested; NC = no correlation found; ncf = number of cycles to failure; P = statistical significance of the correlational study; Prop. Msrd. = property measured; r^2 = correlation coefficient between the mechanical property of the specimen and the specimen property measured using the indirect method; F_{SPF} = screw pullout force (N); Sc.P.out = screw pullout test; Tech. = indirect testing technique used in the presented study; T.E. = method used to simulate the effect of soft tissues present around the bone specimen during the indirect testing; vBMD = Volumetric bone mineral density (mg/cm³); W = this indicates that tissue effect was simulated by using water bath during densitometry measurements; [1] = screw pullout testing done in transverse process position; × = indicates that the effect of bone tissue for the indirect testing was not simulated in the study; - = indicates that no information was given in the referred paper. * = indicates that the coefficient of correlation 'r' (as given in the referred paper), has been converted to r^2 in this table for consistency

- **Effect of bone geometry:** Screw pullout strength is also affected by the change in bone geometry. Zdeblick *et al* [16] investigated the effect of pedicle width on the screw pullout strength and found that there were several specimens having low bone mineral density with higher screw pullout strength, but in those specimens the pedicle diameter was small. Thus, patients with osteoporosis vertebrae can have a good screw purchase with small pedicles. This shows that bone density can result in a wrong prediction of the screw pullout strength. Moreover, the medicines which can change bone geometry without making any considerable change in the bone density would also lead to a wrong prediction of screw pullout strength using bone density measurements.

Based on the presented literature it can be concluded that the in-vitro bone density, as measured using DXA, can be used as a predictor of screw pullout strength. However, more studies are required to investigate its application when non-site specific bone density measurements are used under in-vivo condition. Furthermore, QCT bone density measurements should not be used to predict screw pullout strength.

6.1.2 Use of Screw Insertion Torque to Predict Screw Pullout Strength

The bone screw is a mechanical device that converts the torque applied during screw insertion into a compressive force between the two components that it is placed through. Screw insertion into the bone can be divided into two stages; screw insertion and screw tightening. The screw insertion stage involves cutting or shearing of the bone; hence, the torque applied on the screw if recorded during this stage can be used as a predictor of bone quality or screw pullout strength. The main advantage of using the screw insertion torque is that it can be easily measured intra-operatively during the treatment of bone fracture and can give site specific prediction of the screw pullout strength, unlike bone density measurements. Many investigations have been reported in the literature to study its effectiveness in predicting the screw pullout strength. A tabular summary of such correlational studies are presented in table 6.2.

In all of the correlational studies presented in table 6.2, a significantly high correlation between the screw insertion torque with screw pullout strength was observed, in both homogeneous foam material [147] and bone specimen [2, 62]. This supports the use of screw insertion torque to predict screw pullout strength.

As bone density is another technique which can be used under in-vivo conditions to predict the screw pullout strength; therefore it was compared by various researchers with the screw insertion torque. It was found that the screw insertional torque was a better predictor of the screw pullout strength as compared to the both DXA [146] and QCT [61, 62] bone density measurements. However, Reitman *et al* [145] found that DXA bone density measurement to be a better predictor of screw pullout strength in comparison to the screw insertion torque.

To draw a significantly meaningful conclusion of the reviewed literature, it is important to understand the factors which could affect the measurement of screw insertion torque. A critical discussion on the effect of these factors, in using the screw insertion torque to predict screw pullout strength is presented below [148]:

(i)   **The property of the bone into which the screw is inserted**: During the screw insertion process, the torque applied to shear the bone depends upon the shear property of the bone. Hence, theoretically the screw insertion torque can be used as a method to predict bone strength which in turn can be related to the screw pullout strength.

(ii)   **The quality and size of the pilot hole in relation to the core diameter of the screw**: In the correlational studies presented in table 6.2, no information was provided on the method of bone drilling prior to the screw insertion. This plays a very critical role in defining the quality and size of the pilot hole, which contributes significantly to the magnitude of the screw insertion torque [149, 150].

Table 6.2 **Summary of the Various Correlational Studies Conducted to Evaluate the Use of Screw Insertion Torque in Predicting the Screw Pullout Strength**

Column 1		Column 2					Column 3						Column 4	
		Mechanical Testing (In-vitro)					Indirect Testing						Corr. Coeff.	
	Bone Specimen Source	Bone Specimen		Test Specification			Bone Specimen		Measurement Conditions					
Author		Site	Type	Test	n	Prop. Msrd.	Site	Type	Tech.	T.E.	Meth.	Prop. Msrd.	r^2	P
Zdeblick et al 1993 [16]	Human cadaver	Lumber vertebrae	Whole-bone	Sc.P.out (cyclic test)	6	ncf	Lumber vertebrae	Whole-bone	Sc.Ins.Tor	-	-	T_i (N.m)	Linear relationship was found	
Okuyama et al 1993 [62]	Human cadaver	Lumber vertebrae	Whole-bone	Sc.P.out	15	F_{SPF} (N)	Lumber vertebrae	Whole-bone	Sc.Ins.Tor	-	-	T_i (N.m)	0.85*	<0.01
Snyder et al 1995 [94]	Two week old calf	Lumbar vertebrae	Whole-bone	Sc.P.out	24	Yield moment (N.m)	Lumber vertebrae	Whole-bone	Sc.Ins.Tor	-	-	T_i (N.m)	0.77^2	<0.05
Myers et al 1996 [61]	Human cadaver	Lumber spine	Whole-bone	Sc.P.out	49	F_{SPF} (N)	Lumber spine	Whole-bone	Sc.Ins.Tor	-	-	T_i (N.m)	0.6*	<0.0005
Daftari et al 1994 [2]	Foam	Bi Cortical foam	Bi-cort.	Sc.P.out	112	F_{SPF} (N)	Bi Cortical Foam	Bi-cort.	Sc.Ins.Tor	-	-	T_i (N.m)	0.42*	<0.001
	Calf	Lumbar vertebrae	Whole-bone		60		Lumbar vertebrae	Whole-bone					0.72*	
Reitman et al 2004 [145]	Human cadaver	Cervical spines	Whole-bone	Sc.P.out	54	F_{SPF} (N)	Cervical spines	Whole-bone	Sc.Ins.Tor	-	-	T_i (N.m)	0.42	0.093
Ryken et al 1995 [146]	Human cadaver	Cervical spine	Whole-bone	Sc.P.out	99	Sc.Pu.F (N)	Cervical spines	Whole-bone	Sc.Ins.Tor	-	-	T_i (N.m)	0.77*	<0.0001
Hsu et al 2005 [147]	Foam	Foam (0.32g/cm³)	Canc.	Sc.P.out	9	F_{SPF} (N)	Foam (0.32g/cm³)	Canc.	Sc.Ins.Tor	-	-	T_i (N.m)	0.75*	<0.05

Note: Symbols and abbreviations used in the previous tables presented in this chapter are not repeated here.

Bi-cort. = bi-cortical bone specimen; T_i = screw insertion torque (N.m); Sc.Ins.Tor = screw insertion torque testing; ^{2} = maximum value of correlation coefficient is presented among the four different types of insertional techniques which were used in the referred study

(iii) **The insertion of a screw using continuous or intermittent rotation:** Intermittent motion of the screw inserted manually can cause the stick-slip phenomenon. This will generate relatively a higher magnitude of the torque depending upon the friction between screw and bone. The screw was manually inserted in all of the studies reviewed in table 6.2; thus, the recorded screw insertion torque was not entirely due to the shearing of the bone specimen.

(iv) **Pressure applied on the screw head:** The pressure applied on the screw head during the insertion process was not maintained constant, as the screws were inserted manually in all the review studies presented in table 6.2. Therefore, different surgeons will apply different pressures on the screw during insertion, which would result in different torque and screw pullout values.

(v) **Friction between the bone and screw interface:** This depends upon, (a) the property of lubrication used during the insertion, (b) the surface texture of the screw and bone and (c) the screw design. All of which cannot be maintained constant during the fracture treatment of various patients undergoing surgery at different locations. Hence, the value of the screw insertion torque could be misleading in predicting the bone strength.

(vi) **Angle of screw insertion:** The screw insertion torque depends substantially on the angle at which the screw is inserted with respect to the axis of drilled hole. In all the studies presented in table 6.2, no bushes were used to maintain the alignment during the screw insertion. Therefore, there can be an error in the screw insertion torque values recorded in the reviewed studies.

It can be concluded that the measurement of screw insertion torque can be erroneous and therefore, should not be used by surgeons as the main parameter to predict the screw pullout strength. However, it can be used as an additional or supporting information in predicting the screw fixation quality. This conclusion can also be supported by the recent studies performed by Inceoglu *et al* [151] and Kwok *et al* [152], who found that screw insertion torque was not a reliable predictor of the screw pullout strength.

6.2 USE OF SCREW TIGHTENING TORQUE IN CLINICS TO OPTIMISE SCREW TIGHTENING

The second stage of inserting the screw into the bone is known as the screw tightening stage. It starts when the screw head touches the bone surface or bone plate. The torque applied after this point is called screw tightening torque. The efficiency of bone screw in internal fixation is related to its axial tension. This tension produces compression of the fractured surfaces and presses the bone plate to the bone surface. To permit functional

treatment of a fracture, it is desirable to achieve an optimal clamping force, i.e., the highest amount of compression force without failure of either the bone or the screw. The clamping force achieved in the joint is proportional to the screw tightening torque. When inserting bone screws manually, orthopaedic surgeons adapt to what they perceive as the "optimal" torque depending on the bone quality and stop before stripping occurs based on their feel of screw tightening torque. However, the torque achieved based on the feel is significantly closer to the thread stripping failure limit, as clinical torque tightening levels reach an average of 86% of the failure stripping torque [153], which is generally past the yield point of bone [154]. This shows that there is a small margin of safety if the screw is tightened manually by surgeons based on their feel and perception. Additionally, in immature or osteoporotic bone, even at low screw tightening torque, unexpected stripping of the threads can occur, requiring re-drilling and insertion of a larger diameter screw, hence requiring greater attention of the surgeon during screw tightening and leaving a smaller margin of safety. Another disadvantage of using feel as a measure of optimum tightening is that the tightening torque depends largely on the friction; therefore, as the friction decreases (due to the change in screw and screw plate design or screw coating or lubrication), the surgeon will end up applying more torque to get the same feel resulting in higher axial tension and stripping of threads. Therefore, optimum tightening of the screw during the surgery is significantly important for a good bone-screw fixation quality; as over tightening of the bone screw can result in a loss of approximately 40% of the screw pullout strength [21]. A method of achieving an optimum tightening torque is to use a predetermined torque value (as in case of metals) based on the screw design rather than relying on the feel. However, bone strength of every patient is different and therefore, a preset value of optimum tightening torque just based on the screw design cannot be applied in clinics unless the optimum tightening torque value is determined and set based on the bone strength of the patient who is undergoing the surgery. A device which can estimate the optimum tightening torque value based on the bone strength of the patient undergoing the treatment was proposed by Hearn *et al* [155] and is discussed in next section.

6.2.1   Device for Optimising Screw Tightening Torque

A device which uses screw insertion torque and screw tightening torque information to optimise the screw tightening was proposed by Hearn *et al* [155] in a patent titled, "adaptive apparatus for driving a threaded device into material". To evaluate the effectiveness of the proposed method and device, a test rig was developed and experiments on foam (0.2 and 0.3 g/cm^3), cancellous bone (0.9 g/cm^3), cortical bone (2 g/cm^3) and wood were conducted. They successfully demonstrated the effectiveness of the proposed method on the above mentioned samples tested. The test rig designed to conduct the experiments can perform the following functions:

1) Drill a pilot hole for screw insertion,

2) Record torque data during the insertion of screw into the material,

3) Use the recorded data to determine the material strength,

4) Use the material strength to set the optimum screw insertion torque (for maximum bone fracture joint strength), and

5) Tighten the screw automatically to the pre-defined optimum torque value.

The method used to optimise the screw tightening using the designed test rig is shown below in two steps:

Step 1: Generation of reference data for known material

a)   The reference torque data was initially generated in the lab for known materials. For this, the screw was inserted until the screw head touched the top surface of the bone material. This was referred to as the point of head contact (HC), as shown in figure 6.1. An algorithm was developed to automatically detect the point of HC, based on either the sudden increase in the screw insertion torque value or by recording the screw rotation and multiplying it by the screw pitch to give the length of screw insertion. The screw insertion torque (T_i) profile, as shown in figure 6.1, was continuously recorded and stored during the screw insertion process.

b) The screw was further inserted from the HC point and the applied torque data was recorded and stored. The torque reaches its maximum value (T_{max}) at the start of thread stripping, as shown in figure 6.1.

This generated reference data was used to set the optimum screw tightening torque value for unknown materials, as described in step 2.

HC = point of head contact; T_i = screw insertion torque (mN.m); T_{opt} = optimum torque (mN.m); T_{max} = maximum torque (mN.m).
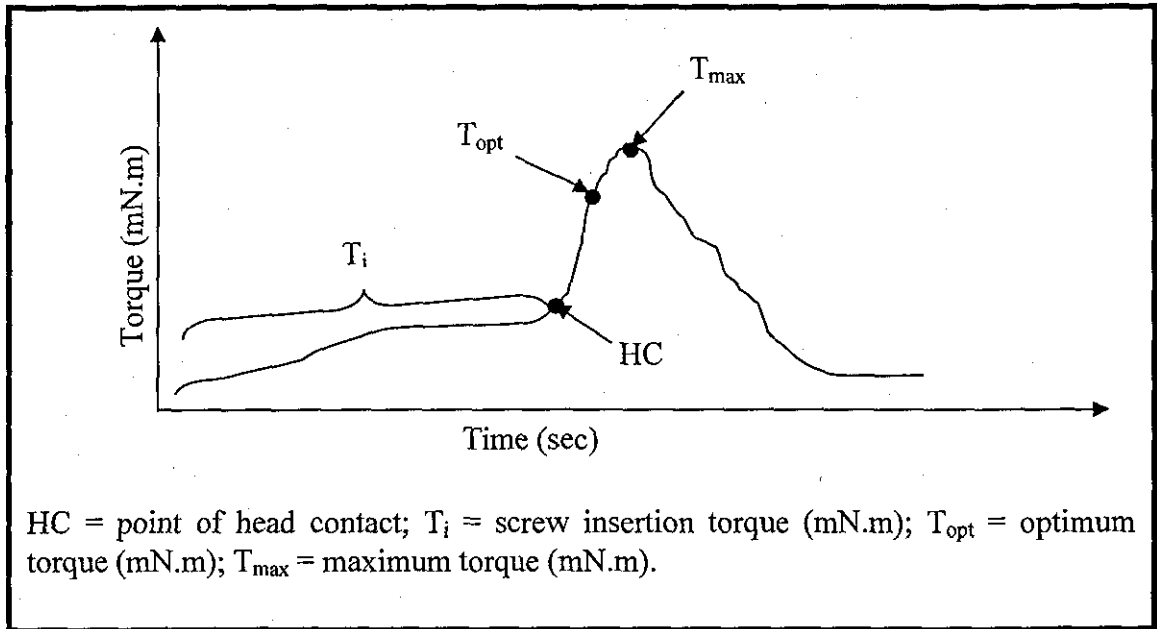
Figure 6.1 Applied Screw Torque vs Time

Step 2: Setting the optimum torque value (T_{opt}) for an unknown material.

The screw was inserted into an unknown material and the screw insertion torque data was recorded and stored for the initial T_i region. This torque data for the T_i region was compared continuously with the already generated reference torque database, as described in step 1 for the T_i region. A close match between the torque data generated for the known and unknown material was made. T_{max} value of the matched reference data was used to define the T_{opt} value for the unknown material. T_{opt} was defined as 70% of T_{max}. After the T_{opt} value was set, a screw was inserted into the unknown material until that torque level was achieved.

6.2.2 Shortcomings in the Hearn *et al* Method and Device

(i)   The experiments conducted by Hearn *et al* [155] to demonstrate the effectiveness of the method and device used the same combination of material and screw for generating both the reference data and to set the optimum torque value. Therefore, before using this device in clinics, the reference data has to be generated for the various combinations of bone and screw design, to cover the entire range of bone strength and screw design before using this device in clinics.

(ii) In the experiments conducted by Hearn *et al* [155] to demonstrate the effectiveness of the proposed device, no closed loop feedback was provided to control the screw insertion speed. This might cause the screw insertion torque value to change because of the variation in the screw insertion speed rather than change in the material property of the specimen under testing.

(iii) After the HC point, no thread cutting is involved; hence, the frictional forces between (i) the screw head and the bone surface or plate and (ii) the screw and bone threads, are the major contributors to the screw tightening torque. Therefore, all the parameters which can affect the above stated frictional forces should be maintained constant while generating the reference data and at the time of setting up the optimum torque value during the fracture treatment surgery. As the reference data has to be generated before hand and stored in the device, therefore, it will be very difficult to maintain all the parameters constant to simulate the exact operating conditions while generating the reference data. This will result in setting up either a lower or higher optimum screw tightening torque value and thus compromising the bone-screw fixation quality. Moreover, once the handheld device comes into operation, the surgeon will rely completely on the optimum torque value that the device would set (one cannot rely on the feel, as the screw insertion would be done automatically) and if the optimum value is set wrongly then there is no way to know if the fixation quality has been compromised or not.

(iv) Screw design (both threads and screw head) has to be maintained the same during the generation of the reference data and the fracture treatment surgery. Different hospitals use screws from different manufacturers; therefore generating the reference data for all the screws which are used in different hospitals would be a difficult task.

(v)   Different surface coating on the screws produces different levels of screw insertion torques [156, 157], e.g., the screw insertion torque can be decreased up to 50% by using a diamond coating on the screws [157]. Since different screw manufacturers use different screw coatings; therefore the reference data should be generated for all the different screws manufactured by the various companies. Not only that, the reference data has to be upgraded every time a new type of screw comes up in the market but it will also be very difficult to upgrade the reference data in the handheld devices if they are already being used in hospitals.

(vi) The reference data cannot be generated under in-vivo conditions on living patients, as bone thread stripping cannot be performed on living patients to determine the maximum torque value. Therefore, reference data would be generated from cadavers, but bone properties of cadaver bones are different to those of living bones. This can be further supported by the investigation of Buhler *et al* [158] who found that the screw insertion torque value under in-vivo conditions is significantly greater than when measured under in-vitro conditions. They also found a significant linear correlation between screw insertion torque and bone density for the in-vitro data but not for the in-vivo data. Hence, a maximum torque value measured in cadavers cannot be used accurately to set the optimum torque value for living human bones

(vii) Blood acts as a lubricant during surgery; therefore blood pressure inside the bone will also have a significant contribution to the screw insertion torque. Blood pressure will vary in every individual and this might give either a higher or a lower value of the screw insertion torque, which in turn might lead to the wrong setting of optimum screw insertion torque value.

From the above presented shortcomings, it can be concluded that a critical review of the above proposed device is required before it can be used in practice. Moreover, all the experimental results which were presented in the patent were under in-vitro condition. Hence, it is important to know the effectiveness of the above method and device under in-vivo conditions. Few studies have been reported in the literature which recorded the screw tightening torque under in-vivo condition on patients undergoing surgery. Okuyama *et al* [159] recorded screw tightening torque intra-operatively on 62 patients undergoing bone fracture treatment. The patients were observed for two years and seven

months for screw loosening as a measure of bone-screw fixation quality. It was concluded in the study that the screw tightening torque could not objectively predict screw loosening. Similar results were also found by Ozawa *et al* [160] who recorded the screw tightening torque intraoperatively on 25 patients undergoing surgery and concluded that the intraoperative screw tightening torque is not a quantitative predictor of screw loosening. It should be noted that in the above two presented studies, the screw tightening torque value was not determined according to the proposed method by Hearn *et al* [155], but they were tightened manually by the surgeons using their experience and feel to limit the tightening torque value.

From the above discussed limitations and drawbacks it is clear that screw tightening torque data could be misleading if used in surgery for optimising screw tightening. Therefore, there is a need of another method to optimise screw tightening which is independent of the friction between the screw and bone surface and which can be recorded under in-vivo condition. Controlling the screw rotation angle, which is independent of the friction between bone and screw, is proposed in this research. So far, there are no studies in the literature which have proposed the use of screw rotation angle to optimise screw tightening.

6.3 USE OF SCREW ROTATION ANGLE TO OPTIMISE SCREW TIGHTENING

As part of this research, it is proposed to use the screw rotation angle after the point of head contact, for optimum screw tightening. Optimum screw tightening depends upon the axial tension, or clamping force, between the mating parts, which is quantified by the amount of torque applied to the screw. This is the concept which is widely used in the fastener industry and all the studies presented previously are based on this concept. However, torque with respect to rotation, only indicate work done on a joint by the operator and not necessarily the clamping force. This is because torque must first overcome under-head and thread friction before getting converted into the clamping load. Figure 6.2 shows a typical curve between the applied screw torque and the screw rotation angle. The area under the curve is proportional to the energy required to tighten the fastener. Hence, screw tightening torque alone does not provide sufficient information to determine the clamping load attained in the fixation.
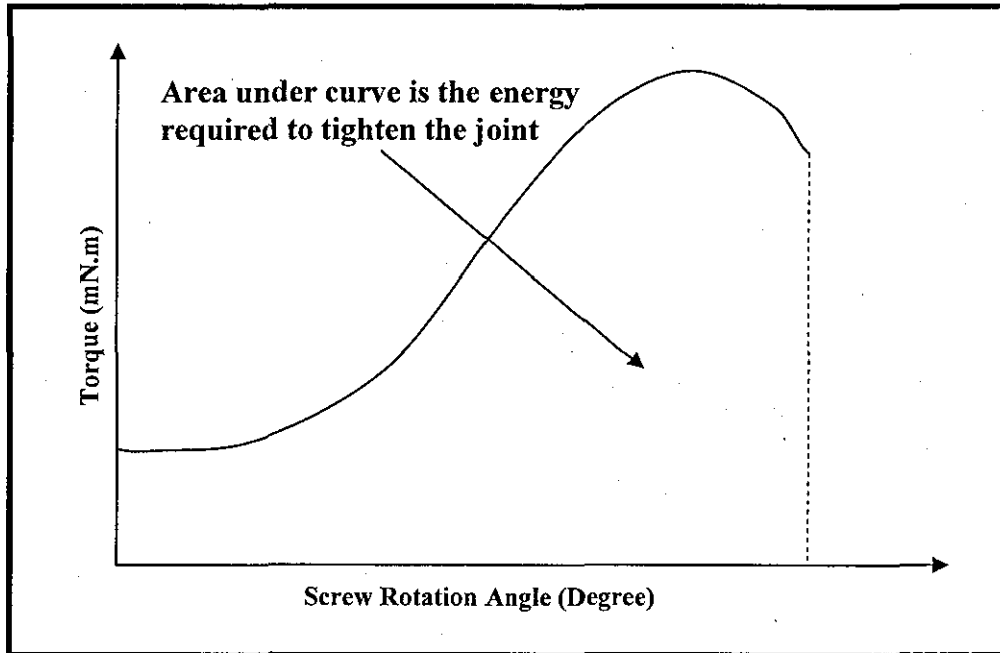
Figure 6.2 Energy Required to Tighten the Fastener

6.3.1 Modelling the Screw Tightening Process

To understand the tightening process of a joint, it is important to first understand the relationship between the screw torque and screw rotation angle in the development of the clamping load. A general model of the screw torque versus angle of screw rotation for the screw insertion and tightening process is shown in figure 6.3. It has four distinct zones.

Zone 1 Rundown: In this zone the screw is being threaded into the pilot hole (in the case of self tapping screws) or inserted into an already threaded pilot hole (in the case of non-self tapping screws) before the screw head contacts the bone surface or bone plate surface (also known as bearing surface). The torque applied in this zone is known as screw insertion torque. Screw insertion torque can be the result of thread cutting (in the case of self tapping screws) and the frictional force between the screw and bone threads. Factors like, misalignment of parts or presence of any foreign material in the threads can also contribute to the frictional force.
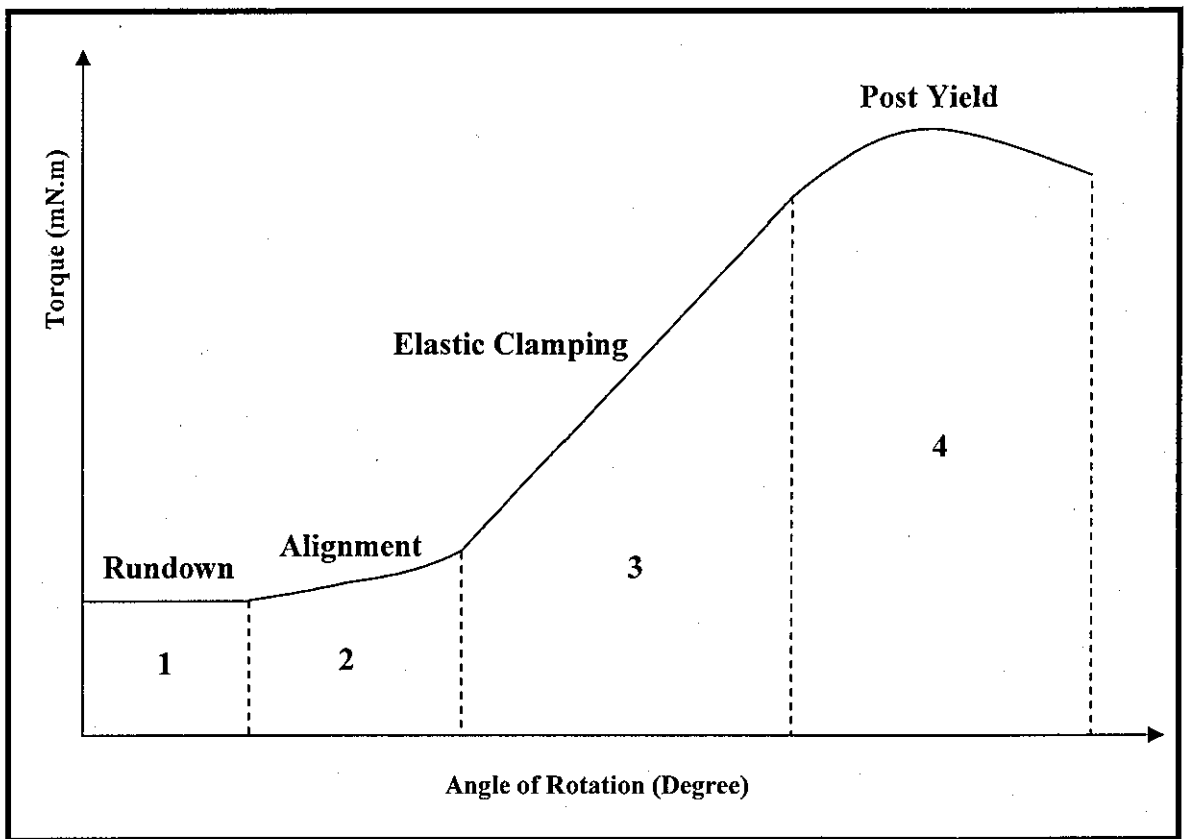
Figure 6.3 Four Zones of the Screw Tightening Process

Zone 2 Alignment: The second zone is the Alignment Zone, wherein the screw and joint mating surfaces are drawn into alignment. This zone, which is non-linear, is a complex function of the process of drawing together the mating threads, bending together of mating parts, bending of the threads as a result of non-parallelism of the bearing surface with the screw under head surface, stress induced deformation of coatings and thread deformation.

Zone 3 Elastic Clamping: The third zone is the Elastic Clamping Zone, wherein the slope of the torque angle curve is normally constant. This portion of the torque-angle signature is most important since this is where most of the tightening energy is transferred from the tool/surgeon to the joint assembly. The angle-of-turn of screw (or screw rotation angle) in the elastic clamping zone is directly proportional to the clamping load developed in the joint. Even if the friction between the threads or in the under head region of the fastener is varied, the clamping load generated will always be proportional to the angle-of-turn in the elastic clamping zone. The angle of the slope is indicative of the amount of friction present in the joint; steeper slopes indicate higher levels of friction, flatter slopes indicate lesser levels of friction.

Zone 4 Post Yield: The fourth zone is the Post-Yield Zone, which begins with an inflection point at the end of the elastic range. This fourth zone is due to yielding in the joint or washer, or due to yielding of the threads.

The above mentioned four zones of the screw tightening process are clearly visible in the graph plotted for the screw tightening torque data recorded for the FR-6718 series foam material, as shown in figure 6.4. A cancellous screw of $\phi 3.5$ mm diameter (Model No. 206.045, Synthes Ltd., UK) was used and the torque data was recorded at a sampling frequency of 250 Hz.
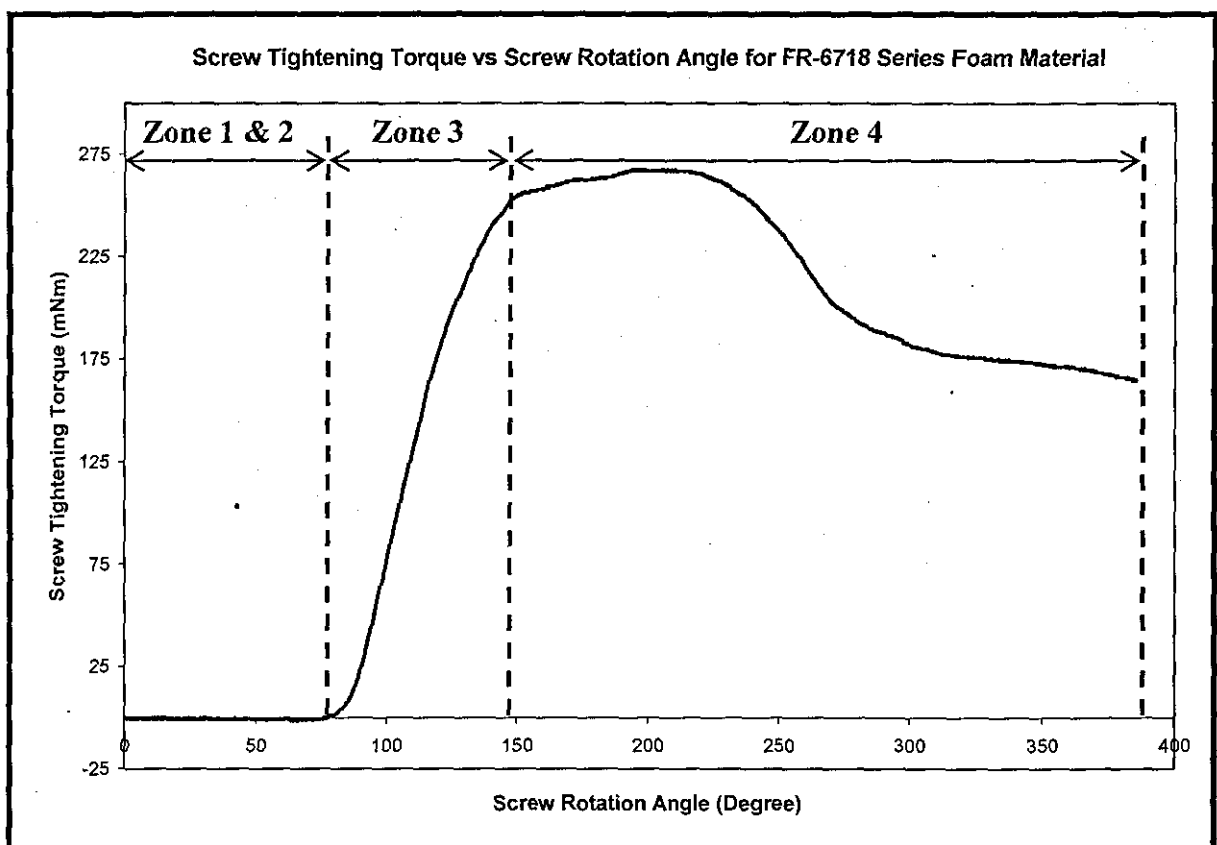
Figure 6.4 Four Zones of Screw Tightening Process Demonstrated on FR-6718 Series Foam Material

6.3.2   Relationship Between the Torque Applied on the Screw and Clamping Load

A schematic diagram of the bone fracture fixation using a bone screw is shown in figure 6.4. The total torque applied on screw is absorbed in three main areas; (i) to overcome the under head friction, (ii) to overcome the thread friction and (iii) to develop the clamping force in the joint. Equation 6.1 gives the formula to calculate the total torque applied on the screw [161]:

$$T_s = \frac{F_c}{2}\left[d_m\,\mu_h + d_n\left(\frac{\mu_t + \cos\theta_f\,\tan\theta_h}{\cos\theta_f - \mu_t\,\tan\theta_h}\right)\right] \qquad (6.1)$$

where

d_m = the mean diameter of the screw head bearing surface (mm)

d_n = the nominal diameter of the screw (mm)

F_c = the clamping load developed in the joint (N)

T_s = total torque applied at the screw (N.m)

μ_h = friction between the screw head and either the bone plate or washer or bone (dimensionless)

μ_t = friction between the screw thread and bone thread (dimensionless)

θ_h = helix angle of the screw thread (degree)

θ_f = screw thread flank angle (degree)
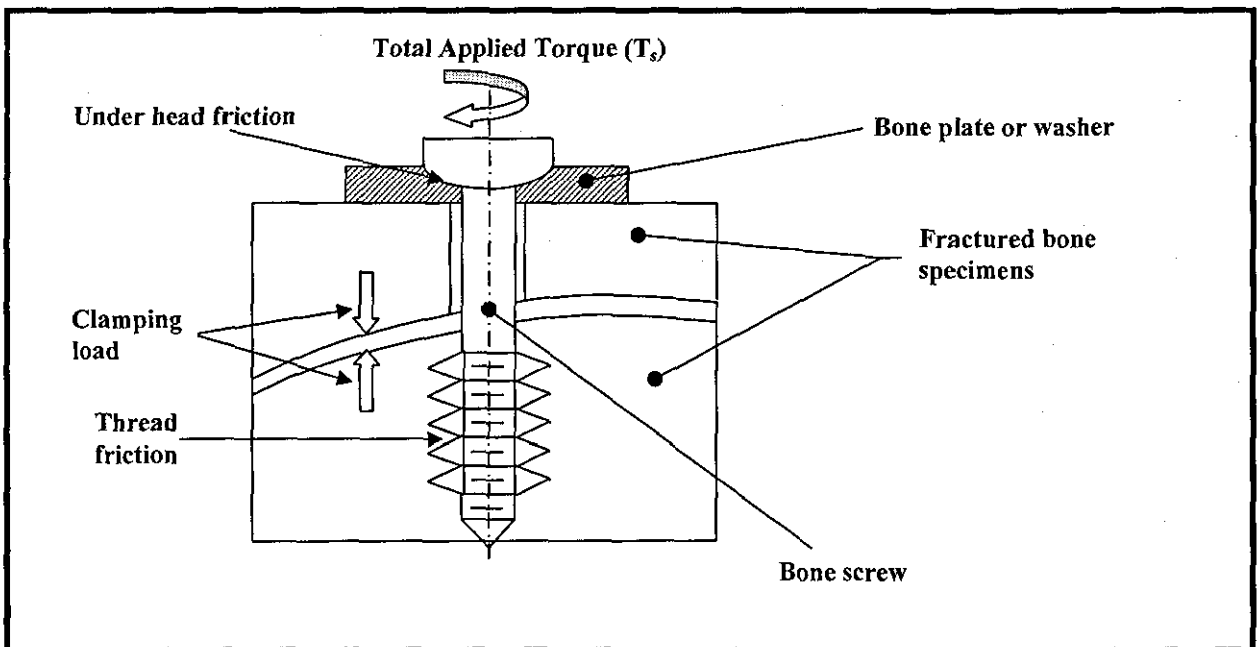
Figure 6.5 Bone Fracture Fixation

It can be seen from equation 6.1 that the total applied torque depends upon the friction between the mating parts. Therefore, any variation in the friction coefficients can dramatically affect the integrity of the joint at a specific torque value. The torque has to overcome both the under head friction and the thread friction before the clamp load is achieved, therefore any increase in either of the friction coefficients will increase the percentage of torque needed to overcome friction, leaving less torque available to produce the clamping load. In other words, if more friction is present in the joint, the less clamping load will be attained at a specific torque value. Hence, any variation which could affect the friction would result in a different clamping force for the same applied torque. Every fracture fixation surgery will have different operating conditions, thus will have different friction between the mating parts. At present, surgeons use either a preset torque value or rely on their feel to optimise the tightening torque to achieve a good quality of fracture fixation. Using a preset torque value can result in either a lower or higher clamping load depending upon the variation in the friction, e.g., if the friction is higher, then more torque would be consumed to overcome the friction and less clamping load would be achieved for the same value of applied torque. Similarly, using manual screw tightening, would also result in either a lower or higher clamping load.

There is another method of achieving optimum clamping load, which is used in the fastener industry where more accuracy is required for critical applications. This method uses the screw rotation angle as a measure of the clamping force instead of torque. Screw rotation angle can be geometrically related with deformation in the joint as given in the following formula.

$$\delta = \frac{\theta_r}{360} \times p \qquad (6.2)$$

where, δ = linear deformation in the joint (mm)
θ_r = screw rotation angle (degree)
p = thread pitch (mm)

It can be observed from equation 6.2 that deformation in the joint depends upon the screw rotation angle and is independent of the friction between the mating parts. Deformation or joint displacement gives a direct measure of the clamping load; therefore, the screw rotation angle can be used as a parameter which can be controlled during surgery to optimise the screw fixation quality. This is further explained using figure 6.5, which gives a relationship plot between: (i) the clamping load and applied screw torque for different

values of coefficient of friction (shown by solid lines) and (ii) clamping load and screw rotation angle (shown by the dotted line).

Let us assume that T_r is the recommended value of screw tightening torque (shown by a vertical line) which should be applied to achieve the optimum clamping load for a particular configuration of screw and bone. Three cases with low, medium and high coefficient of friction between the screw and bone are plotted in figure 6.5. The optimum clamping load (F_{opt}) which should be achieved for the maximum joint strength is shown by the horizontal line in figure 6.5. It can be seen that in case of high friction, the recommended or preset torque value can be reached well before the optimum clamping load is achieved. This is because most of the applied torque will be used to overcome the friction than providing the clamping load. In the case of low friction, tightening up to the recommended or preset torque value might result in over-tightening of the joint as less torque would be used to overcome the friction. Hence, the use of applied torque as a controlling parameter to obtain optimum fixation strength could be misleading and inaccurate, as it depends upon the friction which cannot be maintained constant in all the cases.
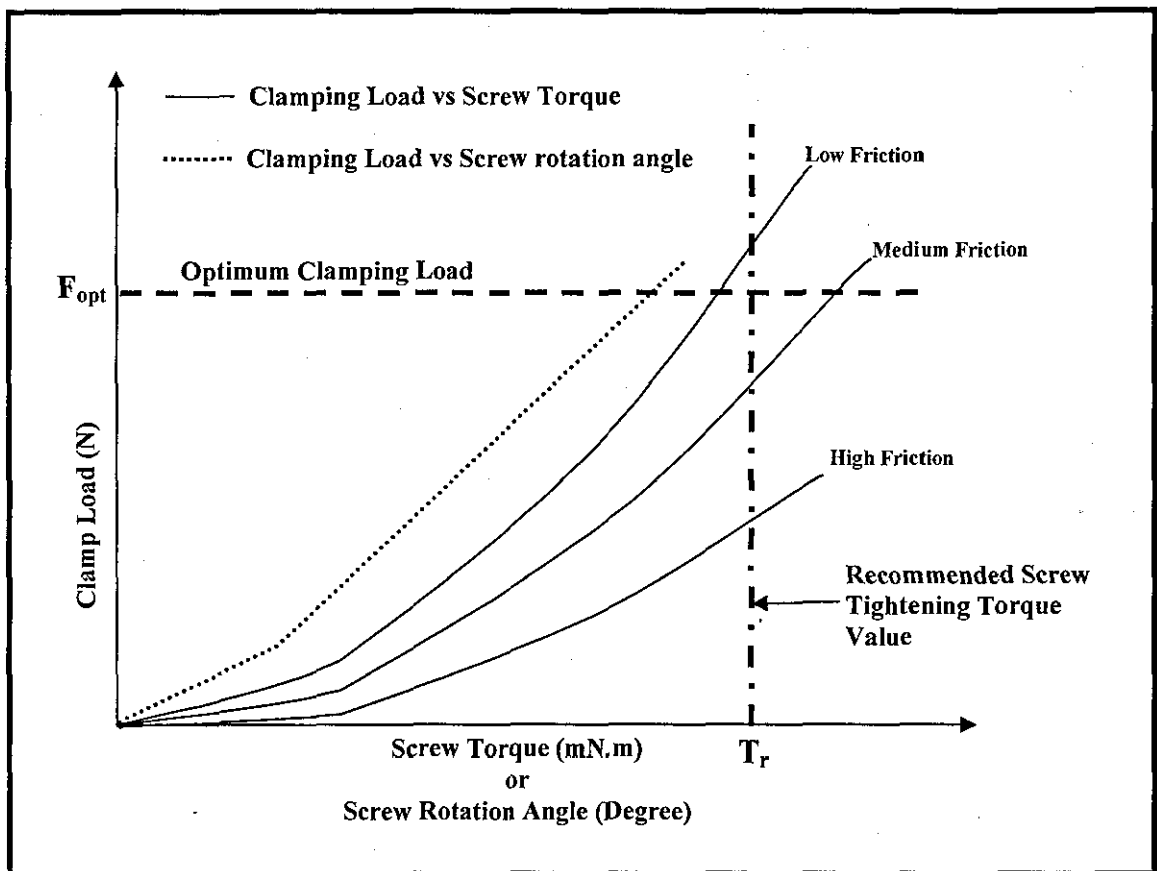
Figure 6.6   **Plot Showing Relationship between (i) Clamp Load and Screw Torque for Different Levels of Friction and (ii) Clamp Load and Screw Rotation**

On the other hand, the clamping load increases linearly with the screw rotation angle (shown by dotted line) irrespective of the friction in the joint. This is because the clamping load depends upon the amount of deformation in the joint which in turn depends linearly on the screw rotation angle. This shows that the screw rotation angle can be used as a better controlling parameter as compared to the screw tightening torque for better fixation quality. Hence, the use of screw rotation angle will be investigated in this research.

6.4 CONCLUDING REMARKS

The quality of bone-screw fixation depends upon, (i) the bone quality and (ii) the size and design of the screw used in fixation. Screw pullout strength can give direct information of the aforementioned parameters; however it cannot be measured in-vivo. Therefore, studies have been conducted to explore the use of bone density measurements and screw insertion torque, which can be measured in-vivo, to estimate the screw pullout strength. Such correlational studies have been presented in this chapter. The main findings of using bone density measurements are that QCT bone density measurements should not be used to predict screw pullout strength, on the other hand DXA measurements can be used; however all the studies presented were conducted in-vitro, thus avoiding the effect of soft tissues and non-site specific measurements. Screw insertion torque was found to be a better predictor of the screw pullout strength in comparison to bone density measurements; however, it can give erroneous results and should not be used by surgeons as a main parameter to predict the quality of screw fixation but can be used as additional information.

Another parameter on which bone-screw fixation quality depends upon is how well the screw is tightened into the bone to avoid loosening. At present, screws are tightened manually by surgeons and they limit the tightening based on their feel of screw tightening torque and the perception of bone quality. The torque achieved by manual insertion of the screw is significantly close to the thread stripping failure limit, therefore the control of screw tightening torque was proposed by many researcher. A critical review of the investigations done to evaluate the use of screw tightening torque to optimise screw tightening have been presented in this chapter. It was concluded that the use of screw tightening torque could be misleading, especially under in-vivo conditions, therefore

another method involving the control of the screw rotation angle, to optimise screw tightening, is proposed. A background study on the use of screw rotation angle has been presented. The next chapter presents the design of the test rig which was developed as a part of this research.

CHAPTER 7

TEST RIG DESIGN

This chapter presents the design and functional description of the electromechanical test rig developed to achieve the objectives of this research. Initially, the need to design such a test rig and its design concept are presented. This is followed by defining the design criteria and description of the test rig.

7.1   NEED OF A TEST RIG

To accomplish the aims of this research, bone drilling, screw insertion, screw tightening and screw pullout tests have to be conducted in a sequence. To eliminate or have minimal errors caused due to the misalignment of the specimen axis and machine axis, all tests have to be conducted with a single setting of specimen. This can be achieved if all the tests are conducted using a single custom designed machine rather than modifying and using different commercial machines, e.g., using a lathe or conventional drilling machine for drilling and screw insertion testing and using MTS or Instron machine for screw pullout testing. Using different machines would require the test specimen to be realigned in each machine thus, a potential for misalignment. Many studies on screw pullout tests have been reported to validate the use of bone mineral density and screw insertion torque in predicting screw pullout strength and also to study the effect of other factors like, screw design and pilot hole, on screw-bone fixation strength. However, none of these studies have followed the standard testing procedures given in ASTM F543-02 [141] (Standard specification and test methods for metallic medical bone screws), making the results from

different studies incomparable with each other. Furthermore, only a few studies have been reported in the area of bone drilling and in all of these studies the drilling was not conducted under controlled conditions (like, using closed loop control for drilling speed, using bushes while drilling, etc.), thus making it non feasible to compare the results from one study to another. Therefore, a custom designed electromechanical test rig that can perform required tests in series with a single setting of specimen as per ASTM F543-02 standard was designed to get repeatable results.

7.2 CONCEPT DESIGN OF THE ELECTROMECHANICAL TEST RIG

Out of various test rig design concepts investigated initially, a schematic diagram of the final design concept is presented in figure 7.1. The main components of the test rig are;

- **Fixed Outer Frame**: this provides support and rigidity to the test rig,
- **Moveable Inner Frame**: this moves freely in the vertical direction using a guide mechanism,
- **Feed Mechanism**: this is mounted on the fixed outer frame and provides drilling feed rate and screw pullout rate,
- **Drilling and Screw Insertion Mechanism**: this performs the desired operation of drilling and screw insertion,
- **Specimen Mounting Arrangement**: this is mounted on the fixed outer frame and is free to rotate,
- **Counterbalancing Weight**: weight of inner frame is counterbalanced using dead weights to stop it from moving down in vertical direction because of its own weight. This is achieved using a combination of pulley and wire rope,
- **Sensors**: load cells are used to record drilling and screw pullout force and a cantilever beam is used for torque measurement,
- **Tool Holder**: this holds the drill bit, the screw driver bit and the attachment for the screw pullout, and
- **Computer and Electronics Interface**: this allows controlling the test rig and data acquisition using a computer.

The main operations which are performed using the test rig are discussed below, with reference to figure 7.1.

1)   Drilling Operation: desired drilling speed is provided by a drilling motor. A closed loop speed feedback controller is used to maintain constant drilling speed. A chuck is used for holding a drill bit which is mounted on the main shaft. The drilling motor assembly along with the main shaft are mounted on the movable inner frame, which is connected to the feed mechanism though a force sensor. The feed mechanism provides a constant feed to the inner frame and is mounted on the fixed outer frame. A rotary table supported on ball bearings is used to mount the specimen. The rotary movement of the specimen mounting table is restricted using a strain gauged (Wheatstone bridge) cantilever beam; thus giving a measure of the drilling torque. The test rig control and data acquisition are done through a computer.

2)   Screw Insertion or Screw Tightening Operation: during this operation the movable inner frame is disconnected from the feed mechanism. To stop the movable inner frame from moving down because of its own weight, it is counterbalanced by hanging dead weights behind the test rig using a rope and pulley arrangement. A screw is inserted into the drilled hole at a constant speed, using a screw insertion motor. A constant pressure or load on the screw head (as per ASTM F543-02) is maintained by adding extra weight to the inner frame. A strain gauge cantilever beam is used to record the screw insertion or screw tightening torque.

3)   Screw Pullout Operation: once the screw is inserted into the specimen, the inner frame is connected to the feed mechanism through a force sensor. The screw is connected to the inner frame using a screw pullout attachment. A feed mechanism provides a constant screw pullout rate and a force sensor is used to record the screw pullout force.
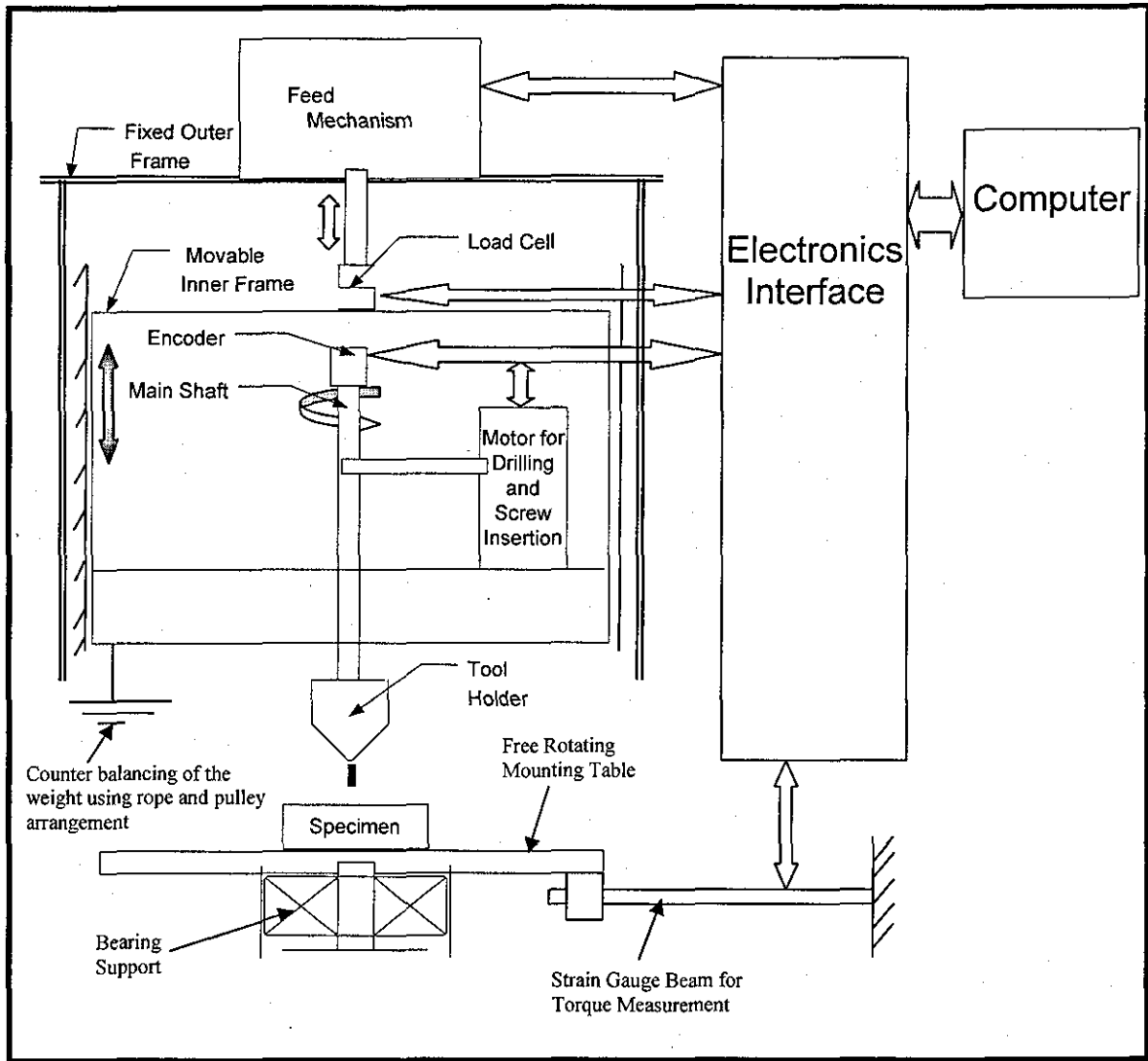
Figure 7.1 Schematic Diagram of the Electromechanical Test Rig

7.3   ESTABLISHING DESIGN CRITERIA OF THE TEST RIG

To design a test rig, an approximate range of the design parameters should be known. These parameters along with their application in designing the test rig are given in table 7.1, 7.2 and 7.3.

Table 7.1   Design Parameters Involved During Drilling Operation

S.No.	Design Parameter	Application of the Design Parameter
1	Feed Rate Range (mm/min)	This helps in designing or selecting of motor, lead screw and gear box for the feed mechanism.
2	Rotational speed (rpm)	This helps in designing or selecting of drilling motor, bearings, encoder and main shaft.
3	Maximum Thickness of the Specimen to be Used (mm)	This helps in determining the height of the test rig and also the maximum travel of the feed mechanism.
4	Drilling Force (N)	This helps in designing or selecting of force sensor, lead screw, lead screw motor and size of the inner and outer frame.
5	Drilling Torque (N.m)	This helps in designing the main shaft and torque sensor cantilever beam.

Table 7.2   Design Parameters Involved During Screw Insertion and Screw Tightening Operation

S.No.	Design Parameter	Application of the Design Parameter
1	Screw Insertion Speed (rpm)	This helps in designing or selecting of screw insertion motor, encoder and gear box.
2	Screw Insertion and Screw Tightening Torque (N.m)	This helps in designing or selecting of torque sensor cantilever beam, screw insertion motor and gear box for the screw insertion mechanism.

Table 7.3 Design Parameters Involved During Screw Pullout Operation

S.No.	Design Parameter	Application of the Design Parameter
1	Screw pullout force (N)	This helps in designing or selecting of force sensor, motor for feed mechanism, lead screw and size of the inner and outer frame.
2	Screw pullout rate (mm/min)	This helps in designing or selecting of feed mechanism motor, lead screw and gear box for the feed mechanism.

7.3.1 Literature Review to Define the Design Criteria for the Drilling Operation

A summary of the review on bone drilling is presented in table 7.4. In this table the range of drilling force and drilling torque along with the value of other test parameters used in the study are presented. The main objective of this review is to identify an approximate range of drilling speed, drilling feed rate, drilling force and drilling torque. Other observations like, (i) type of drill bits used, (ii) type and make of sensors and motors used and (iii) thickness of the specimen used, are also made for each study; however these are not presented in table 7.4 but will help in designing the test rig and experiments.

In addition to the studies presented in table 7.4, other studies have also been conducted in which the drilling force was not recorded; as it was maintained constant to study the effect of other parameters on bone drilling. The magnitude of the drilling force was decided based on the average drilling force value that surgeons would apply during surgery. Such studies are presented below:

- Matthews and Hirsch [162] maintained a constant drilling force of 20 N, 60 N and 120 N while drilling the human cadaver femur diaphysis with a ϕ3.2 mm diameter drill bit.

- Abouzgia and James [17] applied a constant force in the range of 1.5 to 9 N while drilling the bovine femur mid diaphysis cortical bone with a surgical drill bit of ϕ2.5 mm diameter.

- Lee *et al* [163] maintained a constant force of 26 N while drilling the pig scapula and skull with a ϕ3 mm diameter drill bit

In a few studies, drilling was done manually and the drilling force was recorded. This simulates the clinical condition. The drilling force ranges found in such studies are presented below:

- Drilling force ranging from 5.98 N to 24.32 N was applied while drilling bovine mandibles cortical bone using a ϕ2.2 mm and ϕ2.4 mm diameter drill bit at 3600 rpm and 7500 rpm [18]

- Drilling force of 57 N, 83 N, 93 N and 130 N was applied by different surgeons while drilling human cadaver femur shaft using a ϕ3.2 mm standard surgical drill bit at 820 rpm [164]

Table 7.4   Summary of Various Studies Conducted on Bone Drilling

Author	Material	Type	Feed Rate (mm/min)	Speed (rpm)	Drill Diameter (mm)	Drilling Force (N)	Drilling Torque (N.m)
Jacob and Berry 1976 [19]	Mature bovine tibia diaphysis	Cortical	50.8	100-2360	3.2	10 - 135	0.012 - 0.159
Saha and Albright 1982 [119]	Bovine mid diaphysis bone	Cortical	120.3	940	6.35	35 - 70	Not measured
Chagneau and Levasseur 1992 [22]	Human femoral head	Cancellous	10	350	4	100	Not measured
Allotta 1996 [129]	Swine femur shaft	Cortical	100	2000	3.5	52	Not measured
Colla and Allotta 1998 [132]	Bone model	Cortical	100	2000	No information given	60	Not measured
Ong and Bouazza-Marouf 1999 [133]	Porcine proximal femur shaft	Whole-bone	90	1000, 1900	2.5	1 - 62	Not measured
Ong and Bouazza-Marouf 1999 [23]	Porcine femur shaft	Cortical	90	1000, 1900	2.5	30 - 70	Not measured
Rolf 2004 [165]	Timber	-	71	1900	3	7 - 20	Not measured
	Foam	Cancellous	92	1000	3	1.5 - 9	
Studies Conducted Using K-Wires							
Shuaib and Hillery 1995 [166]	Human femoral head	Cancellous	40, 60, 80	400, 800, 1200, 1600	2.5	3.5 - 16	0.048 - 0.05
Bouazza-Marouf et al 1996 [167]	Pig proximal femur and femur shaft	Whole-bone	120	3300	2.5	23	Not measured
Piska et al 2002 [168]	Pig femur	Cortical	28	280	3.2	36 - 144	0.038 - 0.062

Conclusions Drawn From the Review Studies Presented on Bone Drilling

The range of design parameters which are presented in table 7.1 are defined in table 7.5. This range is defined based on the review conducted on bone drilling in this section.

Table 7.5   Range of the Design Parameters (Based on the Review of Studies Conducted on Bone Drilling)

S.No.	Design Parameter	Range as Identified from the Literature
1	Feed rate (mm/min)	10 to 120.3
2	Rotational speed (rpm)	100 to 3300
3	Maximum thickness of the specimen used (mm)	70
4	Drilling force (N)	1 to 144
5	Drilling torque (N.m)	0.012 to 0.05

The following observations are also made from the presented studies in table 7.4.

- No single value of feed rate was used in various studies; hence there is no common platform for comparison of the data between two studies.

- No study was conducted according to the ASTM F543-02.

- The drilling speed was not controlled in any of the studies.

- The surgical bone drilling speed range is between 750 rpm to 1250 rpm.

- Surgical drilling machine have a speed of around 820 rpm.

7.3.2 Literature Review to Define the Design Criteria for the Screw Pullout Operation

A summary of the review on screw insertion, screw tightening and screw pullout testing is presented in table 7.6. The main objective of this review is to find the range of screw pullout rate, screw pullout force, screw insertion speed, screw insertion torque and screw tightening torque.

Table 7.6 **Summary of Various Studies Conducted on Screw Insertion and Screw Pullout**

Author	Specimen	Screw Pullout Rate (mm/min)	Screw Insertion Depth (mm)	Screw Specifications (mm)			Screw Pullout Force (N)	Screw Torque (N.m)
				OD	ID	P		
DeCoster et al 1990 [137]	Foam	60	16	3.5	2.0	1.2	580 - 1935	Not measured
			16	4.5	3.2	1.75	690 - 1755	Not measured
Skinner et al 1990 [169]	Human cadaver lumber vertebrae	10	40	3.66	1.7	1.26	417	Not measured
			40	4.94	3.75	1.75	827	Not measured
			40	5.92	4.26	2.53	624	Not measured
			40	6.45	2.85	2.82	1242	Not measured
			40	6.5	5	1.75	1136	Not measured
Okuyama et al 1993 [62]	Human cadaver vertebrae	1	-	7	4	-	1013 - 151	$(0.15 - 0.65)^{SI}$
Stromsoe et al 1993 [50]	Human cadaver femur shaft	60	-	4.5	-	-	600 - 6400	Not measured
Zdeblick et al 1993 [16]	Human cadaver vertebrae	Cyclic loading	-	6.5	-	-	Not measured	$(0.08 - 0.8)SI$
Daftari et al 1994 [2]	Bicortical foam	125	40	6.5	4.2	-	$859 - 1246$	$(0.75 - 1.36)^{SI}$
	Calf vertebrae		40	5.5	4.2	-	$818 - 1866$	$(0.97 - 1.46)^{SI}$
Halvorson et al 1994 [142]	Cadaver human spine	12.7	-	6.5	-	-	$15 - 2044$	Not measured
Asnis et al 1996 [134]	Foam	6	19	4.5	3.0	$(14 - 32)^{TPI}$	$357 - 595$	Not measured
			19	6.4	3.5	$(12 - 24)^{TPI}$	$520 - 780$	
			19	6.4	4.2	$(14 - 32)^{TPI}$	$465 - 815$	
Chapman et al 1996 [135]	Foam	2.0	16	6.5	3.0	2.75	$367 - 1166$	Not measured

List of symbols used in the table
ID = inner diameter of the screw; OD = outer diameter of the screw; P = screw pitch; [SI] = screw insertion torque; - = No information was given in the referred paper; TPI = tooth per inch; [TPI] = screw pitch is given in TPI instead of mm;

Table 7.6 Summary of Various Studies Conducted on Screw Insertion and Screw Pullout (Contd.)

Author	Specimen	Screw Pullout Rate (mm/min)	Screw Insertion Depth (mm)	Screw specifications (mm)			Screw Pullout Force (N)	Screw Torque (N.m)
				OD	ID	P		
Myers et al 1996 [61]	Human vertebrae	Cyclic loading	-	6.5	-	2.85	Not measured	$(0.52 - 1.06)^{SI}$
				7.0	-	3.0		
Hirano et al 1997 [95]	Human vertebrae	1.0	40	6.25	-	-	277 - 723	Not measured
Ronderos et al 1997 [170]	Human vertebrae	15	-	3.5	-	-	344 - 445	Not measured
Heidemann et al 1998 [171]	Wood	-	2	1.5	-	-	180.5 - 223	$(0.078 - 0.133)^{ST}$
	PVC		2	1.5	-	-	329.6 - 355.7	$(0.094 - 0.16)^{ST}$
	Porcine bone		2	1.5	-	-	252.1 - 403.9	$(0.09 - 0.171)^{ST}$
Okuyama et al 2000 [159]	Human patients vertebrae in-vivo	-	40, 45	7.0	-	-	Not measured	$(0.91 - 1.9)^{ST}$
Gausepohl et al 2001 [138]	Foam	50	13	4.0	-	-	97.6 - 112.2	Not measured
			13	3.5	-	-	92.7 - 99.5	
			13	2.7	-	-	70.2 - 79.6	
			13	2.2	-	-	73.2 - 83.2	
			13	1.6	-	-	59.8 - 69	
			13	1.2	-	-	50.5 - 57.7	
	Bovine	50	13	4.0	-	-	109.9 - 156.7	Not measured
			13	3.5	-	-	92.7 - 132.7	
			13	2.7	-	-	64.9 - 101.7	
			13	2.2	-	-	95.5 - 126.9	
			13	1.6	-	-	56.8 - 90.2	
			13	1.2	-	-	42.1 - 62.1	
Oktenoglu et al 2001 [150]	Foam	2.5	10	4.0	2.8	1.65	157.5 - 239.5	$(0.14 - 0.24)^{SI}$
			10	3.5	2.0	0.5	143.1 - 254.1	$(0.10 - 0.22)^{SI}$
			24	5.5	3.5	1.5	741.2 - 1155.6	$(0.74 - 1.10)^{SI}$

List of symbols used in the table
ST = screw tightening torque

Conclusions Drawn From the Review Studies Presented on Screw Insertion and Screw Pullout

The range of design parameters presented in table 7.2 and table 7.3 are summarised in table 7.7 and table 7.8, respectively. The specified ranges are based on the review conducted on screw insertion and screw pullout in this section which are tabulated in table 7.6.

Table 7.7   Range of the Design Parameters (Based on the Review of Studies Conducted on Screw Insertion)

S.No.	Design Parameter	Range as Identified from the Literature
1	Screw insertion speed (rpm)	In all of the studies presented in table 7.6, the screws were inserted manually. However, according to ASTM F543-02 screws should be inserted at a constant speed of 3 rpm.
2	Screw insertion and screw tightening torque (N.m)	0.08 to 1.46 (screw insertion torque) 0.078 to 1.9 (screw tightening torque)

Table 7.8   Range of the Design Parameters (Based on the Review of Studies Conducted on Screw Pullout)

S.No.	Design Parameter	Range as Identified from the Literature
1	Screw pullout force (N)	15 to 6400
2	Screw pullout rate (mm/min)	1 to 125 According to ASTM F543-02 it should be maintained constant at 5 mm/min

The following observations are also made from the presented studies in table 7.6.

- No studies were conducted according to the test conditions specified in the ASTM standard F543-02.

- No bushes were used during both screw insertion and screw pullout testing. Bush ensures the insertion of screw at 90° with respect to the bone surface and it also prevents rupture of the specimen's outer layer during screw pullout. Use of bush is

also specified as one of the requirement in ASTM F543-02 in both screw insertion and screw pullout testing.

- Lag screws are available in length ranging from 70 to 120 mm (Stryker Trauma GmbH). This gives an idea of typical thickness of the human proximal femur bone which will be used to define the maximum specimen thickness that can be tested using the proposed test rig.

7.4   DESCRIPTION AND DESIGN OF THE TEST RIG

The test rig is designed based on the design concept presented in section 7.2 and the design parameters established in tables 7.5, 7.7 and 7.8. The assembly drawing of the designed test rig is given in appendix C. IDEAS software is used for modelling and drafting of the test rig. The softcopy of the IDEAS file containing the solid model, assembly and engineering drawing of the test rig components is copied on to a CD which is attached with this thesis. All engineering drawings are also converted from IDEAS to AutoCAD format because AutoCAD format can be easily used or imported into any engineering drawing software. The AutoCAD drawings are also given in the CD.

The three main test operations performed using test rig are described below. Design calculations of the critical components are also presented.

7.4.1   Drilling Operation

The main components of the test rig involved in the drilling operation are labelled in figure 7.2. A constant feed rate during drilling is provided using the ball screw feed mechanism. An encoder (En_{Lead}) is mounted on the lead screw shaft to record drill bit displacement and feed rate. Ball screw feed mechanism assembly is mounted on the fixed outer frame. A stepper motor (SM_{Feed}) provides the rotary motion to the ball screw. Rotary motion is converted by the ball screw mechanism into a linear motion of the actuator arm. The actuator arm pushes the inner frame through a drilling load cell (LC_{Drill}); thus transferring the feed motion to the inner frame. A drilling load cell is used to record the drilling force profile. The inner frame moves linearly on two linear bearing shafts. The required speed

for drilling is provided by a DC servo motor, which is part of the drilling motor assembly mounted on the inner frame. A tachometer is used to provide speed feedback to control the drilling speed. The drilling motor shaft is attached to the main shaft which encompasses a chuck at the free end. The weight of the inner frame is counter balanced. The specimen to be drilled is mounted on a plate which is part of the specimen mounting assembly. The specimen mounting assembly is free to rotate on the ball bearings and its rotation is restricted using a torque sensing cantilever beam. The two limit switches, upper and lower, limit the linear movement of the inner frame for safety purposes. Drill bushes are used to ensure that the drill bit is driven into the specimen at an angle of 90 degree.

According to the range of design parameters given in table 7.5, the maximum drilling feed rate used in the literature is 120.3 mm/min. There is no standard which defines the optimum value of the feed rate, as the drilling of bone is done manually. In this research the maximum value of the drilling feed rate chosen is 250 mm/min. This is based on the assumption that surgeons take approximately 15 seconds to drill the proximal femur bone whose thickness is approximately 70 mm. Therefore, to achieve a feed rate of 250 mm/min, the required rotational speed of the ball screw ($(\text{rpm})_{\text{Ball\_Sc.}}$, rev/min) can be calculated as,

$$(\text{rpm})_{\text{Ball\_Sc.}} = \frac{f_{\text{Drill}}}{L_{\text{Ball\_Sc.}}} \tag{7.1}$$

where, $(\text{rpm})_{\text{Ball\_Sc.}}$ = rotational speed of the ball screw (rev/min)

f_{Drill} = drill feed rate (mm/min)

$L_{\text{Ball\_Sc.}}$ = Lead of ball screw (mm/rotation)

Substituting the value of f_{Drill} = 250 mm/min and $L_{\text{Ball\_Sc.}}$ = 2.54 mm/rotation in equation 7.1, we get

$$(\text{rpm})_{\text{Ball\_Sc.}} = \frac{250\,(\text{mm/min})}{2.54\,(\text{mm/rotation})} = 98.4\,\text{rev/min} \tag{7.2}$$
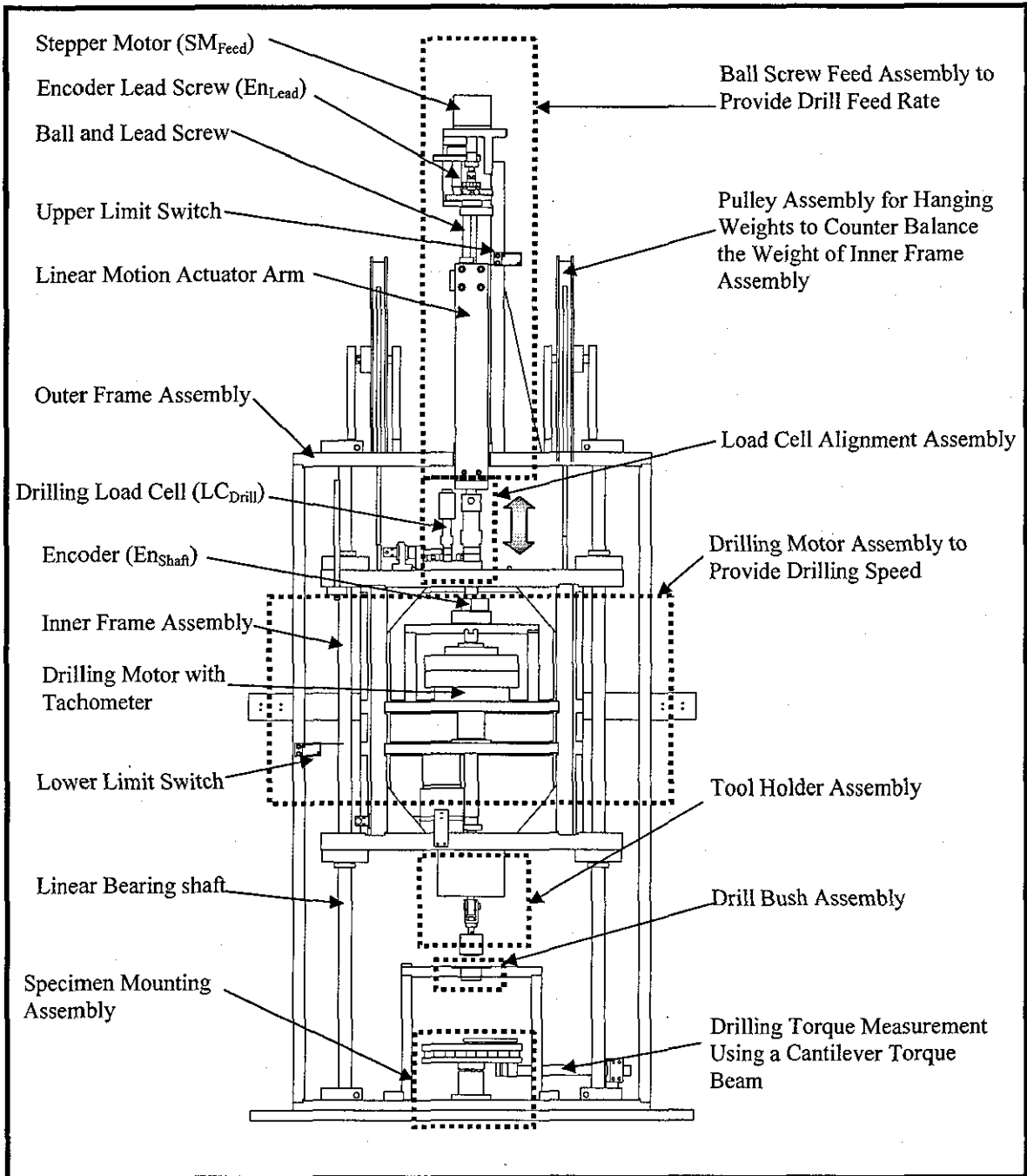
Figure 7.2 Test Rig Components Used During Drilling Operation

The ball screw is directly connected to the stepper motor shaft through a coupling (shown in figure 7.3); therefore the rotational speed of the stepper motor shaft is the same as that of ball screw. The stepper motor drive board is configured to run in full step mode, i.e., there are 200 steps or pulses in one revolution of the stepper motor shaft. The frequency (f_{Hz}, Hz) value which should be supplied to the control board to get 98.4 rev/min can be calculated as,

$$f_{Hz} = \frac{(rpm)_{SM_{Feed}}}{60} \times SM_{Step}$$ (7.3)

where, f_{Hz} = frequency supplied to the control board (Hz)

$(rpm)_{SM_{Feed}}$ = rotational speed of feed stepper motor shaft (rev/min)
= $(rpm)_{Ball\_Sc.}$ = 98.4 rev/min

SM_{Step} = number of steps per revolution of stepper motor shaft (steps/rev)
= 200 steps/rev

Substituting the above values in equation 7.3, we get

$$f_{Hz} = \frac{98.4}{60}(rev/sec) \times 200(steps/rev) = 328 \text{ Hz}$$ (7.4)

The graph of the stepper motor (SM_{Feed}) torque performance, provided by the manufacturer, shows that the stepper motor can deliver a significantly consistent torque of 340 mN.m up to 400 Hz. Hence, the torque requirement for drilling operations should be less than 340 mN.m at 98.4 rev/min.

Drilling Configuration: The stepper motor is directly connected to the ball screw using an Oldham coupling, shown with solid line. Gear Z = 20, is not connected to gear Z = 70. The torque from the motor shaft is directly transferred to the ball screw.

Screw Pullout Configuration: The two coupling ends are disconnected by changing the position of the gear shifter. Gear Z = 20 is connected to gear Z = 70, shown with dotted line. The torque from the motor shaft is transferred to the ball screw through two gear pairs, Z = 20 & Z=70 and Z = 9 & Z = 80.

Figure 7.3 Schematic Diagram Illustrating Gear Shifting Mechanism used for Drilling and Screw Pullout Configuration in Feed Mechanism

From table 7.5, the maximum drilling force value found in the literature is 144 N. Lets take a factor of safety of 2.5 and calculate the required torque at the stepper motor shaft, for a drilling force of 400 N. The efficiency (η_{bs}) of the ball screw is assumed 80%. Therefore,

$$\eta_{bs} T_{SM_{Feed}} \theta_{SM_{Feed}} = F_d \cdot x \tag{7.5}$$

where,　　η_{bs} = efficiency of ball screw = 80 %

$T_{SM_{Feed}}$ = torque at feed stepper motor (SM_{Feed}) shaft (N.m)

$\theta_{SM_{Feed}}$ = rotational displacement of stepper motor (SM_{Feed}) shaft (radians)

F_d = drilling force (N)

x = linear displacement of the ball screw (mm)

For one revolution of the ball screw, i.e., for $\theta_{SM_{Feed}} = 2\pi$, the linear displacement of the ball screw (x) is equal to the lead of the ball screw, i.e., 2.54 mm. Substituting the value of variables in equation 7.5, we get

$$0.8 \times T_{SM_{Feed}} \times 2\pi = 400(N) \times 2.54(mm) \tag{7.6}$$

$$\therefore T_{SM_{Feed}} = \frac{400\,(N) \times 2.54\,(mm)}{0.8 \times 2\pi} = 202\ mN.m \tag{7.7}$$

$T_{SM_{Feed}}$ = 202 mN.m is well below the maximum torque value (340 mN.m) which can be provided by the motor at 250 mm/min feed rate. Before mounting the stepper motor on the test rig, the maximum value of the stepper motor torque was checked experimentally using a pulley and weights to provide the torque. It was found that the motor torque was above the required value of 202 mN.m up to 500 Hz.

The maximum torque (4.89 N.m at a rated speed of 3000 rpm) and the maximum speed (6000 rpm) which can be delivered by the DC servo motor and its controller, used to provide the drilling torque and the drilling speed, is significantly above the maximum expected drilling torque (approximately 0.05 N.m) and maximum drilling speed used in the literature (3300 rpm). Furthermore, the maximum drilling speed is also within the upper limit (30,000 rpm.) of the encoder coupled to the end of the drilling motor shaft (En_{Shaft}).

7.4.2   Screw Insertion and Screw Tightening Operation

The main components of the test rig involved in the screw insertion or screw tightening test operation are highlighted in figure 7.4. The inner frame is disconnected from the ball screw mechanism assembly and is free to move in the vertical direction on linear bearing shafts. As stated previously, the vertical movement of the inner frame is controlled by counterbalancing its weight using wire rope and pulley arrangement. A chuck attached to the main shaft is used to hold the screw driver bit. To have a constant engagement of the screw driver bit into the screw, a constant pressure on the screw head has to be applied by the screw driver bit. As the chuck moves with the inner frame therefore, a weight added on to the inner frame will apply a constant load on the screw head. A constant load of 1.14 Kgf has been used in accordance with the ASTM F543-02 [172]. A stepper motor (SM_{Sc_Ins}) provides the driving torque for screw insertion or screw tightening. The screw insertion mechanism assembly is engaged with the main shaft using a gear pair, as shown in figure 7.5. For safety purposes, a limit switch and an opto-switch are used, which ensure that the drilling servo motor is not powered when the screw insertion mechanism assembly is engaged with the main shaft. This ensures that both motors, i.e., screw insertion stepper motor (SM_{Sc_Ins}) and drilling servo motor are never switched on at the same time. The encoder on the main shaft is used to record and control the screw rotation angle. Similar to the drilling operation, the specimen is mounted on the specimen mounting assembly. Screw insertion and screw tightening torques are recorded using the torque sensing cantilever beam. Bushing for the screw is used during screw insertion into the predrilled hole.
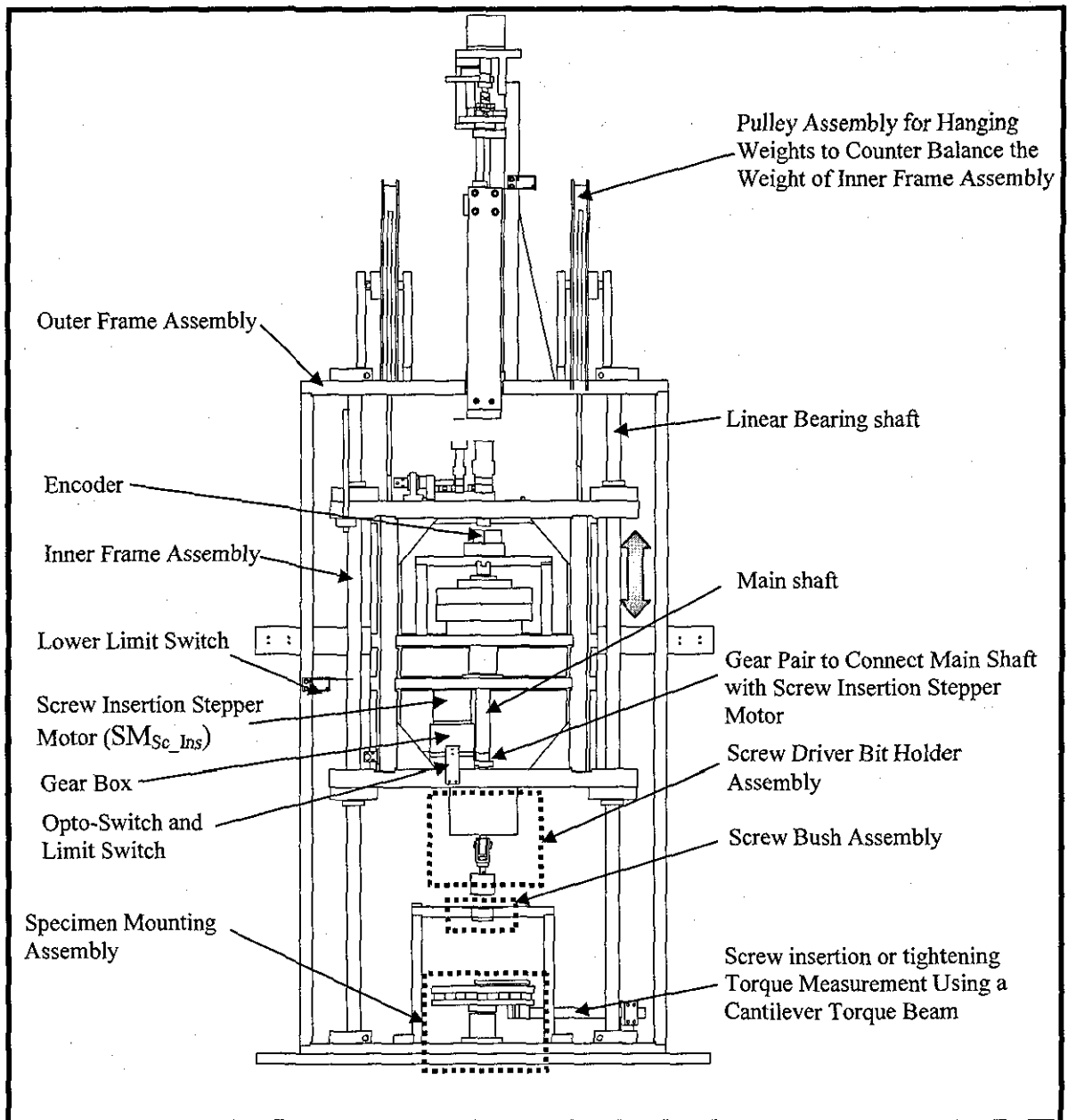
Figure 7.4 Test Rig Components Used During Screw Insertion or Screw Tightening Operation
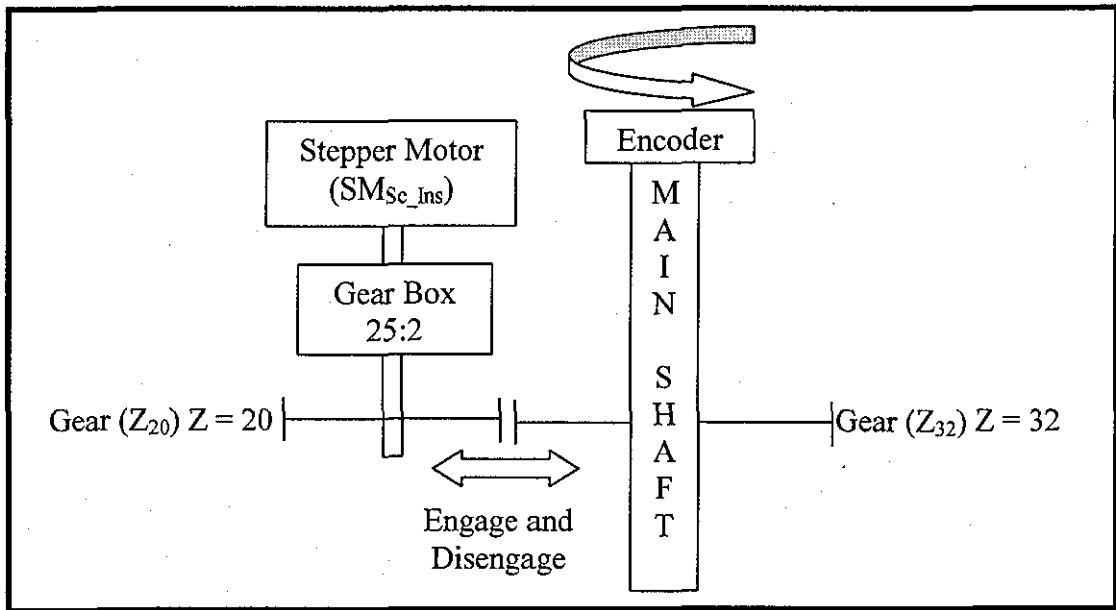
Figure 7.5 Schematic Diagram of the Screw Insertion Mechanism Assembly

The screw insertion speed should be maintained at 3 rpm (refer to table 7.7 for design criteria). However, the calculations are performed for 10 rpm to have an increased speed range for future tests.

$$\therefore (\text{rpm})_{\text{shaft}} = \text{screw insertion speed} = 10 \text{ rpm} \tag{7.8}$$

where, $(\text{rpm})_{\text{shaft}}$ = rotational speed of main shaft, as shown in figure 7.5.

There is a two step reduction of speed from the stepper motor shaft to the main shaft. First, a reduction of 12.5 is through a reduction gear box on which the motor is mounted. Second, a reduction of 1.6 is through a pair of spur gears, as shown in figure 7.5.

$$\therefore \text{Total reduction in speed (gr)} = 12.5 \times 1.6 = 20 \tag{7.9}$$

$$(\text{rpm})_{SM_{Sc\_Ins}} = (\text{rpm})_{\text{shaft}} \times \text{gr} \tag{7.10}$$

where, $(\text{rpm})_{SM_{Sc\_Ins}}$ = rotational speed of the screw insertion stepper motor (SM_{Sc_Ins})
(rev/min)

$$\therefore \ (\text{rpm})_{SM_{Sc\_Ins}} = 10 \, (\text{rev/min}) \times 20 = 200 \, \text{rev/min} \tag{7.11}$$

In full step mode, the frequency (f_{Hz}) value which should be supplied to the control board to get 200 rev/min can be calculated as,

$$f_{Hz} = \frac{(rpm)_{SM_{Sc\_Ins}}}{60} \times SM_{Step} \qquad (7.12)$$

Substituting the values in equation 7.12, we get

$$f_{Hz} = \frac{200}{60}(rev/sec) \times 200(steps/rev) = 667\,Hz \qquad (7.13)$$

The graph of the screw insertion stepper motor (SM_{Sc_Ins}) torque performance, provided by the manufacturer, shows that the stepper motor can deliver a significantly consistent torque of 360 mN.m up to 700 Hz. Hence, the torque requirement for screw insertion or screw tightening operations should be less than 360 mN.m at 200 rev/min.

From table 7.7, the maximum expected torque at the main shaft is 1.9 N.m. Therefore, to get 1.9 N.m torque at the main shaft, the torque at the screw insertion stepper motor shaft can be calculated as,

$$T_{SM_{Sc\_Ins}} = \frac{T_{Shaft}}{gr \times \eta_{sg} \times \eta_{gb}} \qquad (7.14)$$

where, $T_{SM_{Sc\_Ins}}$ = torque at screw insertion stepper motor shaft (N.m)

η_{sg} = efficiency of spur gear $\cong$ 80 %

η_{gb} = efficiency of reduction gear box $\cong$ 70 %

$$\therefore T_{SM_{Sc\_Ins}} = \frac{1.9\,(N.m) \times 1000}{20 \times 0.8 \times 0.7} = 170\,mN.m \qquad (7.15)$$

Hence, the stepper motor torque and speed requirements are well within its specifications.

7.4.3   Screw Pullout Operation

The main components of the test rig involved in the screw pullout test operation are highlighted in figure 7.6. The inner frame assembly is connected to the ball screw feed assembly through screw pullout load cell ($LC_{Pullout}$). The ball screw feed mechanism

assembly is changed to the screw pullout configuration, as shown in figure 7.3. The drilling load cell is replaced by the screw pullout load cell, which connects the ball screw assembly to the inner frame assembly. The screw (which is inserted into the specimen) is connected to the screw pullout attachment assembly and is pullout out at the required pullout rate. The screw pullout attachment assembly is mounted on the inner frame.

According to ASTM F543-02, the screw pullout rate should be maintained constant at 5 mm/min. Therefore, to achieve a screw pullout rate of 5 mm/min, the required rotational speed of the ball screw ($(rpm)_{Ball\_Sc.}$, rev/min) can be calculated as,

$$(rpm)_{Ball\_Sc.} = \frac{f_{Pullout}}{L_{Ball\_Sc.}} \qquad (7.16)$$

where, $\qquad f_{Pullout}$ = screw pullout rate (mm/min)

Substituting the value of $f_{Pullout}$ = 5 mm/min and $L_{Ball\_Sc.}$ = 2.54 mm/rotation in equation 7.16, we get

$$(rpm)_{Ball\_Sc.} = \frac{5\,(mm/min)}{2.54\,(mm/rotation)} = 1.97\,rev/min \qquad (7.17)$$

The ball screw is connected to the feed stepper motor shaft (SM_{Feed}) through two gear pairs, Z_{20} & Z_{70} and Z_9 & Z_{80}, as shown in the screw pullout configuration in figure 7.3. Therefore, the rotational speed of feed stepper motor shaft ($(rpm)_{SM_{Feed}}$) can be calculated as,

$$(rpm)_{SM_{Feed}} = (rpm)_{Ball\_Sc.} \times \frac{Z_{80}}{Z_9} \times \frac{Z_{70}}{Z_{20}} \qquad (7.18)$$

where, $\qquad Z_{80}$ = numbers of teeth in the gear having 80 teeth

$\qquad Z_9$ = numbers of teeth in the gear having 9 teeth

$\qquad Z_{70}$ = numbers of teeth in the gear having 70 teeth

$\qquad Z_{20}$ = numbers of teeth in the gear having 20 teeth

$$\therefore (rpm)_{SM_{Feed}} = 1.97\,(rev/min) \times \frac{80}{9} \times \frac{70}{20} = 61.3\,rev/min \qquad (7.19)$$
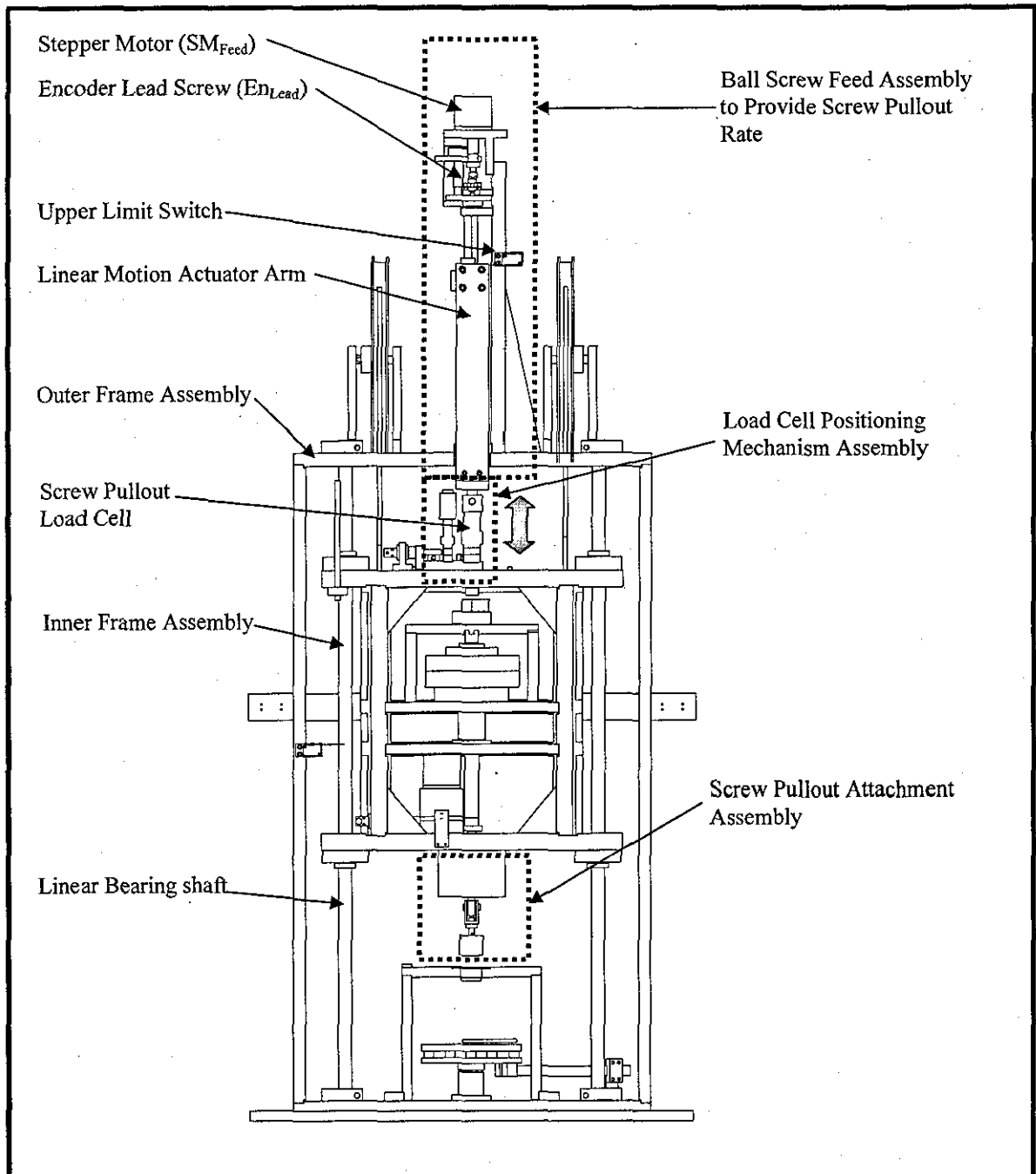
Figure 7.6 Test Rig Components Used During Screw Pullout Operation

The stepper motor drive board is configured to run in full step mode, i.e., there are 200 steps or pulses in one revolution (SM_{Step}) of the stepper motor shaft. The frequency (f_{Hz}) value which should be supplied to the control board to get 61.3 rev/min can be calculated as,

$$f_{Hz} = \frac{(rpm)_{SM_{Feed}}}{60} \times SM_{Step} = \frac{61.3}{60}(rev/sec) \times 200\,(steps/rev) = 204.2\,Hz \qquad (7.20)$$

The graph of the stepper motor (SM_{Feed}) torque performance, provided by the manufacturer, shows that the stepper motor can deliver a significantly consistent torque of 340 mN.m up to 400 Hz. Hence, the torque requirement for screw pullout operations should be less than 340 mN.m at 61.3 rev/min.

From table 7.8, the maximum screw pullout force value found in the literature is 6400 N. Lets take a factor of safety of 1.25 and calculate the required torque at the stepper motor shaft, for a screw pullout force of 8000 N. The torque at ball screw (T_{bs}, N.m) can be calculated as,

$$T_{bs} = \frac{F_{SPF} \cdot x}{\eta_{bs} \times \theta_{SM_{Feed}}} \qquad (7.21)$$

where, T_{bs} = torque at the ball screw (N.m)

F_{SPF} = screw pullout force (N)

For one revolution of the ball screw, i.e., for $\theta_{SM_{Feed}} = 2\pi$, the linear displacement of the ball screw (x) is equal to the lead of the ball screw, i.e., 2.54 mm

Substituting the value of variables in equation 7.21, we get

$$\therefore T_{bs} = \frac{8000\,(N) \times 2.54\,(mm)}{0.8 \times 2\pi} = 4040.9\,mN.m \qquad (7.22)$$

The torque at the feed stepper motor shaft ($T_{SM_{Feed}}$) can be calculated as,

$$T_{SM_{Feed}} = T_{bs} \times \left(\frac{Z_9}{Z_{80}} \times \frac{1}{\eta_{sg}} \right) \times \left(\frac{Z_{20}}{Z_{70}} \times \frac{1}{\eta_{sg}} \right) \qquad (7.23)$$

Substituting the value of variables in equation 7.23, we get

$$T_{SM_{Feed}} = 4040.9\,(mN-m) \times \left(\frac{9}{80} \times \frac{1}{80} \right) \times \left(\frac{20}{70} \times \frac{1}{80} \right) = 202.9\,mN.m \qquad (7.24)$$

$T_{SM_{Feed}}$ = 202.9 mN.m is well below the maximum torque value (340 mN.m) which can be provided by the motor at 5 mm/min screw pullout rate.

7.5   DESCRIPTION OF TEST RIG ELECTRONICS

The location of sensors and other electronic components on the test rig are shown in figure 7.7. A microcontroller PIC18F6620 from Microchip is used for interfacing the test rig with the computer. Visual basic programs written to control the test rig and to acquire data are given in CD attached with this thesis. A complete electronics control system diagram is shown in figure 7.8. A 12-bit, eight channel data acquisition system is used for data acquisition.

A picture of the final test rig after commissioning is shown in figure 7.9.
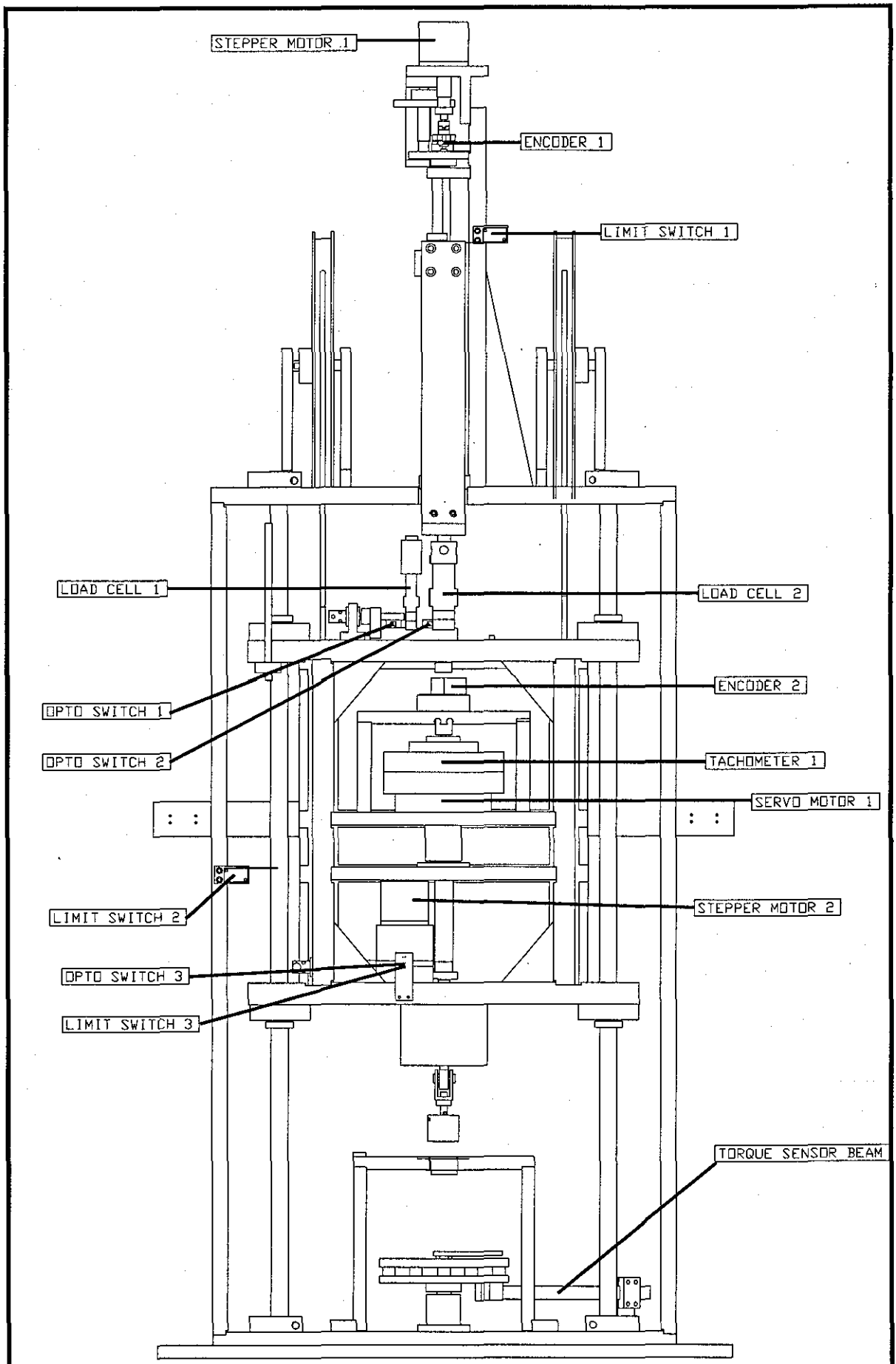
Figure 7.7 Locations of Sensors and Electronic Components on the Test Rig
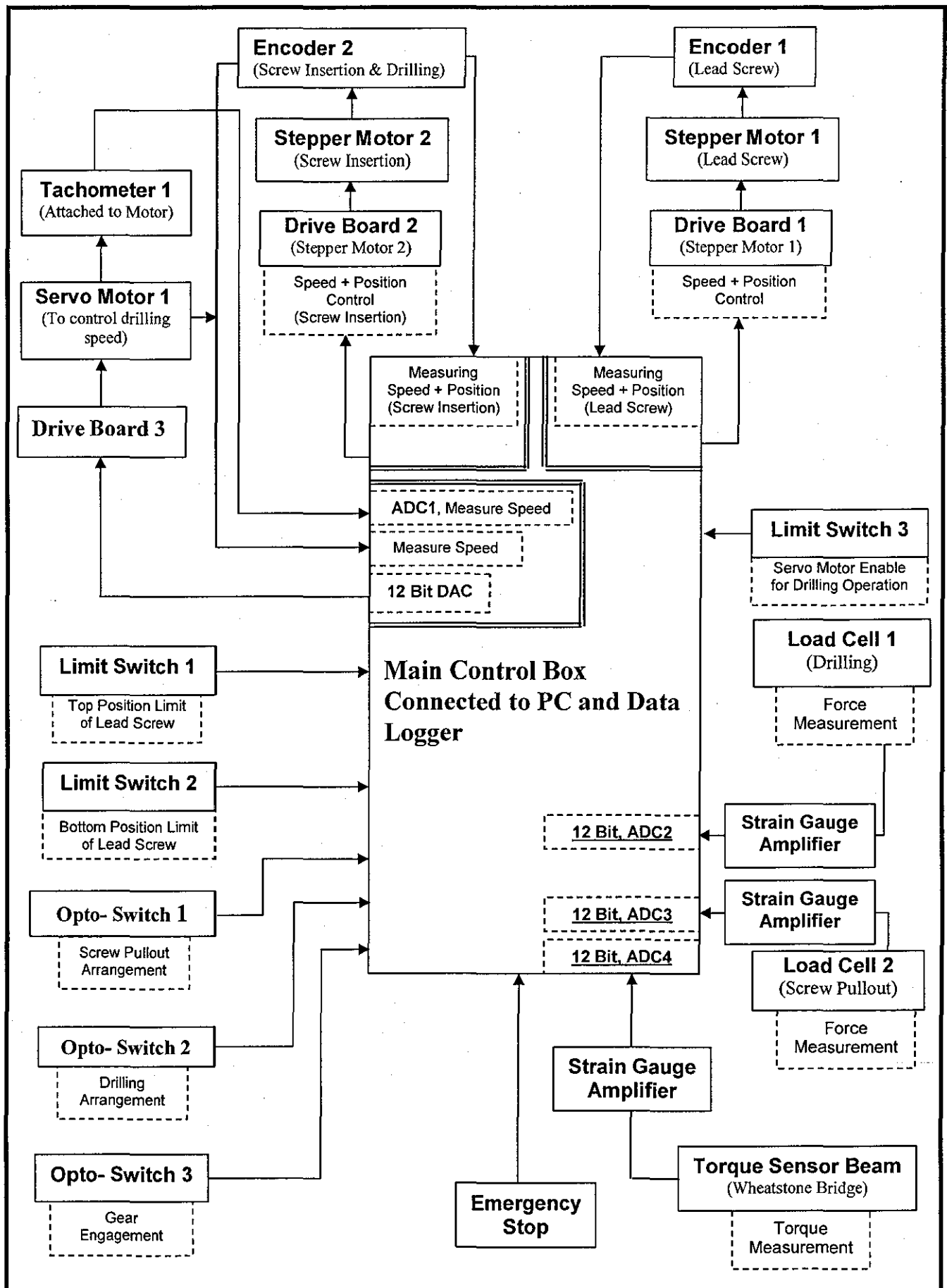
Figure 7.8 Electronics Control System Diagram of Test Rig
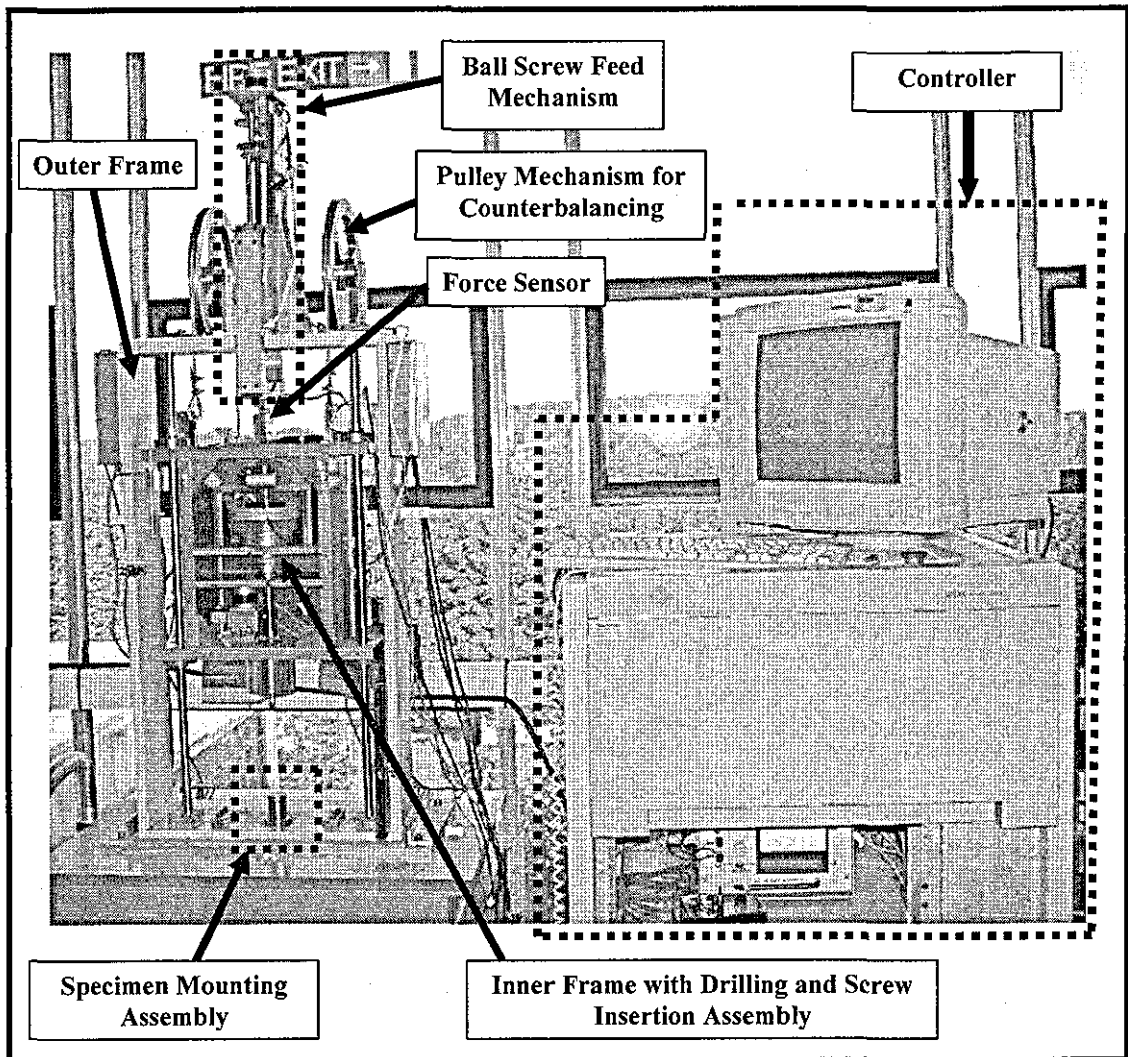
Figure 7.9 Picture of the Commissioned Test Rig

7.6 TEST RIG MAXIMUM MEASUREMENT ERRORS

The measurement errors of the designed test rig are presented in this section.

7.6.1 Drill Force Measurement Error

Based on the maximum magnitude of the drilling force to be recorded, data given in table 7.5, two load cells of 100 N and 800 N capacities were purchased. To have higher accuracy and sensitivity, the lower capacity load cell is used to record the drilling force of cancellous and osteoporotic bone. The maximum error of the drilling force measurement depends upon the inherent noise of the complete data acquisition system, which includes

sensor, amplifier, and ADC data acquisition board and external noise. Hence, to measure the overall noise level of the drilling force measurement, the drilling force data was recorded when the test rig was operated in the drilling configuration but without actually drilling a specimen. The overall noise level of the 100 N load cell was recorded as 0.089 N and the overall noise level of the 800 N load cell was recorded as 0.284 N.

7.6.2 Screw Pullout Force Measurement Error

Based on the maximum magnitude of the screw pullout force to be recorded, as given in table 7.8, a load cell of 8000 N capacity was purchased. The overall inherent noise level of the screw pullout force measurement was found in the similar way the noise level of the drilling force was determined. The overall noise level of the screw pullout force found, while the test rig was operated in the screw pullout configuration, was 4N.

7.6.3 Minimum Measurement of Drill Bit Displacement

To measure the displacement of the drill bit during drilling operation, an encoder (En_{Lead}) of resolution of 500 pulses per revolution was used. The resolution of the encoder was increased from 500 pulses per revolution to 2000 pulses per revolution through electronic quadrature. Therefore the minimum drill bit displacement, x_{min}, which can be measured is derived from the minimum number of pulses, n_{pmin}, which can be recorded (i.e. 1 pulse).

The ball screw used has a lead of 2.54 mm (per revolution), hence,

$$x_{min} = \frac{2.54}{2000} = 0.00127 \text{ mm}$$

7.6.4 Minimum Measurement of the Screw Rotation Angle

To measure the screw rotation angle, an encoder (En_{Shaft}) of resolution of 500 pulses per revolution was used. The resolution of the encoder was increased from 500 pulses per revolution to 2000 pulse per revolution through electronic quadrature. The minimum screw rotation angle, θ_{min}, which can be measured is derived from the minimum number of pulses, n_{pmin}, which can be recorded (i.e. 1 pulse). Therefore,

$\theta_{min} = 360/2000 = 0.18$ degree

7.7   CONCLUDING REMARKS

The design and functional description of the electromechanical test rig developed to achieve the objectives of this research has been presented. The designed test rig can perform drilling, screw insertion, screw removal and screw pullout tests, according to the standard test procedures described in ASTM F543-02 with a single setting of specimen. Various design variables for the different test operations have been identified and based on that, the design criteria for the test rig was established. The final conceptual design, operational description and critical design calculations of the test rig have been presented. An IDEAS software was used for modelling and drafting of the designed test rig. A computer was interfaced with the test rig for control and data acquisition. The test rig was successfully commissioned with a noise level of 0.089 N for the drilling force, 4 N for the screw pullout force and a least count of 0.00127 mm for the drill bit displacement and 0.18 degree for the screw rotation angle. The next chapter presents the description and results of experiments conducted on the synthetic bone material.

CHAPTER 8

TESTING OF SYNTHETIC BONE MATERIAL

Polyurethane foam was used as a synthetic bone material for initial testing in this research. It is a homogenous material and thus it would give repeatable results. Another advantage of using foam is that it is inexpensive and easily available for a complete range of cancellous and osteoporotic bone density. Foam also facilitates uncontaminated and clean test environment that is not possible in bone testing. According to the American Society for Testing and Materials Standard (ASTM) F1839-97 [173] (Standard specification for rigid polyurethane foam for use as a standard material for testing orthopaedic devices and instruments), foam can be used as an alternative material for bone testing when the material properties of the foam are uniform and within an approximate range of the human bone. Therefore, the selection criteria of suitable foam material for testing are presented in this chapter. Following this, the results obtained from the experiments conducted on the foam are presented and discussed.

8.1   SELECTION OF THE FOAM MATERIAL

The details of the foam material used by other researchers are presented in table 8.1. The table also provides the type of the respective bone the foam is used to stimulate.

Table 8.1   Details of the Foam Material used in the Published Research Studies

Source	Foam Company	Foam Model	Foam Density (g/cm³)	Type of Bone
Chapman *et al* 1992 [174]	General Plastics, USA	R-9315	0.04	Cancellous
			0.23	
			0.29	
Daftari *et al* 1994 [2]	Pacific Research, USA (Used foam representing bi-cortical bone. Sandwiched polyurethane foam between top and bottom layer of fiberglass epoxy laminates stimulating cortical bone)	Foam	0.141	Cancellous
		Fiberglass epoxy	No Information	Cortical
Asnis *et al* 1996 [134]	Pedilen, Ottobock, USA	Pedilen	0.15	Cancellous
			0.22	
Chapman *et al* 1996 [135]	General Plastics, USA	FR-3710	0.16	Cancellous
		FR-3715	0.24	
		FR-3720	0.32	
Gausepohl *et al* 2001 [138]	Bayer, Germany	Foam	1.6	Cortical
Koistinen *et al* 2003 [156]	No information of the company was given. Used Teflon (polytetrafluoroethylene)	Teflon	2.2	Cortical
Hou *et al* 2004 [175]	Bayer, Germany	Cylindrical tube	0.25	Cancellous
			0.5	
Hsu *et al* 2005 [147]	Pacific Research, USA	Foam	0.32	Cancellous
		Foam	0.16	

The foam material to be used for testing should have similar material properties to human bone. These are specified in the ASTM F1839-97 [173] and given in table 8.2.

Table 8.2   Foam Properties, as per ASTM F1839-97 [173], for use as Alternate Material to Bone

Grade	Density Range (lbs/ft³)	Density Range (g/cm³)	Compressive Strength (MPa)	Compressive Modulus (MPa)	Shear Strength (MPa)	Shear Modulus (MPa)
10	9 -11	0.1442 – 0.1762	2.095 – 2.895	56.3-76.7	1.660-2.170	20.82-27.68
12	11 - 13	0.1762-0.2082	2.895 – 3.790	76.7-99.2	2.17 – 2.725	27.68-35.10
15	14 – 16	0.2243-0.2583	4.280 – 5.315	111.2-136.65	3.000-3.620	39.00-47.13
20	19 – 21	0.3044-0.3364	7.000 – 8.245	178.1-207.8	4.580-5.276	60.16-69.40
40	39 - 41	0.6247-0.6568	22.41 – 24.300	539.6-582.8	12.34-13.24	167.17-179.47

Among the various foam manufacturing companies given in table 8.1, foam samples were purchased from General Plastics, USA as their material properties are in accordance with the required property given in table 8.2.

It can also be observed from table 8.1 that no research has been conducted in which the used foam samples cover a good range of the cancellous bone density. The human cancellous bone density ranges from 0.09 g/cm^3 to 1.26 g/cm^3 [30, 176] and cortical bone density ranges from 1.8 g/cm^3 to 2.0 g/cm^3 [30, 176]. Bone strength evaluation of the cancellous bone is more important than the cortical bone because it is the cancellous bone which is affected by osteoporosis. The foam samples purchased for this research cover the density range from 0.0481 g/cm^3 to 0.6407 g/cm^3. This range covers the low and medium density of the cancellous bone.

It is also important to decide on how many different densities of foam are required within the chosen density range, in order for the results to be statistically significant. The main objectives of doing experiments on foam are to conduct correlational studies. For any correlation study to be statistically significant, the minimum number of sample size required can be calculated using the equation given below [177]:

$$n = 3 + \frac{4C_c}{\left[\ln\left(\frac{1+r_n}{1-r_n} \times \frac{1-r_a}{1+r_a}\right)\right]^2} \qquad (8.1)$$

where, n = number of foam samples required of different densities,

C_c = constant that depends on the values chosen for α and β,

α = probability of detecting a false effect,

β = probability of detecting a true effect (or power of the experiment),

r_n = correlation coefficient under the null hypothesis and

r_a = correlation coefficient under the alternative hypothesis.

$$C_c = \left(z_{\alpha/2} + z_{(1-\beta)}\right)^2 \qquad (8.2)$$

where, $z_{\alpha/2}$ = is the upper $\alpha/2$ critical value of the standard normal distribution which is found in the table of the standard normal distribution

$z_{(1-\beta)}$ = is the upper $(1-\beta)$ critical value of the standard normal distribution which is found in the table of the standard normal distribution

For research experiments,

$\alpha = 5\%$ $\qquad (8.3)$

$\beta = 80\%$ $\qquad (8.4)$

For $\alpha/2 = 0.025$, $z_{\alpha/2}$ from the table of standard normal distribution [178] is,

$z_{\alpha/2} = 1.96$ $\qquad (8.5)$

Similarly,

For $(1-\beta) = 0.2$, $z_{(1-\beta)}$ from the table of standard normal distribution [178] is,

$z_{(1-\beta)} = 0.841$ $\qquad (8.6)$

$$\therefore C_c = \left(z_{\alpha/2} + z_{(1-\beta)}\right)^2 = (1.96 + 0.841)^2 = 7.85 \qquad (8.7)$$

To calculate number of samples, an assumption has to be made on the expected correlation coefficient value between the variables under study. As foam is a homogeneous material and testing is done under controlled conditions; therefore a significantly strong relationship between the variables is expected, which is also seen in

the study conducted by Chapman *et al* 1996 [135]. Hence, let us assume the expected value of correlation coefficient (r_a) to be higher than 0.9. In case the value of correlation coefficient found after doing the experiments is less than 0.9, then the sample size will need to be recalculated.

The value of r_n, in equation 8.1, is taken as zero because null hypothesis means there is no relationship between the variables under comparison. Substituting the value of C_c, r_n and r_a in equation 8.1, we get

$$n = 3 + \frac{4 \times 7.85}{\left[\ln\left(\frac{1+0}{1-0} \times \frac{1-0.9}{1+0.9} \right) \right]^2} = 6.6 \qquad (8.8)$$

Therefore, we would need foam material of at least seven different densities for the results to be statistically significant.

Two different types of foam material, General Plastics FR-6700 series foam and FR-3700 series foam, with more than seven different densities from each series have been used. Various experiments conducted on these foam samples are presented in the following sections.

8.2 TO FIND A RELATIONSHIP BETWEEN DRILLING FORCE AND SYNTHETIC BONE MATERIAL STRENGTH

8.2.1 Aims

1. To investigate if drilling force can estimate the strength of the foam material.

Drilling involves shearing of material; therefore shear strength of the foam is used as the material property to find the correlation.

2. To investigate if drilling force be used to estimate the difference in strength in materials having the same densities.

As discussed in chapter 3, the prediction of bone strength using bone density measurements can be inaccurate because two different materials having the same density can have different strengths. Therefore, test will be conducted to investigate if the difference in the material strength (of materials having the same densities) could be predicted by analysing drilling force data. For this

investigation two different series of foam (FR-3700 and FR-6700) which have the same densities but different material properties are used.

8.2.2   Material Used

The details of various foam densities tested in both FR-3700 and FR-6700 series foam are given in table 8.4 and table 8.5, respectively.

An industrial drill bit of Dormer make was used for drilling foam specimens. The specification of the drill bit is given in figure 8.1. Industrial drill bits were used because they are inexpensive and easily available as compared to surgical drill bits. Although surgical drill bits would give a better drilling performance, like lower drilling temperature, less cutting force, etc., however the aim of this study is not to enhance the drilling performance but to compare the drilling forces recorded for different foam material. Such a comparison can be done by maintaining the same type and make of drill bit throughout the experiments irrespective of the drill bit performance.

Drill bits of $\phi 2.5$ mm were used because the same drilled holes are also used as the pilot holes for the screws used in screw pullout testing, in section 8.3.

Chisel Edge Thickness 0.7 mm

Point Angle 118°

Helix Angle 28.28°

Flute Length 80 mm

$\phi 2.5$

Overall Length 125 mm
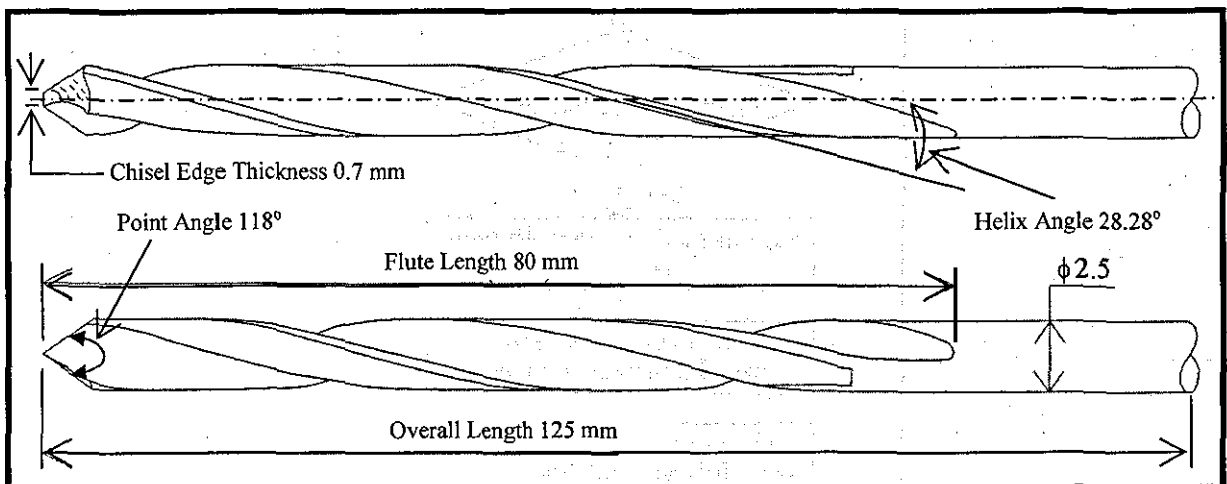
Figure 8.1 Specification of the Industrial Drill Bit of Dormer Make

8.2.3   Method Used

The method used for determining experimentally the shear strength of foam and the procedure for the drilling experiments are described in this section.

SHEAR TESTING OF FOAM

The shear strength of foam samples were determined experimentally using the punch tool method described in the ASTM D732-90 [179] (Standard test method for shear strength of plastics by punch tool). The same method was also used by Asnis *et al* (1996) [134] and Chapman *et al* (1996) [135] to find the shear strength of the foam material. In this test, the foam specimen under testing was rigidly fixed in a stationary block. A punch type shear tool was used to shear a cylinder of known dimension out of the foam specimen, at a constant shear rate of 1.25 mm/min. The maximum load required to shear the foam material was recorded at a sampling frequency of 25 Hz. The shear strength of each foam sample was calculated as the maximum recorded load divided by the area of the sheared cylindrical surface. For each foam density, five samples were tested as specified in the ASTM D732-90. Average shear strength of the five tested samples are presented in table 8.4 for FR-3700 series and in table 8.5 for FR-6700 series. Instron-3366 material testing machine, shown in figure 8.2, was used for the shear testing.
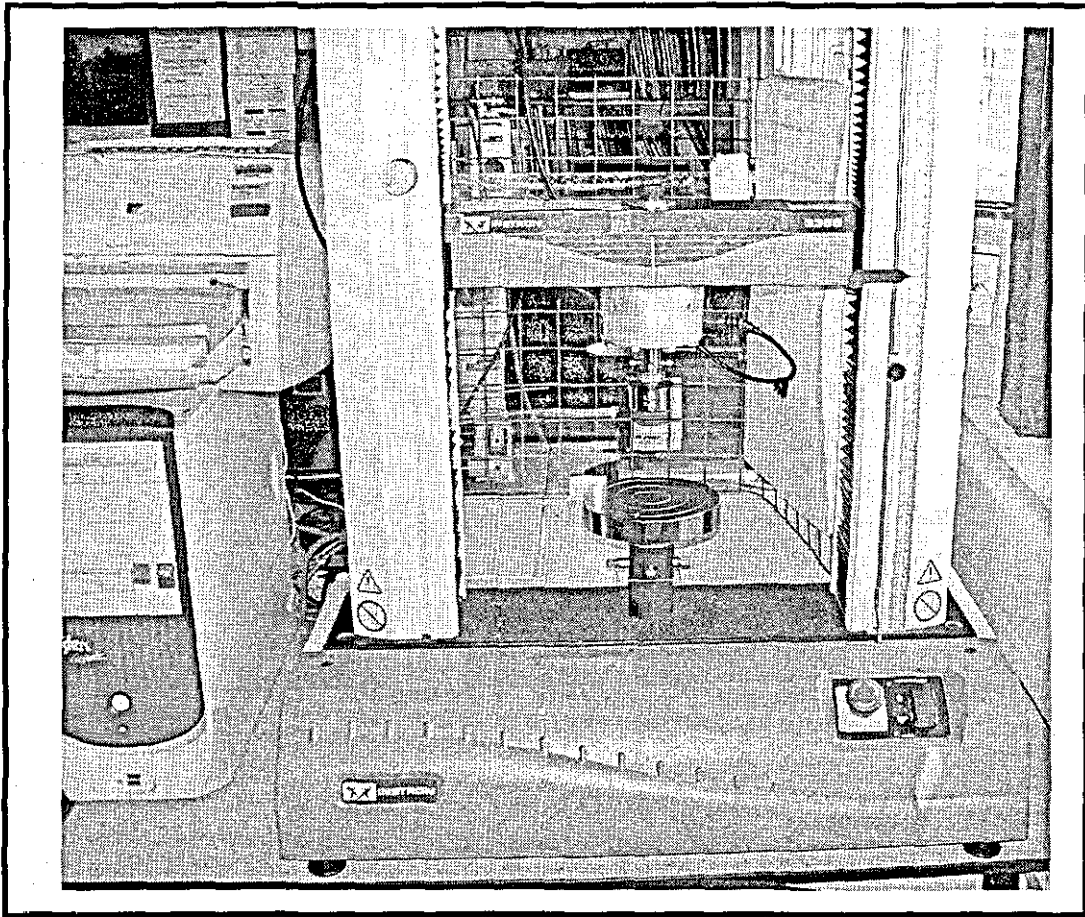
Figure 8.2 Instron 3366 Material Testing Machine Used for Shear Testing

DRILLING OF FOAM

Before conducting the drilling experiments on foam, it is important to calculate the number of holes, which should be drilled in each density foam sample. This will make the study cost effective and statistically significant. The sample size can be calculated using equation 8.2 given below [178].

$$ n = \left(\frac{\sigma \, z_{\alpha/2}}{E_e} \right)^2 \tag{8.9} $$

where, n = number of samples required in the study,

   σ = standard deviation of the data and

   E_e = margin of error

To calculate the sample size using equation 8.9, the standard deviation of the drilling force data recorded using the designed test rig setup should be known. Therefore, to calculate the standard deviation of our experimental set up, initially ten holes were drilled, according to the process described in section 7.4.1, into the foam sample FR-6740 and the drilling force profile were recorded. The test parameters used for this sample size calculation study are given below:

Drilling feed rate = 150 mm/min
Drilling Speed = 800 rpm
Data sampling frequency = 1000 Hz

A typical profile of the drilling force plotted with respect to the drill bit displacement for a single hole is shown in figure 8.3. The drilling profile is divided into three zones. Zone 1 represents the idle downward movement of the drill bit before it starts cutting the specimen. The drill bit starts to penetrate the specimen at the start of Zone 2, which can be seen by a sharp rise in the drilling force. A small variation in the drilling force magnitude is observed throughout the drilling process, which could be due to the porous nature of the foam material. The breakthrough of the dill bit from the specimen can be seen by a sharp fall in the drilling force at the end of Zone 2. No drilling is performed after the drill bit breakthrough, which is represented by Zone 3. Similar drilling force profiles having different drilling force magnitude were observed for all the ten holes drilled into the foam sample.
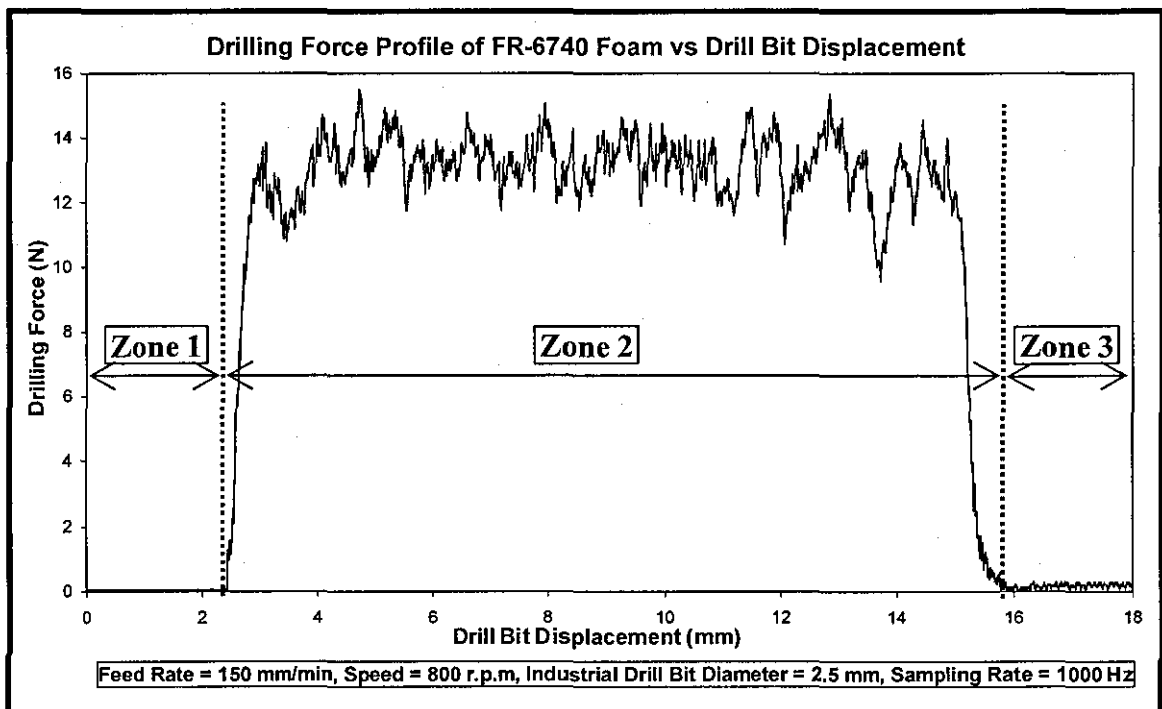
Figure 8.3 Drilling Force Profile of Foam Sample FR-6740

The recorded drilling force for all the ten holes drilled into FR-6740 foam in Zone 2 is averaged and is presented in table 8.3. For the data presented in table 8.3,

$$\overline{x} = 11.2884 \, N \tag{8.10}$$

$$\sigma = 0.0418 \, N \tag{8.11}$$

where, $\overline{x}$ = mean of the data

Table 8.3   Average Drilling Forces (N) Recorded for Ten FR-6740 Foam Samples

Hole No.	1	2	3	4	5	6	7	8	9	10
Drilling Force (N)	11.352	11.3746	11.2832	11.2477	11.2716	11.2822	11.2618	11.283	11.276	11.2515

The margin of error (E_e) in equation 8.9, in our case, can be defined as the minimum acceptable error in the drilling force. Let us assume that for any two different samples of foam of two different densities, there would be a minimum difference of 0.05 N in the drilling force, i.e., the designed test set up should be able to record a difference of at least 0.05 N. Therefore, the margin of error (E_e) is chosen as 0.05 N.

Substituting the value of standard deviation (σ) and margin of error (E_e) in equation 8.9, we get,

$$n = \left(\frac{\sigma \, z_{\alpha/2}}{E} \right)^2 = \left(\frac{0.0418 \times 1.96}{0.05} \right)^2 = 2.68 \tag{8.12}$$

Hence, three holes if drilled into one particular density of the foam sample will give an accurate measure of the drilling force. However, considering the chances of any human error to occur during the experiments, a sample size of five is selected.

Drilling of foam samples was performed according to the method described in section 7.4.1. Two sets of drilling force data were recorded at two different feed rate values, 150 mm/min and 250 mm/min. These feed rates were selected based on the assumption made about the approximate drilling time that a surgeon would take to perform drilling in clinics. Two different feed rate values were used to get two sets of data for comparison. The surgical bone drilling speed range is between 750 rpm to 1250 rpm (as given in section 7.3.1); this range is for handheld (manual) drilling and as thus for a variable feed rate. A constant drilling speed of 800 rpm was used to drill foam at a constant drill feed rate of 150 mm/min and 250 mm/min. The low speed of 800 rpm was chosen to avoid

damaging drill bits and generation of high temperature (in bone drilling). The drilling force data was recorded at a sampling rate of 1000 Hz.

It is important to avoid drilling holes with a blunt drill bit. Therefore, it is critical to know after how many holes the drill bit should be changed. As there is no standard which gives information on this, a procedure was developed to identify when there is a need to change the drill bit. According to the adopted procedure, the drilling force recorded for the first hole in foam sample FR-6740 was taken as the reference drilling force value. After drilling ten holes into the different foam samples, a hole is then drilled into the foam sample FR-6740 and the recorded drilling force is compared with the reference value. If a significant difference was found between the two drilling forces, the drill bit was replaced otherwise the same drill bit was used to drill another ten holes.

A cantilever torque beam is designed to record the drilling torque (as explained in section 7.4.1). However, for the chosen test parameters the magnitude of the drilling torque was significantly small to overcome the bearing friction in the specimen mounting assembly. Therefore, no torque could be recorded as there was no deflection of the cantilever torque beam. This puts a limit on the minimum value of the torque which can be measured using the designed system. Measurement of the torque either by measuring the change in the current supplied to the drilling motor or by stain gauging the drive shaft is proposed as a part of the future work.

8.2.4   Results and Discussions

The shear and drilling test results for the foam samples of series FR-3700 and FR-6700 are given in tables 8.4 and 8.5, respectively.

For FR-3730 and FR-3740, the standard deviation of the drilling force data was significantly high as compared to the estimated standard deviation, given in equation 8.11. Therefore, the sample size is recalculated for the above two foam samples with the actual standard deviation value given in table 8.4. The margin of error (E_e) was assumed 0.05 N for the sample size calculation performed in equation 8.12. However, as the difference in the drilling force is high between FR-3730 and FR-3740, therefore margin of error (E_e) is taken as 1 N for sample size calculation. Using equation 8.9, sample size for FR-3740 is calculated as,

$$n = \left(\frac{\sigma \, z_{\alpha/2}}{E}\right)^2 = \left(\frac{0.7981 \times 1.96}{1}\right)^2 = 2.5 \qquad (8.13)$$

Hence, sample size of five was used for FR-3740. The standard deviation of FR-3730 was lower than that of FR-3740, therefore sample size calculation for FR-3730 is not performed.

Table 8.4   Shear and Drilling Test Results of FR-3700 Series Foam Samples

Foam Samples Used			Shear Testing Results		Drilling Test Results			
					At 150 mm/min Feed Rate		At 250 mm/min Feed Rate	
Foam Model Number	Density of Foam (g/cm^3)	Specimen Thickness (mm)	Shear Strength[1] (N/mm^2)	Standard Deviation (N/mm^2)	Drilling Force[1] (N)	Standard Deviation (N)	Drilling Force[1] (N)	Standard Deviation (N)
3703	0.0481	19.20	0.2900	0.0151	0.1645	0.0031	0.2390	0.0040
3704	0.0641	19.05	0.3842	0.0597	0.2238	0.0051	0.3009	0.0143
3705	0.0801	19.20	0.6120	0.0102	0.3679	0.0227	0.5328	0.0093
3710	0.1602	25.40	1.6700	0.0378	1.1487	0.0519	1.5210	0.0338
3712	0.1922	25.40	2.1159	0.0267	1.4340	0.0106	1.9479	0.0310
3715	0.2403	25.40	3.3060	0.0601	2.4585	0.0354	3.0908	0.0547
3720	0.3204	25.50	5.1670	0.0920	3.9092	0.0174	5.0797	0.0297
3730	0.4806	19.06	10.6200	0.0187	7.5432	0.1088	10.2346	0.2902
3740	0.6407	19.10	17.2400	0.0662	12.4056	0.7981	16.9441	0.3388

[1] = average reading of five samples is given in the table

Table 8.5 Shear Test and Drilling Test Results of FR-6700 Series Foam Samples

Foam Samples Used			Shear Testing Results		Drilling Test Results			
					At 150 mm/min Feed Rate		At 250 mm/min Feed Rate	
Foam Model Number	Density of Foam (g/cm³)	Specimen Thickness (mm)	Shear Strength[1] (N/mm²)	Standard Deviation	Drilling Force[1] (N)	Standard Deviation	Drilling Force[1] (N)	Standard Deviation
6706	0.0961	19.10	0.4700	0.0636	0.3445	0.0077	0.4814	0.0185
6708	0.1282	17.86	1.2000	0.0052	0.8864	0.0127	1.2333	0.0137
6710	0.1602	19.40	1.4600	0.0495	1.0147	0.0211	1.3711	0.0145
6712	0.1922	18.80	1.6400	0.0047	1.1252	0.0140	1.5610	0.0166
6715	0.2403	19.00	3.2800	0.0046	2.1062	0.0538	2.8082	0.0650
6718	0.2884	19.10	4.1920	0.0344	2.7820	0.0241	3.7080	0.0638
6720	0.3204	18.80	4.7100	0.0741	3.0869	0.0257	4.0647	0.0257
6725	0.4005	19.10	6.6100	0.0202	4.0504	0.0638	5.8751	0.0402
6730	0.4806	19.10	10.7900	0.0778	6.5332	0.0710	9.3540	0.1194
6740	0.6407	13.00	18.3746	0.0586	11.2807	0.0978	16.7926	0.0772

[1] = average reading of five samples is given in the table

Correlation between Drilling Force and Shear Strength

Graphs generated based on the data presented in tables 8.3 and 8.4, to evaluate the relationship between the drilling force and shear strength for FR-3700 and FR-6700 series foam samples, are given in figures 8.4 and 8.5, respectively.

Figure 8.4   **Relationship between Drilling Force and Shear Strength of the FR-3700 Series Foam Material**
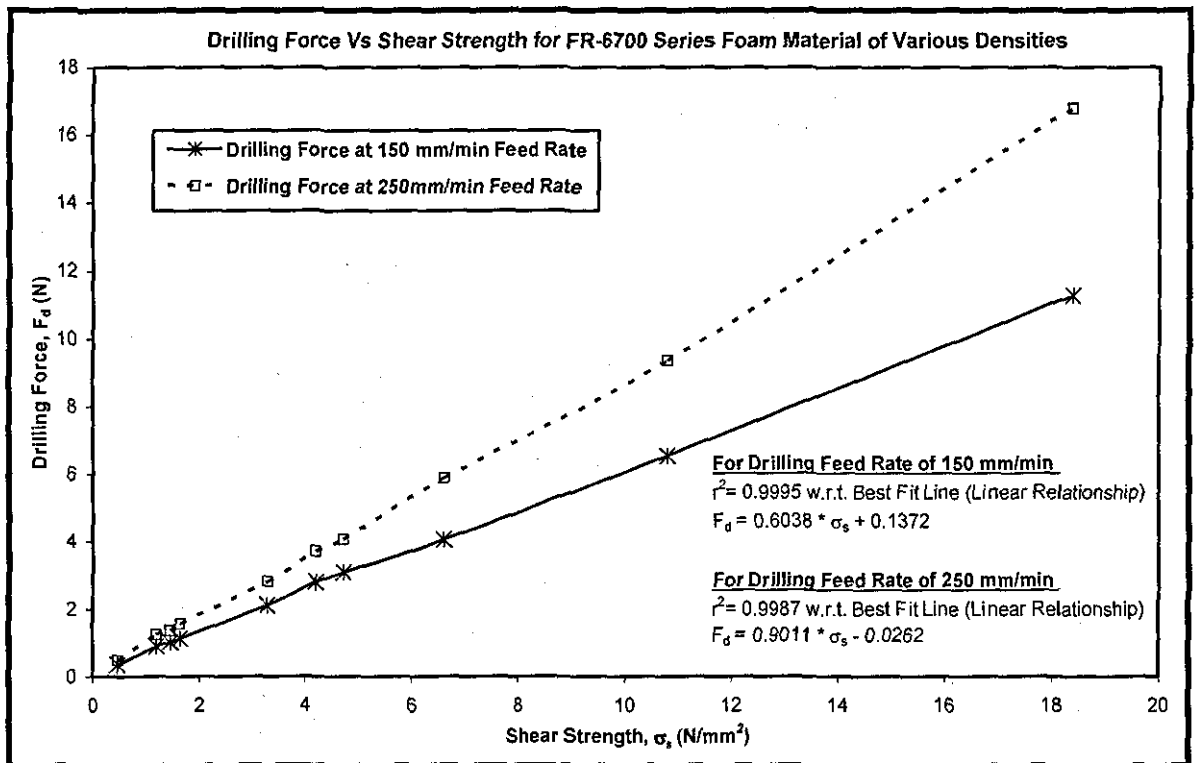
Figure 8.5 Relationship between Drilling Force and Shear Strength of the FR-6700 Series Foam Material

It can be seen from figures 8.4 and 8.5, that there exists a strong correlation (linear relationship) between the drilling force and shear strength for both FR-3700 and FR-6700 series foam material, at feed rate values of 150 mm/min and 250 mm/min. Hence, drilling force can be used to estimate foam strength. The above findings are also supported by the various theoretical models presented in chapter 4 to calculate the drilling force.

According to the model presented by Cook (1966) [180] in equation 4.3 and Jacob *et al* (1976) [19] in equation 4.36, the drilling force is function of the specific energy required to cut the material.

Whereas, according to the model presented by Mauch and Lauderbaugh (1990) [124] in equations 4.7, 4.9 and 4.22, the drilling force is function of the yield shear strength.

Since specific energy is a function of shear strength [19], therefore in all the models presented above (by Cook, Jacob and Mauch & Lauderbaugh), the drilling force is a function of shear strength. This justifies the strong relationship that is found between the drilling force and shear strength in the graphs presented in figures 8.4 and 8.5.

The use of bone density to predict bone strength was criticised in chapter 3, i.e., using density to predict bone strength can give erroneous results. This can also be supported by the results found in this experiment. FR-3740 and FR-6740 are two different foam materials with different material properties; however, they have the same densities. Different drilling forces were found for FR-3740 and FR-6740 which shows that drilling force does take into account the material property.

It can also be observed that feed rate only affected the magnitude of drilling force and did not change the linear relationship of drilling force with shear strength. Hence, in animal testing, drilling experiments will be carried out at a single feed rate value of 150 mm/min. 250 mm/min feed rate was not chosen as there are higher chances of damaging the drill bit at higher feed rate.

Relationship between Shear Strength and Density (ρ) of the Foam Material

Graphs generated based on the data presented in tables 8.3 and 8.4 to evaluate the relationship between the shear strength and density for FR-3700 and FR-6700 series foam material are given in figures 8.6 and figure 8.7, respectively. In both foam materials, shear strength showed a power relationship with the density and a strong correlation ($r^2 > 0.98$) was found in both series of foam material. However, a different power relationship was found for FR-3700 series [$\sigma_s = 32.575 \times \rho^{1.5923}$] and FR-6700 series [$\sigma_s = 39.727 \times \rho^{1.827}$]. A Similar power relationship was also found for both animal bone and synthetic bone material by other researchers [104, 135]. Their results are given below,

$\sigma_s = 21.6 \times \rho^{1.65}$ (for bovine bone) [104]

$\sigma_s = 23.9 \times \rho^{1.54}$ (for polyurethane foam) [135]
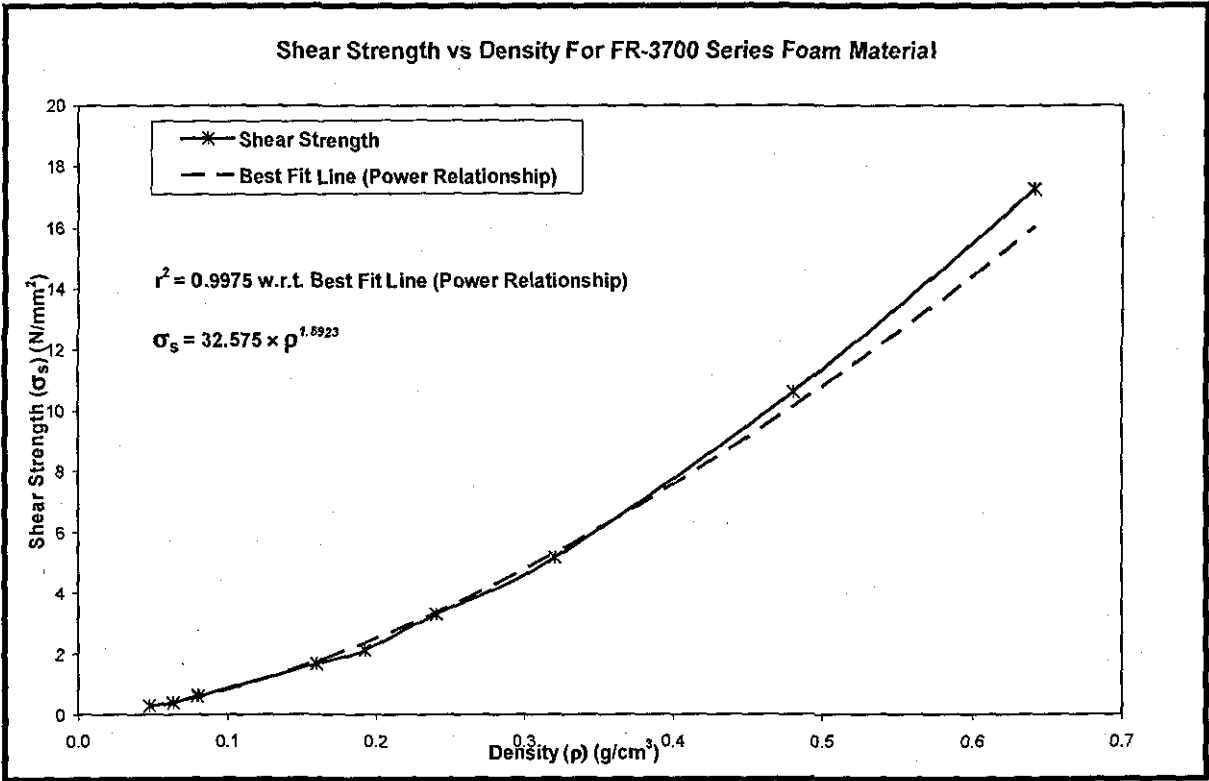
Figure 8.6 Relationship between Shear Strength and Density of the FR-3700 Series Foam Material
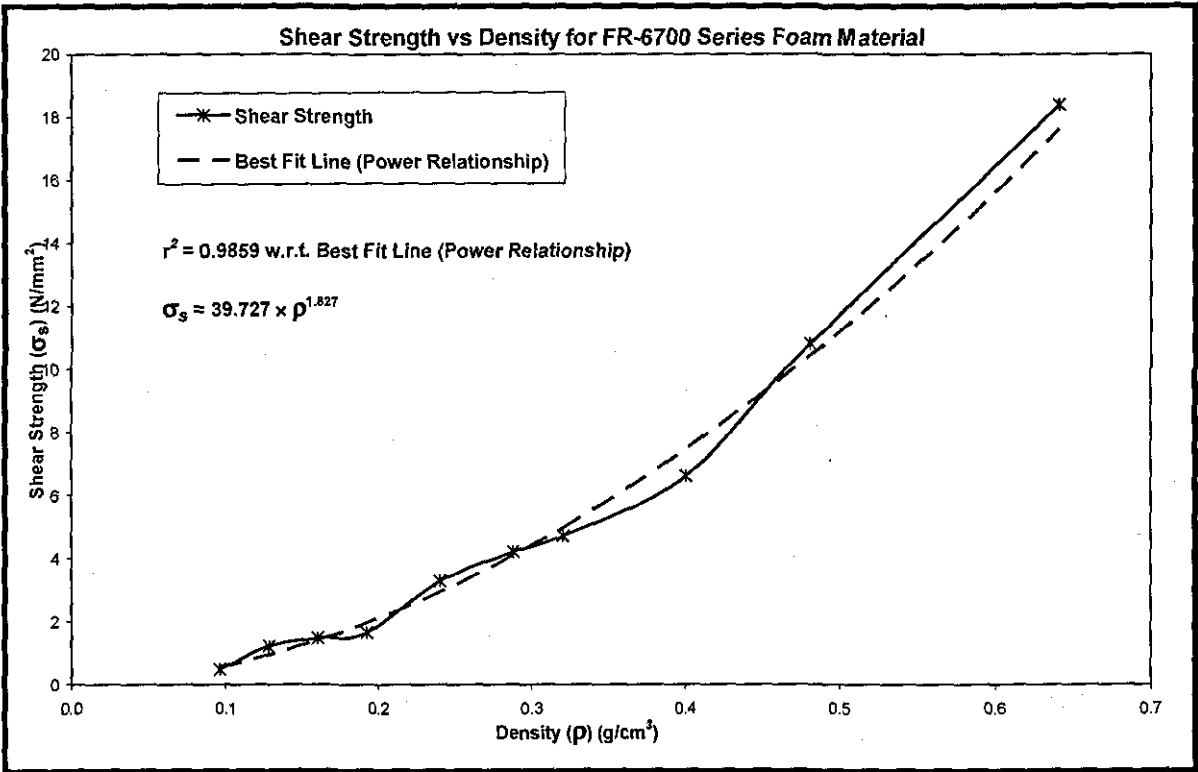
Figure 8.7 Relationship between Shear Strength and Density of the FR-6700 Series Foam Material

Relationship between Drilling Force and density of the foam material

Graphs generated based on the data presented in tables 8.3 and 8.4 to evaluate the relationship between the drilling force and foam density for FR-3700 and FR-6700 series foam material are given in figures 8.8 and 8.9, respectively.

In both foam materials, the drilling force showed a power relationship with the density and a strong correlation ($r^2 > 0.98$) was found. A better correlation is obtained for FR-3700 series foam.

Drilling Force vs Density for FR-3700 Series Foam Material

Legend:
—✳— Drilling Force at 150 mm/min Feed Rate
- ▫ - Drilling Force at 250 mm/min Feed Rate

For Drilling Feed Rate of 150 mm/min
r^2= 0.9983 w.r.t. Best Fit Line (Power Relationship)
$F_d = 26.226 \times \rho^{1.7002}$

For Drilling Feed Rate of 250 mm/min
r^2= 0.9972 w.r.t. Best Fit Line (Power Relationship)
$F_d = 33.966 \times \rho^{1.674}$

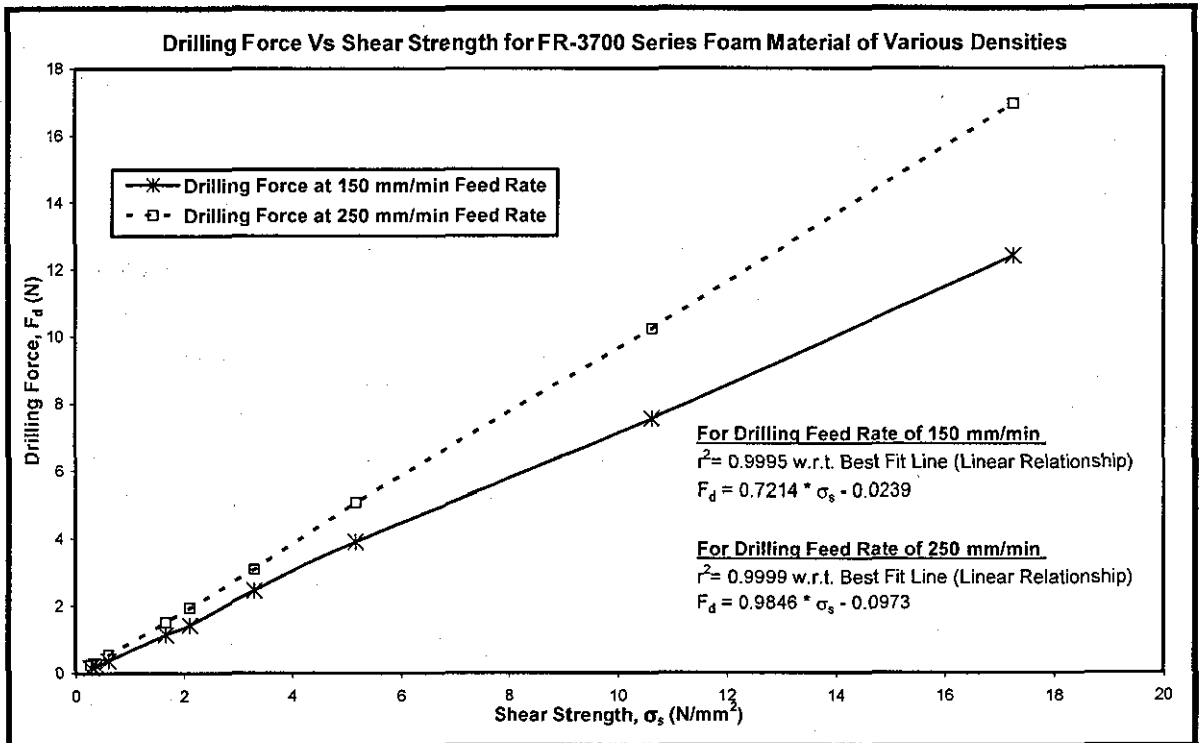Y-axis: Drilling Force (F_d) (N)
X-axis: Density (ρ) (g/cm^3)

Figure 8.8 Relationship between Drilling Force and Density of the FR-3700 Series Foam Material
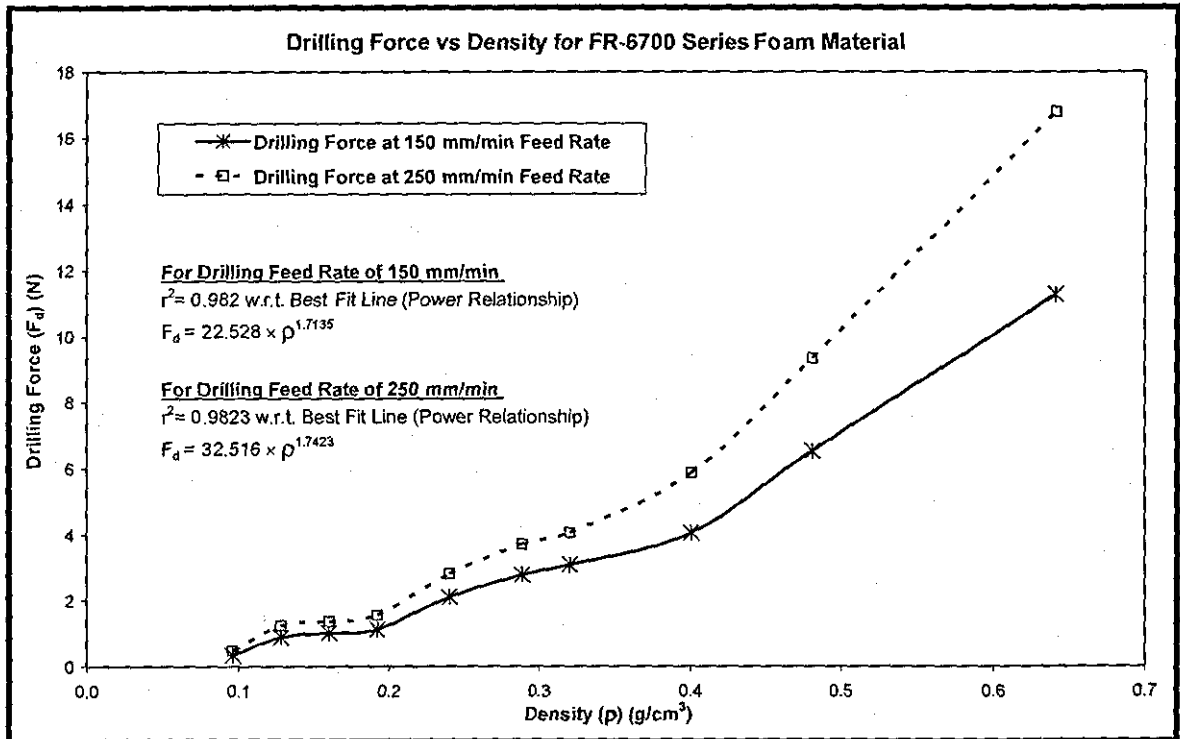
Figure 8.9 Relationship between Drilling Force and Density of the FR-6700 Series Foam Material

8.3 RELATIONSHIP BETWEEN DRILLING FORCE AND SCREW PULLOUT STRENGTH

8.3.1 Aims

1. To investigate if screw pullout strength can estimate shear strength of the foam material.

From the experimental results presented in section 8.2.4, it was established that drilling is a significantly good predictor of the shear strength of foam material. Foam is a homogeneous material, therefore shear testing and drilling could be done at different locations to find the correlation. However, bone is anisotropic and to avoid non-site specific correlations it is important to do shear testing at the site of drilling. But, shear testing is destructive in nature and therefore cannot be done at the site of drilling. On the other hand, screw pullout testing can be performed at the site of drilling. Hence, it is important to investigate the correlation between screw pullout strength and shear strength in synthetic bone material.

2. To find a correlation between the drilling force and screw pullout force

> This aim is to investigate the relationship between drilling force and screw pullout force. A strong relationship between them will prove that bone drilling data if recorded could be used as a predictor of bone screw fixation strength and give a quantitative evaluation of the bone quality.

8.3.2   Material Used

The same foam samples and drill bit, as used in section 8.2.2 were used. Surgical cancellous screws (Model No. 206.045, Synthes Ltd., UK) were used for testing. The key dimensions of the screw were measured using an optical microscope of 1 µm least count and are given in figure 8.10.

8.3.3   Method Used

Holes drilled in the experiment described in section 8.2 were used as pilot holes for screw insertion. Therefore, drilling force data as given in table 8.4 and table 8.5 is used in this study.

Screw pullout testing of foam

Tapping of pilot holes (ϕ2.5 mm diameter) were done using a tap supplied by the manufacturer for the corresponding screw type used in this study. Tapping of holes, using a tap, was selected over using the self tapping screws because pre-tapping decreases the stress and potential damage applied to the surrounding foam material and decreases the shearing forces on the screw during insertion, thereby increasing the life of screw used [181]. However, self-tapping screws create their fit by cutting and compacting bone around the screw threads at insertion and thus would result in a better fixation quality. Our study is a comparison based study; therefore the interest is not to have the better quality of fixation but to keep the testing parameters constant for comparison.

Thread Diameter or Outer Diameter = 3.444 mm
Core Diameter = 1.927 mm
Pitch = 1.754 mm
Thread Length = 41 mm
Screw Length = 45 mm
Thread Angle = 30°
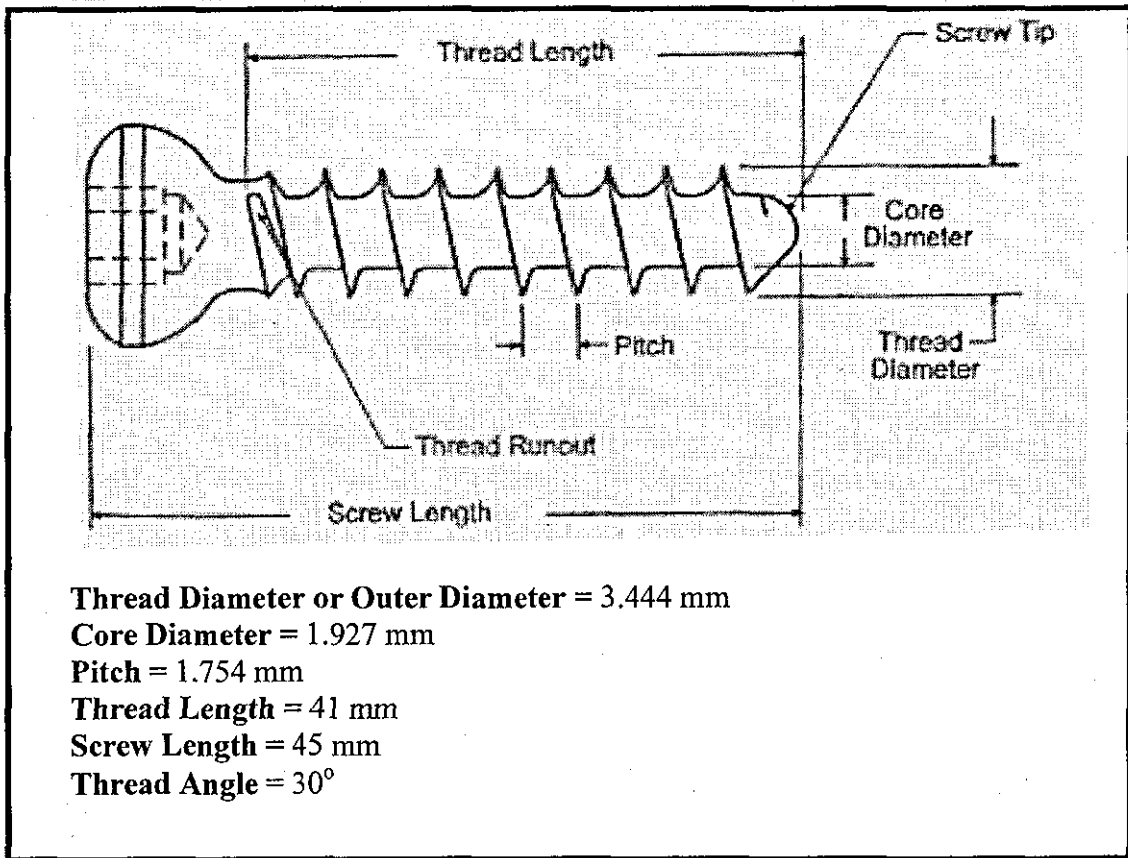
Figure 8.10   Surgical Cancellous Screw (Model No. 206.045, Synthes Ltd., UK) used for Screw Pullout Testing

Insertion of screw using the designed test rig was done according to the process described in section 7.4.2. Both tapping and screw insertion were done at a constant speed of 10 rpm.

Screws were pulled out using the designed test rig according to the process described in section 7.4.3. The maximum force required to pullout the screws was recorded at a sampling frequency of 500 Hz. The screws were pulled out at a rate of 5 mm/min (as per ASTM F543-02).

The same method, as described above for drilling test in section 8.2.3, was used to calculate the minimum sample size required for screw pullout testing. Screw pullout data for ten holes in foam samples FR-6740 was recorded initially. The standard deviation (σ) of the data was found to be 11.81 N. Assuming that for any two different samples of foam there would be a minimum difference of 12 N in the screw pullout force, hence, the

designed test set up should be able to record a difference of at least 12 N, which is the margin of error (E_e). Substituting the value of the standard deviation and margin of error in equation 8.9, we get

$$n = \left(\frac{\sigma \, Z_{\alpha/2}}{E}\right)^2 = \left(\frac{11.81 \times 1.96}{12}\right)^2 = 3.72 \qquad \qquad (8.14)$$

Therefore, a minimum sample size of five was selected for the screw pullout testing.

A typical plot of screw pullout force vs screw displacement for FR-6740 material is shown in figure 8.11.
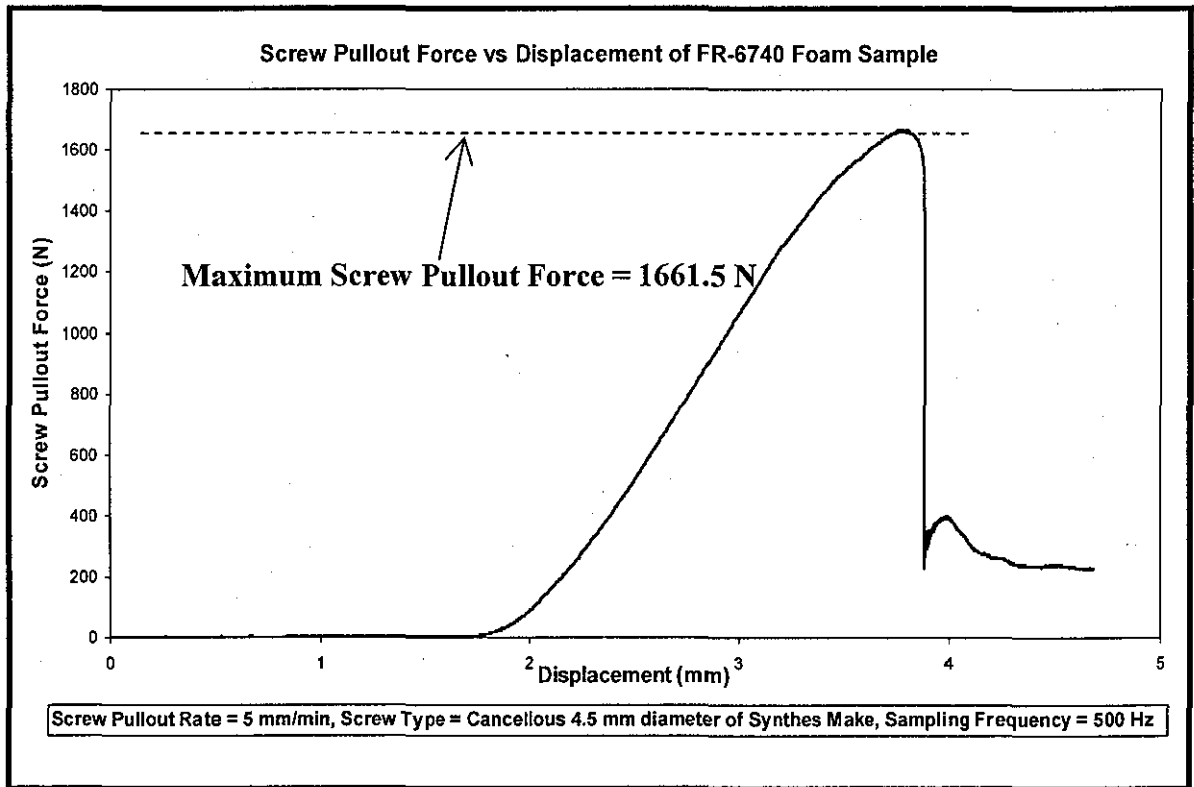
Figure 8.11   Screw Pullout Force vs Screw Displacement for FR-6740 Foam Sample

8.3.4 Results and Discussions

Screw pullout test results for foam samples of series FR-3700 and FR-6700 are given in table 8.6 and 8.7, respectively.

The maximum screw pullout force depends upon the specimen thickness; therefore it was normalised by dividing with the specimen thickness. The normalised screw pullout force (F_{NSPF}) value is also given in table 8.6 and table 8.7. Normalising will give a common platform for comparison among different foam samples.

Table 8.6   Screw Pullout Test Results of FR-3700 Series Foam Samples

Foam Samples Used			Screw Pullout Test Results		
Foam Model Number	Density of Foam (g/cm^3)	Specimen Thickness (mm)	Screw Pullout Force[1] (N)	Standard Deviation (N)	Screw Pullout Force/Specimen Thickness[1] (N/mm)
3703	0.0481	19.20	18.7106	1.4976	0.9745
3704	0.0641	19.05	36.7723	2.8505	1.9303
3705	0.0801	19.20	64.3418	2.0104	3.3511
3710	0.1602	25.40	261.1914	5.1949	10.2831
3712	0.1922	25.40	349.7507	6.1290	13.7697
3715	0.2403	25.40	562.4668	10.5862	22.1444
3720	0.3204	25.50	919.2580	13.9120	36.0493
3730	0.4806	19.06	1482.0960	14.6634	77.7595
3740	0.6407	19.10	2323.9813	4.9910	121.6744

[1] = average reading of five samples is given in the table

Table 8.7   Screw Pullout Test Results of FR-6700 Series Foam Samples

Foam Samples Used			Screw Pullout Test Results		
Foam Model Number	Density of Foam (g/cm^3)	Specimen Thickness (mm)	Screw Pullout Force[1] (N)	Standard Deviation (N)	Screw Pullout Force/Specimen Thickness[1] (N/mm)
6706	0.0961	19.10	46.6294	11.6167	2.4413
6708	0.1282	17.86	142.6484	12.9299	7.9870
6710	0.1602	19.40	191.2473	6.1051	9.8581
6712	0.1922	18.80	205.2935	8.5963	10.9199
6715	0.2403	19.00	382.2228	15.1901	20.1170
6718	0.2884	19.10	507.8230	7.3028	26.5876
6720	0.3204	18.80	593.7362	2.5463	31.5817
6725	0.4005	19.10	846.1010	13.3448	44.2985
6730	0.4806	19.10	1459.7240	11.2538	76.4253
6740	0.6407	13.00	1661.5790	11.8105	127.8138

[1] = average reading of five samples is given in the table

Correlation between Normalised Screw Pullout Force (F_{NSPF}) and Shear Strength (σ_s)

Graphs generated based on the data presented in tables 8.6 and 8.7 to evaluate the relationship between the normalised screw pullout force and shear strength for FR-3700 and FR-6700 series foam samples are given in figures 8.12 and 8.13 respectively.
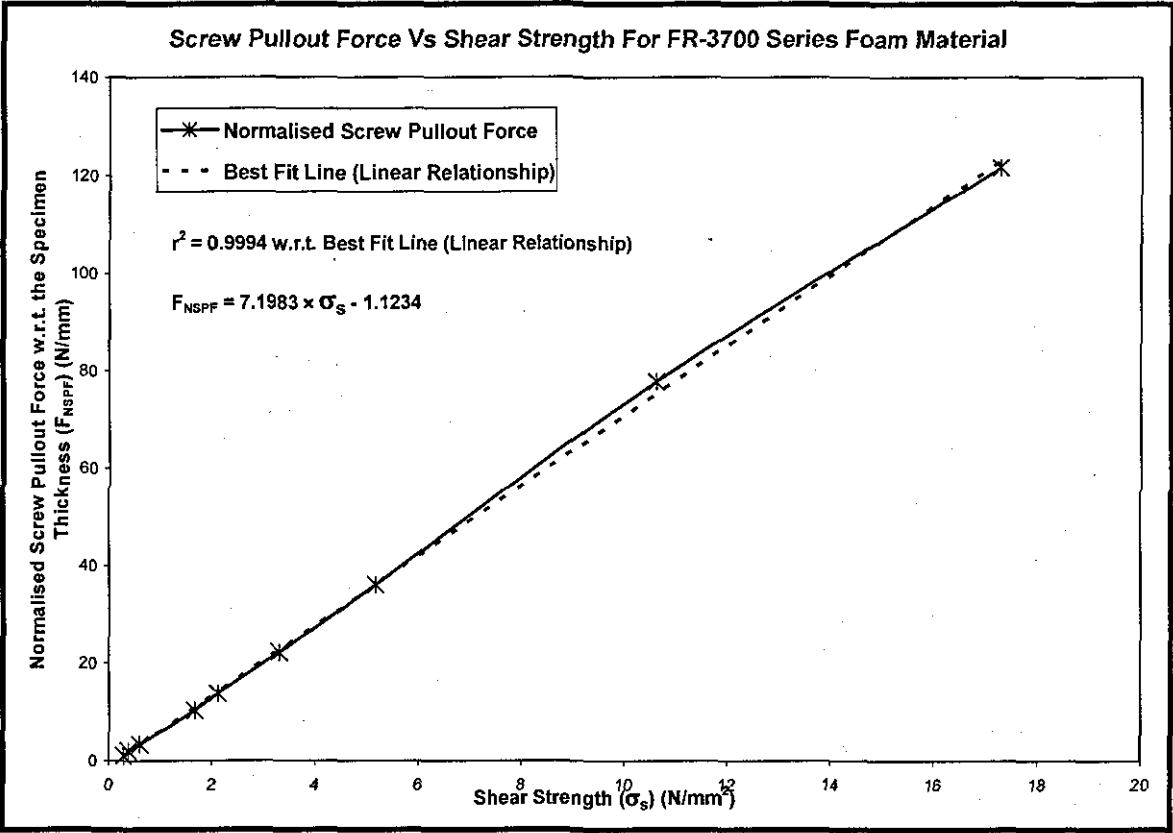
Figure 8.12 Relationship between Normalised Screw Pullout Force and Shear Strength of FR-3700 Series Foam Material
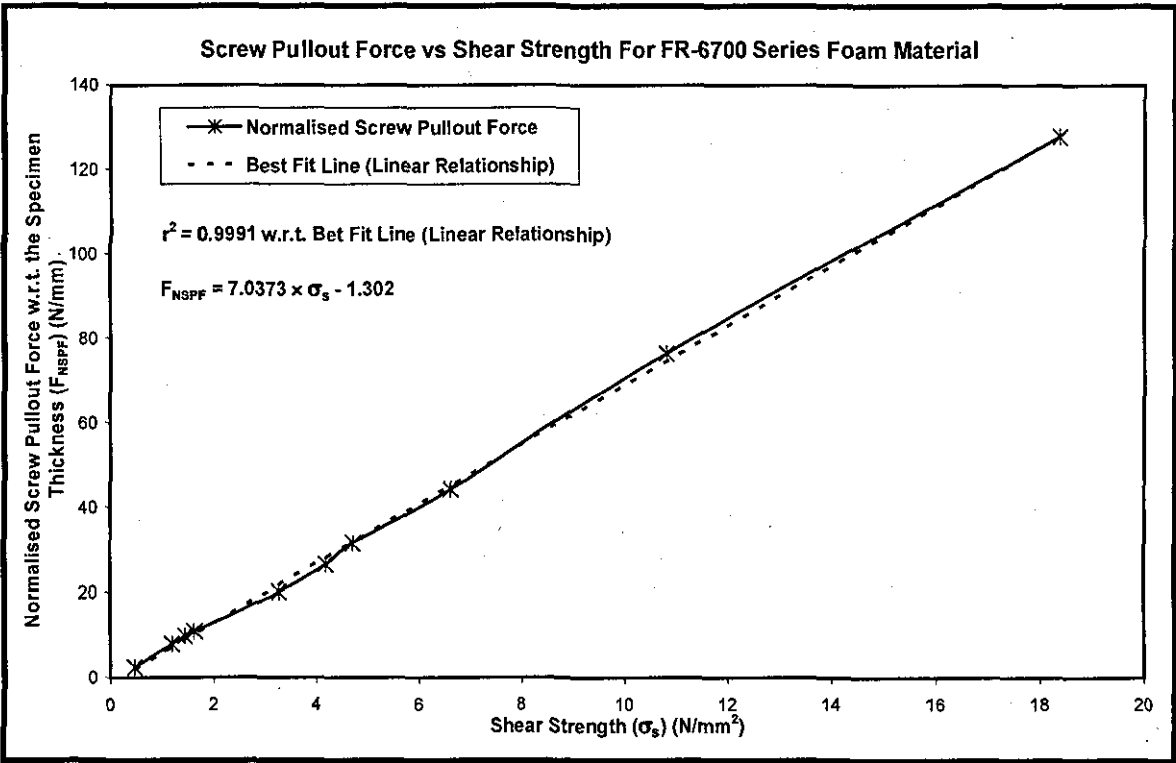
Figure 8.13 Relationship between Normalised Screw Pullout Force and Shear Strength of FR-6700 Series Foam Material

A significantly strong linear relationship ($r^2 > 0.99$) was found between the normalized maximum screw pullout force and shear strength, for both types of foam material tested. Hence, screw pullout force can be used as an alternative method to give the measure of the material shear strength.

Correlation between Normalised Screw Pullout Force and Drilling Force

Graphs generated, based on the data presented in tables 8.4, 8.5, 8.6 and 8.7, to evaluate the relationship between the drilling force and normalised screw pullout force for FR-3700 and FR-6700 series foam samples are given in figure 8.14 and figure 8.15, respectively.
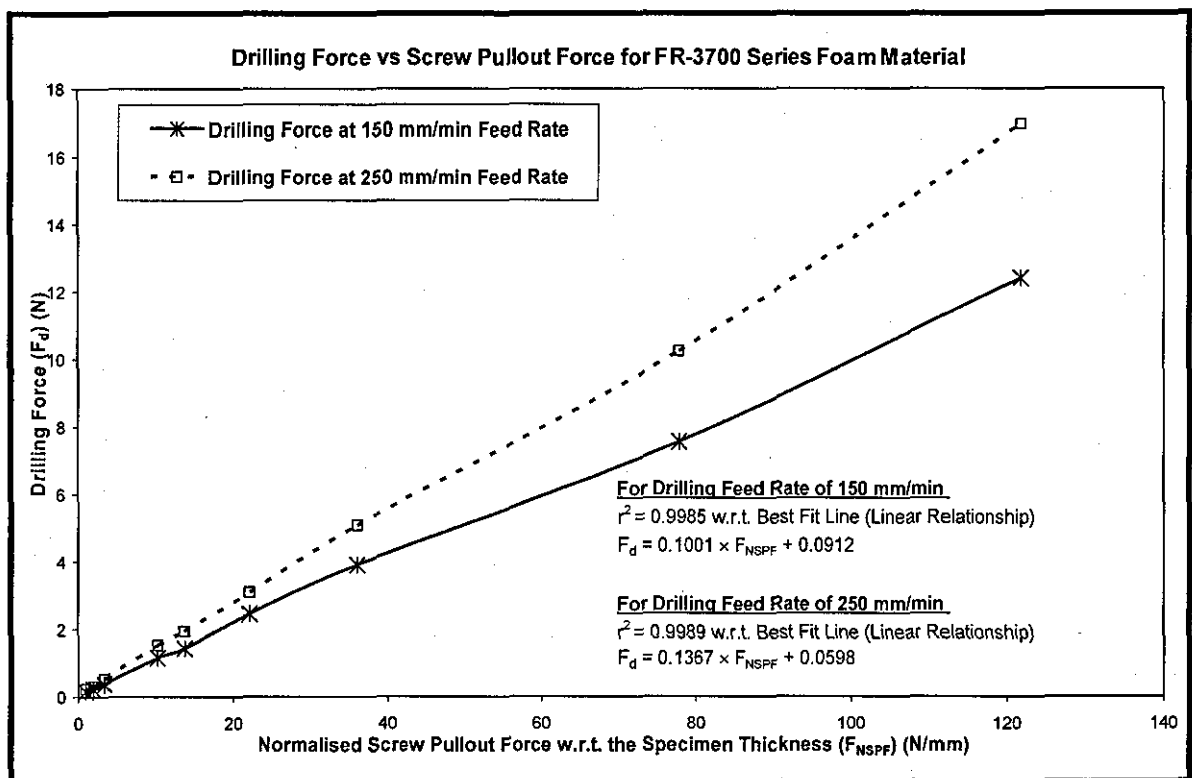
Figure 8.14 Relationship between Drilling Force and Normalised Screw Pullout Force for FR-3700 Series Foam Material
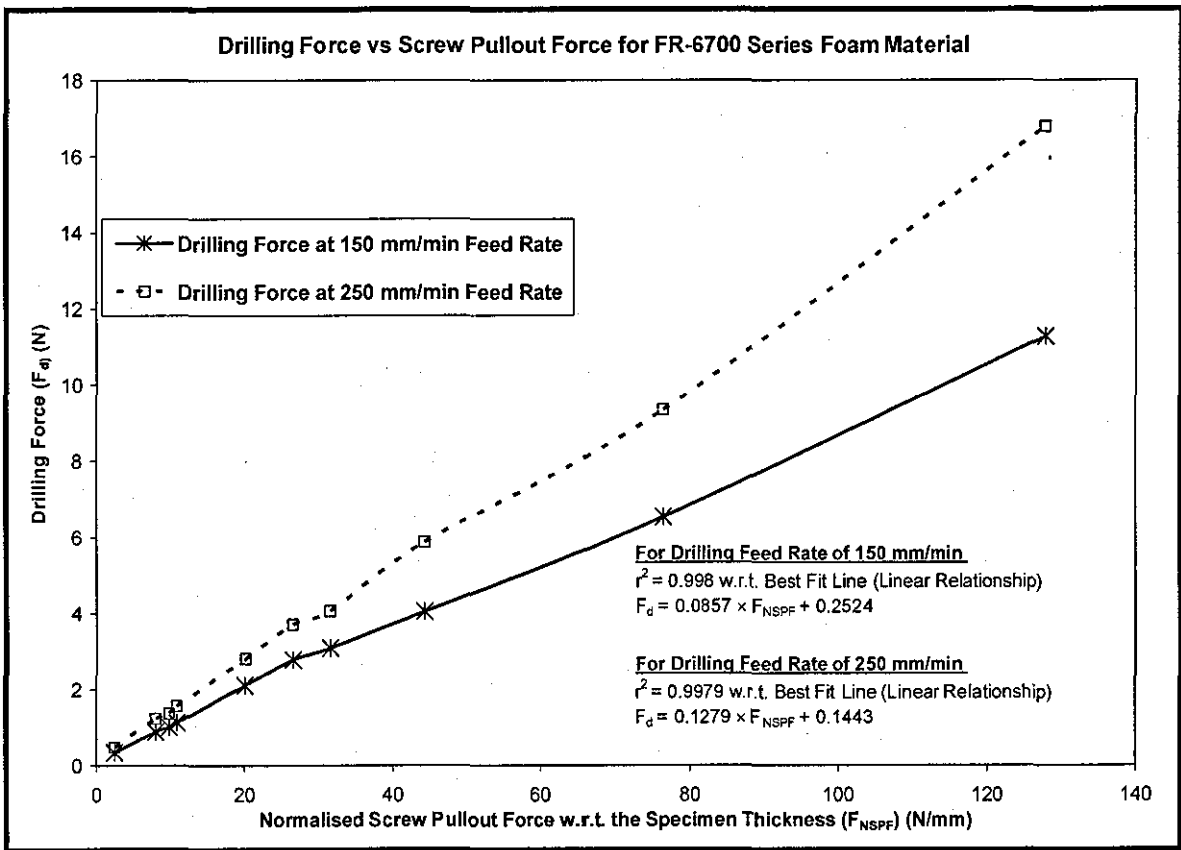
Figure 8.15 Relationship between Drilling Force and Normalised Screw Pullout Force for FR-6700 Series Foam Material

In both foam materials, a strong linear relationship ($r^2 > 0.99$) was found between the drilling force and normalized screw pullout force. This shows that bone drilling data can be used as a means to estimate the bone strength. Experiments to evaluate such relationship on animal bone are presented in chapter 9.

8.4 DRILLING EXPERIMENTS USING A SURGICAL DRILL BIT

8.4.1 Aim

To investigate the relationship between drilling force data obtained using surgical drill bit and screw pullout strength.

Surgical drill bits are not easily available and are expensive to buy; hence initial experiments were done using an industrial drill bit to investigate the relation of drilling force with other parameters. In the experiment described in section 8.3, using an

industrial drill bit, a strong correlation was found between the drilling force and screw pullout force. Surgical drill bits have different design as compared to the industrial drill bits. Therefore, it is also important to investigate the relationship between drilling force data obtained using a surgical drill bit and screw pullout strength.

8.4.2   Material Used

The same foam materials as used in section 8.2.2, i.e., FR-3700 series and FR-6700 series, were used for these experiments. Synthes surgical drill bits of ϕ2.5 mm diameter and Synthes surgical cancellous screws were used (refer section 8.3.2 for details).

8.4.3   Method Used

Drilling of Foam Using a Surgical Drill Bit

The same method as described in section 8.2.3 is used. Results found for the industrial drill bit in section 8.3 showed similar relationship between drilling force, measured at a feed rate of 150 mm/min and 350 mm/min, and normalised screw pullout force; therefore in this study only the relationship of drilling force measured at 150 mm/min feed rate was investigated.

Screw Pullout Testing of Foam

The screw pullout force depends upon the diameter of the pilot hole. The diameter of the surgical drill bit used in this study is the same as that of the industrial drill bit used in the study described in section 8.3. Hence, the screw pullout test data given in tables 8.6 and 8.7 was used in this study to find the correlation between drilling force and normalised screw pullout force.

8.4.4   Results and Discussions

The drilling force data for foam samples of series FR-3700 and FR-6700 are given in tables 8.8 and 8.9, respectively.

Table 8.8 Drilling Test Results of FR-3700 Series Foam Samples Using Surgical Drill Bit

Foam Samples Used			Drilling Test Results	
Foam Model Number	Density of Foam (g/cm^3)	Specimen Thickness (mm)	At 150 mm/min Feed Rate	
			Drilling Force[1] (N)	Standard Deviation (N)
3703	0.0481	19.20	0.2660	0.0095
3704	0.0641	19.05	0.2938	0.0063
3705	0.0801	19.20	0.4785	0.0093
3710	0.1602	25.40	1.3369	0.0133
3712	0.1922	25.40	1.6274	0.0105
3715	0.2403	25.40	2.5639	0.0349
3720	0.3204	25.50	4.4872	0.0319
3730	0.4806	19.06	10.6128	0.8220
3740	0.6407	19.10	16.2872	0.1188

[1] = average reading of five samples is given in the table

Table 8.9   Drilling Test Results of FR-6700 Series Foam Samples using Surgical Drill Bit

Foam Samples Used			Drilling Test Results	
			At 150 mm/min Feed Rate	
Foam Model Number	Density of Foam (g/cm^3)	Specimen Thickness (mm)	Drilling Force[1] (N)	Standard Deviation (N)
6706	0.0961	19.10	0.4755	0.0204
6708	0.1282	17.86	1.0313	0.0241
6710	0.1602	19.40	1.1638	0.0165
6712	0.1922	18.80	1.3768	0.0095
6715	0.2403	19.00	2.4782	0.0138
6718	0.2884	19.10	3.3403	0.0118
6720	0.3204	18.80	3.7550	0.0288
6725	0.4005	19.10	4.9836	0.0497
6730	0.4806	19.10	8.0008	0.0554
6740	0.6407	13.00	13.1446	0.1782

[1] = average reading of five samples is given in the table

Correlation between Normalised Screw Pullout Force and Drilling Force

Graphs generated based on the data presented in tables 8.6, 8.7, 8.8 and 8.9, to evaluate the relationship between the drilling force (using a surgical drill bit) and the normalised screw pullout force, are given in figures 8.16 and 8.17, for FR-3700 and FR-6700 series foam samples respectively.

As expected and similar to the previous results using industrial drill bits, a strong linear relationship ($r^2 > 0.99$) was found in both foam materials between the drilling force (measured using the surgical drill bit) and the normalized screw pullout force. Hence, the results obtained using industrial drill bits are representative for surgical drill bit. Thus, industrial drill bits can be used, instead of surgical drill bits, in the further investigations.
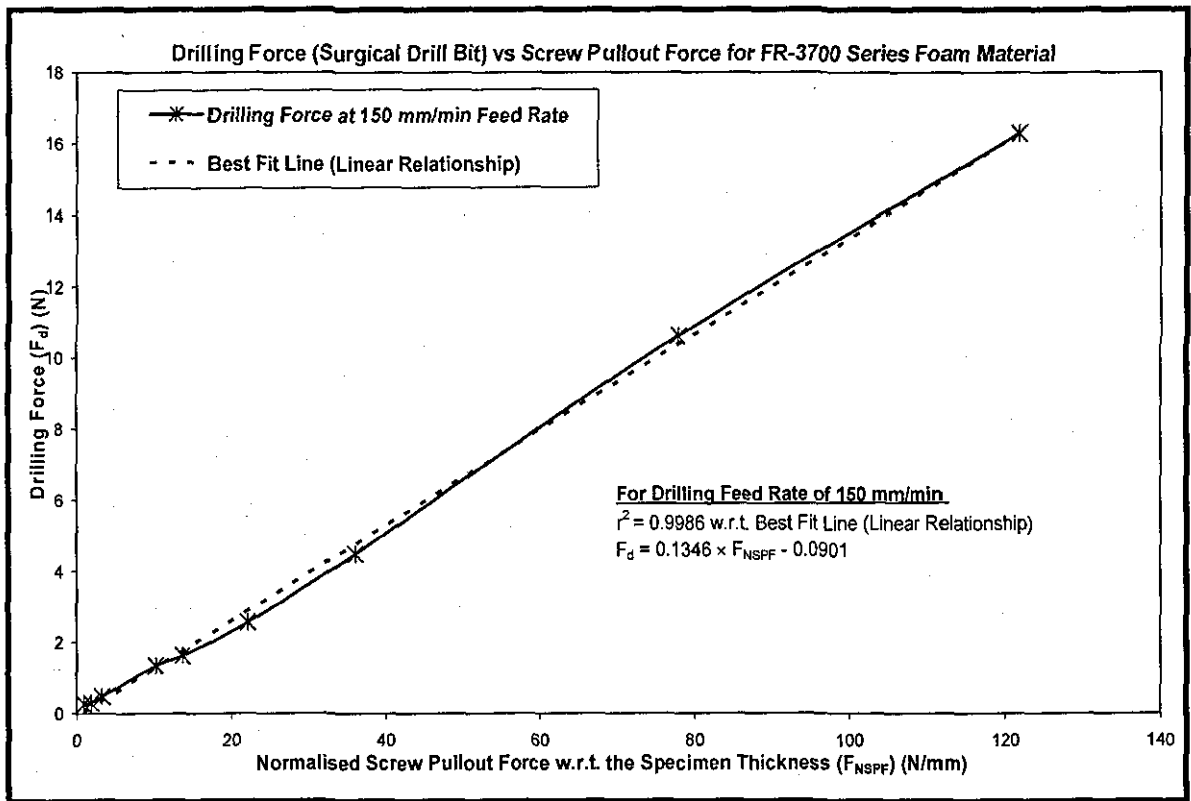
Figure 8.16   Relationship between Drilling Force (Measured Using Surgical Drill Bit) and Normalised Screw Pullout Force for FR-3700 Series Foam Material
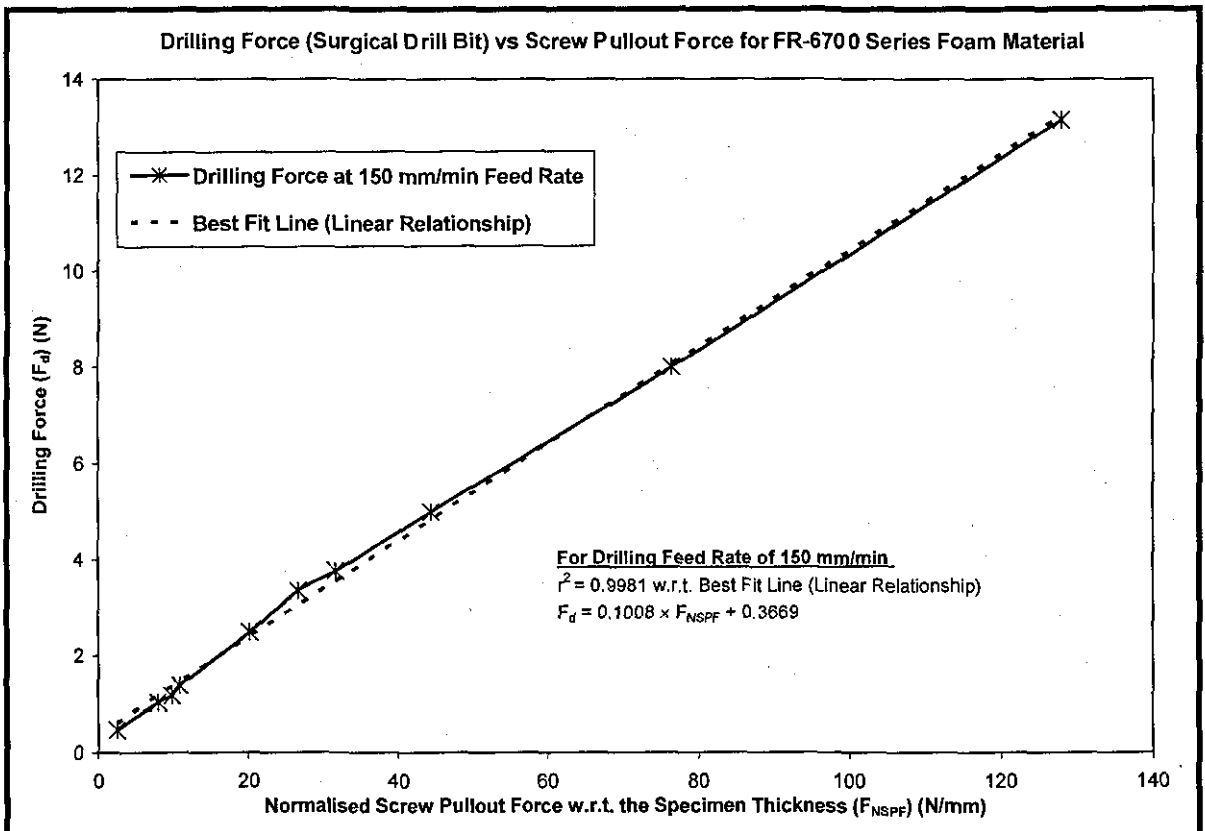
Figure 8.17 Relationship between Drilling Force (Measured Using Surgical Drill Bit) and Normalised Screw Pullout Force for FR-6700 Series Foam Material

8.5 USE OF SCREW ROTATION ANGLE FOR THE OPTIMISATION OF SCREW TIGHTENING

8.5.1 Aim

To investigate the use of screw rotation angle in optimising the screw tightening by conducting screw stripping tests.

As discussed in chapter 6, the use of screw insertion torque or screw tightening torque to optimize screw tightening can be erroneous. Hence, the use of screw rotation angle which was proposed as another method for optimizing screw tightening was explored in this study.

8.5.2 Material Used

FR-6700 series foam material was used for these experiments. Industrial drill bit of $\phi 2.5$ mm diameter was used to drill pilot holes (refer section 8.2.2 for details). Synthes surgical cancellous screws were used (refer section 8.3.2 for details).

8.5.3 Method Used

Controlled screw tightening and screw pullout test are used in this study. Pilot holes of $\phi 2.5$ mm were drilled according to the method described in section 8.2.3. Prior to screw insertion, tapping was carried out using a Synthes tap for the corresponding cancellous screw used in the study.

The screw insertion torque, screw angular rotation and screw tightening torque were monitored using an appropriate algorithm. The screw was inserted until the screw head touched the top surface of the foam material. This was referred to as the point of head contact (HC). A control algorithm was written in Visual Basic (VB) to detect the point of head contact, which is given by a sudden increase in the screw insertion torque value. The screw was further inserted by a specified angle from the HC point. The process of inserting the screw to a specified angle was achieved by controlling the rotation of the screw insertion stepper motor (SM_{Sc_Ins}) using an encoder (En_{Shaft}) mounted on the main shaft. Then, screw pullout testing was carried out for different tightening angles. The

screw pullout testing was conducted according to the process described in section 8.3.3. For every tightening angle, five samples were tested for the results to be statistically significant.

Initially, foam sample FR-6712 (density 0.1922 g/cm^3) was tested. This selection was made on a random basis. The screw was inserted in steps of 15 degree after the HC point and the screw pullout force, given in table 8.10, was recorded for each angle. The tests were stopped when the screw pullout force was reduced to approximately 60% w.r.t. the zero degree value. It can be seen, in table 8.10, that this occurred at 180 degrees from the HC point.

To verify the results, another foam sample FR-6720 (density 0.3204 g/cm^3) was tested according to the test procedure described above. The results of FR-6720 are also given in table 8.10.

It was observed from these initial tests performed on FR-6712 and FR-6720, that until 120 degree of screw rotation after the HC point, there was no reduction in the screw pullout force. Therefore, for the other density foam samples, the screw was not inserted in steps of 15 degree to save time and resources; but the tests were carried out at 0, 90, 120, 135, 150 and 180 degrees.

8.5.4   Results and Discussions

Based on the results of the initial tests, carried out on FR-6712 and FR-6720 foam material and presented in table 8.10, further testing of other foam density materials were carried out with the results presented in table 8.11.

Based on the previous screw pullout test data of FR-6700 series foam, presented in table 8.7, a standard deviation value of the screw pullout force for the current screw pullout tests could be expected in between 2 N and 15 N. Hence, any difference in the screw pullout force, recorded at two different screw insertion angle, less than 15 N was not considered as a loss in the screw pullout force.

From the data presented in tables 8.10 and 8.11, it can be observed that for the entire density of foam samples tested, there is no reduction in the screw pullout force until 120

degree of screw rotation after the HC point. This means that the threads in the foam material were not damaged or stripped until the screw was rotated beyond 120 degree. Further rotation of screw after 120 degree results in the loss of screw pullout force. Therefore, 120 degree can be taken as the critical angle for this type of screw. The results presented show that the critical angle was independent of the material strength and density and remained constant for a particular type of screw design. Furthermore, from the screw tightening torque data plotted against the screw rotation angle, for FR-6718 foam material in figure 6.4, shows that after 120 degrees of screw rotation from the HC point the screw tightening torque reaches its maximum value and further rotation of screw decreases the tightening torque.

The pitch of the screw used is 1.754 mm. Therefore, 120 degree of screw rotation, which is equivalent to 33% of the screw pitch, results in a linear displacement of 0.584 mm.

Similar tests should be conducted for the different surgical screws available in the market to establish the corresponding critical angle. Once the critical angle is established for all the screws, a table can be established for use in clinics, for optimum screw fixation.

Table 8.10   Screw Pullout Force of FR-6712 and FR-6720 Foam Material, after Inserting Screw at Various Angles from the Head Contact Point

		Screw Insertion Angle After Head Contact Point (Degree)														
		0	15	30	45	60	75	90	105	120	130	135	140	150	165	180
FR-6712 (0.1922 g/cm3)	Screw Pullout Force (N)[1]	209	213	210	207	210	204	208	210	209	201	195	190	171	152	125
	% Reduction in Screw Pullout Force[2]	100	102	101	99	101	98	100	100	100	96	94	90	82	73	60
FR-6720 (0.3204 g/cm3)	Screw Pullout Force (N)[1]	592	595	597	588	591	589	596	590	583	559	526	520	444	410	347
	% Reduction in Screw Pullout Force[2]	100	101	101	99	100	100	101	100	99	94	89	87	75	69	59

[1] = average reading of the five samples is given in the table

[2] = percentage reduction in screw pullout force value with respect to the screw pullout force value recorded at the zero degree

Table 8.11   Screw Pullout Force of FR-6700 series Foam Material, after Inserting Screw at Various Angles from the Head Contact Point

		Screw Insertion Angle After Head Contact Point (Degree)					
		0	90	120	135	150	180
FR-6708	Screw Pullout Force (N)[1]	140	137	138	126	122	93
	% Reduction in Screw Pullout Force[2]	100	98	99	90	87	67
FR-6710	Screw Pullout Force (N)[1]	191	193	195	181	175	128
	% Reduction in Screw Pullout Force[2]	100	101	102	94	91	67
FR-6715	Screw Pullout Force (N)[1]	382	388	383	360	322	226
	% Reduction in Screw Pullout Force[2]	100	102	100	94	84	59
FR-6718	Screw Pullout Force (N)[1]	479	475	467	423	365	247
	% Reduction in Screw Pullout Force[2]	100	99	98	88	76	52
FR-6725	Screw Pullout Force (N)[1]	797	803	795	719	607	436
	% Reduction in Screw Pullout Force[2]	100	101	100	90	76	55
FR-6730	Screw Pullout Force (N)[1]	1444	1417	1434	1357	1039	721
	% Reduction in Screw Pullout Force[2]	100	98	99	94	72	50
FR-6740	Screw Pullout Force (N)[1]	1659	1656	1650	1488	1371	1099
	% Reduction in Screw Pullout Force[2]	100	100	99	90	83	66

[1] = average reading of five samples is given in the table

[2] = percentage reduction in screw pullout force value with respect to the screw pullout force value recorded at the zero degree

8.6 TO INVESTIGATE THE USE OF SCREW PULLOUT FORCE THEORETICAL MODEL

8.6.1 Aim

To investigate the validity of the theoretical screw pullout force model, given in equation 2.5, using the experimental screw pullout force data.

As discussed in section 5.1.6, there have been no studies reported in the literature which have correctly applied the screw pullout force theoretical model developed for metals in synthetic bone material. This study was conducted to investigate the validity of screw pullout force theoretical model using synthetic bone material.

8.6.2 Material Used

The same foam materials as used in section 8.2.2, i.e., FR-3700 series and FR-6700 series, were used for these experiments. Dormer industrial drill bits of $\phi2.5$ mm diameter and Synthes surgical cancellous screws were used (refer section 8.3.2 for details).

8.6.3 Method Used

The theoretical model to calculate screw pullout force is presented in equation 2.5; it is repeated below in equation 8.14 for clarity. It should be noted that this theoretical model was originally derived for metals, and it was used previously by Asnis *et al* [134] and Chapman *et al* [135] to calculate screw pullout force in synthetic bone material.

$$F_{SPF} = \sigma_s \times \pi \times D_o \times L_{th} \times \left[0.5 + \left(\frac{D_o - d_i}{2 \times p} \right) \times \tan \frac{\theta}{2} \right] \qquad (8.14)$$

where, F_{SPF} = screw pullout force (N),

σ_s = shear strength of thread material (N/mm^2),

D_o = maximum diameter of the external thread (mm),

L_{th} = length of thread engagement (mm),

d_i = minimum diameter of the internal thread (mm),

p = thread pitch (mm) and

θ = included thread angle (degree)

Using equation 8.14, a theoretical value of screw pullout force, given in table 8.12, was calculated for the different foam samples used in this study. The values of the variables used in equation 8.14 are given below,

σ_s = shear strength of various foam samples determined using shear testing, refer section 8.2.3, was used

D_o = outer diameter of the screw used = 3.444 mm

L_{th} = thickness of foam specimen, as the screw was inserted into the whole thickness of the foam specimen,

d_i = diameter of pilot hole = 2.5 mm,

p = 1.754 mm and

$\theta = 30^\circ$

The experimental screw pullout force data given in section 8.3.4 was used to validate the theoretical screw pullout force.

8.6.4 Results and Discussions

The theoretical ($^{th}F_{Pullout}$) and experimental ($^{exp}F_{Pullout}$) screw pullout force determined for the various foam samples tested is given in table 8.12. The calculated error ($E_{Pullout}$) between the theoretical and experimental screw pullout force is also given in table 8.12. This calculated error was plotted for FR-3700 and FR-6700 series foam samples as shown in figures 8.18 and 8.19. From these plots it can be seen that for both foam materials, FR-3700 and FR-6700, the error ($E_{Pullout}$) is significantly low in the lower density foam samples and it is substantially high in the higher density foam material. Hence, equation 8.14 should only be used for lower density synthetic bone samples to calculate the screw pullout strength. Its use for higher density synthetic bone materials is questionable and should be further investigated.

Table 8.12   Error between Theoretical and Experimental Screw Pullout Force for
FR-3700 Series Foam Material

Foam Model Number	Density of Foam (g/cm^3)	Specimen Thickness (mm)	Shear Strength[1] (N/mm^2)	Theoretical Screw Pullout Force ($^{th}F_{Pullout}$) (N)	Experimental Screw Pullout Force ($^{exp}F_{Pullout}$) (N)	Error ($E_{Pullout}$) (N)
3703	0.0481	19.20	0.2900	34.4658	18.7106	15.7551
3704	0.0641	19.05	0.3842	45.3045	36.7723	8.5322
3705	0.0801	19.20	0.6120	72.7346	64.3418	8.3928
3710	0.1602	25.40	1.6700	262.5662	261.1914	1.3748
3712	0.1922	25.40	2.1159	332.6730	349.7507	-17.0777
3715	0.2403	25.40	3.3060	519.7868	562.4668	-42.6800
3720	0.3204	25.50	5.1670	815.5814	919.2580	-103.6766
3730	0.4806	19.06	10.6200	1252.9568	1482.0960	-229.1392
3740	0.6407	19.10	17.2400	2038.2588	2323.9813	-285.7225

Table 8.13   Error Between Theoretical and Experimental Screw Pullout Force for FR-6700 Series Foam Material

Foam Model Number	Density of Foam (g/cm^3)	Specimen Thickness (mm)	Shear Strength[1] (N/mm^2)	Theoretical Screw Pullout Force ($^{th}F_{Pullout}$) (N)	Experimental Screw Pullout Force ($^{exp}F_{Pullout}$) (N)	Error ($E_{Pullout}$) (N)
6706	0.0961	19.10	0.4700	55.5674	46.6294	8.9380
6708	0.1282	17.86	1.2000	132.6635	142.6484	-9.9849
6710	0.1602	19.40	1.4600	175.3248	191.2473	-15.9226
6712	0.1922	18.80	1.6400	190.8492	205.2935	-14.4443
6715	0.2403	19.00	3.2800	385.7591	382.2228	3.5362
6718	0.2884	19.10	4.1920	495.6152	507.8230	-12.2079
6720	0.3204	18.80	4.7100	548.1097	593.7362	-45.6266
6725	0.4005	19.10	6.6100	781.4902	846.1010	-64.6108
6730	0.4806	19.10	10.7900	1275.6852	1459.7240	-184.0389
6740	0.6407	13.00	18.3746	1478.5974	1661.5790	-182.9816
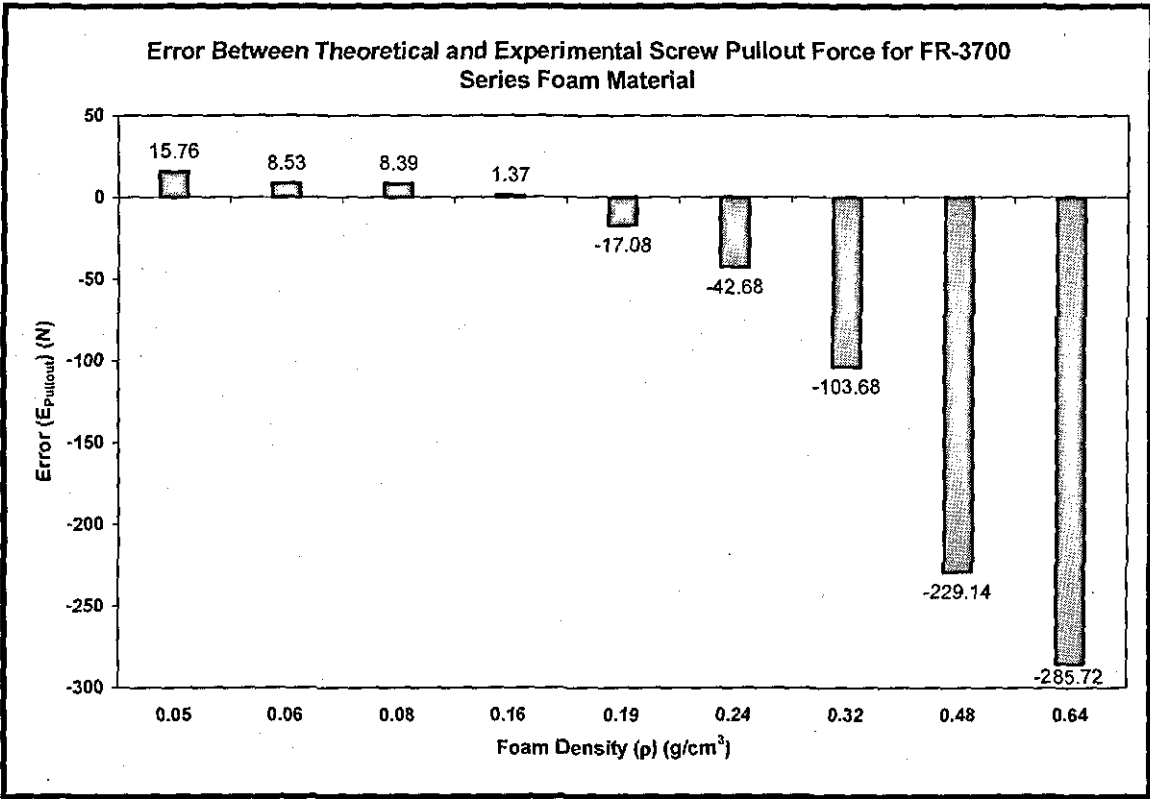
Figure 8.18 Error between Theoretical and Experimental Screw Pullout Force Plotted For FR-3700 Series Foam Material
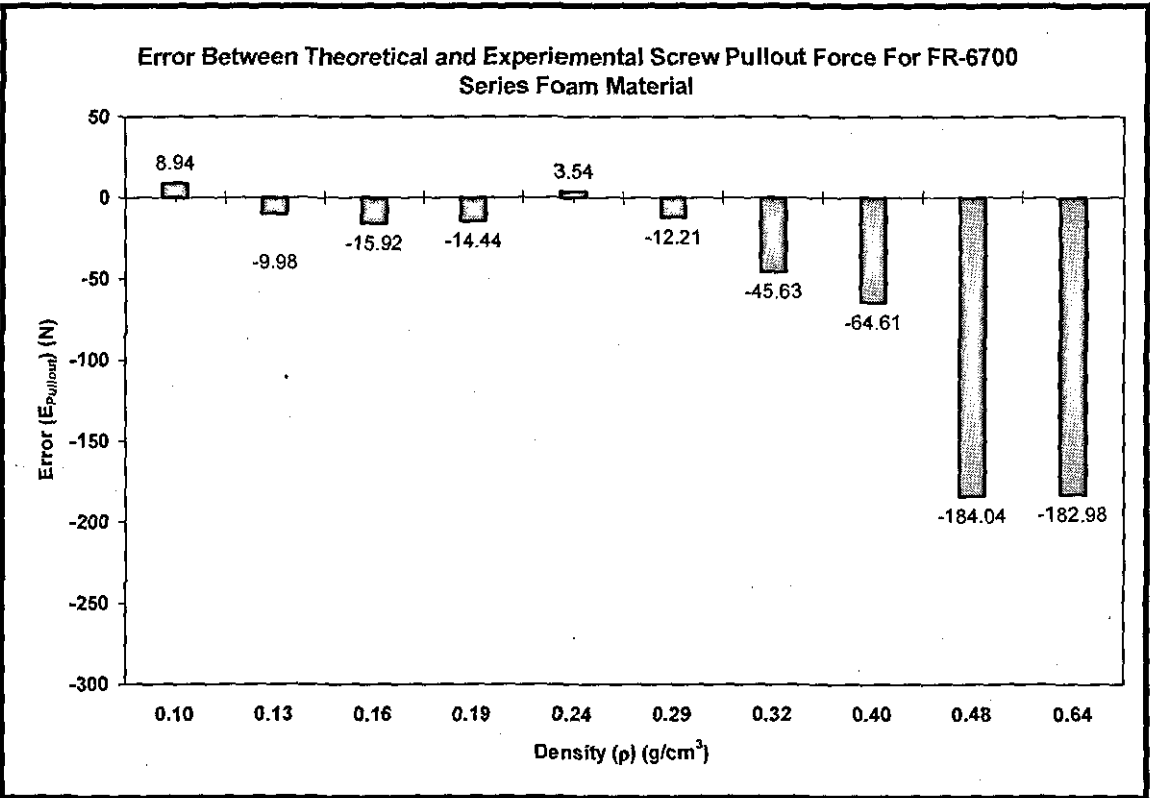
Figure 8.19 Error between Theoretical and Experimental Screw Pullout Force Plotted For FR-6700 Series Foam Material

8.7   CONCLUDING REMARKS

Various tests conducted on the synthetic bone material have been presented. The two different types of foam material, FR-3700 series and FR-6700 series, covering a density range of between 0.0481 g/cm^3 to 0.6407 g/cm^3 were tested. This density range simulates the osteoporotic and cancellous bone. For the correlations to be statistically significant, more than seven different densities of the foam material within the selected range were tested. Significantly high correlation coefficient of r^2 > 0.99 between the drilling force and shear strength of the foam material suggests that the drilling force can give a good estimation of the material quality. Different magnitudes of the drilling force and shear strength were found for the two different foam materials that had the same density, e.g., FR-3730 and FR-6730. This supports the conclusion drawn in chapter 3 that using bone density as a predictor of bone strength can be erroneous. Similar correlations and drilling results were found when drilling was conducted at two different drilling feed rate values, 150 mm/min and 250 mm/min. Therefore, future experiments can be designed to be conducted at a single drill feed rate value. A strong power correlation (r^2 > 0.98) was found between the drilling force and density of the synthetic bone material. A strong correlation (r^2 > 0.99) found between the screw pullout force and shear strength for the synthetic bone material suggests that the screw pullout force is a good predictor of the material shear strength and therefore it can be used in the correlational studies to evaluate the efficacy of drilling force in estimating the material strength. The strong correlation (r^2 > 0.99) which was found between the drilling force and screw pullout force in the synthetic foam material suggests that the drilling force is a good predictor of the material shear strength. The drilling tests were conducted using both industrial and surgical drill bits and similar relationships were found for both drill bits. This suggests that industrial drill bits can be used to conduct future experiments. The use of screw rotation angle to optimise the screw tightening was successfully demonstrated for the FR-6700 series synthetic bone material. The optimum angle for the tested screw was found to be 120° which is equivalent to 33% of the screw pitch. This technique was found to be independent of the friction between the screw & bone or screw & screw plate/washer and material density. The theoretical equation used in the literature to calculate the screw pullout force was evaluated. It was found that the equation should be modified for the porous material and surgical screws. The next chapter presents the description and results of the tests conducted on the animal bones.

CHAPTER 9

TESTING OF ANIMAL BONES

Following the testing of synthetic bone material, tests on animal bones were conducted to investigate the correlation between drilling force and screw pullout strength. Pig, Lamb and Cow bones were tested. This chapter describes the experiments conducted on animal bones.

9.1 RELATIONSHIP BETWEEN DRILLING FORCE AND SCREW PULLOUT STRENGTH

9.1.1 Aim

To find a correlation between the drilling force and screw pullout force

The aim of this experiment was to investigate if the drilling force can be used to estimate the shear strength of bone. Since shear strength of bone cannot be determined without destructive testing, therefore screw pullout force is used instead to find the correlation. A strong correlation between the screw pullout force and shear strength found in the initial experiments conducted on the synthetic bone material (as discussed in section 8.3.4) justifies the use of screw pullout force.

9.1.2   Material Used

Bone samples were purchased from a local butcher and were frozen before testing. Any extra tissues or muscles present around the bone were cleaned using a knife and scrapper before testing. The following bone samples were used,

- Right side and left side pig femur bones of the same animal: a picture of the pig femur after cleaning is shown in figure 9.1.
- Right side and left side pig tibia bones of the same animal
- Right side and left side lamb femur bones of the same animal
- Left side cow femur bone

The shaft portion of the above bone samples was tested, which is predominantly cortical bone, because it was difficult to clean all the extra tissues and muscles around the proximal head of the femur or tibia. Moreover, only one or two holes can be drilled at the proximal head of the femur and therefore a large number of femur bone samples would be required, which is not possible in this scale of research.
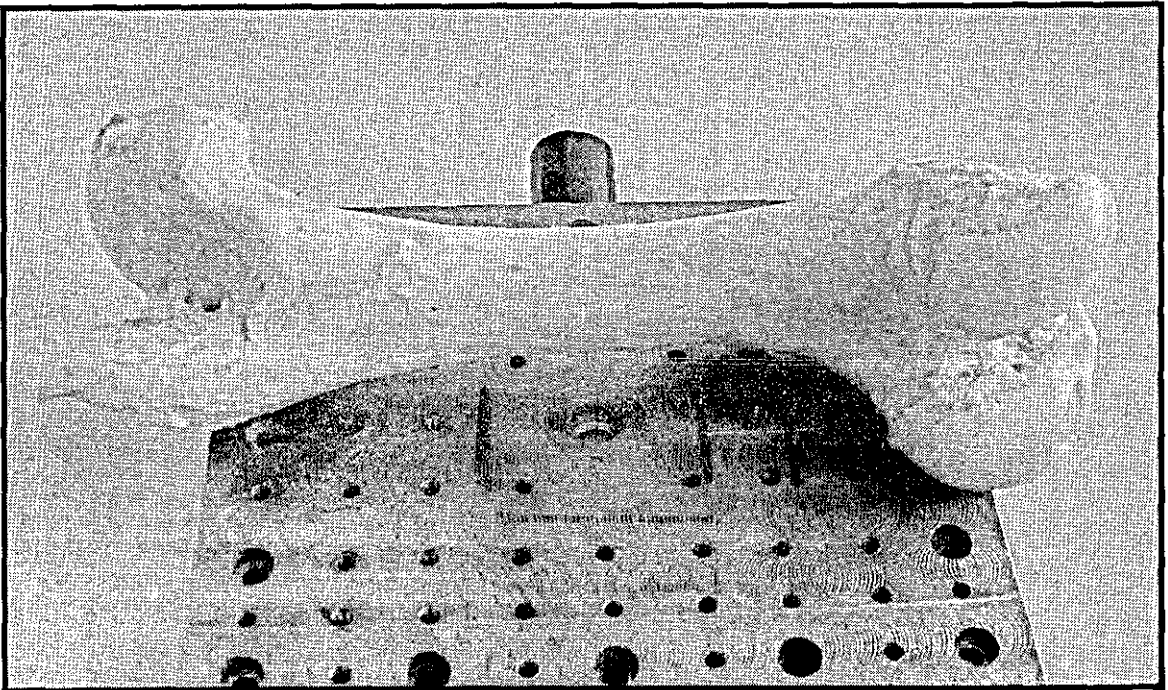
Figure 9.1   Pig Femur Bone Sample

A Dormer make industrial drill bit of $\phi 2.5$ mm diameter was used for drilling and surgical cancellous screws (Model No. 206.045, Synthes Ltd., UK) were used for screw pullout testing (refer to sections 8.2.2 and 8.3.2 for details).

9.1.3   Method Used and Observations

Drilling of bone was conducted at a constant speed of 800 rpm and a feed rate of 150 mm/min was selected based on the discussion in section 8.2.4.

The first few holes were drilled into the cow femoral shaft using a surgical drill bit. The drill bit broke after drilling the first two holes. This was because the cow femoral shaft was significantly hard (resulting in a higher drilling force) and the slippery and uneven surface of the bone caused drill misalignment. Slippery and uneven surface would be a common situation in the case of bone drilling which can cause frequent breaking of drill bits; therefore further experiments were carried out using an industrial drill bit as surgical drill bits are expensive and difficult to obtain. Also, similar results were obtained for surgical and industrial drill bits, as discussed in section 8.4.4.

Drilling was first carried out on pig femur and tibia bones using an industrial drill bit. This was followed by lamb femur bones then cow bones. The drilling force was recorded at a sampling rate of 1000 Hz. A typical bi-cortical drilling profile of the pig femoral shaft is shown in figure 9.2.
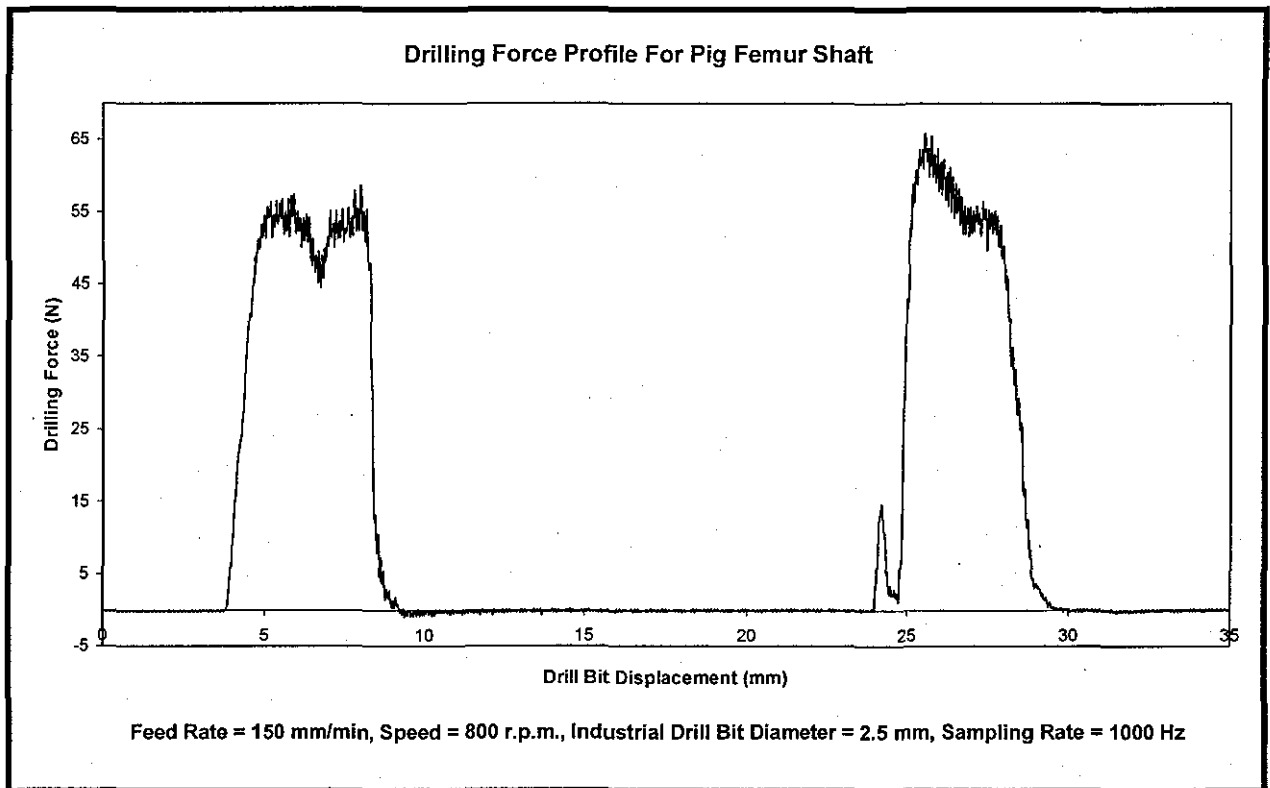
Figure 9.2   Bi-Cortical Drilling Force Profile for the Pig Femoral Shaft

Drilled holes were tapped using a tap supplied by the screw manufacturer. The screw pullout testing was carried out at a constant screw pullout rate of 5 mm/min and the screw pullout force data was recorded at a sampling rate of 500 Hz. A sampling rate of 500 Hz was used because screw pullout takes relatively a longer time compared to drilling which would result in a big data file. Moreover, there are no sudden changes that are expected in the screw pullout force profile as in the case of drilling force profile.

Initially, the screw was inserted into both cortices of the pig femoral shaft bone. After screw pullout testing, the screw was found bent and, because of this, a new screw was used for the next hole. The same observation was found for the first three holes tested. To visualise the cause of screw bending, the bone shaft was sawn perpendicular to the long axis of the femoral shaft, as shown in figure 9.3 (A). The bone marrow was removed to have a clear side view of the bone shaft. The side view of the bone shaft was visually observed during the drilling and screw pullout operation.
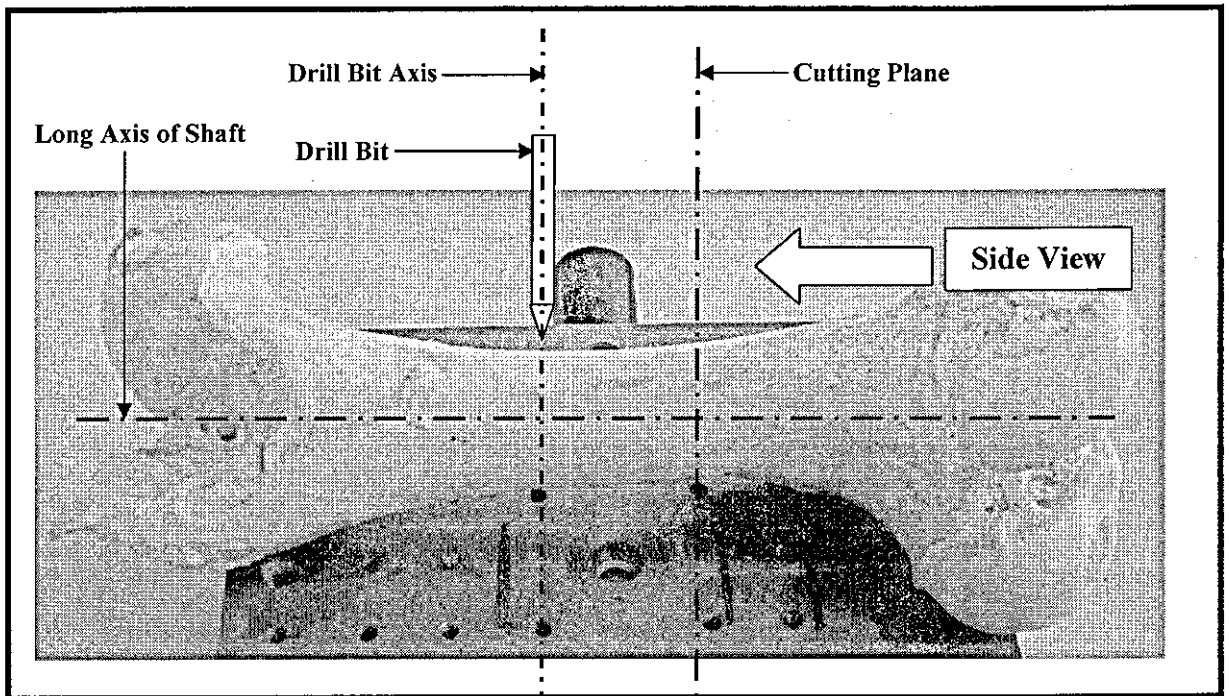
(A)   Cutting Plane, Drill Bit Axis and Long Axis of the Pig Femoral Shaft
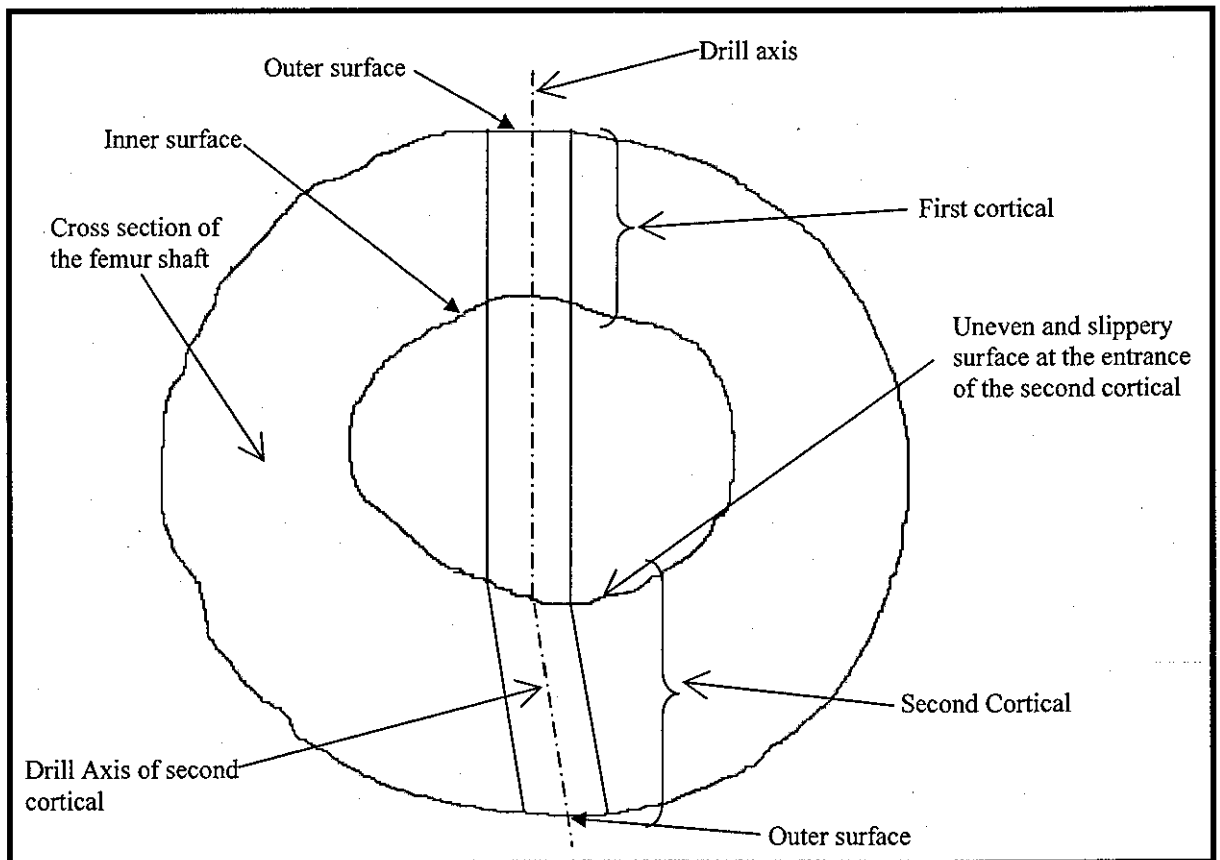
(B)   Side View Sketch of Pig Femoral Shaft Highlighting the Problem of Misalignment

Figure 9.3 Cutting Plane and Side View Sketch of the Pig Femoral Shaft

It was found that drilling in the first cortical was done without any error; however at the entrance of second cortical, the bone surface was very slippery and uneven which caused a slight bending of the drill bit, as shown schematically in figure 9.3 (B). This resulted in a different axis of the hole drilled into the second cortical. A comparatively higher torque was observed while inserting screw into the second cortical as compared to the first cortical (both cortices were pre tapped); this also supports the observation of the misalignment of the drilled hole axes in the two cortices. During the screw pullout operation, bending of the screw was visually observed from the side view. The bending of the screw could be because of the misalignment in the drilled hole axis and the higher force required to pullout the screw. To resolve this problem, further testing was done on the single cortical of the bone shaft. Single cortical testing can be justified because the screw pullout force depends directly on the length of the screw thread engaged into the bone. Inserting the screw in both cortices simply increases the screw pullout force; however, normalising the screw pullout force with respect to the length of screw thread engagement should make no difference to the results. The thickness of the bone shaft cortices was measured using the drill bit displacement and the force profiles. To further reduce the errors caused by uneven and slippery bone surface, a small indent on the bone surface was made prior to drilling. This would help to locate the drill bit during constant feed rate and would avoid a spike of high drilling force at the entrance of the drill bit.

Femur bones of pig, lamb and cow and tibia bones of pig were divided into three regions, (i) proximal end region, (ii) mid-shaft region and (iii) distal end region. This division is demonstrated in figure 9.4 for a pig femur bone. The location and numbers assigned to the holes drilled into the pig femur bone are also shown in figure 9.4.
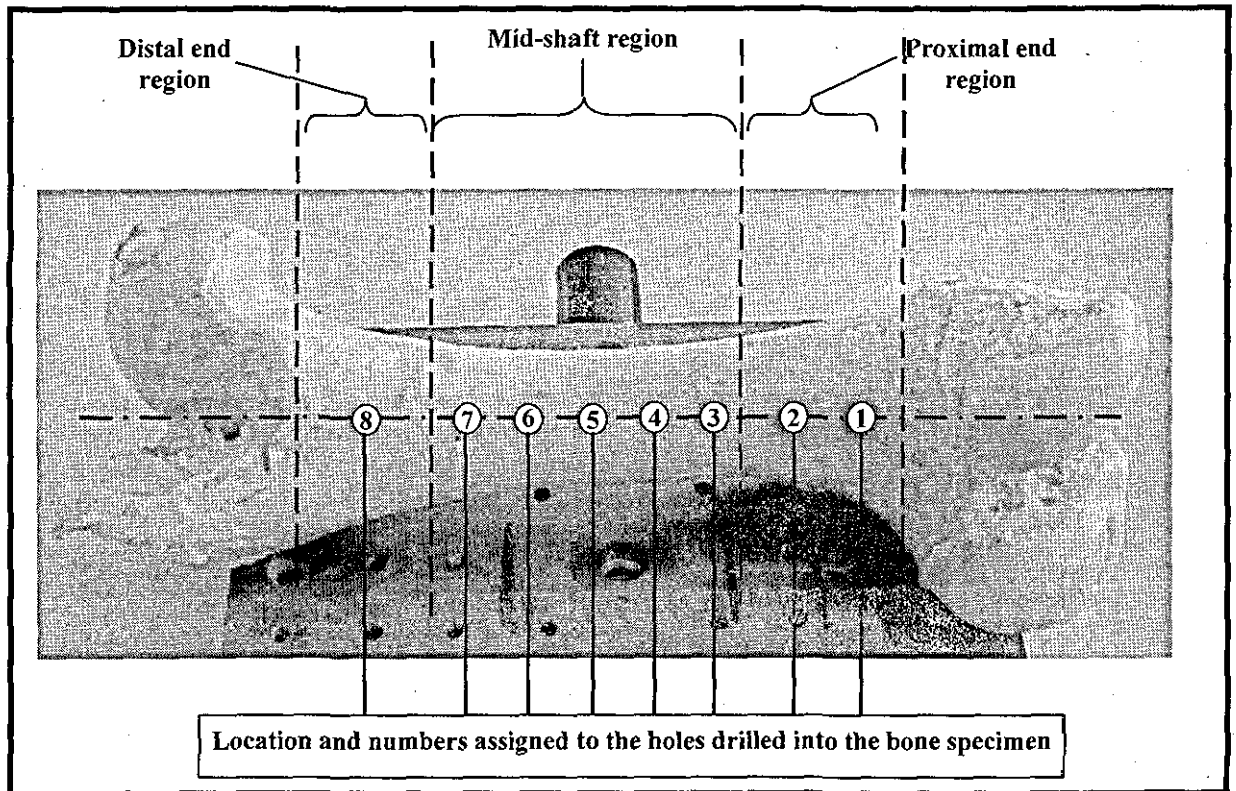
Figure 9.4   Location of Holes Drilled into the Femoral Shaft of a Pig

9.1.4   Results and Discussions

The thickness of bone samples vary for different drilling locations. Therefore, to have a standard platform, to find the correlation between drilling force and screw pullout force, the screw pullout force was normalised with respect to the bone thickness and the drilling force recorded over the entire length of the specimen thickness was averaged (for the drilled holes in the mid-shaft region) to find the correlation. A typical drilling force profile of the drilling locations in the mid-shaft region is shown in figure 9.5.

A typical drilling profile of a single cortical at the proximal end region (at location 1) of the pig femur bone is shown in figure 9.6. A sharp rise in the drilling force at the entrance (outer region of the bone) of the bone can be seen. However, no sharp fall in the drilling force was observed towards the exist of the drill bit (inner region of the bone).
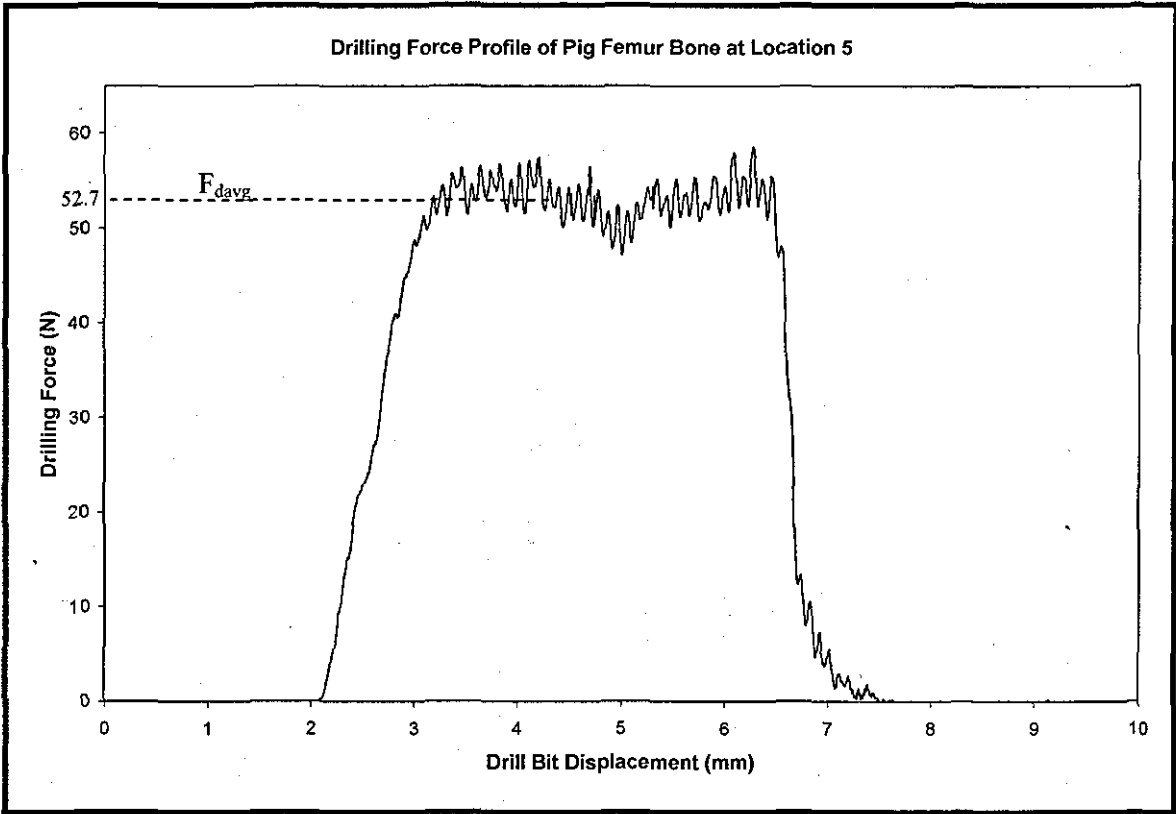
Figure 9.5 **Drilling Profile of a Single Cortical at the Mid-Shaft Region (at Drilling Location 5) of the Pig Femur Bone**

Feed Rate = 150 mm/min, Speed = 800 r.p.m., Industrial Drill Bit Diameter = 2.5 mm, Sampling Rate = 1000 Hz

t_t = total thickness of the specimen
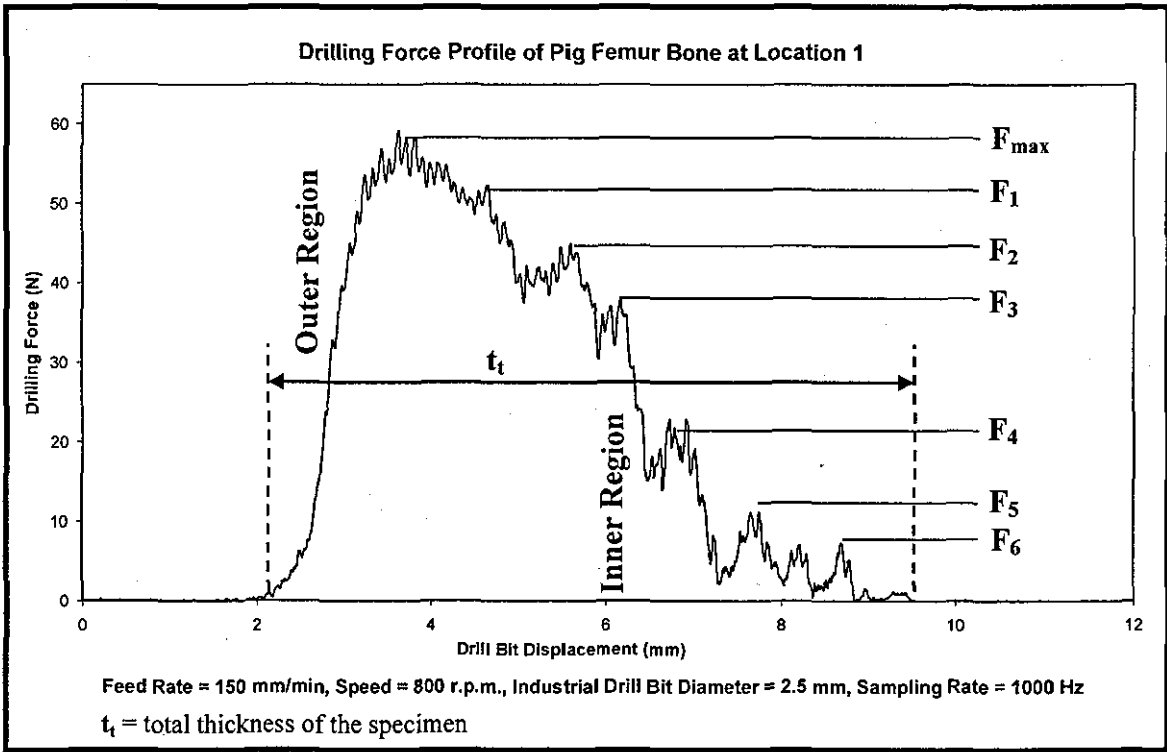
Figure 9.6 Drilling Profile of a Single Cortical at the Proximal End Region (at Drilling Location 1) of the Pig Femur Bone

Approximately six different regions of the different bone strength, in the inner region of location 1, can be identified from the six different magnitudes of the drilling force (i.e., F_{max}, F_1, F_2, ..., F_6) observed in the drilling profile. This shows that near the proximal end of the pig femur bone, the inner region is relatively not as strong as the outer region. This can be justified because towards the proximal and distal ends of the femur bone there would be more cancellous bone towards the inner side, which can be seen by the low magnitude of the drilling force. Similar observations can also be made in the drilling force profile of the single cortical in the proximal end region at drilling location 2, as shown in figure 9.7. Different regions of bone strength are shown by horizontal lines in the drilling force profile of location 2.
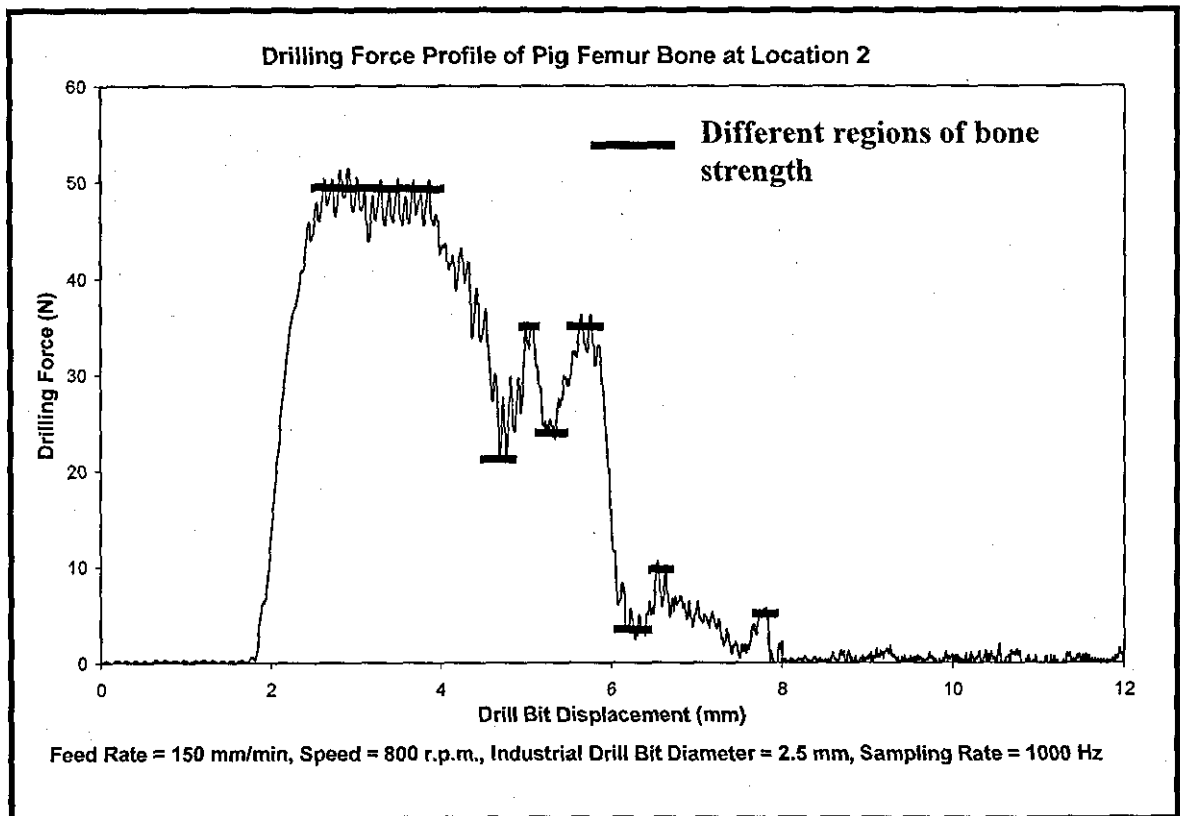
Figure 9.7   Drilling Profile of a Single Cortical at the Proximal End Region (at Drilling Location 2) of the Pig Femur Bone

As bone is non homogeneous in nature, its strength varies across the bone thickness. The change in the magnitude of the drilling force through the bone thickness was observed in the drilling profiles at the proximal end region and the distal end regions of both femur and tibia bones, reflecting different regions of bone strength. For the correlational study it will be erroneous to average the drilling force for the entire bone thickness in the case of the bone specimens having different regions of bone strengths. Moreover, normalising the screw pullout force over the entire thickness of the bone specimen in the case of the specimen with multi bone strength regions would again give inaccurate results. The contribution of the bone strength region thickness of different strengths to the overall screw pullout force could be established through multilayer testing proposed as part of future work in chapter 10. To have a meaningful correlational study, the drilling force should be significantly constant over the entire bone thickness and as such drilling profiles at the mid-shaft region of the femur and tibia shafts have been used. One such drilling profile of the mid-shaft region at drilling location 5 is shown in figure 9.5. Hence, for the correlational study only the mid shaft regions are considered which have fairly consistent bone strength over the entire bone thickness.

The locations of the holes drilled into the pig's mid-shaft region of the tibia are shown in figure 9.8. Drilling and screw pullout test results of pig femur and tibia mid-shaft regions are presented in table 9.1.
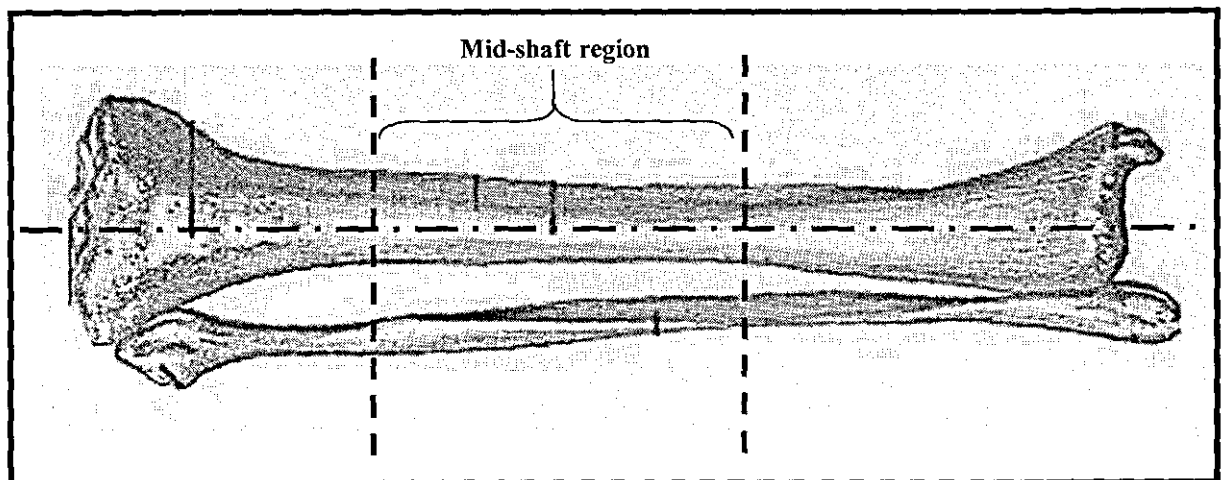
Figure 9.8   **Location of Holes Drilled into the Tibia Shaft of a Pig [182]**

Table 9.1 Drilling and Screw Pullout Test Results at the Mid-Region of Pig Femur and Tibia Bones

Drilling Location	Average Drilling Force (F_{davg}) (N)	Screw Pullout Force / Bone Thickness (F_{NSPF}) (N/mm)
Experimental Data of Pig Femoral Shafts (a & b)		
3a	49.77795	444.5822
4a	40.81792	329.4029
5a	52.74216	460.0652
6a	53.86781	469.0735
7a	52.17267	458.6496
3b	50.28918	441.928
4b	51.95742	444.914
5b	56.69305	518.7109
6b	53.08751	462.83
7b	51.25784	439.5392
Experimental Data of Pig Tibia Shafts (a&b)		
1a	48.08281	429.984
2a	52.57628	467.1431
3a	53.30277	456.5262
4a	52.36102	446.6017
1b	45.23067	386.9856
2b	42.78213	358.32
3b	46.57602	402.0395
4b	48.37879	421.6422

a = left side of the same animal

b = right side of the same animal

Figure 9.9 shows the average drilling force (F_{davg}) plotted against the normalised screw pullout force (F_{NSPF}). A correlation coefficient of $r^2 = 0.9587$ shows a strong relationship between the average drilling force and normalised screw pullout force.
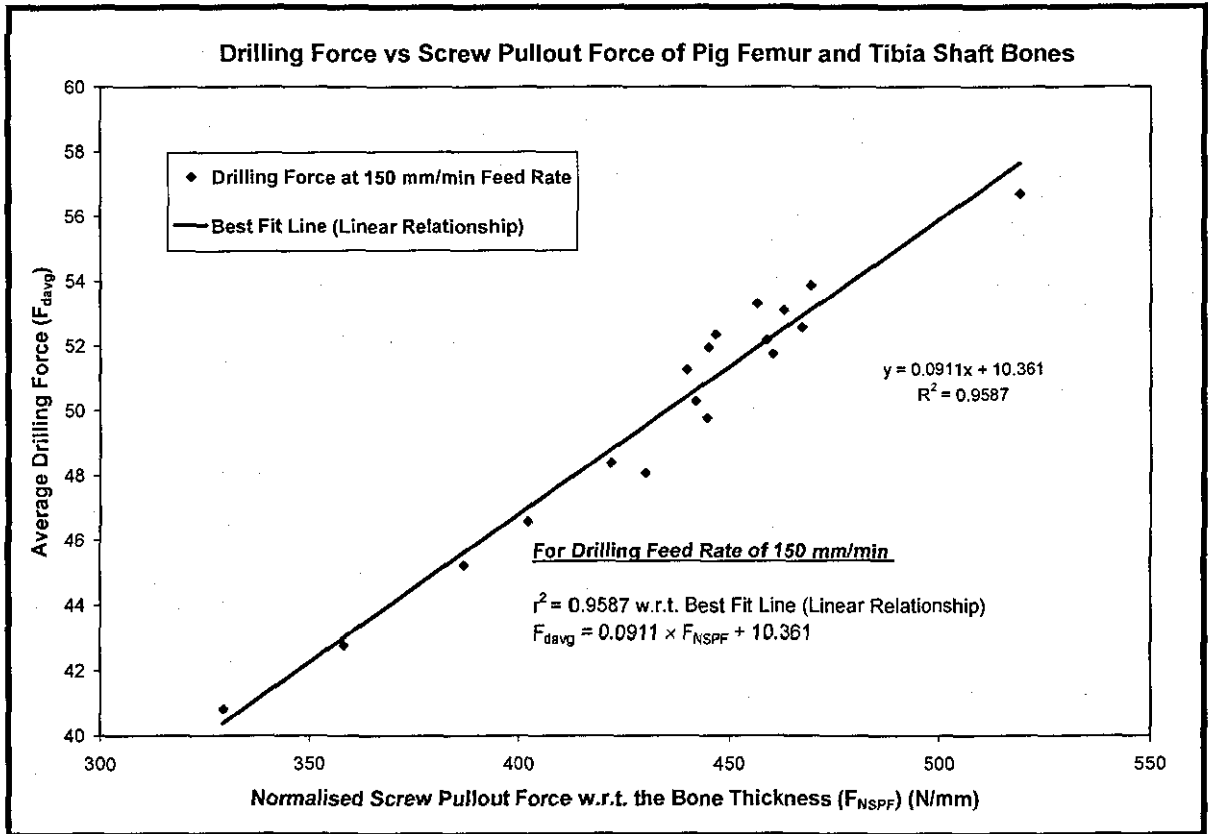
Figure 9.9 Relationship between Drilling Force and Screw Pullout Force For Pig Femur and Tibia Shaft Bone

Similar drilling and screw pullout tests were carried out on a lamb's left and right side femur bones. The drilling locations on the femoral shaft are shown in figure 9.10 and the test results are presented on table 9.2. Figure 9.11 shows the average drilling force (F_{davg}) plotted against the normalised screw pullout force (F_{NSPF}) for the lamb femur bone. A correlation coefficient of $r^2 = 0.9018$ shows a strong relationship between the drilling force and normalised screw pullout force. It can be seen that the results are not as good as for the pig femoral bones. This could be because the cortices in the lamb bones are thinner which results in a reduced number of engaged threads and thus increased error in computing the normalised screw pullout force.
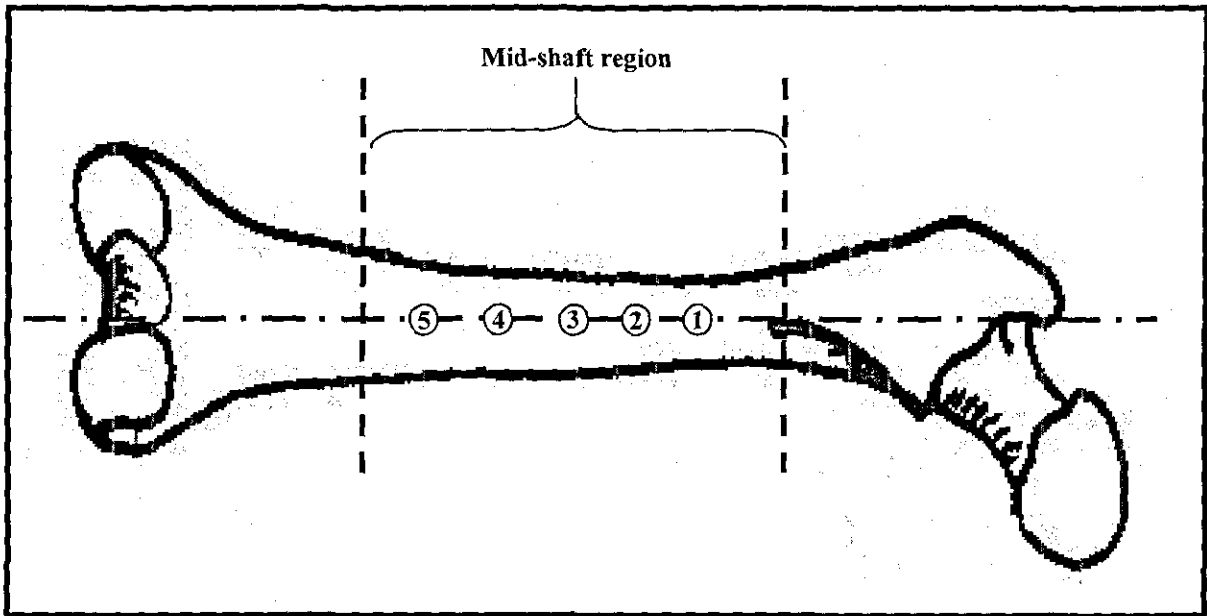
Figure 9.10   Location of Holes Drilled into the Femoral Shaft of a Lamb [183]

Table 9.2   Drilling and Screw Pullout Test Results of Lamb Femoral Shaft

Drilling Location	Maximum Drilling Force (N)	Screw Pullout Force / Bone Thickness (N/mm)
1a	56.1011	497.4936
2a	54.64812	489.704
3a	52.03814	463.3656
4a	53.59874	494.2345
5a	53.38349	474.5749
1b	48.45951	375.1821
2b	55.50914	505.6293
3b	56.61233	514.5873
4b	49.72414	380.1178
5b	54.94409	477.76

a = left side of the same animal

b = right side of the same animal
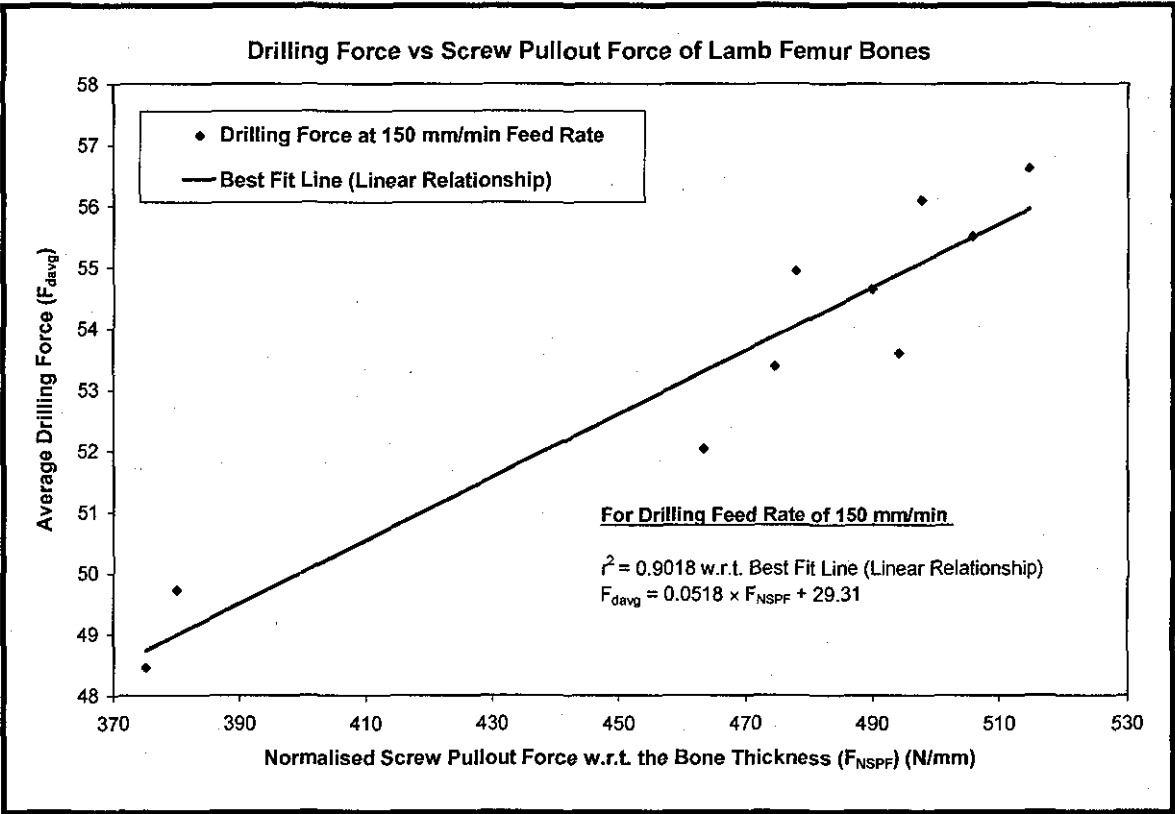
Figure 9.11   Relationship between Drilling Force and Screw Pullout Force For Lamb Femoral Shaft Bone

As discussed in section 9.1.3, the cow femur bone is stronger in comparison to the pig and lamb bones. A maximum drilling force of 197.69 N was observed in the case of the cow bone as compared to the maximum drilling force of 56.69 N observed in the case of pig and lamb bones. The screw pullout testing of the cow bone could not be carried out as the screws failed during pullout because of the required high screw pullout force. Hence, the relationship between drilling force and screw pullout force was not determined in the case of cow bones. For reference and future use, the single cortical drilling data recorded, at the drilling locations shown in figure 9.12, for the cow femur bone is presented in table 9.3.
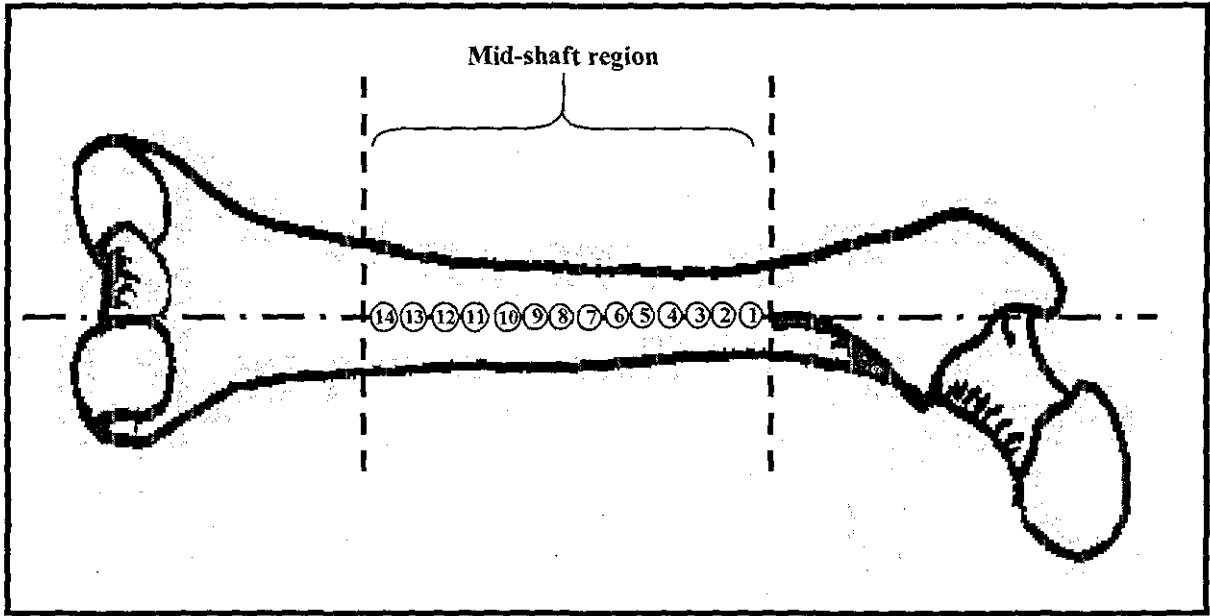
Figure 9.12   Location of Holes Drilled into the Femoral Shaft of a Cow

Table 9.3   Drilling Test Results of Cow Femoral Shaft Bone

Hole No.	1	2	3	4	5	6	7
Maximum Drilling Force (N)	191.60	193.78	197.69	190.69	151.70	136.31	91.59

Table 9.3   Drilling Test Results of Cow Femoral Shaft Bone (continued)

Hole No.	8	9	10	11	12	13	14
Maximum Drilling Force (N)	88.36	65.18	64.37	61.26	60.96	61.65	62.92

Table 9.3 shows that the maximum drilling force at drilling locations 1 to 6 is significantly higher than at other drilling locations. This was because in the region of drilling locations 1 to 6, there was a muscle or a ligament attached to the bone. This could have made the outer surface of the femoral shaft comparatively harder than the inner surface. A drilling profile of location 3 is shown in figure 9.13, which is a typical drilling profile of the drilling locations 1 to 6. Higher drilling force at the outer surface

of the femoral shaft clearly shows that the outer surface has higher strength as compared to the inner surface. The drilling force of the inner surface (61.1 N) was of the order of the drilling force found at locations 7 to 14, a typical profile of which is given in figure 9.14. This indicates that the inner region at drilling locations 1 to 6 is cortical and not cancellous. There were no muscles or ligaments attached at the drilling locations 7 to 14. Hence, a reasonable constant drilling force was observed throughout the bone thickness, as shown in figure 9.14. This observation shows that when considering the shaft of a bone for a study which requires a homogeneous bone sample, care should be taken to avoid the bone regions to which a ligament or muscle is attached.
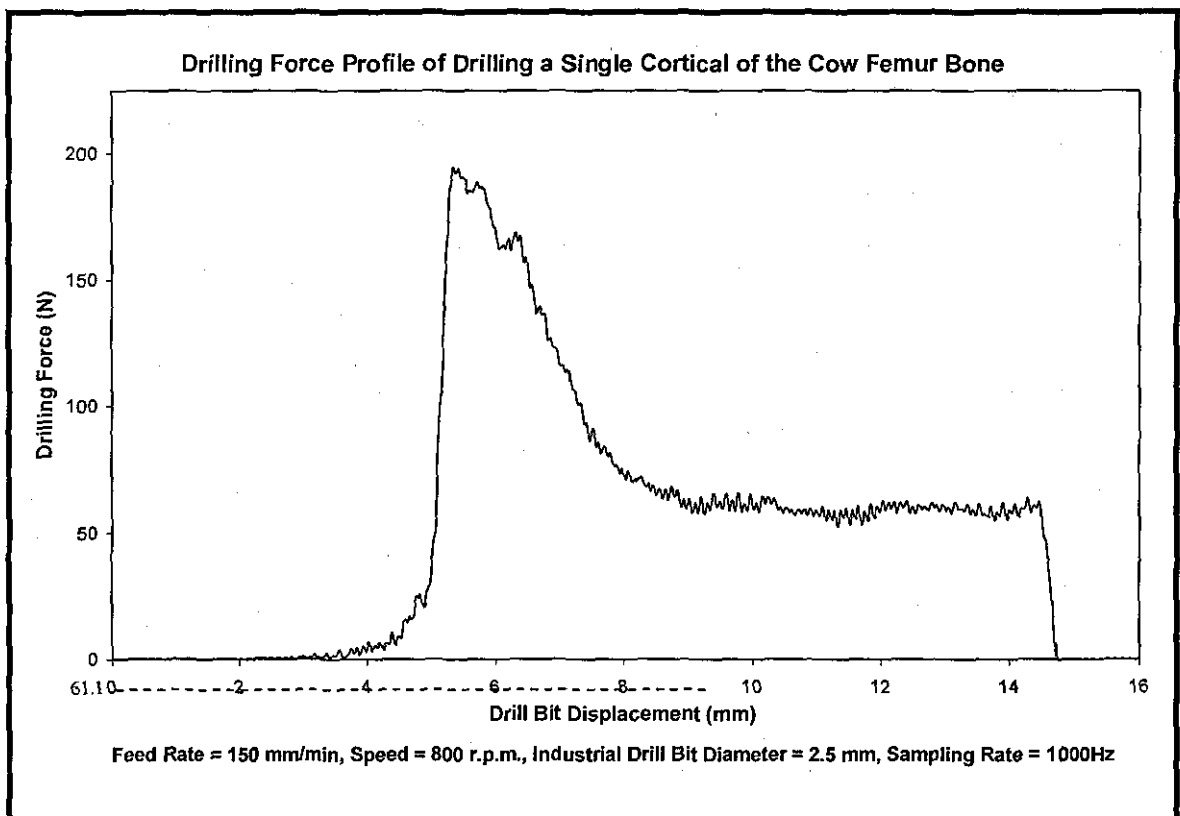
Figure 9.13   **Single Cortical Drilling Force Profile of Cow Femur at Drilling Location 3**
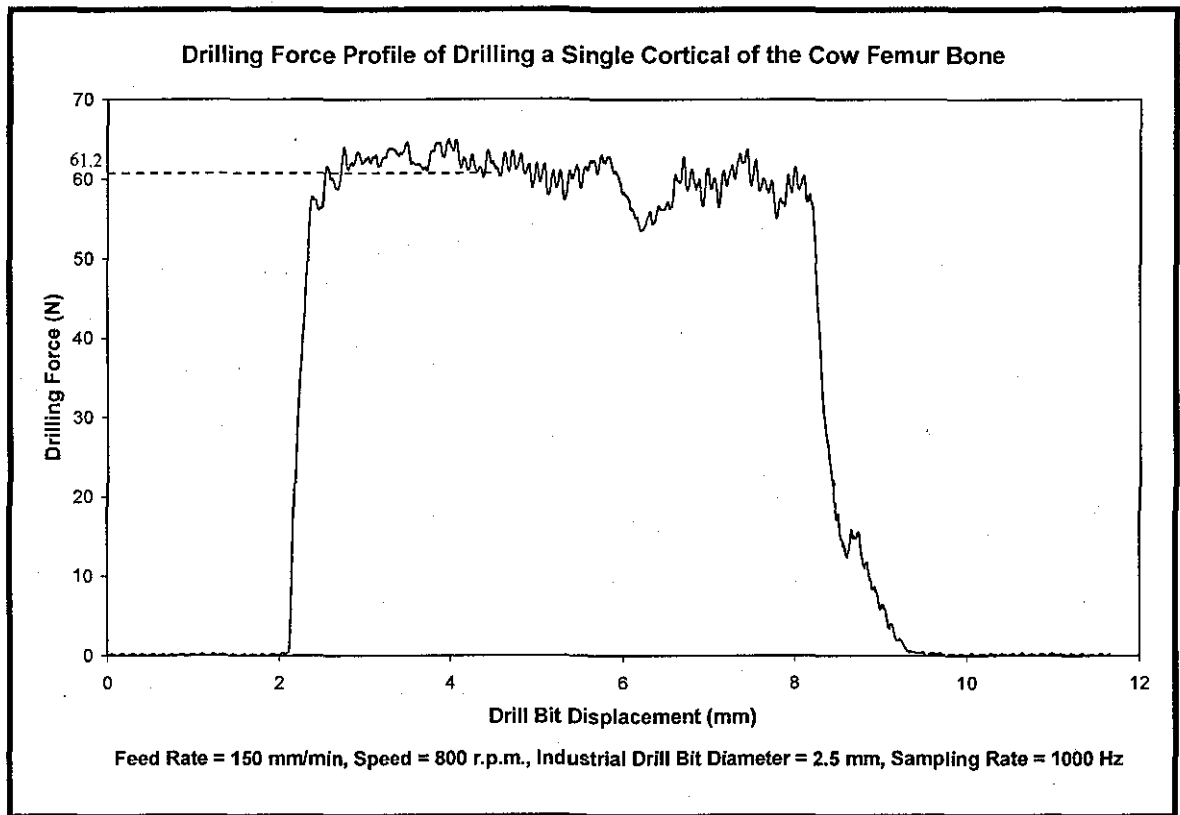
Figure 9.14   Single Cortical Drilling Force Profile of Cow Femur at Drilling Location 10

The average thickness of the bones used for testing was between 5 mm to 6 mm for the pig bones and between 3 mm to 5 mm for the lamb bones. This is deduced from the drilling profiles. The pitch of the screw used for pullout testing was 1.754 mm. Therefore, the approximate number of screw threads engaged into the bone specimens are 3 for pig bones and 2 for the lamb bones. This shows that the number of threads engaged are significantly low. To overcome this problem bone samples of higher thickness should be tested in the future, e.g., spine. Engagement of fewer threads in the case of lamb as compared to pig bones could be a reason of relatively lower correlation coefficient found in case of lamb bone ($r^2 = 0.901$) as compared to the pig bone ($r^2 = 0.958$). Hence, testing of lamb bones should be avoided for higher accuracy.

Cancellous screws were used in this research. These have a coarse pitch as compared to cortical screws. Hence, fine pitch cortical screws should also be used in future work to increase the number of threads engaged into the bone samples.

The screw pullout testing setup can be modified to get more accurate and consistent results in the case of bone testing. The main areas of improvement include the method of clamping the bone specimen and universal joint attachment used for the pullout operation.

Also, the outer surface of the bone samples can be filed to get a flat surface. This will avoid the walking of drill bit on the bone surface and would increase the accuracy of drilled holes.

The bone samples used in the experiments were the left side and right side bones of the same animal. Therefore, a wide range of bone strength was not tested. More bone samples of animals of different age should be tested to get a wider range of bone strength.

9.2   CONCLUDING REMARKS

Tests conducted on animal bones to investigate the correlation between drilling force and screw pullout force have been presented. A strong correlation of $r^2 = 0.958$ for pig bones and $r^2 = 0.901$ for lamb bones was found between the drilling force and screw pullout force. This verifies that drilling force data could be used to predict bone strength. Screw pullout tests could not be performed on cow femur bone as the screws failed due to the high screw pullout force. Further experimental tests using bone samples of animals of different age and on bones from different skeletal locations are necessary, in future work, to confirm the results of this study.

CHAPTER 10

CONCLUSIONS AND RECOMMENDATIONS FOR FURTHER WORK

In this chapter the conclusions that can be drawn from this study are summarised. The chapter aims to show how the objectives presented in Chapter 1 have been met. The chapter concludes with recommendations for further work. A list of proposed publications that are to be made as part of this study is also included.

10.1 CONTRIBUTION OF THE RESEARCH

This research has demonstrated the significant contribution of automation/mechatronics technology to orthopaedic surgery in two key areas, (i) the use of drilling force data to provide information about the strength of bone and (ii) the use of screw rotation angle during screw tightening to optimise the bone-screw fixation strength.

A significantly high value of correlation between drilling force and both the shear strength and screw pullout strength in synthetic bone material, of different densities, demonstrated the effectiveness of drilling force. The effectiveness of using drilling force data was also demonstrated for pig femur, pig tibia and lamb femur bones.

A new method of using screw rotation angle during screw tightening to optimise the bone-screw fixation strength was demonstrated successfully in synthetic bone material. This method overcomes the various disadvantages of the current system which was

proposed in the literature by other researchers. The current system uses screw insertion and screw tightening torque as control variables which depend upon the friction present between the screw and bone or screw and screw plate/washer interface. The proposed system is independent of the friction and depends only on the pitch of the screw used. Hence, the proposed method can be used effectively for any type of bone and also under any operating condition.

The contribution of this research is aided by the development of a novel experimental rig which enables bone tests to be carried out under a controlled environment.

10.2 CONCLUSIONS FROM THIS RESEARCH

This section aims to show how the objectives presented in chapter 1 have been met. The eight objectives are repeated here for clarity and are defined as:

Objective 1. To critically review the efficacy of using indirect methods to estimate bone strength in clinics and identify the limitations and errors involved in the estimations.

Objective 2. To investigate the advantages and limitations of using the screw pullout test against the available direct methods of bone strength measurement. This will support the use of screw pullout testing in this research to validate the use of bone drilling data for bone strength prediction.

Objective 3. To review the screw pullout test method and to identify the parameters affecting screw pullout strength. Also to identify the range of various screw pullout test parameters used in the literature. This helps in setting the design specifications of the test rig.

Objective 4. To study and review the use of screw insertion torque, screw tightening torque and screw rotation angle in optimising screw tightening.

Objective 5. To study and review the current progress of bone drilling. Also to identify the range and effect of various drilling parameters. This helps in setting the design specification of the test rig.

Objective 6. To design and develop an electromechanical test rig which can cater for bone drilling, screw insertion, screw removal, screw pullout and screw stripping tests. This development involves also interfacing of the rig with a personal computer and software programming for the control of the tests and data acquisition.

Objective 7. To demonstrate a correlation between the drilling force and screw pullout strength by using the data acquired during the drilling and screw pullout testing of synthetic bone material and animal bone. This is to verify the use of drilling data in predicting bone strength.

Objective 8. To investigate the relationship between the screw rotation angle and screw pullout strength of foam in order to investigate the use of screw rotation angle in optimising the strength of bone-screw fixation.

To support objective 1, a critical literature review of the indirect methods was conducted and subsequently a review journal paper was submitted. The various commercial indirect methods evaluated in this research are not very accurate, effective and reliable methods for in-vivo bone strength prediction. An ideal method of in-vivo bone strength prediction should be cheap, accurate, easy to use and easy to interpret. Hence, the use of bone drilling data as an alternative in-vivo method to predict bone strength has been explored in this research. The following conclusions were drawn from the review:

- Bone density, when measured using a standard method, can predict bone strength more accurately as compared to the commonly available commercial densitometry techniques (QCT, pQCT and DXA).

- The use of QCT is limited because it is expensive and exposes patients to high radiation.

- pQCT has a limited use as it can only be used at the peripheral bone sites and DXA bone density measurements, when performed in-vivo, could lead to an inaccurate or wrong prediction of the bone strength.

- Variation in bone geometry, use of non-site specific bone density measurement, and bone anisotropy affect the bone strength prediction using the indirect methods.

- Bone densitometry methods were found to be better predictors of bone strength as compared to the Singh Index and ultrasound methods.

- The Singh Index is subjective and its use to predict bone strength was not recommended.

- Among ultrasound measurements, SOS can be used to predict bone strength, and the use of BUA is not recommended as it can lead to a wrong prediction of bone strength. Moreover, the use of ultrasound methods is limited to only the peripheral sites.

To satisfy objective 2, screw pullout testing was evaluated against other direct testing methods. Based on the following advantages, screw pullout testing was selected for the validation of the drilling force data to predict bone strength. The advantages of screw pullout testing are:

- Any shape and size of bone specimen can be tested.

- Less number of bone samples are required

- Specimen preparation is easy

- The specimen is not removed from its parent bone; hence the tests are carried out under physiologic boundary conditions.

- Location of failure or region of interest can be controlled.

- No special fixtures are required for specimen clamping.

- Combined strength of cortical and cancellous bone can be evaluated.

- It simulates the actual or practical condition of bone-screw failure; hence it gives a direct measure of bone-screw fixation strength.

- Screw pullout test data can also be used in future to optimise the parameters which affect bone-screw fixation strength, e.g., bone screw design.

- Additional information, like screw insertion/tightening torque and screw rotation angle during screw tightening can be collected during testing and analysed to optimise the bone-screw fixation strength.

To accomplish objective 3, various parameters affecting the screw pullout force were identified. These parameters are shear strength of the material under testing and thread geometry which includes the major and minor diameters of the thread, thread pitch and thread angle. Based on these parameters, a formula to calculate screw pullout force (developed for metals) was validated in the literature for two different densities of synthetic bone material. After a critical evaluation, in this study, it was found that a wrong formula was applied by the researchers in the case of surgical screws. The values of thread angle and minor diameter of the thread were not used accurately. Using the correct values and applying the formula over a wide range of foam density, it was found that the formula gave inconsistent results with respect to experimental results and therefore it should be modified for it to be used accurately in the case of surgical screws and bone material. A journal paper will be published on this highlighting an accurate use of the formula and will present the results found in this research showing how this formula does not give an accurate result for different density of synthetic bone material.

An electromechanical test rig was successfully designed and commissioned based on the design parameters identified from the literature. The test rig can conduct drilling, screw insertion, screw removal, screw stripping and screw pullout testing under a controlled environment in a single setting of the specimen, satisfying objective 3, 5 and 6. The designed test rig was controlled using a computer and had an accuracy of 0.089 N in the measurement of drilling force, 4 N in the measurement of screw pullout force and 0.18 degree in the control of the screw rotation angle during screw insertion or screw tightening. The test rig has high precision or repeatability which was demonstrated by a small average standard deviation value of 0.039 N for drilling force

tests and 10 N for screw pullout force tests, for the homogeneous FR-6700 synthetic bone material.

The bone drilling process was reviewed to accomplish objective 5. In all the models presented in the literature to calculate drilling force, there is no model which can be used to calculate drilling force without conducting experiments, as all models have some parameters the values of which have to be determined experimentally. However, there was a direct relationship in all the models between drilling force and the material property (either specific energy or yield shear strength). This means that drilling force can be used to give information about the material strength. This was proved experimentally for two different types of synthetic bone materials, FR-3700 and FR-6700, tested over a wide density range. Drilling force showed a significantly high correlation coefficient of $r^2 > 0.99$ with material shear strength, for both type of foam materials. Hence, drilling force can predict the material shear strength.

Similar drilling results were found when drilling was conducted at two different drilling feed rate values, 150 mm/min and 250 mm/min. Therefore, future experiments can be designed to be conducted at a single drill feed rate value.

The current method of using bone density measurements to predict bone strength was not supported in this research, as bone strength depends upon many factors and bone mineral density is only one of them. This was verified when a different value of shear strength and drilling force was found for two different foam material having the same density, e.g., FR-3730 and FR-6730.

A strong power correlation ($r^2 > 0.98$) was found between the drilling force and density of synthetic bone material.

A strong correlation ($r^2 > 0.99$) found between screw pullout force and shear strength for the synthetic bone material verifies that the screw pullout force gives a significantly good estimation of shear strength. Hence, screw pullout force can be used for the correlation of drilling force to investigate the efficacy of drilling force in estimating the shear strength of the bone. This supports objective 2.

The strong correlation ($r^2 > 0.99$) which was found between drilling force and screw pullout force in synthetic foam material suggests that drilling force is a good predictor of material shear strength. This satisfies objective 7.

Similar relationships were found in synthetic bone material for both industrial and surgical drill bits. This suggests that industrial drill bits can be used to conduct future experiments as they are easily available and inexpensive.

The use of screw rotation angle to optimise bone-screw fixation strength was successfully demonstrated for the synthetic bone material FR-6700. This meets objectives 4 and 8. The optimum angle for the tested screw was found to be 120° which is equivalent to 33% of the screw pitch. This technique was found to be independent of the friction between the screw and bone or screw and screw plate/washer and material density.

A strong correlation of $r^2 = 0.958$ for pig bones and $r^2 = 0.901$ for lamb bones was found between drilling force and screw pullout force. This verifies that drilling force data can be used to predict bone strength. This achieves objective 7. The strong value of correlation suggests that drilling force data is a better predictor of screw pullout strength or bone-screw fixation strength in comparison to the bone density and screw insertion torque.

10.3   RECOMMENDATIONS FOR FUTURE WORK

This research has successfully demonstrated the efficacy of using drilling force data to give information about the strength of bone and the use of screw rotation angle to optimise the bone-screw fixation strength. This was achieved with the help of an electromechanical test rig which was designed and developed as a part of this research. During the process of this research a number of interesting areas worthy of future work have been identified; these are:

1. <u>Number of Samples of Animal Bone.</u> The number of animal bone samples used in this investigation is relatively small, which can have a significant effect on the correlation. In order to verify the relationship between drilling force and screw pullout force in animal bones, a lot more experimental measurements are needed.

2. <u>Improvement of Screw Pullout Testing Set Up.</u> The present setup used for screw pullout testing has significantly negligible errors when testing regular shape specimens, like synthetic bone material. However, maintaining the direction of screw pullout force in line with the screw axis, in the case of irregular shaped specimens like animal bone was found difficult. This misalignment can be the cause of the lower correlations found for animal bones. Therefore, screw pullout testing setup should be modified to minimise the error caused due to the misalignment.

3. <u>Recording the Screw Clamping Force.</u> Further insertion of screw after head contact (HC) point generates a clamping force in the screw joint. This clamping force can be recorded by using a washer type load cell and placing it in between the screw head and specimen surface, as shown in figure 10.1. It is believed that during screw tightening there should be a relationship between clamping force and screw rotation angle and also with the screw pullout force, as explained in section 6.3.2 and in equations 6.1 and 6.2. Experiments should be conducted to explore these relationships. If a relationship is found then the clamping force could be used, instead of the screw pullout force, to determine the critical screw rotation angle during screw insertion to optimise the bone-screw fixation strength. This will avoid the alignment errors associated with the screw pullout testing in animal bones and the requirement of having to use a large sample size.
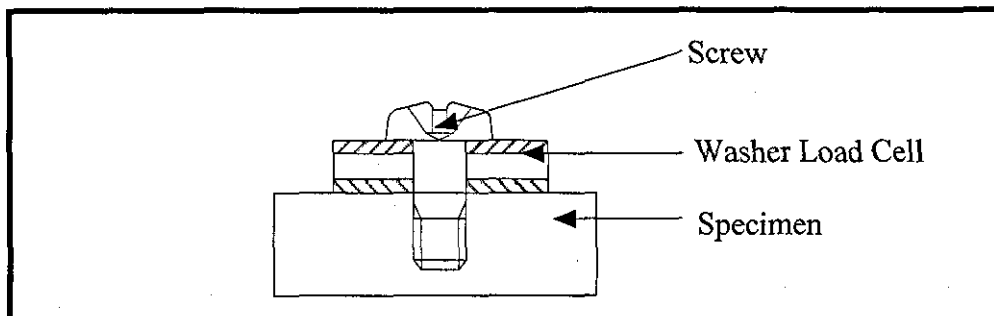
Figure 10.1   Use of Washer Load Cell to Record Clamping Force in the Screw Joint

4. <u>Using Different Animal Bone Samples with a Wide Range of Strength.</u> The correlation between drilling force and screw pullout force of cortical bone from the femoral and tibia shaft of pig and femoral shaft of lamb can be improved by conducting experiments on pig and lamb bones of different ages which will give a wider range of bone strength.

5. <u>Testing Various Screw Designs to Verify the Use of Rotation Angle to Optimise Bone-Screw Fixation Strength.</u> Only one type of screw was tested to successfully demonstrate the use of screw rotation to optimise the bone-screw fixation strength. Further test should be carried out to confirm the concept using different screw designs with different pitches.

6. <u>Verify the Use of Screw Rotation Angle in Animal Bones.</u> The use of screw rotation angle to optimise the bone-screw fixation strength was successfully demonstrated on synthetic bone material in this research. Further tests on animal bones should be conducted to verify this concept in animal bones. However, the following points should be considered during the experiment design process:

    • Since bone is non-homogeneous, anisotropic in nature and moreover the bone strength is site specific; therefore it will be erroneous to use the screw pullout force value measured at one location, at zero degree of screw rotation, as a reference value for comparison with the screw pullout force reading taken for a different screw rotation angle at another location. To overcome this problem, one should consider using vertebrae bones (see below) and/or doing tests at a same location in left and right bones from the same animal/human bones.

    • Smaller length of screws would be needed when testing the single cortex of the femur or tibia shaft bone. This is to ensure that the screw does not penetrate into the second cortex of the bone.

    • Instead of using femur or tibia shaft bone samples, vertebrae bone should be tested. Vertebra bone is mostly cancellous bone and may give better results.

7. Drill Bit Clogging Problem. Consideration has to be given to the problem of drill bit clogging due to the large drilling depth in the case of drilling the cancellous bone, like femoral head. This is to ensure that possible correlations are not adversely affected by the drill bit clogging. In addition, the flow of blood in the proximal femur during drilling may have an effect on the drilling forces.

8. Multi Layer Testing of Synthetic Bone to Evaluate the Contribution of Cancellous Layer of Bone to the Combined Screw Pullout Strength of Cortical and Cancellous Bone. Different synthetic bone samples can be made by joining two or more different synthetic bone samples having different densities. This will create a multilayer sample. A different combination of densities and thicknesses can be used. Drilling and screw pullout forces of various multilayer samples should be recorded. Different values of drilling force should be observed for two or more different layers. Knowing the screw pullout force of the individual layers (from this research), the contribution of each layer to the combined screw pullout strength can be calculated. This will provide information on how the drilling force of different layers is related to the combined screw pullout strength. The results of this exercise will be useful when analysing the bone drilling data, to get an approximate contribution of each layer to the overall screw pullout strength.

9. Conducting Experiments on Human Bones. The present investigation has used pig femur, pig tibia and lamb femur bones to show the correlation between drilling force and screw pullout force. However, the characteristics of drilling force and screw pullout force may be different on human bones. Therefore, sufficient numbers of experiments need to be conducted on human bones in order to establish the relevant relationship. In addition, the experimental rig may have to be modified to cater for human bones. Ethical issues must be considered before the tests are considered.

10. Development of a Handheld Mechatronics Drilling Device. A handheld mechatronics drill, screw insertion and screw tightening system for orthopaedic surgery can be developed to provide in-vivo information on bone strength and to

control the screw rotation angle to achieve the optimum bone-screw fixation strength. The aim is to assist orthopaedic surgeons in the decision making related to the treatment of a fracture, improvement in the quality of fixation and the management of post-operative treatment.

10.4 PUBLICATIONS

As part of this research the planned journal papers for the publication are given below.

Submitted:

A. Jain, K. Bouazza-Marouf, G. J. S. Taylor and A. Gulihar., Evaluation of indirect bone strength measurement methods. Osteoporosis International.

Planned:

A. Jain, K. Bouazza-Marouf, G. J. S. Taylor and A. Gulihar., Validation of the theoretical screw pullout force model in synthetic bone material. Journal of Biomechanical Engineering.

A. Jain, K. Bouazza-Marouf, G. J. S. Taylor and A. Gulihar., Use of drilling force to predict bone quality. Proceedings of the Institution of Mechanical Engineers. Part H, Journal of Engineering in Medicine.

A. Jain, K. Bouazza-Marouf, G. J. S. Taylor and A. Gulihar., Use of screw rotation angle to optimise the bone-screw fixation quality. Clinical Biomechanics.

REFERENCES

1. Faulkner K.G., Gluer C.C., Majumdar S., Lang P., Engelke K., and Genant H.K., Non-invasive measurements of bone mass, structure, and strength: current methods and experimental techniques. *American Journal Roentgenology (AJR)*, 1991, Vol. 157(6), pp. 1229-37.

2. Daftari T.K., Horton W.C., and Hutton W.C., Correlations between screw hole preparation, torque of insertion, and pullout strength for spinal screws. *Journal of Spinal Disorder*, 1994, Vol. 7(2), pp. 139-45.

3. Cheng X.G., Lowet G., Boonen S., Nicholson P.H., Van der Perre G., and Dequeker J., Prediction of vertebral and femoral strength in vitro by bone mineral density measured at different skeletal sites. *Journal of Bone and Mineral Research*, 1998, Vol. 13(9), pp. 1439-1443.

4. Lochmuller E.M., Groll O., Kuhn V., and Eckstein F., Mechanical strength of the proximal femur as predicted from geometric and densitometric bone properties at the lower limb versus the distal radius. *Bone*, 2002, Vol. 30(1), pp. 207-16.

5. Lochmuller E.M., Lill C.A., Kuhn V., Schneider E., and Eckstein F., Radius bone strength in bending, compression, and falling and its correlation with clinical densitometry at multiple sites. *Journal of Bone and Mineral Research*, 2002, Vol. 17(9), pp. 1629-38.

6. Koo M.W., Yang K.H., Begeman P., Hammami M., and Koo W.W., Prediction of bone strength in growing animals using noninvasive bone mass measurements. *Calcified Tissue International*, 2001, Vol. 68(4), pp. 230-4.

7.   **Robert. M D.F., Jennifer.K,** Osteoporosis, ed. Edition, S. Vol. One. 2001, *Academic Press.*

8.   **Eckstein F., Kuhn V., and Lochmuller E.-M.,** Strength prediction of the distal radius by bone densitometry-evaluation using biomechanical tests. *Annals of Biomedical Engineering,* 2004, Vol. 32(3), pp. 487-503.

9.   **Morgan E.F., Bayraktar H.H., and Keaveny T.M.,** Trabecular bone modulus-density relationships depend on anatomic site. *Journal of Biomechanics,* 2003, Vol. 36(7), pp. 897-904.

10.   **Cefalu C.A.,** Is bone mineral density predictive of fracture risk reduction? *Current Medical Research and Opinion,* 2004, Vol. 20(3), pp. 341-349.

11.   **Rubin C.D.,** Emerging concepts in osteoporosis and bone strength. *Current Medical Research and Opinion,* 2005, Vol. 21(7), pp. 1049-56.

12.   **Bolotin H.H.,** The significant effects of bone structure on inherent patient-specific DXA in vivo bone mineral density measurement inaccuracies. *Medical Physics,* 2004, Vol. 31(4), pp. 774-88.

13.   **Bolotin H.H.,** Inaccuracies inherent in dual-energy X-ray absorptiometry in vivo bone mineral densitometry may flaw osteopenic/osteoporotic interpretations and mislead assessment of antiresorptive therapy effectiveness. *Bone,* 2001, Vol. 28(5), pp. 548-55.

14.   **Bolotin H.H.,** A new perspective on the causal influence of soft tissue composition on DXA-measured in vivo bone mineral density. *Journal of Bone and Mineral Research,* 1998, Vol. 13(11), pp. 1739-46.

15. **Bolotin H.H.**, Analytic and quantitative exposition of patient-specific systematic inaccuracies inherent in planar DXA-derived in vivo BMD measurements. *Medical Physics*, 1998, Vol. 25(2), pp. 139-51.

16. **Zdeblick T.A., Kunz D.N., Cooke M.E., and McCabe R.**, Pedicle screw pullout strength. Correlation with insertional torque. *Spine*, 1993, Vol. 18(12), pp. 1673-6.

17. **Abouzgia M.B. and James D.F.**, Measurements of shaft speed while drilling through bone. *Journal of Oral and Maxillofacial Surgery*, 1995, Vol. 53(11), pp. 1308-15; discussion 1315-6.

18. **Hobkirk J.A. and Rusiniak K.**, Investigation of variable factors in drilling bone. *Journal of Oral Surgery (American Dental Association : 1965)*, 1977, Vol. 35(12), pp. 968-973.

19. **Jacob C.H. and Berry J.T.**, A study of the bone machining process--drilling. *Journal of Biomechanics*, 1976, Vol. 9(5), pp. 343-349.

20. **Wiggins K.L. and Malkin S.**, Drilling of bone. *Journal of Biomechanics*, 1976, Vol. 9(9), pp. 553-559.

21. **Lawson K.J. and Brems J.**, Effect of insertion torque on bone screw pullout strength. *Orthopedics*, 2001, Vol. 24(5), pp. 451-4.

22. **Chagneau F. and Levasseur M.**, Mechanical Analysis of bone structures by Dynamostratigraphy. *European Journal of Mechanics - A/Solids*, 1992, Vol. 11(4), pp. 551-571.

23. **Ong F.R. and Bouazza-Marouf K.**, Evaluation of bone strength: correlation between measurements of bone mineral density and drilling force. *Proceedings of the Institution of Mechanical Engineers. Part H, Journal of Engineering in Medicine*, 2000, Vol. 214(4), pp. 385-99.

24. **Bouazza-Marouf K.**, Development of a handheld Mechatronic drill. *Internal document defining the original outlines of the research, Loughborough University,* 2000.

25. **Khurmi R.S. and Gupta J.K.**, A textbook of machine design. 2006, *S. Chand & Company Ltd., India.*

26. **Currey J.D.**, Bone strength: What are we trying to measure? *Calcified Tissue International,* 2001, Vol. 68(4), pp. 205-10.

27. **Ammann P.**, Bone strength and its determinants. *Therapie,* 2003, Vol. 58(5), pp. 403-407.

28. **Beck T.**, Measuring the structural strength of bones with dual-energy X-ray absorptiometry: principles, technical limitations, and future possibilities. *Osteoporosis International,* 2003, Vol. 14 Supplement 5, pp. 81-8.

29. **Evans F.G.**, Mechanical properties of bone. 1973, *Charles C Thomas Publisher.*

30. **An Y.H.**, *Mechanical testing of bone and the bone-implant interface.* 2000, CRC Press.

31. **Turner C.H. and Burr D.B.**, Basic biomechanical measurements of bone: a tutorial. *Bone,* 1993, Vol. 14(4), pp. 595-608.

32. **Athanasiou K.A., Zhu C., Lanctot D.R., Agrawal C.M., and Wang X.**, Fundamentals of biomechanics in tissue engineering of bone. *Tissue Engineering,* 2000, Vol. 6(4), pp. 361-81.

33. **Bouxsein M.L.**, Bone quality: where do we go from here? *Osteoporosis International,* 2003, Vol. 14 Supplement 5, pp. 118-27.

34. **Watts N.B.,** Bone quality: getting closer to a definition. *Journal of Bone and Mineral Research*, 2002, Vol. 17(7), pp. 1148-50.

35. **Stromsoe K., Hoiseth A., Alho A., and Kok W.L.,** Bending strength of the femur in relation to non-invasive bone mineral assessment. *Journal of Biomechanics*, 1995, Vol. 28(7), pp. 857-61.

36. **Ferrari S.L.,** Genetic determinants of bone strength and fracture in humans: dreams and realities. *Osteoporosis International*, 2003, Vol. 14 Supplement 5, pp. 107-12.

37. **Snyder S.M. and Schneider E.,** Estimation of mechanical properties of cortical bone by computed tomography. *Journal of Orthopaedic Research*, 1991, Vol. 9(3), pp. 422-31.

38. **Ammann P. and Rizzoli R.,** Bone strength and its determinants. *Osteoporosis International*, 2003, Vol. 14 Supplement 3, pp. S13-8.

39. **Kowalchuk R.M. and Dalinka M.K.,** The Radiologic Assessment of Osteoporosis. *University of Pennsylvania Orthopaedic Journal*, 1998, Vol. 11, pp. 67-72.

40. **Faulkner K.G.,** Bone matters: are density increases necessary to reduce fracture risk? *Journal of Bone and Mineral Research*, 2000, Vol. 15(2), pp. 183-7.

41. **Friedman A.W.,** Important determinants of bone strength: beyond bone mineral density. *Journal of Clinical Rheumatology*, 2006, Vol. 12(2), pp. 70-7.

42. **Rho J.Y., Kuhn-Spearing L., and Zioupos P.,** Mechanical properties and the hierarchical structure of bone. *Medical Engineering and Physics*, 1998, Vol. 20(2), pp. 92-102.

43. **Follet H., Boivin G., Rumelhart C., and Meunier P.J.,** The degree of mineralization is a determinant of bone strength: a study on human calcanei. *Bone*, 2004, Vol. 34(5), pp. 783-9.

44. **Linde F. and Sorensen H.C.,** The effect of different storage methods on the mechanical properties of trabecular bone. *Journal of Biomechanics*, 1993, Vol. 26(10), pp. 1249-52.

45. **Keaveny T.M., Guo X.E., Wachtel E.F., McMahon T.A., and Hayes W.C.,** Trabecular bone exhibits fully linear elastic behavior and yields at low strains. *Journal of Biomechanics*, 1994, Vol. 27(9), pp. 1127-1136.

46. **Beaupied H., Lespessailles E., and Benhamou C.L.,** Evaluation of macrostructural bone biomechanics. *Joint Bone Spine*, 2007, Vol. 74(3), pp. 233-9.

47. **Levenston M.E., Beaupre G.S., and van der Meulen M.C.,** Improved method for analysis of whole bone torsion tests. *Journal of Bone and Mineral Research*, 1994, Vol. 9(9), pp. 1459-65.

48. **Oberg Erik, Jones Franklin D., L H.H., and Ryffel H.,** Machinery's Handbook. 27 ed. 2004, *Industrial Press, Inc.*

49. **FED-STD,** Screw-thread standards for federal services. *Federal Standard*, 1991, Vol. FED-STD-H28/2B(August).

50. **Stromsoe K., Kok W.L., Hoiseth A., and Alho A.,** Holding power of the 4.5 mm AO/ASIF cortex screw in cortical bone in relation to bone mineral. *Injury*, 1993, Vol. 24(10), pp. 656-9.

51. **ASTM,** Standard test method for determining axial pull-out strength of medical bone screws. *ASTM*, 1996, Vol. F1691-96.

52. **Petersen M.M., Jensen N.C., Gehrchen P.M., Nielsen P.K., and Nielsen P.T.,** The relation between trabecular bone strength and bone mineral density assessed by dual photon and dual energy X-ray absorptiometry in the proximal tibia. *Calcified Tissue International*, 1996, Vol. 59(4), pp. 311-314.

53. **Bentzen S.M., Hvid I., and Jorgensen J.,** Mechanical strength of tibial trabecular bone evaluated by X-ray computed tomography. *Journal of Biomechanics*, 1987, Vol. 20(8), pp. 743-52.

54. **Sneppen O., Christensen P., Larsen H., and Vang P.S.,** Mechanical testing of trabecular bone in knee replacement. *International orthopaedics*, 1981, Vol. 5(4), pp. 251-256.

55. **Hvid I., Christensen P., Soondergaard J., Christensen P.B., and Larsen C.G.,** Compressive strength of tibial cancellous bone. Instron and osteopenetrometer measurements in an autopsy material. *Acta Orthopaedica Scandinavica*, 1983, Vol. 54(6), pp. 819-25.

56. **Hvid I., Andersen K., and Olesen S.,** Cancellous bone strength measurements with the osteopenetrometer. *Engineering in Medicine*, 1984, Vol. 13(2), pp. 73-8.

57. **Cheng X.G., Lowet G., Boonen S., Nicholson P.H., Brys P., Nijs J., and Dequeker J.,** Assessment of the strength of proximal femur in vitro: relationship to femoral bone mineral density and femoral geometry. *Bone*, 1997, Vol. 20(3), pp. 213-8.

58. **Wahner H.W. and Fogelman I.,** The evaluation of osteoporosis:Dual energy X-Ray absorptiometry in clinical practice. 1995, *Martin Dunitz, London.*

59. **Mazess R.B., Barden H., Vetter J., and Ettinger M.,** Advances in noninvasive bone measurement. *Annals of Biomedical Engineering*, 1989, Vol. 17(2), pp. 177-81.

60. Adams J.E., Single and dual energy X-ray absorptiometry. *European Radiology*, 1997, Vol. 7(Suplement No. 2), pp. S20-S31.

61. **Myers B.S., Belmont P.J., Jr., Richardson W.J., Yu J.R., Harper K.D., and Nightingale R.W.,** The role of imaging and in situ biomechanical testing in assessing pedicle screw pull-out strength. *Spine*, 1996, Vol. 21(17), pp. 1962-8.

62. **Okuyama K., Sato K., Abe E., Inaba H., Shimada Y., and Murai H.,** Stability of transpedicle screwing for the osteoporotic spine. An in vitro study of the mechanical stability. *Spine*, 1993, Vol. 18(15), pp. 2240-5.

63. **Singh M., Nagrath A.R., and Maini P.S.,** Changes in trabecular pattern of the upper end of the femur as an index of osteoporosis. *American Journal of Bone and Joint Surgery*, 1970, Vol. 52(3), pp. 457-67.

64. **Krischak G.D., Augat P., Wachter N.J., Kinzl L., and Claes L.E.,** Predictive value of bone mineral density and Singh index for the in vitro mechanical properties of cancellous bone in the femoral head. *Clinical Biomechanics (Bristol, Avon)*, 1999, Vol. 14(5), pp. 346-51.

65. **Svendsen O.L., Hassager C., Skodt V., and Christiansen C.,** Impact of soft tissue on in vivo accuracy of bone mineral measurements in the spine, hip, and forearm: a human cadaver study. *Journal of Bone and Mineral Research*, 1995, Vol. 10(6), pp. 868-73.

66. **Lochmuller E.M., Krefting N., Burklein D., and Eckstein F.,** Effect of fixation, soft-tissues, and scan projection on bone mineral measurements with dual energy X-ray absorptiometry (DXA). *Calcified Tissue International*, 2001, Vol. 68(3), pp. 140-5.

67. **McCalden R.W., McGeough J.A., and Court-Brown C.M.,** Age-related changes in the compressive strength of cancellous bone. The relative importance

of changes in density and trabecular architecture. *Journal of Bone and Joint Surgery-American Volume*, 1997, Vol. 79(3), pp. 421-427.

68. **Keller T.S.**, Predicting the compressive mechanical behavior of bone. *Journal of Biomechanics*, 1994, Vol. 27(9), pp. 1159-68.

69. **Brear K., Currey J.D., Raines S., and Smith K.J.**, Density and temperature effects on some mechanical properties of cancellous bone. *Engineering in Medicine*, 1988, Vol. 17(4), pp. 163-7.

70. **Rice J.C., Cowin S.C., and Bowman J.A.**, On the dependence of the elasticity and strength of cancellous bone on apparent density. *Journal of Biomechanics*, 1988, Vol. 21(2), pp. 155-68.

71. **Lang S.M., Moyle D.D., Berg E.W., Detorie N., Gilpin A.T., Pappas N.J., Jr., Reynolds J.C., Tkacik M., and Waldron R.L., 2nd**, Correlation of mechanical properties of vertebral trabecular bone with equivalent mineral density as measured by computed tomography. *Journal of Bone and Joint Surgery - American Volume*, 1988, Vol. 70(10), pp. 1531-8.

72. **Wachter N.J., Krischak G.D., Mentzel M., Sarkar M.R., Ebinger T., Kinzl L., Claes L., and Augat P.**, Correlation of bone mineral density with strength and microstructural parameters of cortical bone in vitro. *Bone*, 2002, Vol. 31(1), pp. 90-5.

73. **Lang T.F., Keyak J.H., Heitz M.W., Augat P., Lu Y., Mathur A., and Genant H.K.**, Volumetric quantitative computed tomography of the proximal femur: precision and relation to bone strength. *Bone*, 1997, Vol. 21(1), pp. 101-8.

74. **Lotz J.C. and Hayes W.C.**, The use of quantitative computed tomography to estimate risk of fracture of the hip from falls. *Journal of Bone and Joint Surgery - American Volume*, 1990, Vol. 72(5), pp. 689-700.

75. **Currey J.D.,** The effects of drying and re-wetting on some mechanical properties of cortical bone. *Journal of Biomechanics*, 1988, Vol. 21(5), pp. 439-41.

76. **Smeathers J.E. and Joanes D.N.,** Dynamic compressive properties of human lumbar intervertebral joints: a comparison between fresh and thawed specimens. *Journal of Biomechanics*, 1988, Vol. 21(5), pp. 425-33.

77. **Jameson M.W., Hood J.A., and Tidmarsh B.G.,** The effects of dehydration and rehydration on some mechanical properties of human dentine. *Journal of Biomechanics*, 1993, Vol. 26(9), pp. 1055-65.

78. **Nyman J.S., Roy A., Shen X., Acuna R.L., Tyler J.H., and Wang X.,** The influence of water removal on the strength and toughness of cortical bone. *Journal of Biomechanics*, 2006, Vol. 39(5), pp. 931-8.

79. **Martin D.E., Severns A.E., and Kabo J.M.,** Determination of mechanical stiffness of bone by pQCT measurements: correlation with non-destructive mechanical four-point bending test data. *Journal of Biomechanics*, 2004, Vol. 37(8), pp. 1289-93.

80. **Carter D.R. and Hayes W.C.,** Bone compressive strength: the influence of density and strain rate. *Science*, 1976, Vol. 194(4270), pp. 1174-6.

81. **Carter D.R. and Hayes W.C.,** The compressive behaviour of bone as a two-phase porous structure. *Journal of Bone and Joint Surgery - American Volume*, 1977, Vol. 59(7), pp. 954-62.

82. **Jamsa T., Jalovaara P., Peng Z., Vaananen H.K., and Tuukkanen J.,** Comparison of three-point bending test and peripheral quantitative computed tomography analysis in the evaluation of the strength of mouse femur and tibia. *Bone*, 1998, Vol. 23(2), pp. 155-161.

83. Lill C.A., Goldhahn J., Albrecht A., Eckstein F., Gatzka C., and Schneider E., Impact of bone density on distal radius fracture patterns and comparison between five different fracture classifications. *Journal of Orthopaedic Trauma,* 2003, Vol. 17(4), pp. 271-8.

84. Bouxsein M.L., Courtney A.C., and Hayes W.C., Ultrasound and densitometry of the calcaneus correlate with the failure loads of cadaveric femurs. *Calcified Tissue International,* 1995, Vol. 56(2), pp. 99-103.

85. Courtney A.C., Wachtel E.F., Myers E.R., and Hayes W.C., Age-related reductions in the strength of the femur tested in a fall-loading configuration. *Journal of Bone and Joint Surgery - American Volume,* 1995, Vol. 77(3), pp. 387-95.

86. Toyras J., Nieminen M.T., Kroger H., and Jurvelin J.S., Bone mineral density, ultrasound velocity, and broadband attenuation predict mechanical properties of trabecular bone differently. *Bone,* 2002, Vol. 31(4), pp. 503-7.

87. Toyras J., Kroger H., and Jurvelin J.S., Bone properties as estimated by mineral density, ultrasound attenuation, and velocity. *Bone,* 1999, Vol. 25(6), pp. 725-31.

88. Nicholson P.H., Lowet G., Cheng X.G., Boonen S., van der Perre G., and Dequeker J., Assessment of the strength of the proximal femur in vitro: relationship with ultrasonic measurements of the calcaneus. *Bone,* 1997, Vol. 20(3), pp. 219-24.

89. Lee S.C., Coan B.S., and Bouxsein M.L., Tibial ultrasound velocity measured in situ predicts the material properties of tibial cortical bone. *Bone,* 1997, Vol. 21(1), pp. 119-25.

90. Augat P., Link T., Lang T.F., Lin J.C., Majumdar S., and Genant H.K., Anisotropy of the elastic modulus of trabecular bone specimens from different

anatomical locations. *Medical Engineering & Physics*, 1998, Vol. 20(2), pp. 124-131.

91. **Watts N.B.,** Fundamentals and pitfalls of bone densitometry using dual-energy X-ray absorptiometry (DXA). *Osteoporosis International*, 2004, Vol. 15(11), pp. 847-54.

92. **Block J.E., Smith R., Glueer C.C., Steiger P., Ettinger B., and Genant H.K.,** Models of spinal trabecular bone loss as determined by quantitative computed tomography. *Journal of Bone and Mineral Research*, 1989, Vol. 4(2), pp. 249-57.

93. **Guglielmi G., Grimston S.K., Fischer K.C., and Pacifici R.,** Osteoporosis: diagnosis with lateral and posteroanterior dual x-ray absorptiometry compared with quantitative CT. *Radiology*, 1994, Vol. 192(3), pp. 845-50.

94. **Snyder B.D., Zaltz I., Hall J.E., and Emans J.B.,** Predicting the integrity of vertebral bone screw fixation in anterior spinal instrumentation. *Spine*, 1995, Vol. 20(14), pp. 1568-74.

95. **Hirano T., Hasegawa K., Takahashi H.E., Uchiyama S., Hara T., Washio T., Sugiura T., Yokaichiya M., and Ikeda M.,** Structural characteristics of the pedicle and its role in screw stability. *Spine*, 1997, Vol. 22(21), pp. 2504-9; discussion 2510.

96. **Heller J.G., Shuster J.K., and Hutton W.C.,** Pedicle and transverse process screws of the upper thoracic spine. Biomechanical comparison of loads to failure. *Spine*, 1999, Vol. 24(7), pp. 654-8.

97. **Harnroongroj T. and Techataweewan A.,** Determination of the role of the cancellous bone in generation of screw holding power at metaphysis. *Clinical Biomechanics (Bristol, Avon)*, 1999, Vol. 14(5), pp. 364-6.

98. **Pierson R.N., Jr., Wang J., Thornton J.C., Kotler D.P., Heymsfield S.B., Weber D.A., and Ma R.M.,** Bone mineral and body fat measurements by two absorptiometry systems: comparisons with neutron activation analysis. *Calcified Tissue International*, 1995, Vol. 56(2), pp. 93-8.

99. **Bonnaire F.A., Buitrago-Tellez C., Schmal H., Gotze B., and Weber A.T.,** Correlation of bone density and geometric parameters to the mechanical strength of the femoral neck. *Injury*, 2002, Vol. 33 Suppl 3, pp. C47-53.

100. **Ejersted C., Andreassen T.T., Oxlund H., Jorgensen P.H., Bak B., Haggblad J., Torring O., and Nilsson M.H.,** Human parathyroid hormone (1-34) and (1-84) increase the mechanical strength and thickness of cortical bone in rats. *Journal of Bone and Mineral Research*, 1993, Vol. 8(9), pp. 1097-101.

101. **Bonfield W. and Grynpas M.D.,** Anisotropy of the Young's modulus of bone. *Nature*, 1977, Vol. 270(5636), pp. 453-4.

102. **Brown T.D. and Ferguson A.B., Jr.,** Mechanical property distributions in the cancellous bone of the human proximal femur. *Acta Orthopaedica Scandinavica*, 1980, Vol. 51(3), pp. 429-37.

103. **Katz J.L.,** Anisotropy of Young's modulus of bone. *Nature*, 1980, Vol. 283(5742), pp. 106-7.

104. **Stone J.L., Beaupre G.S., and Hayes W.C.,** Multiaxial strength characteristics of trabecular bone. *Journal of Biomechanics*, 1983, Vol. 16(9), pp. 743-52.

105. **Dalstra M., Huiskes R., Odgaard A., and van Erning L.,** Mechanical and textural properties of pelvic trabecular bone. *Journal of Biomechanics*, 1993, Vol. 26(4-5), pp. 523-535.

106. **Pope M.H. and Outwater J.O.**, Mechanical properties of bone as a function of position and orientation. *Journal of Biomechanics*, 1974, Vol. 7(1), pp. 61-6.

107. **Wachter N.J., Augat P., Hoellen I.P., Krischak G.D., Sarkar M.R., Mentzel M., Kinzl L., and Claes L.**, Predictive value of Singh index and bone mineral density measured by quantitative computed tomography in determining the local cancellous bone quality of the proximal femur. *Clinical Biomechanics (Bristol, Avon)*, 2001, Vol. 16(3), pp. 257-62.

108. **Koot V.C., Kesselaer S.M., Clevers G.J., de Hooge P., Weits T., and van der Werken C.**, Evaluation of the Singh index for measuring osteoporosis. *Journal of Bone and Joint Surgery - British Volume*, 1996, Vol. 78(5), pp. 831-4.

109. **Serpe L. and Rho J.Y.**, The nonlinear transition period of broadband ultrasound attenuation as bone density varies. *Journal of Biomechanics*, 1996, Vol. 29(7), pp. 963-6.

110. **Martens M., Van Audekercke R., Delport P., De Meester P., and Mulier J.C.**, The mechanical characteristics of cancellous bone at the upper femoral region. *Journal of Biomechanics*, 1983, Vol. 16(12), pp. 971-83.

111. **Keaveny T.M. and Hayes W.C.**, A 20-year perspective on the mechanical properties of trabecular bone. *Journal of Biomechanical Engineering*, 1993, Vol. 115(4B), pp. 534-542.

112. **Morgan E.F. and Keaveny T.M.**, Dependence of yield strain of human trabecular bone on anatomic site. *Journal of Biomechanics*, 2001, Vol. 34(5), pp. 569-577.

113. **Goldstein S.A.**, The mechanical properties of trabecular bone: dependence on anatomic location and function. *Journal of Biomechanics*, 1987, Vol. 20(11-12), pp. 1055-61.

114. **Linde F., Hvid I., and Madsen F.**, The effect of specimen geometry on the mechanical behaviour of trabecular bone specimens. *Journal of Biomechanics*, 1992, Vol. 25(4), pp. 359-68.

115. **Keaveny T.M., Borchers R.E., Gibson L.J., and Hayes W.C.**, Trabecular bone modulus and strength can depend on specimen geometry. *Journal of Biomechanics*, 1993, Vol. 26(8), pp. 991-1000.

116. **David A.S. and John S.A.**, Metal Cutting Theory and Practice. Second ed. 2006, *CRC Press*.

117. **Nathan H.C.**, Manufacturing Analysis. 1966, *Addison-Wesley Educational Publishers Inc.*

118. **Williams R.A.**, A study of the drilling process. *Journal of Engineering for Industry*, 1974, Vol. 96, pp. 1207-1215.

119. **Saha S., Pal S., and Albright J.A.**, Surgical drilling: design and performance of an improved drill. *Journal of Biomechanical Engineering*, 1982, Vol. 104(3), pp. 245-252.

120. **Armarego E.J.A. and Brown R.H.**, The machining of metals. 1969, *Prentice-Hall*.

121. **Shaw M.C. and Oxford C.J.J.**, On the drilling of metals: Part 2 - The torque and thrust in drilling. *Transactions- ASME*, 1957, Vol. 79, pp. 139-148.

122. **Jacob C.H., Pope M.H., Berry J.T., and Hoaglund F.**, A study of the bone machining process-orthogonal cutting. *Journal of Biomechanics*, 1974, Vol. 7(2), pp. 131-136.

123. **Robinson R.C., Mosby E.L., and Eick J.D.**, Bone hole diameter as a function of drill guide length and drilling method in rigid internal fixation. *Journal of Oral and Maxillofacial Surgery*, 1992, Vol. 50(6), pp. 613-617.

124. **Mauch C.A. and Lauderbaugh L.K.** *Modeling the drilling process. An analytical model to predict thrust force and torque.* in *Winter Annual Meeting of the American Society of Mechanical Engineers, Nov 25-30.* 1990. Dallas, TX, USA: Published by ASME, New York, NY, USA.

125. **Kuppuswamy G.**, Principles of metal cutting. 1996, Hyderabad, *Sangam Bks.*

126. **Chandrasekharan V., Kapoor S.G., and DeVor R.E.**, A Mechanistic Approach to Predicting the Cutting Forces in Drilling: With Application to Fiber-Reinforced Composite Materials. *Transactions- American Society of Mechanical Engineers Journal of Engineering for Industry*, 1995, Vol. 117(4), pp. 559-570.

127. **Langella A., Nele L., and Maio A.**, A torque and thrust prediction model for drilling of composite materials. *Composites Part A*, 2005, Vol. 36(1), pp. 83-93.

128. **Somerton W.H.**, A laboratory study of rock breakage by rotary drilling. *AIME Petroleum Transactions*, 1959, Vol. 216, pp. 92-97.

129. **Allotta B., Belmonte F., Bosio L., and Dario P.**, Study on a mechatronic tool for drilling in the osteosynthesis of long bones: tool/bone interaction, modeling and experiments. *Mechatronics*, 1996, Vol. 6(4), pp. 447-459.

130. **Karalis T. and Galanos P.**, Research on the mechanical impedance of human bone by a drilling test. *Journal of Biomechanics*, 1982, Vol. 15(8), pp. 561-581.

131. **Brett P.N., Baker D.A., Reyes L., and Blanshard J.**, An automatic technique for micro-drilling a stapedotomy in the flexible stapes footplate. *Proceedings of the*

Institution of Mechanical Engineers. Part H, Journal of engineering in medicine, 1995, Vol. 209(4), pp. 255-262.

132. **Colla V. and Allotta B.** *Wavelet-based control of penetration in a mechatronic drill for orthopaedic surgery.* in *Proceedings of the 1998 IEEE International Conference on Robotics and Automation. Part 1 (of 4), May 16-20 1998.* 1998. Leuven, Belgium: IEEE, Piscataway, NJ, USA.

133. **Ong F.R. and Bouazza-Marouf K.,** Detection of drill bit break-through for the enhancement of safety in mechatronic assisted orthopaedic drilling. *Mechatronics,* 1999, Vol. 9(6), pp. 565-588.

134. **Asnis S.E., Ernberg J.J., Bostrom M.P., Wright T.M., Harrington R.M., Tencer A., and Peterson M.,** Cancellous bone screw thread design and holding power. *Journal of Orthopaedic Trauma,* 1996, Vol. 10(7), pp. 462-9.

135. **Chapman J.R., Harrington R.M., Lee K.M., Anderson P.A., Tencer A.F., and Kowalski D.,** Factors affecting the pullout strength of cancellous bone screws. *Journal of Biomechanical Engineering,* 1996, Vol. 118(3), pp. 391-8.

136. **Oberg, Jones, Horton, McCauley, Heald, and Hussain,** Machinery's Handbook. 27th ed, *Industrial Press.*

137. **DeCoster T.A., Heetderks D.B., Downey D.J., Ferries J.S., and Jones W.,** Optimizing bone screw pullout force. *Journal of Orthopaedic Trauma,* 1990, Vol. 4(2), pp. 169-74.

138. **Gausepohl T., Mohring R., Pennig D., and Koebke J.,** Fine thread versus coarse thread. A comparison of the maximum holding power. *Injury,* 2001, Vol. 32 Supplement 4, pp. SD1-7.

139. **Nunamaker D.M. and Perren S.M.**, Force measurements in screw fixation. *Journal of Biomechanics*, 1976, Vol. 9(11), pp. 669-75.

140. **Uhl R.L.**, The biomechanics of screws. *Orthopaedic Review*, 1989, Vol. 18(12), pp. 1302-7.

141. **ASTM**, Standard specification and test methods for metallic medical bone screws. 2002, Vol. F543-02.

142. **Halvorson T.L., Kelley L.A., Thomas K.A., Whitecloud T.S., 3rd, and Cook S.D.**, Effects of bone mineral density on pedicle screw fixation. *Spine*, 1994, Vol. 19(21), pp. 2415-20.

143. **Heller J.G., Estes B.T., Zaouali M., and Diop A.**, Biomechanical study of screws in the lateral masses: variables affecting pull-out resistance. *Journal of Bone and Joint Surgery - American Volume*, 1996, Vol. 78(9), pp. 1315-21.

144. **Jones E.L., Heller J.G., Silcox D.H., and Hutton W.C.**, Cervical pedicle screws versus lateral mass screws. Anatomic feasibility and biomechanical comparison. *Spine*, 1997, Vol. 22(9), pp. 977-82.

145. **Reitman C.A., Nguyen L., and Fogel G.R.**, Biomechanical evaluation of relationship of screw pullout strength, insertional torque, and bone mineral density in the cervical spine. *Journal of Spinal Disorders and Techniques*, 2004, Vol. 17(4), pp. 306-11.

146. **Ryken T.C., Clausen J.D., Traynelis V.C., and Goel V.K.**, Biomechanical analysis of bone mineral density, insertion technique, screw torque, and holding strength of anterior cervical plate screws. *Journal of Neurosurgery*, 1995, Vol. 83(2), pp. 325-9.

147. **Hsu C.C., Chao C.K., Wang J.L., Hou S.M., Tsai Y.T., and Lin J.**, Increase of pullout strength of spinal pedicle screws with conical core: biomechanical tests and finite element analyses. *Journal of Orthopaedic Research*, 2005, Vol. 23(4), pp. 788-94.

148. **Ansell R.H. and Scales J.T.**, A Study of some factors which affect the strength of screws and their insertion and holding power in bone. *Journal of Biomechanics*, 1968, Vol. 1, pp. 279-302.

149. **Steeves M., Stone C., Mogaard J., and Byrne S.**, How pilot-hole size affects bone-screw pullout strength in human cadaveric cancellous bone. *Canadian Journal of Surgery*, 2005, Vol. 48(3), pp. 207-12.

150. **Oktenoglu B.T., Ferrara L.A., Andalkar N., Ozer A.F., Sarioglu A.C., and Benzel E.C.**, Effects of hole preparation on screw pullout resistance and insertional torque: a biomechanical study. *Journal of Neurosurgery*, 2001, Vol. 94(1 Suppl), pp. 91-6.

151. **Inceoglu S., Ferrara L., and McLain R.F.**, Pedicle screw fixation strength: pullout versus insertional torque. *The Spine Journal*, 2004, Vol. 4(5), pp. 513-8.

152. **Kwok A.W., Finkelstein J.A., Woodside T., Hearn T.C., and Hu R.W.**, Insertional torque and pull-out strengths of conical and cylindrical pedicle screws in cadaveric bone. *Spine*, 1996, Vol. 21(21), pp. 2429-34.

153. **Cordey J., Rahn B.A., and Perren S.M.**, Human torque control in the use of bone screws. *In: Uhthoff HK, ed. Current concepts of internal fixation of fractures. Berlin, Heidelberg, New York: Springer-Verlag*, 1980, pp. 235-243.

154. **Cleek T.M., Reynolds K.J., and Hearn T.C.**, Effect of screw torque level on cortical bone pullout strength. *Journal of Orthopaedic Trauma*, 2007, Vol. 21(2), pp. 117-23.

155. **Hearn T.C. and Reynolds K.J.,** Adaptive appratus for driving a threaded device into material such as biological tissue, in *WIPO*. 2003.

156. **Koistinen A., Santavirta S., and Lappalainen R.,** Apparatus to test insertion and removal torque of bone screws. *Proceedings- Institution of Mechanical Engineers Part H Journal of Engineering in Medicine*, 2003, Vol. 217(6), pp. 503-508.

157. **Koistinen A., Santavirta S.S., Kroger H., and Lappalainen R.,** Effect of bone mineral density and amorphous diamond coatings on insertion torque of bone screws. *Biomaterials*, 2005, Vol. 26(28), pp. 5687-94.

158. **Buhler D.W., Berlemann U., Oxland T.R., and Nolte L.P.,** Moments and forces during pedicle screw insertion. In vitro and in vivo measurements. *Spine*, 1998, Vol. 23(11), pp. 1220-7; discussion 1228.

159. **Okuyama K., Abe E., Suzuki T., Tamura Y., Chiba M., and Sato K.,** Can insertional torque predict screw loosening and related failures? An in vivo study of pedicle screw fixation augmenting posterior lumbar interbody fusion. *Spine*, 2000, Vol. 25(7), pp. 858-64.

160. **Ozawa T., Takahashi K., Yamagata M., Ohtori S., Aoki Y., Saito T., Inoue G., Ito T., and Moriya H.,** Insertional torque of the lumbar pedicle screw during surgery. *Journal of Orthopaedic Science*, 2005, Vol. 10(2), pp. 133-6.

161. **John H. Bickford and Nassar S.,** Handbook of Bolts and Bolted Joints. 1998, *Marcel Dekker Ltd.*

162. **Matthews L.S. and Hirsch C.,** Temperatures measured in human cortical bone when drilling. *The Journal of Bone and Joint Surgery - American Volume*, 1972, Vol. 54(2), pp. 297-308.

163. **Lee W.Y., Shih C.L., and Lee S.T.**, Force Control and Breakthrough Detection of a Bone-Drilling System. *IEEE ASME Transactions on Mechatronics*, 2004, Vol. 9(1), pp. 20-29.

164. **Bachus K.N., Rondina M.T., and Hutchinson D.T.**, The effects of drilling force on cortical temperatures and their duration: an in vitro study. *Medical Engineering Physics*, 2000, Vol. 22(10), pp. 685-91.

165. **Thomas R.L.**, Use of mechatronic devices for enhancement of safety during screw placement in orthopaedic surgery, in *PhD Thesis. Wolfson School of Mechanical and Manufacturing Engineering.* 2004, *Loughborough University.*

166. **Shuaib I. and Hillery M.**, Forces generated in guide-wires when drilling human bone. *Proceedings of the Institution of Mechanical Engineers. Part H, Journal of engineering in medicine*, 1995, Vol. 209(3), pp. 157-162.

167. **Bouazza-Marouf K., Browbank I., and Hewi J.R.**, Robot-assisted invasive orthopaedic surgery. *Mechatronics*, 1996, Vol. 6(4), pp. 381-398.

168. **Piska M., Yang L., Reed M., and Saleh M.**, Drilling efficiency and temperature elevation of three types of Kirschner-wire point. *Journal of Bone and Joint Surgery - British Volume*, 2002, Vol. 84(1), pp. 137-40.

169. **Skinner R., Maybee J., Transfeldt E., Venter R., and Chalmers W.**, Experimental pullout testing and comparison of variables in transpedicular screw fixation. A biomechanical study. *Spine*, 1990, Vol. 15(3), pp. 195-201.

170. **Ronderos J.F., Jacobowitz R., Sonntag V.K., Crawford N.R., and Dickman C.A.**, Comparative pull-out strength of tapped and untapped pilot holes for bicortical anterior cervical screws. *Spine*, 1997, Vol. 22(2), pp. 167-70.

171. **Heidemann W., Gerlach K.L., Grobel K.H., and Kollner H.G.,** Drill Free Screws: a new form of osteosynthesis screw. *Journal of Craniomaxillofacial Surgery*, 1998, Vol. 26(3), pp. 163-8.

172. **ASTM,** Standard Test Method for Driving Torque of Medical Bone Screws. 1999, Vol. F 117-95.

173. **ASTM,** Standard specification for Rigid Polyurethane Foam for use as a standard material for testing Orthopaedic devices and instruments. 1997, Vol. F1839-97.

174. **Chapman J.R., Harrington R.M., K L., E F., and P.A A.** *The influence of screw design and insertion technique on pullout strength of screws in porous materials.* in *38th Annual meeting, Orthopaedic Research Society.* 1992.

175. **Hou S.M., Hsu C.C., Wang J.L., Chao C.K., and Lin J.,** Mechanical tests and finite element models for bone holding power of tibial locking screws. *Clinical Biomechanics (Bristol, Avon)*, 2004, Vol. 19(7), pp. 738-45.

176. **Gibson L.J. and Ashby M.F.,** Cellular solids: structure and properties. *Cambridge University Press.*, 1997, Vol. Second ed.

177. **Dell R.B., Holleran S., and Ramakrishnan R.,** Sample size determination. *ILAR Journal / National Research Council, Institute of Laboratory Animal Resources*, 2002, Vol. 43(4), pp. 207-13.

178. **Moore D.S.,** The basic practice of statistics. 3rd ed. 2004, New York, *W.H. Freeman.*

179. **ASTM,** Standard test method for shear strength of plastics by punch tool. 1990, Vol. D732-90.

180. **Cook N.H.**, Manufacturing Analysis. 1966, *Addison-Wesley Publishing Company, Reading, Massachusetts, USA.*

181. **Phillips J.H. and Rahn B.A.**, Comparison of compression and torque measurements of self-tapping and pretapped screws. *Plastic and Reconstructive Surgery*, 1989, Vol. 83(3), pp. 447-58.

182. **http://academic.wsc.edu/faculty/jatodd1/351/tibia_fibula.jpg**.

183. http://upload.wikimedia.org/wikibooks/en/0/01/Anatomy_and_physiology_of_animals_Femur.jpg.

184. **Kent M.V.D.G.**, Human Anatomy, ed. Edition, F. 1998, *Mc Graw-Hill.*

185. http://www.drugdevelopment-technology.com/projects/lasofoxifene/lasofoxifene2.html.

186. **Boyle J.M., 3rd, Frost D.E., Foley W.L., and Grady J.J.**, Torque and pullout analysis of six currently available self-tapping and "emergency" screws. *J Oral Maxillofac Surg*, 1993, Vol. 51(1), pp. 45-50.

APPENDIX A

BONE

The main objective of this research is to evaluate bone strength. To understand more about the bone, a brief overview of the bone structure, types, properties and functions are discussed within this appendix. The process of bone remodelling and bone fracture healing is also presented.

A.1   BONE – AN INTRODUCTION

Bone is a vital dynamic connective tissue which is composed of cells, fibres and minerals. The major functions of bone are;

- **Structure:** provides mechanical integrity or internal support to the body and attachment for muscles and tendons for locomotion.

- **Protection:** protects vital organs of the body, and encloses the blood forming elements of the bone marrow.

- **Reservoir:** provides a reservoir of ionic calcium (mineral homeostasis) essential for many cellular processes of the body.

The intercellular matrix of the bone consists of organic and inorganic substances. The organic components contain collagenous fibres and small quantity of other bone proteins. The inorganic component of bone contributes to the rigidity of tissues and is composed of calcium phosphate and calcium carbonate (responsible for the compressive strength of the bone) with small amounts of magnesium fluoride, sulphates and hydroxides. These inorganic minerals are present as long, slender crystals called

hydroxyapatites lying within the collagen fibres. Organic component forms 40% of the dry weight while inorganic component forms 60% of the dry weight of the bone.

A.2   CLASSIFICATION OF BONE

Bone can be broadly classified based on its shape, density and the presence of Osteons/Haversian systems.

A.2.1 Classification Based on the Shape of Bone

Bones are classifications based on its shape and location in the human body as:

Long Bone: Long bones are significantly longer in length as compared to their width. *Most of the bones in the upper and lower limbs have long axis and are of this* type. Examples of long bones are humerus, radius, ulna, femur, tibia, metacarpals, metatarsals and phalanges. Macroscopic structure of a particular long bone is shown in figure A.1.

Short Bone: *Bones that do not have a long axis, such as those of the wrist (carpals)* and ankles (tarsals) are called short bone. They are generally cube-shaped.

Flat Bone: Flat bones have a broad surface for muscle attachment or protection of underlying organs, e.g., the cranial bones, ribs, and shoulder girdle.

Irregular Bone: Irregular bones have varied shapes and many surface features for muscle attachment or articulation, e.g., the vertebrae and certain bones of the skull.

A.2.2 Classification Based on the Density of Bone

Bone is classified into two types based on its density:

1. **Compact Bone:**

The compact bone is also known as Harversian or cortical bone. They form a protective covering or external surface of the bone, as shown in figure A.1. Cortical bone surrounds cancellous bone and is mainly responsible for the skeleton's strength. It mainly consists of protein (collagen) and hydroxyapatites (calcium phosphate salts). It consists of three layers, they are:

- **The Periosteal Envelope**: the outer surface of the bone.

- **The Intracortical Envelope**: the next layer down.

- **The Endosteal Envelope**: the layer next to the bone marrow cavity.

2. **Trabecular or Cancellous Bone**

The trabecular bone is also known as the spongy or cancellous bone. The cancellous bone provides only a small part of the skeletal strength as compared to the cortical bone, but has a very important part to play in metabolic duties. Cancellous bone is composed of a network of tiny strands of bone called trabeculae, as shown in figure A.2. The load and pressure which is applied on bones during the development stage of human, determines the way the trabeculae are positioned.

Diaphysis: Shaft of the Bone

Epiphysis: End of the Long Bone

Metaphysis: Area between the Diaphysis and Epiphysis

Epipyseal: Plate (Growth Plate)

Medullary Cavity: Central Cavity of Bone Occupied by Bone Marrow

Trabeculae: Irregular Lattice of Thin Columns of Bone Surrounded by Bone Marrow

Articular cartilage: Hyaline Cartilage Covering the Joint Surfaces

Periosteum: External Covering of the Bone

Endosteum: Internal Covering of Bone

Figure A.1   Macroscopic Structure of Long Bone [184]

A.2.3   Classification Based on the Presence or Absence of Lamellae (Layers) and Osteons/Haversian Systems

Bone can be classified as woven, primary or secondary based on the presence of Haversian system.

Woven Bone

Woven bone has the most disorganised bone tissue as it does not contain osteons like primary or secondary bones. Formation of a woven bone tissue does not need any

existing bone or cartilage tissue. These bones are often found in very young growing skeletons which are under the age of five. However, woven bones are also found in adult skeletons in the case of trauma and it occurs around the bone fracture site. Woven bone is laid down very rapidly which makes its structure disorganised, hence it is less dense.
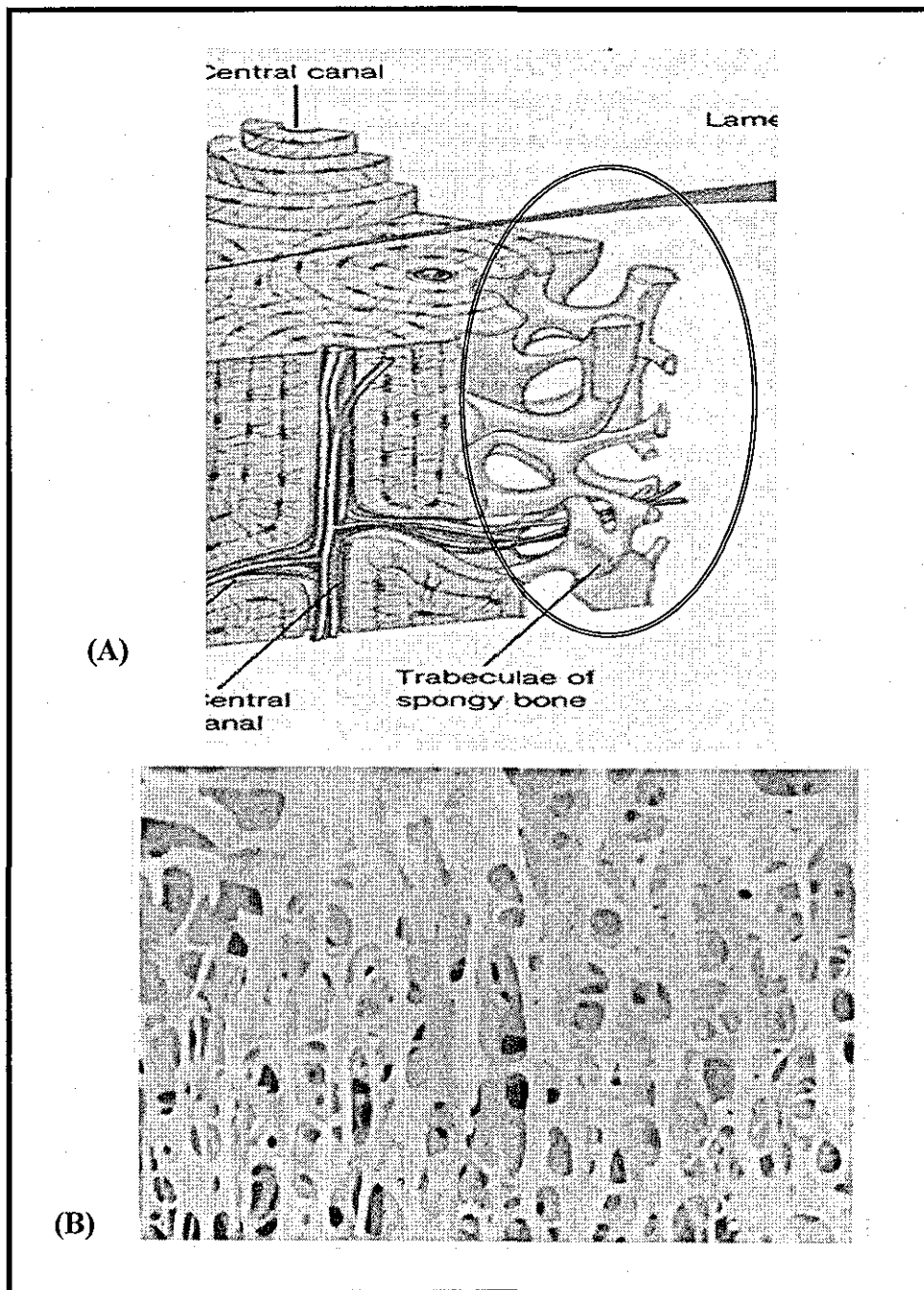
Figure A.2 Cancellous Bone: (A) Structure of Cancellous Bone [184], (B) Radiograph Honeycomb Structure of Cancellous Bone [7]

3. Primary Bone

The primary tissue of bone, osseous tissue, is a relatively hard and lightweight composite material, formed mostly of calcium phosphate (this is the osseous tissue that gives bones their rigidity). It has a relatively high compressive strength but a poor tensile strength, which means it can, resists pushing forces well, but not pulling forces. The structure which includes a central blood vessel surrounded with the concentric bone tissues is called an osteon. Primary osteons does not have any precise delimitation or cement line and are formed by mineralization of the cartilage resulting in narrowing the vascular space of the woven bone.

4. Secondary Bone

The new bone formed by the bone remodelling system is known as the secondary osteons or Haversian system. The secondary bone is also known as lamellar or mature bone. Secondary Osteons are separated from the surrounding matrix by a reversal or cement line. The microstructure of Haversian system is shown in the figure A.3. The Haversian system has a central haversian canal which is surrounded by the concentrically arranged lamellae of bone. In the longitudinal section, the Haversian canal appears as a long tube, as they generally run parallel to the long axis of bone, thus contributing to the compressive force capacity of the bone. Lacunae are small cavities, containing osteocytes, which are located between adjacent lamellae. The lacunae are connected by tiny channels called canaliculi through which nutrient diffuses. The haversian canals are linked to periosteum and endosteum by blood vessels & nerves and are linked to each other via oblique and perpendicular perforating channels known as Volkmann's canals.

The cancellous bone has trabeculae as its unit component and cortical bone has Haversian system or osteons. Trabeculae are made up of fragmented superimposed lamellae with numerous intervening cement lines. Nutrient to the trabeculae is provided by blood vessels in the red marrow.
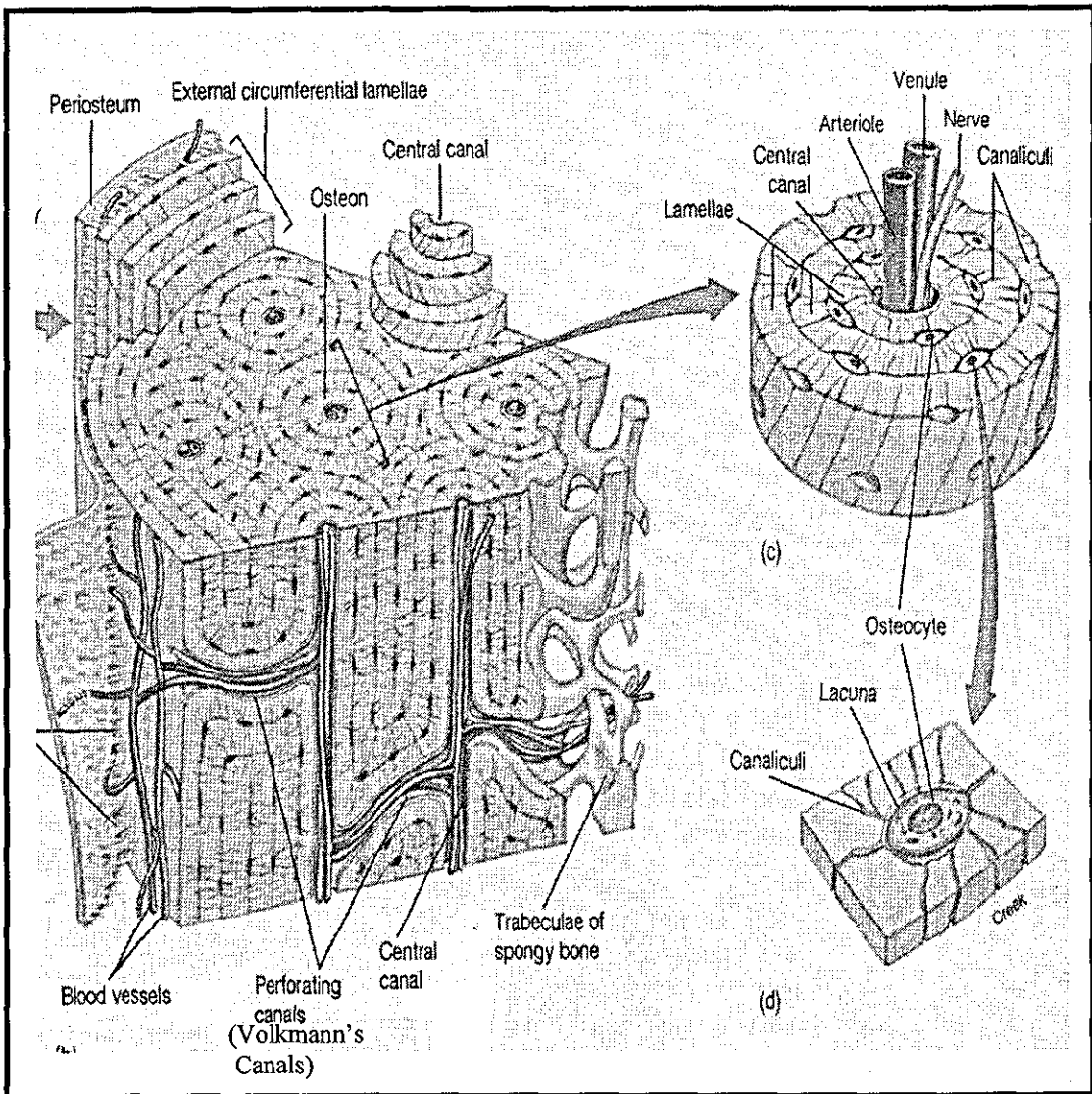
Figure A.3 Microstructure and Haversian System of the Bone [184]

A.3 SKELETAL LIFE CYCLE – BONE MODELLING AND REMODELLING

The basic bone cycle consist of three stages, during the first stage (0 to 25 years of age) calcium, phosphate and other minerals are deposited in the bone. Peak bone mass is achieved between the age of 25-30 years. In the second stage, bone mass remains almost constant till the age of 40 years. After 40 years of age, the third stage, bone loss occurs at an average rate of 0.5% per year. These three stages of bone cycle are shown in figure A.4.
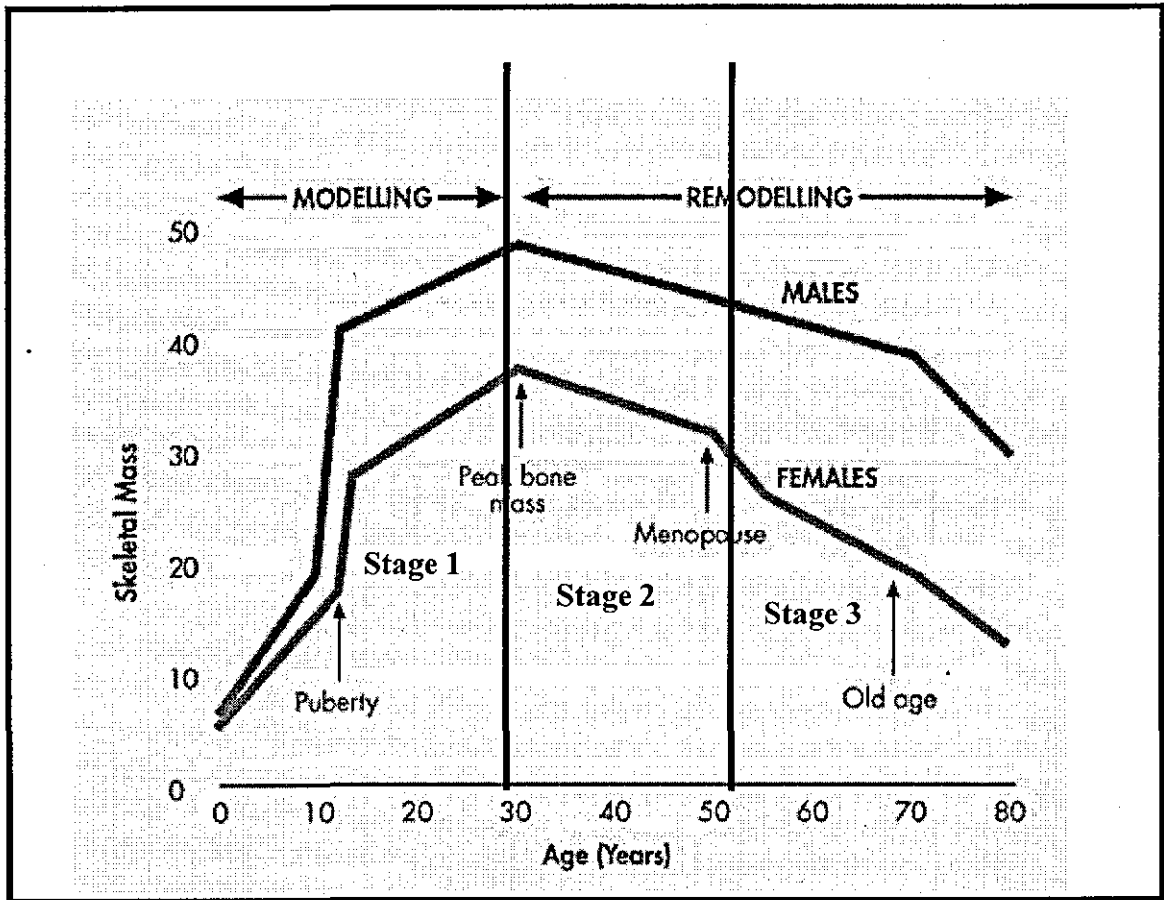
Figure A.4   Human Skeletal Life Cycle [185]

The process of bone formation begins in utero and continues throughout adolescence until skeletal maturity. This initial process of bone formation is called bone modelling. During bone modelling, shape and size of the bone is formed depending upon the load applied to the bone. Following skeletal maturity, the bone continues to remodel throughout its life and adapt its material properties to the mechanical demands placed upon it. Remodelling is a continuous process whereby there is a constant removal and replacement of the whole bone. The bone remodelling cycle consists of three continuous processes: bone removal, formation and maintenance. These three processes are governed by three types of bone cells, osteoclasts (destroys old bone), osteoblasts (grow new bone) and osteocytes (maintain existing bone). Osteoclasts dissolve older bone minerals, releasing them into the blood stream in order to satisfy other bodily needs and to provide room for newer mineral deposits. This process is called bone resorption. Resorption cavity is produced by continuous resorption for approximately two weeks.

Osteoblasts deposits hydroxipatite (calcium phosphate salt) in the protein matrix called collagen. They gradually harden into the protein mesh forming the bone, which is called bone formation. The complete bone formation process lasts for approximately three to four months. Osteocytes are responsible for maintaining the bone tissue by controlling local mineralisation and mineral exchange between bone and serum. The bone remodelling process is shown in figure A.5. The relationship between the processes of bone resorption and bone formation is extremely critical in maintaining bone mass during bone remodelling. The increase in the bone resorption with respect to bone formation would imply a loss in bone mass and this result in a disease called osteoporosis.
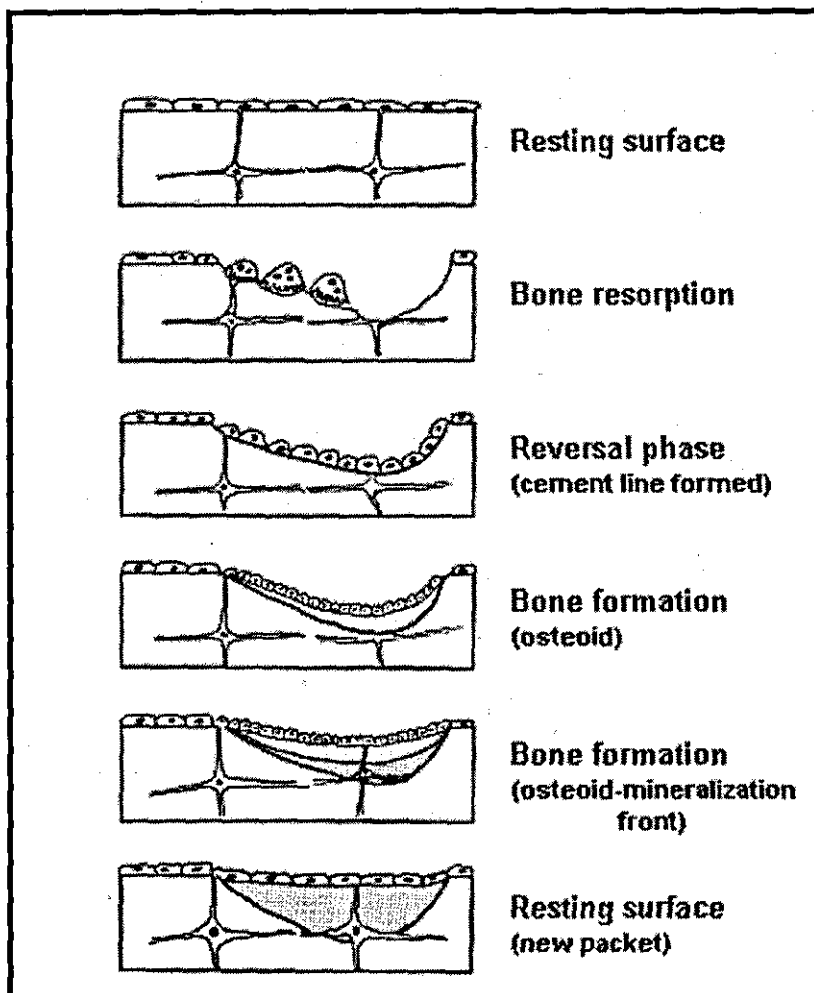
Figure A.5   Bone Remodelling Cycle [186]

A.4   HEALING PROCESS OF BONE FRACTURES

When a bone fractures, its functionality is lost. Medical treatment involves realigning the broken ends of bone and then immobilising them until a new bone tissue has formed and the fracture has healed. The skeletal site, severity of the fracture and the patient's age determines the type of immobilisation. The method of immobilisation includes traction, plaster casting, internal and external fixation.

When a bone is fractured, the surrounding periosteum is usually torn and blood vessels in the bone tissues are ruptured. A blood clot called a fracture hematoma is formed throughout the damaged area. A disrupted blood supply to osteocytes at the fracture site causes localised cellular death. This is followed by swelling and inflammation. The traumatised area is cleaned up by the activity of phagocytic cells within the blood and osteoclasts which resorbs bone fragments. It is followed by rapid formation of the bony callus or woven bone to bridge the fracture gap as well as to provide temporary strength and support. Finally, the bone callus undergoes the process of bone remodelling to produce lamellar bone. The complete fracture healing process is shown in figure A.6.

(a) Blood escapes from ruptured blood vessels and forms a hematoma.

(b) Spongy bone forms in regions close to developing blood vessels; fibrocartilage forms in more distant regions.

(c) Fibrocartilage is replaced by a bony callus.

(d) Osteoclasts remove excess bony tissue, making new bone structure much like the original.
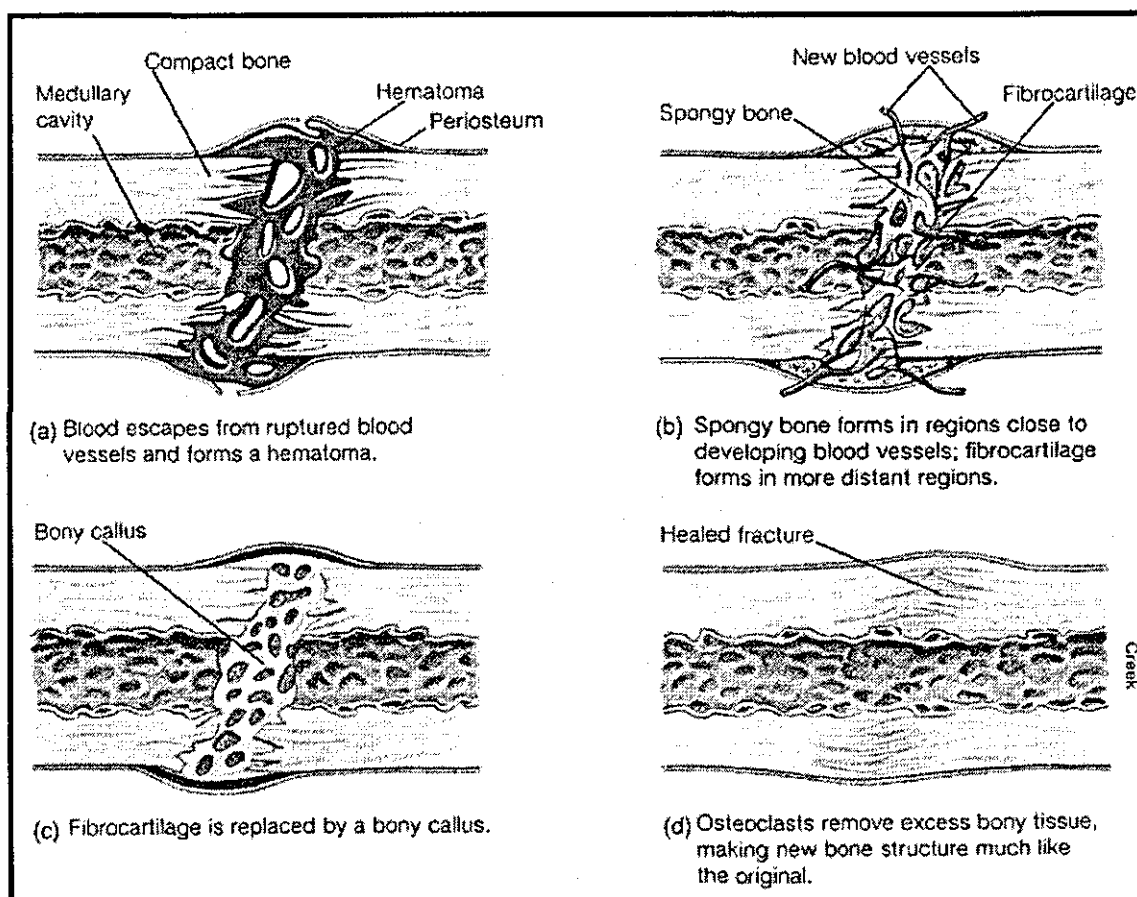
Figure A.6   Fracture Healing Process [184]

APPENDIX B

TEST RIG DESIGN RELATED INFORMATION

This appendix present the details related to designing of the test rig which was used in this research.

B.1   TEST RIG DESIGN PROCESS

The flow chart of the design process used for designing the test rig in this research is shown in figure B.1.

B.2   DETAIL OF COMPONENTS USED IN THE TEST RIG

The details of components used in the designed test rig are presented below.

Feed Stepper Motor (SM$_{Feed}$)

Stepper motor used for drilling feed rate and screw pullout rate was supplied by RS components, stock number 440-458. The drive board used for the stepper motor was supplied by RS Components, stock no. 217-3611. A power supply of 30 V, 3A was used for the stepper motor and 24 V, 2.5 A was used for the drive board.
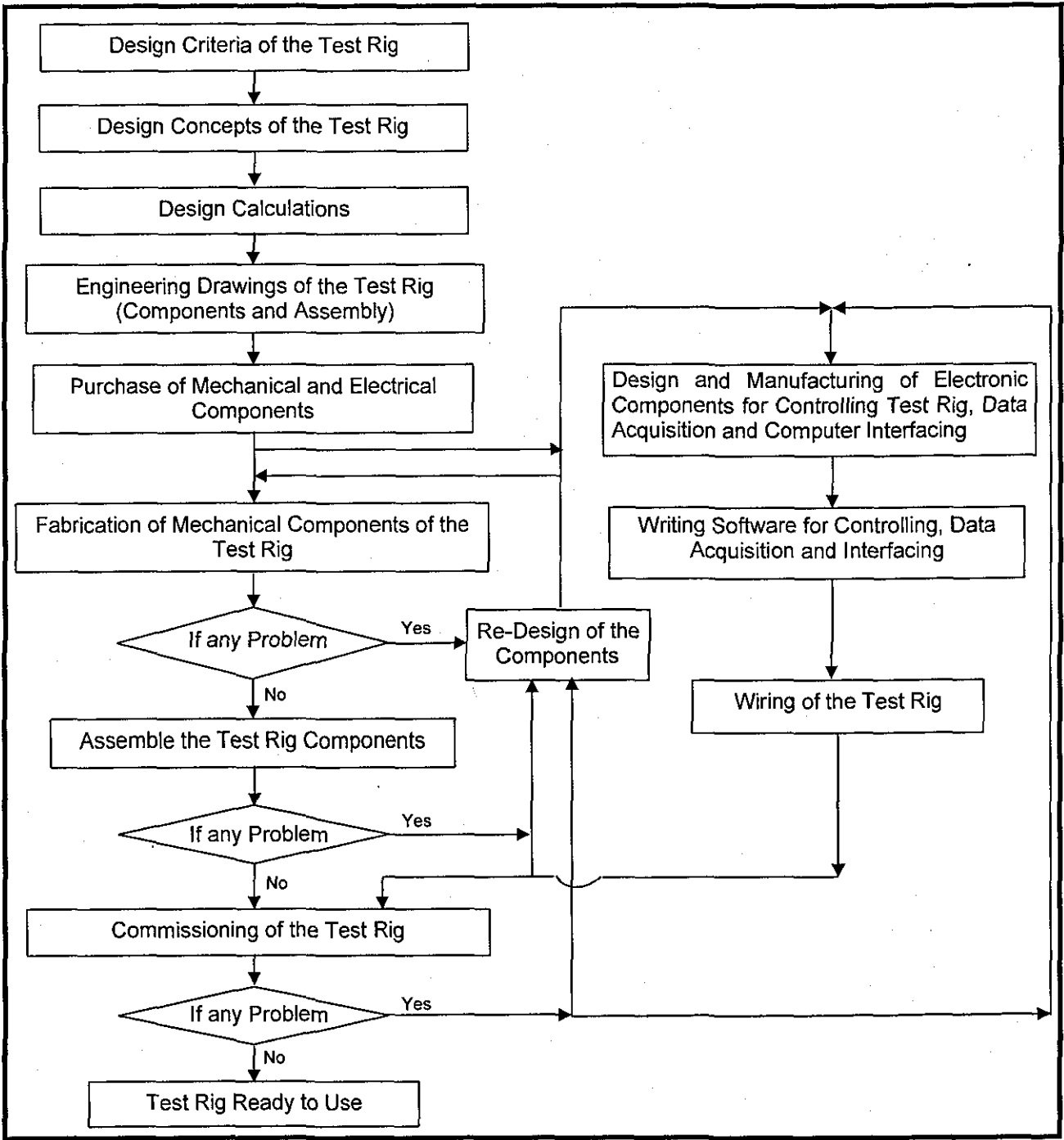
Figure B.1   Flow Chart of the Test Rig Design Process

Screw Insertion Stepper Motor (SM$_{Sc\_Ins}$)

Stepper motor used for screw insertion and screw tightening was supplied by RS components, stock number 440-442. The drive board used for the stepper motor was supplied by RS Components, stock no. 217-3611. A power supply of 30 V, 3A was used for the stepper motor and 24 V, 2.5 A was used for the drive board.

DC Servo Motor for Drilling

DC servo motor (model number N9M4T) and servo controller (model number KXA-48-16/AUX) supplied by Kollmorgen Motion Technology Group are used.

Encoder Mounted on the Ball Screw (En$_{Lead}$)

A separate encoder wheel, which gives an output of 500 pulses per revolution, was mounted at the motor end of the ball screw. The encoder reader was mounted on a fixed frame. Both encoder wheel and encoder reader were supplied by Farnell, stock numbers HEDS5140-A11 and HEDS-9140-A11, respectively.

Encoder Mounted on the Drilling Motor Shaft (En$_{Shaft}$)

A three channel encoder (stock number HEDS-5540-A11, supplied by Farnell) was mounted at the end of the DC servo drilling motor shaft for recording drilling speed and angular displacement.

Load Cell to Record the Drilling Force (LC$_{Drill}$)

Two load cells of S-type having the same size were purchased from Omega Engineering. The first load cell (model number LCM101-10) can record up to 100 N and the second load cell (model number LC101-200) can record up to 800 N.

Load Cell to Record Screw Pullout Force (LC$_{Pullout}$)

S-type load cell was purchased from Omega Engineering. Model Number of the load cell is LC101-2000. The load cell can record up to 8800 N.

<u>**Gear Box (25:2) Attached to the Screw Insertion Stepper Motor**</u>:

Reduction gear box was attached to the screw insertion stepper motor. The gear box was supplied by RS components, stock number 718-868.

<u>**Data Acquisition Board**</u>

4 channel ADC data acquisition board, model number USB-1208FS, from Measurement Computing Corporation was used for recording sensor data.

B.3 OBSERVATIONS AND TROUBLESHOOTING OF THE TEST RIG DURING ITS COMMISSIONING

Various observations during the commissioning of test rig and the troubleshooting tasks which were carried out are presented here. This would help in the future design process.

<u>**Drilling Feed Rate and Screw Pullout Stepper Motor**</u>

Stepper motor 34HSX-312 (7.8 N.m holding torque) manufactured by Mclennan Servo Supplies Ltd. and micro-stepping drive board P-808 (7.8A, 24 to 90V DC) manufactured by ASTROSYN was used initially for the ball screw feed mechanism. It was found that this resulted in a significantly large amount of electromagnetic noise which affected the sensor signal. Different methods to reduce or remove the electromagnetic noise were adopted, which are using a Butterworth noise filter, shielding the stepper motor & controller from the test rig and shielding the sensors from the test rig; however none of them were successful in reducing the noise level to within acceptable limits. Finally, the complete feed mechanism design has to be changed for the new combination of stepper motor and its drive board which are currently used.

Position of Drilling Load Cell

In the drilling operation configuration of the test rig, shown in figure 7.2, the drilling load cell connects the ball screw feed assembly to the inner frame. Recording of the drilling force at this sensor position had a significantly higher and inconsistent magnitude of the noise along the inner frame travel length. Variations in the noise could be due to alignment errors between the liner bearing & inner frame. To eliminate these errors the position of drilling force sensor was change and it was placed below the specimen mounting plate. The ball screw feed mechanism assembly was connected directly to the inner frame. Satisfactory results were found with the new position of the drilling force sensor; hence new position of the drilling force sensor was used to conduct drilling experiments.

Encoder Mounted on the Drilling Motor Shaft (En$_{Shaft}$)

Initially an encoder of Hengstler make (model number RI 58D/5000AE.42KB) was used to record the drilling speed and angular displacement of the shaft. This encoder was directly mounted on the rear shaft of the drilling motor. During the commissioning of test rig, initial drilling was performed at a drilling speed of 1000 rpm, the encoder from Hengstler failed twice. The maximum operating speed of the encoder was 6000 rpm. It was concluded that this type of encoder should not be used at higher speeds. Hence, the test rig design was changed to use the currently mounted encoder supplied by Farnell.

APPENDIX C

ENGINEERING DRAWINGS

C.1 LIST OF THE SUB ASSEMBLIES USED IN THE DESIGN OF TEST RIG

Various sub assemblies were used to design the test rig. These subassemblies are presented in this section along with the list of various components used in the sub assembly. Engineering drawing of all sub assemblies along with the complete assembly drawing of the test rig is presented at the end of this section. A CD is also attached with this thesis which contains all engineering and assembly drawings listed in this appendix.

Every drawing numbers has a prefix and they stand for,

- Prefix 'S' stands for the standard components which were purchased from the market
- Prefix 'A' stands for the assembly drawing
- Prefix 'P' stands for the part or component drawing

Fixed Outer Frame Assembly (Drawing number A-001)

Drawing No.	Name	Quantity
P-001	Outer Frame Bottom Plate	01
P-002	Outer Frame Left Side Plate	01
P-003	Outer Frame Top Plate	01
P-004	Outer Frame Right Side Plate	01
P-005	Linear Bearing Shaft Clamp	04
P-006	Lower Limit Switch Mounting	01
P-007	Dowel Pin 6mm	02
P-008	Dowel Pin 6mm	02
P-009	Dowel Pin 6mm	02
P-010	Base Plate	01
S-001	Linear Bearing Shaft	02
S-002	Limit Switch	01
A-002	Specimen Mounting Plate Holder Assembly	01
A-003	Specimen Mounting Plate Assembly	01

Specimen Mounting Plate Holder Assembly (Drawing Number A-002)

Drawing No.	Name	Quantity
P-011	Bearing Housing	01
P-012	Clamp Shaft	01
P-013	Spacer	01
P-014	Washer	01
S-003	Nut M12	01
S-004	Bearing ϕ12 mm Regular	01
S-005	Bearing ϕ12 mm Special	01

Specimen Mounting Plate Assembly (Drawing Number   A-003)

Drawing No.	Name	Quantity
P-015	Specimen Mounting Bottom Plate	01
P-016	Specimen Mounting Top Plate`	01
P-017	Spacer Specimen Mounting	12
P-018	Torque Sensing Beam	01
P-019	Beam Mounting	01
P-020	Beam Clamp	01
P-021	Bush Breakthrough	01
P-022	Locking Pin	01

Base Bracket Assembly (Drawing Number A-004)

Drawing No.	Name	Quantity
P-023	Base Bracket Bottom Left Plate	01
P-024	Base Bracket Left Side Plate	01
P-025	Base Bracket Top Plate	01
P-026	Base Bracket Right Side Plate	01
P-027	Base Bracket Bottom Right Plate	01
P-028	Aligning Plate Bottom	01
P-029	Aligning Plate Top	01
P-008	Dowel Pin 6mm	02
A-005	Drill Bush Assembly	01

Drill Bush Assembly (Drawing Number A-005)

Drawing No.	Name	Quantity
S-006	Drill Bush	01
P-030	Bush Nut	01
P-031	Locking Nut	01
P-032	Drill Bush Nut Housing	01

Inner Frame Assembly (Drawing Number A-006)

Drawing No.	Name	Quantity
P-009	Dowel Pin 6mm	06
P-033	Inner Frame Bottom Plate	01
P-034	Inner Frame Left Side Plate	01
P-035	Inner Frame Top Plate	01
P-036	Inner Frame Right Side Plate	01
P-037	Inner Frame Back Plate	01
P-038	Mounting Bracket 15mm Bearing	01
P-039	Ribs Inner Frame	08
P-040	Plate	01
P-041	Drag Chain Mounting Plate	01
S-007	Screw Rod	01
A-007	Linear Bearing Assembly	04
A-008	Screw Pullout Attachment Assembly	01

Linear Bearing Assembly (Drawing Number A-007)

Drawing No.	Name	Quantity
P-042	Linear Bearing Housing	01
S-008	Linear Bearing	01

Screw Pullout Attachment Assembly (Drawing Number A-008)

Drawing No.	Name	Quantity
P-043	Screw Pullout Nut Adapter	01
P-044	Screw Pullout Nut	01
P-045	Screw Pullout Rod	01
P-046	Screw Pullout Attachment	01
P-047	Screw Pullout Bush	01
S-009	Screw Pullout Ball Joint	01
S-010	Screw Pullout Fork	01
S-011	Screw Pullout Locking Pin	01

Drilling Motor Assembly (Drawing Number A-009)

Drawing No.	Name	Quantity
P-048	Drilling Motor Mounting Plate	01
P-049	Encoder Mounting Vertical Plate	02
P-050	Encoder Mounting Horizontal Plate	01
P-051	Tacho Mounting Plate	01
P-052	Encoder Mounting Coupling	01
P-053	Encoder Shaft	01
P-054	Bearing Housing	01
P-055	Bearing Locking Plate Motor Side	01
P-056	Bearing Locking Plate Encoder Side	01
S-012	Drilling Motor	01
S-013	Tachometer	01
S-014	Coupling 6 mm	01
S-015	Bearing 6 mm	01
S-016	Bearing 4 mm	01
S-017	Encoder Drilling Motor	01

Main Shaft Assembly (Drawing Number A-010)

Drawing No.	Name	Quantity
P-057	Main Shaft	01
P-058	Bearing Cover 15 mm	01
P-059	Bearing Cover 10mm	01
S-018	Coupling	01
S-019	Bearing 15mm	01
S-020	Gear 32	01
S-021	Bearing 10mm	01
S-022	Chuck	01

Screw Insertion Mechanism Assembly (Drawing Number A-011)

Drawing No.	Name	Quantity
P-060	Gear Box Shifter Arm	01
P-061	Gear Box Shifting Rod	01
P-062	Brass Bush 8 mm id	01
P-063	Washer 3 mm	02
P-064	Rotating Rod	01
S-023	Screw Insertion Motor	01
S-024	Gear Box 25:2	01
S-025	Gear Z = 20	01
A-012	Gear Box Mounting Bracket Assembly	01

Gear Box Mounting Bracket Assembly (Drawing Number A-012)

Drawing No.	Name	Quantity
P-065	Gear Box Mounting Side Plate	02
P-066	Gear Box Mounting Top Plate	01
P-067	Opto-Switch Actuator	01
P-068	Opto-Switch Mounting Plate	01
S-026	Opto-Switch	01

Load Cell Mounting Assembly (Drawing Number A-013)

Drawing No.	Name	Quantity
P-063	Washer 3 mm	02
P-069	Load Cell Mounting Base Plate	01
P-070	Load Cell Mounting Side Plate	01
P-071	Load Cell Shifting Bracket	01
P-072	Brass Bush 10mm	01
P-073	Shifter Rod	01
P-074	Shifter Arm	01
P-075	Opto Switch Actuator Load Cell	01
P-076	Opto Switch Mounting Plate Load Cell	02
P-077	Mounting Bracket	02
P-078	Adaptor Pull Out	01
P-079	Adaptor Drilling	01
S-026	Opto-Switch	02
S-027	Load Cell Drilling	01
S-028	Load Cell Screw Pull Out	01
S-029	Bolt ½"-20	01

Lead Screw and Nut Assembly (Drawing Number A-014)

Drawing No.	Name	Quantity
P-080	Lead Screw Nut Holder	01
P-081	Lead Screw Nut Holder Cover	01
P-082	Linear Bearing Housing (Right)	01
P-083	Linear Bearing Housing (Left)	01
P-084	Connecting Plate	01
P-085	Base Side Bracket	01
P-086	Base Plate	01
P-087	Side Bracket Motor Side	01
P-088	Bush Gear Z80	01
P-089	Lead Screw Actuator Arm	02
P-090	Lead Screw Actuator Load Plate	01
P-091	Rib Lead Screw Arm	04
P-092	Rib Lead Screw	02
P-093	Limit Switch Mounting Plate	01
P-094	Load Cell Screw Pull Out Adaptor	01
P-095	Locking Pin	01
P-096	Bush Gear Z20	01
P-097	Shaft of $Z = 9$ and $z = 70$	01
P-098	Bearing Housing $Z = 9$ Gear	01
P-099	Encoder Reader Mounting Plate	01
P-100	Washer	01
P-101	Motor Mounting Bracket	01
S-002	Limit Switch	01
S-030	Lead Screw	01
S-031	Lead Screw Nut	01
S-032	Linear Bearing	02
S-033	Linear Bearing Shaft	02
S-034	Bearing 9mm	02
S-035	Gear $Z = 80$	01
S-036	Stepper Motor	01
S-037	Gear $Z = 9$	01
S-038	Gear $Z = 20$	01
S-039	Gear $Z = 70$	01
S-040	Encoder Wheel	01
S-041	Encoder Reader	01
S-042	Coupling 4mm End	01
S-043	Coupling 5mm End	01
S-044	Coupling Coupler	01
S-045	Bearing 8 mm	01
S-046	Bearing 4 mm	01

Wire Rope Assembly (Drawing Number A-015)

Drawing No.	Name	Quantity
S-047	Hook	02
S-048	Rope	02

Pulley Housing Right Assembly (Drawing Number A-016)

Drawing No.	Name	Quantity
P-102	Pulley Housing Left	01
P-103	Pulley Housing Right	01
P-104	Shaft Pulley	01
S-049	Pulley	01
S-050	Bearing 8mm	02

Pulley Housing Left Assembly (Drawing Number A-017)

Drawing No.	Name	Quantity
P-102	Pulley Housing Left	01
P-103	Pulley Housing Right	01
P-104	Shaft Pulley	01
S-049	Pulley	01
S-050	Bearing 8mm	02
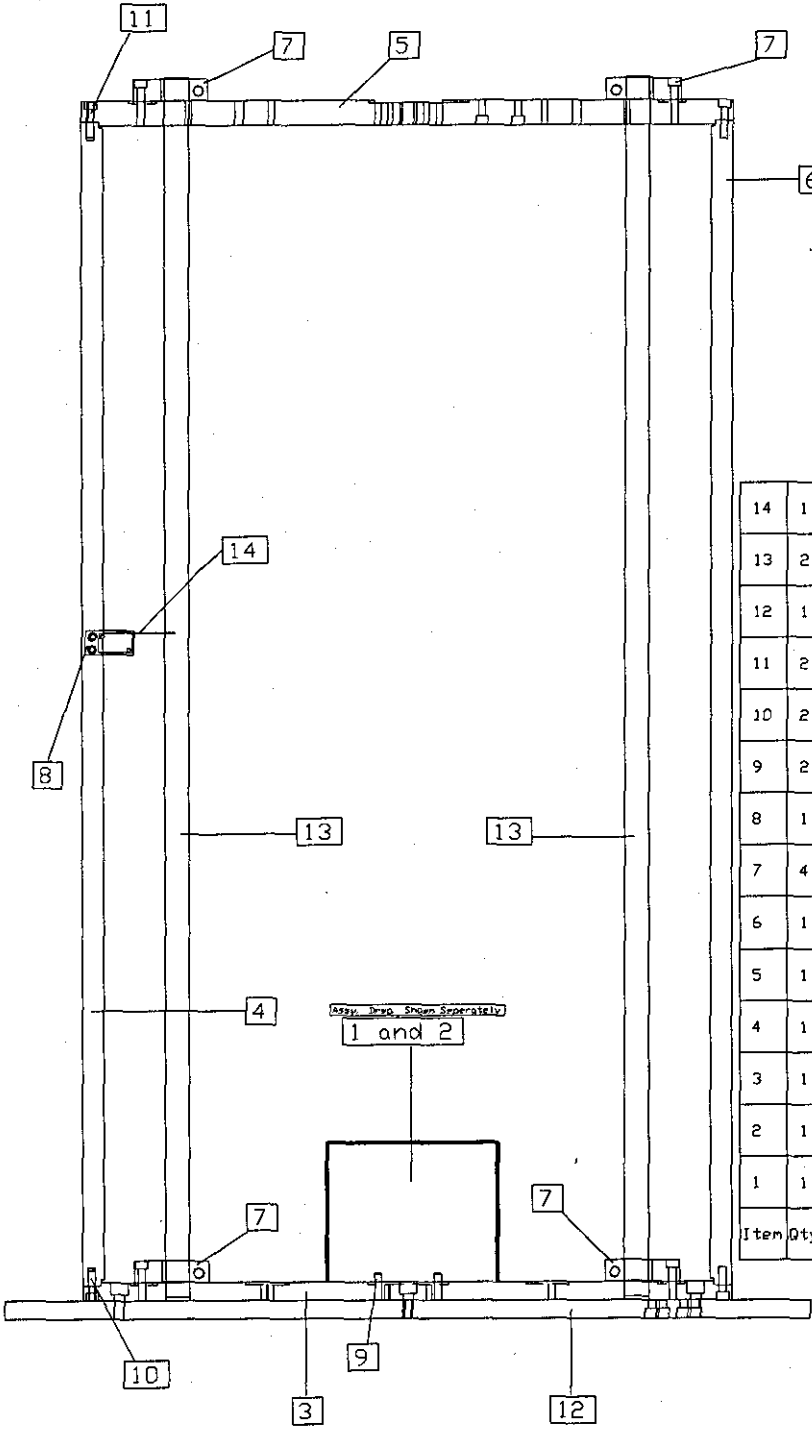
Item	Qty	Name	Part #
14	1	Limit Switch	S-002
13	2	Linear Bearing Shaft	S-001
12	1	Base Plate	P-010
11	2	Dowel Pin 6mm	P-009
10	2	Dowel Pin 6mm	P-008
9	2	Dowel Pin 6mm	P-007
8	1	Lower Limit Switch Mounting	P-006
7	4	Linear Bearing Shaft Clamp	P-005
6	1	Outer Frame Right Side Plate	P-004
5	1	Outer Frame Top Plate	P-003
4	1	Outer Frame Left Side Plate	P-002
3	1	Outer Frame Bottom Plate	P-001
2	1	Sp. Mtg. Plate Assembly	A-003
1	1	Sp. Mtg. Plate Holder Assy.	A-002

LOUGHBOROUGH UNIVERSITY	TITLE: FIXED OUTER FRAME ASSEMBLY				
DEPARTMENT OF MECHANICAL ENGINEERING	SCALE 0.2:1	QTY. 01	MATERIAL M.S.	DRWG NO. A-001	
Tol. If not mentioned is ±0.1	PROJECTION: THIRD ANGLE		DIMENSION: MM	DRAWN BY: Atul Jain	PART NO.

- 283 -

7	1	Bearing 12mm Special	S-005
6	1	Bearing 12mm Reg.	S-004
5	1	Nut M12	S-003
4	1	Washer	P-014
3	1	Spacer	P-013
2	1	Clamp Shaft	P-012
1	1	Bearing Housing	P-011
Item	Qty	Name	Part #

LOUGHBOROUGH UNIVERSITY	TITLE: SPECIMEN MOUNTING PLATE HOLDER ASSEMBLY			
DEPARTMENT OF MECHANICAL ENGINEERING	SCALE 2:1	QTY. 01	MATERIAL M. S.	DRWG NO. A-002
Tol. If not mentioned is ±0.1	PROJECTION: THIRD ANGLE	DIMENSION: MM	DRAWN BY: Atul Jain	PART NO.

- 284 -
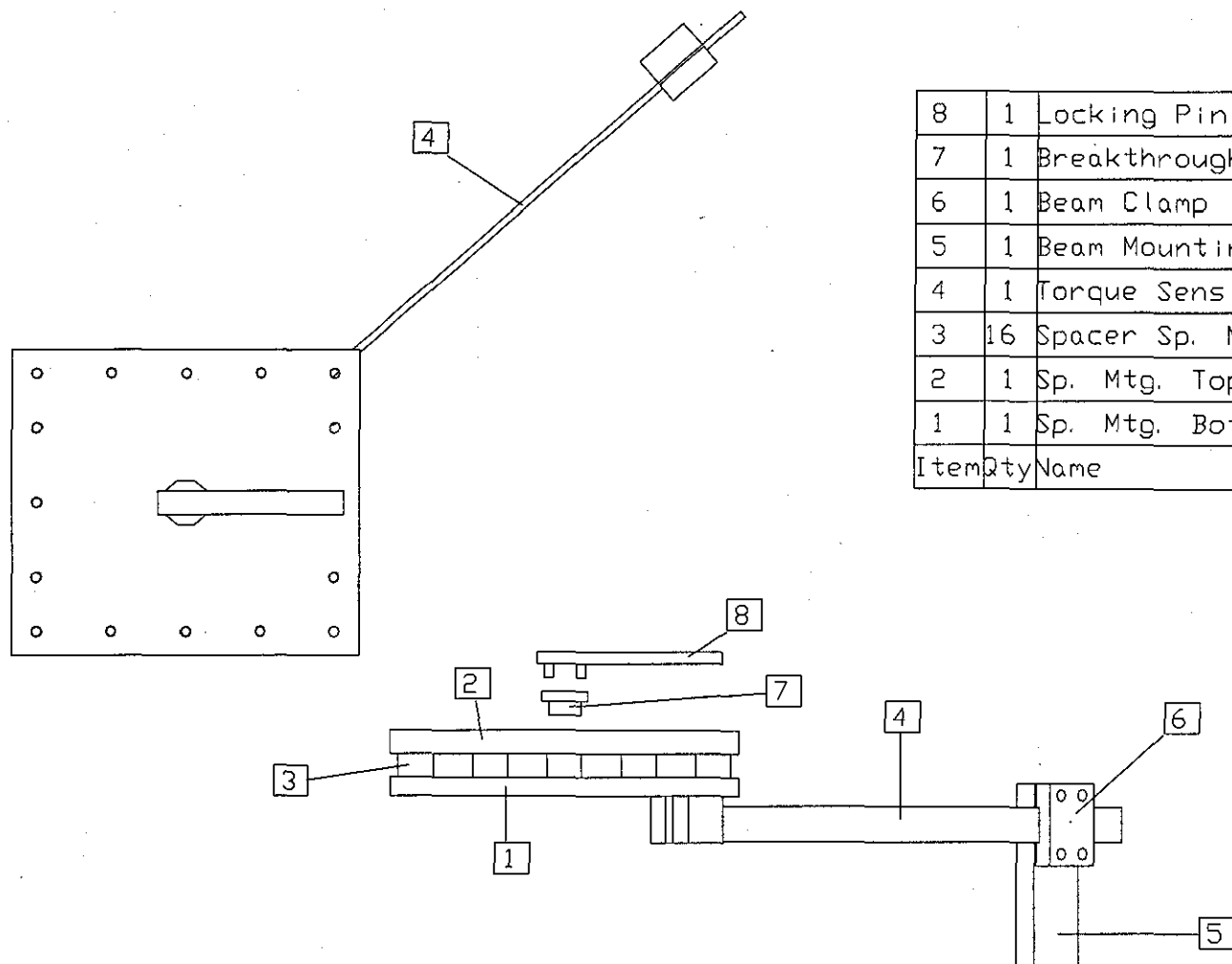
Item	Qty	Name	Part #
8	1	Locking Pin	P-022
7	1	Breakthrough Bush	P-021
6	1	Beam Clamp	P-020
5	1	Beam Mounting	P-019
4	1	Torque Sensing Beam	P-018
3	16	Spacer Sp. Mtg.	P-017
2	1	Sp. Mtg. Top Plate	P-016
1	1	Sp. Mtg. Bottom Plate	P-015

LOUGHBOROUGH UNIVERSITY	TITLE: Specimen Mounting Plate Assembly				
DEPARTMENT OF MECHANICAL ENGINEERING	SCALE As Shown	QTY. 01	MATERIAL M. S.	DRWG NO. A-003	
Tol. If not mentioned is ±0.1	PROJECTION: THIRD ANGLE		DIMENSION: MM	DRAWN BY: Atul Jain	PART NO.

9	1	Aligning Plate Top	P-029
8	1	Alingning Plate Bottom	P-028
7	1	Base Bkt. Bottom Right Plate	P-027
6	1	Base Bkt. Right Side Plate	P-026
5	1	Base Bkt. Top Plate	P-025
4	1	Base Bkt. Left Side Plate	P-024
3	1	Base Bkt. Bottom Left Plate	P-023
2	2	Dowel Pin 6mm	P-008
1	1	Drill Bush Assembly	A-005
Item	Qty	Name	Part #

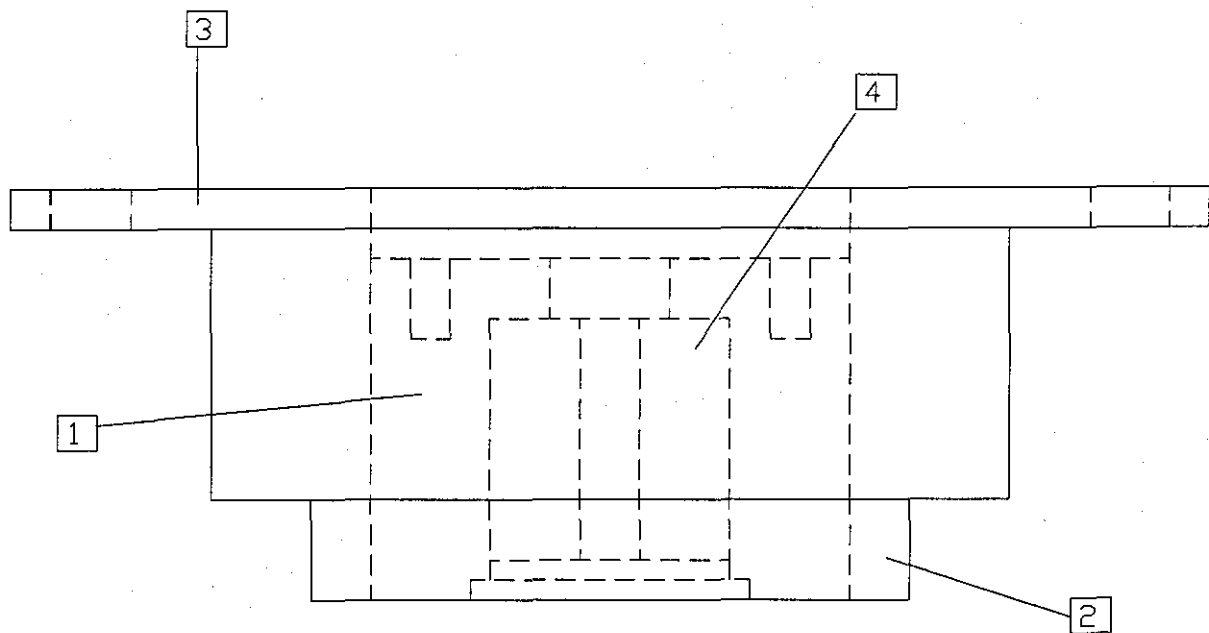| LOUGHBOROUGH UNIVERSITY	TITLE: BASE BRACKET ASSEMBLY			
——— DEPARTMENT OF MECHANICAL ENGINEERING	SCALE 1: 2. 5	QTY. 01	MATERIAL M. S.	DRWG NO. A-004
Tol. If not mentioned is ±0. 1	PROJECTION: THIRD ANGLE	DIMENSION: MM	DRAWN BY: Atul Jain	PART NO.

4	1	Drill Bush	S-006
3	1	Drill Bush Nut Housing	P-032
2	1	Locking Nut	P-031
1	1	Bush Nut	P-030
Item	Qty	Name	Part #

LOUGHBOROUGH UNIVERSITY DEPARTMENT OF MECHANICAL ENGINEERING	TITLE: Drill and Screw Insetion Bush Assembly			
	SCALE As Shown	QTY. 01	MATERIAL M. S.	DRWG NO. A-005
Tol. If not mentioned is ±0.1	PROJECTION: THIRD ANGLE	DIMENSION: MM	DRAWN BY: Atul Jain	PART NO.
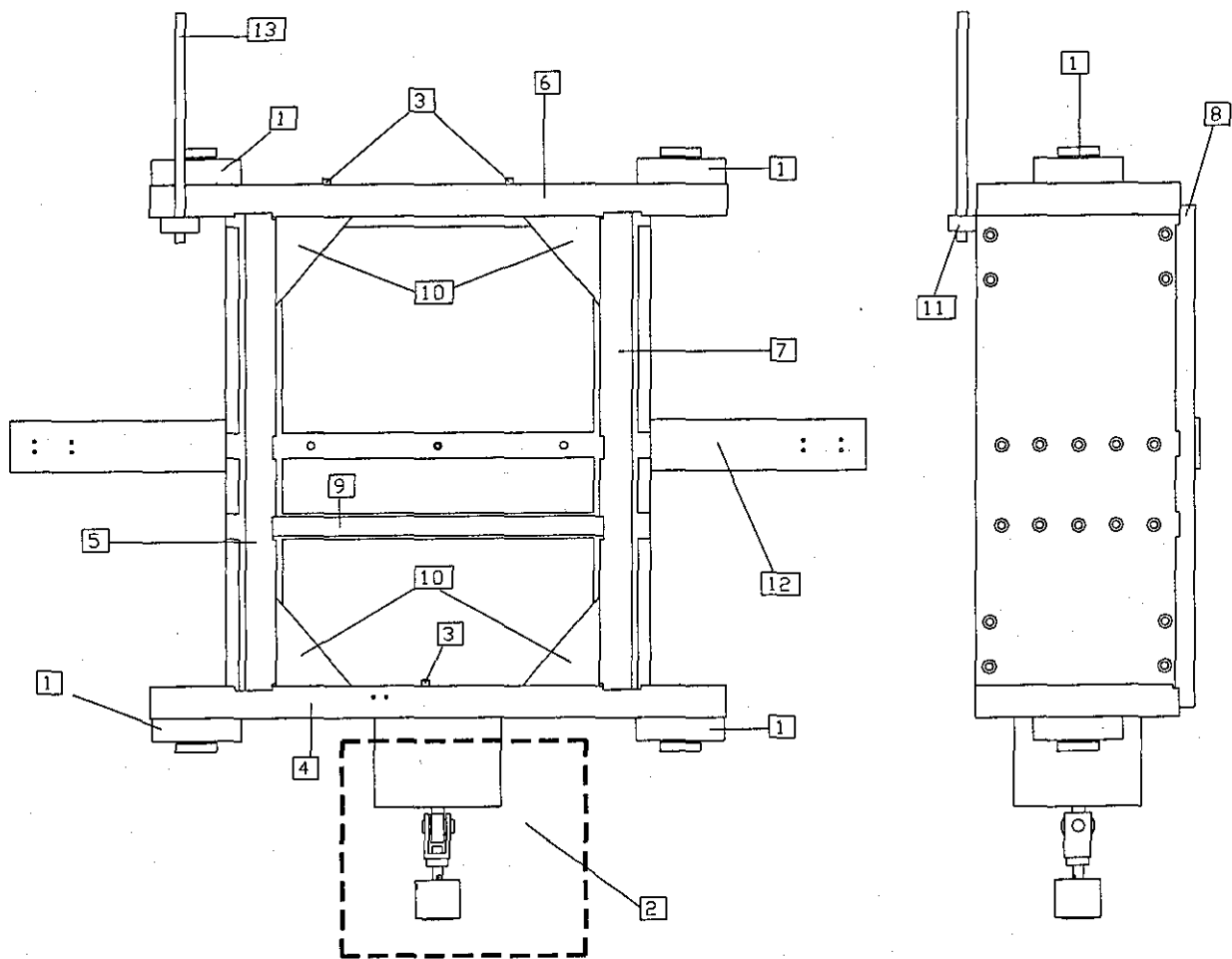
13	1	Screw Rod	S-007
12	1	Drag Chain Mtg. PLate	P-041
11	1	Plate	P-040
10	8	Ribs Inner Frame	P-039
9	1	Mtg. Bkt. 15mm Brg.	P-038
8	1	Inner Frame Back Plate	P-037
7	1	Inner Frame Right Side Plate	P-036
6	1	Inner Frame Top Plate	P-035
5	1	Inner Frame Left Side Plate	P-034
4	1	Inner Frame Bottom Plate	P-033
3	6	Dowel Pin 6mm	P-009
2	1	Screw Pullout Attachment Assy.	A-008
1	4	Linear Bearing Assembly	A-007
Item	Qty	Name	Part #

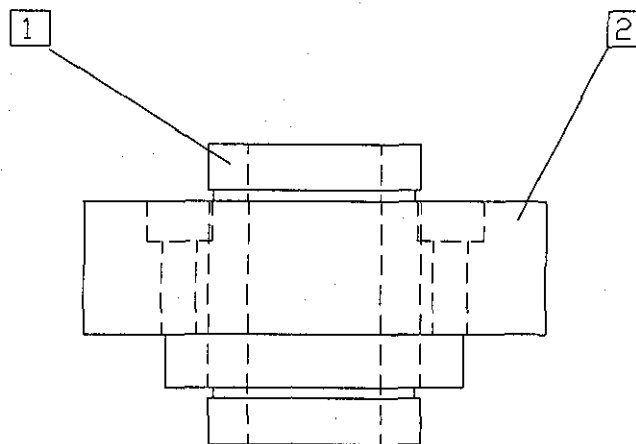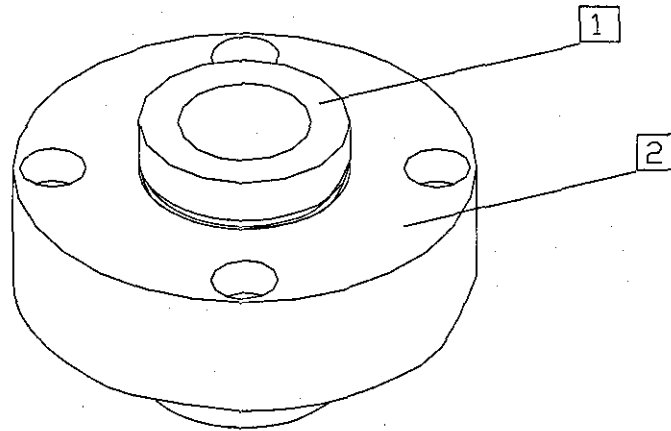| LOUGHBOROUGH UNIVERSITY	TITLE: INNER FRAME ASSEMBLY			
DEPARTMENT OF MECHANICAL ENGINEERING	SCALE 0.2:1	QTY. 01	MATERIAL M. S.	DRWG NO. A-006
Tol. If not mentioned is ±0.1	PROJECTION: THIRD ANGLE	DIMENSION: MM	DRAWN BY: Atul Jain	PART NO.

2	1	Linear Brg. Housing	P-042
1	1	Linear Bearing	S-008
Item	Qty	Name	Part #

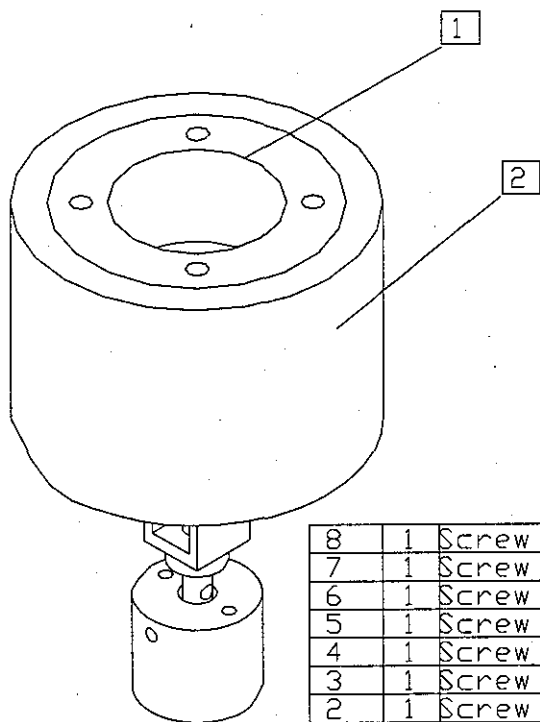| LOUGHBOROUGH UNIVERSITY DEPARTMENT OF MECHANICAL ENGINEERING	TITLE: Linear Bearing Assembly			
	SCALE 1:1	QTY. 01	MATERIAL M. S.	DRWG NO. A-007
Tol. If not mentioned is ±0.1	PROJECTION: THIRD ANGLE	DIMENSION: MM	DRAWN BY: Atul Jain	PART NO.

8	1	Screw Pullout Loacking Pin	S-011
7	1	Screw Pullout Fork	S-010
6	1	Screw Pullout Ball Joint	S-009
5	1	Screw Pullout Bush	P-047
4	1	Screw Pullout Attachment	P-046
3	1	Screw Pullout Rod	P-045
2	1	Screw Pullout Nut	P-044
1	1	Screw Pullout Nut Adapter	P-043
Item	Qty	Name	Part #

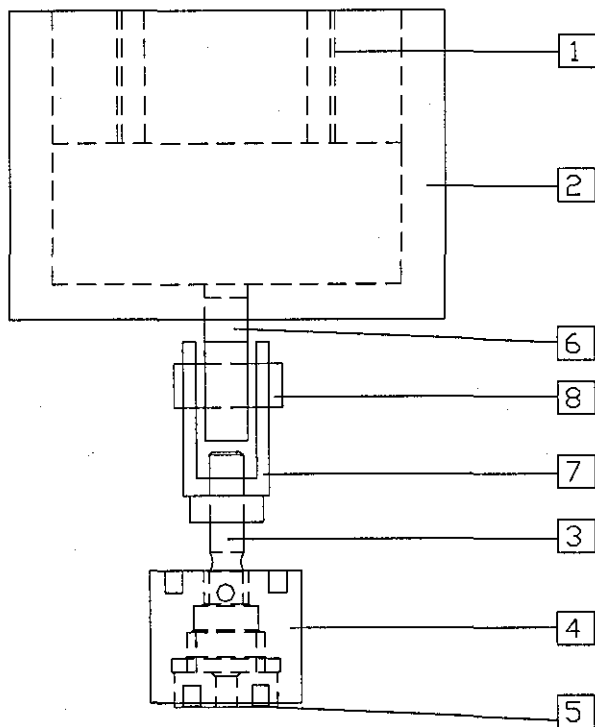| LOUGHBOROUGH UNIVERSITY	TITLE: Screw Pullout Attachment Assembly				
DEPARTMENT OF MECHANICAL ENGINEERING	SCALE As Shown	QTY. 01	MATERIAL M. S.	DRWG NO. A-008	
Tol. If not mentioned is ±0.1	PROJECTION: THIRD ANGLE		DIMENSION: MM	DRAWN BY: Atul Jain	PART NO.
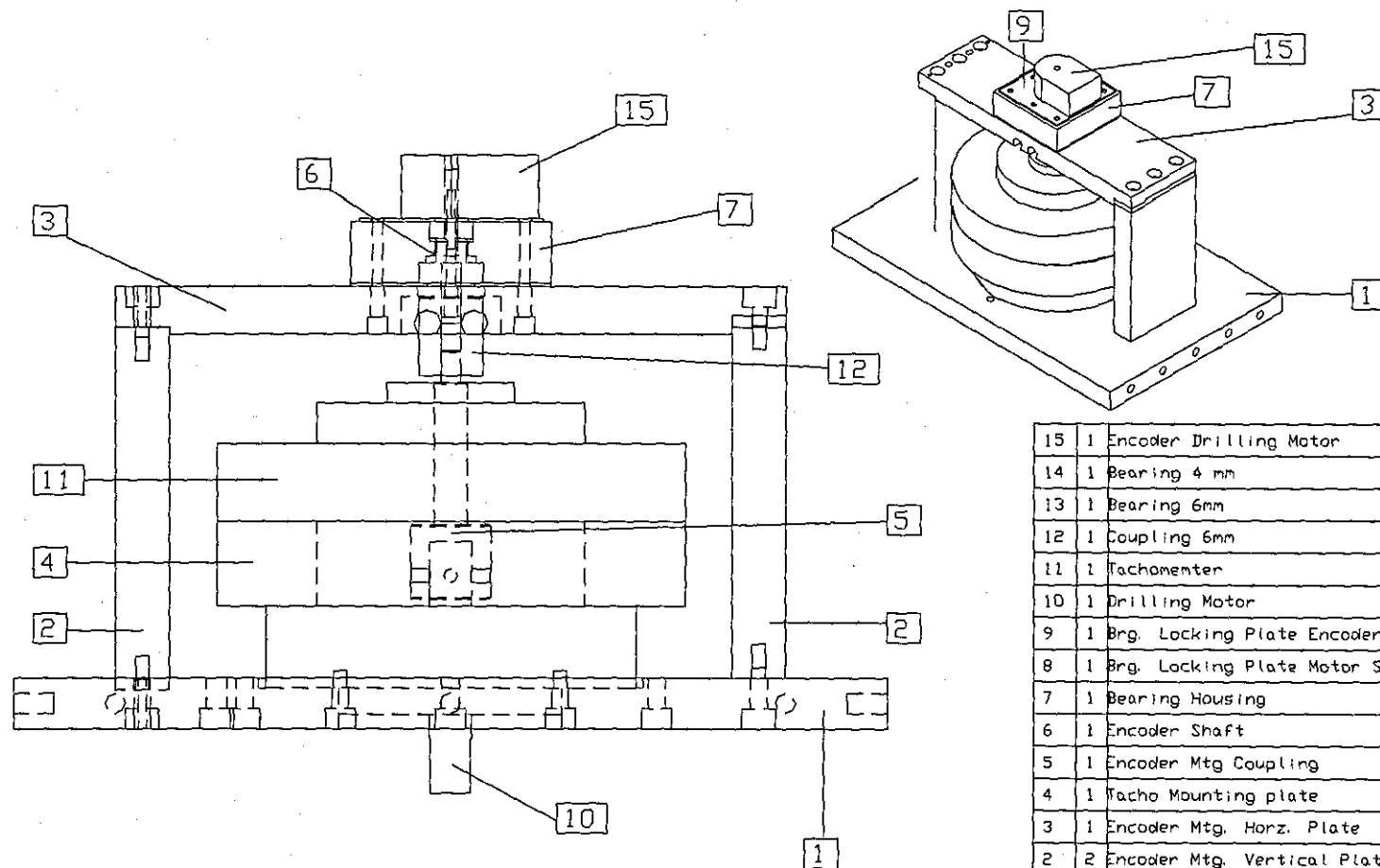
15	1	Encoder Drilling Motor	S-017
14	1	Bearing 4 mm	S-016
13	1	Bearing 6mm	S-015
12	1	Coupling 6mm	S-014
11	1	Tachomemter	S-013
10	1	Drilling Motor	S-012
9	1	Brg. Locking Plate Encoder Side	P-056
8	1	Brg. Locking Plate Motor Side	P-055
7	1	Bearing Housing	P-054
6	1	Encoder Shaft	P-053
5	1	Encoder Mtg Coupling	P-052
4	1	Tacho Mounting plate	P-051
3	1	Encoder Mtg. Horz. Plate	P-050
2	2	Encoder Mtg. Vertical Plate	P-049
1	1	Drilling Motor Mtg. Plate	P-048
Item	Qty	Name	Part #

LOUGHBOROUGH UNIVERSITY	TITLE:	Drilling Motor Assembly			
DEPARTMENT OF MECHANICAL ENGINEERING	SCALE As Shown	QTY. 01	MATERIAL M. S.	DRWG NO. A-009	
Tol. If not mentioned is ±0.1	PROJECTION: THIRD ANGLE		DIMENSION: MM	DRAWN BY: Atul Jain	PART NO.

Appendix C: Engineering Drawings
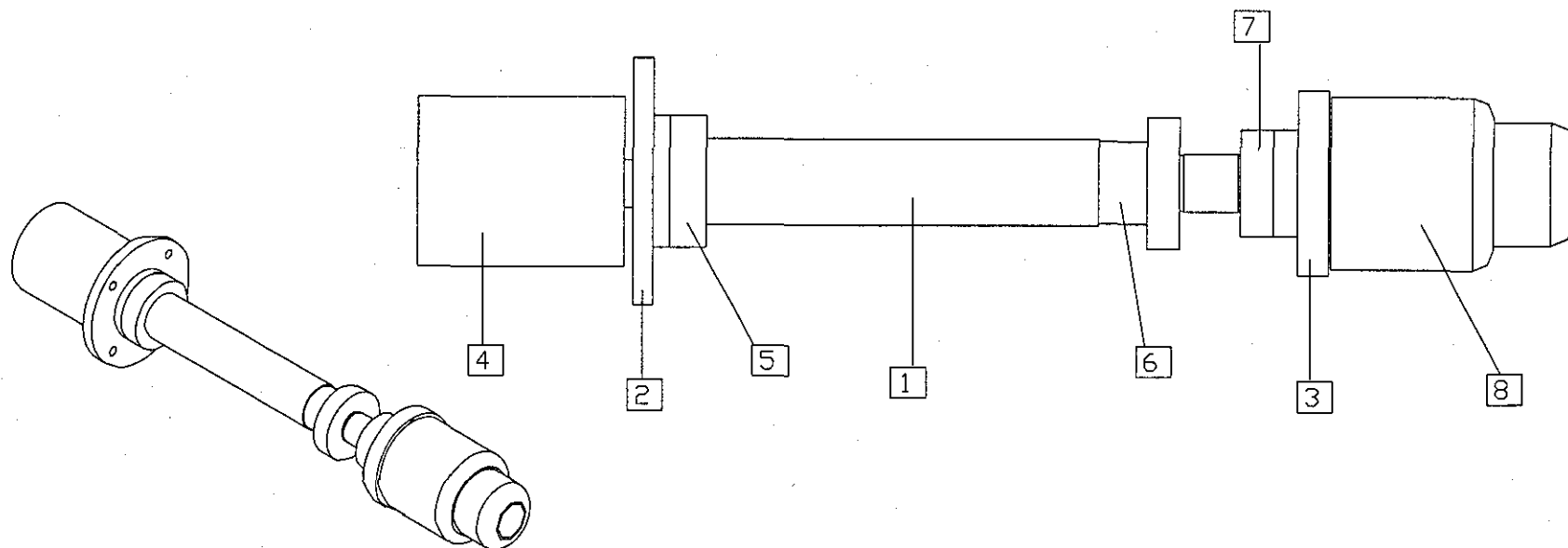
Item	Qty	Name	Part #
8	1	Chuck	S-022
7	1	Bearing 10 mm	S-021
6	1	Gear Z32	S-020
5	1	Bearing 15 mm	S-019
4	1	Coupling	S-018
3	1	Bearing Cover 10 mm	P-059
2	1	Bearing Cover 15 mm	P-058
1	1	Main Shaft	P-057
Item	Qty	Name	Part #

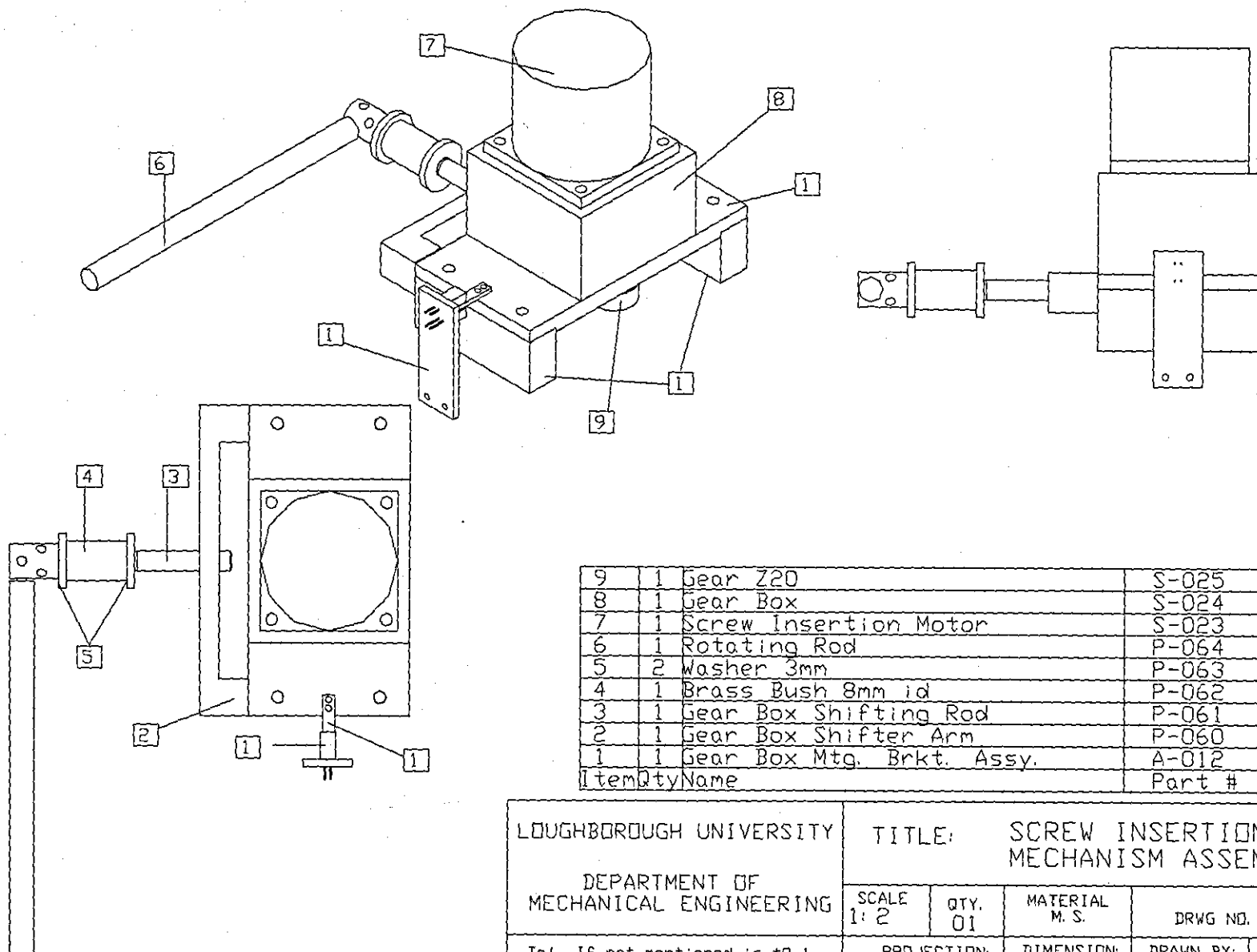| LOUGHBOROUGH UNIVERSITY	TITLE: MAIN SHAFT ASSEMBLY				
DEPARTMENT OF MECHANICAL ENGINEERING	SCALE As Shown	QTY. 01	MATERIAL M. S.	DRWG NO. A-010	
Tol. If not mentioned is ±0.1	PROJECTION: THIRD ANGLE	DIMENSION: MM	DRAWN BY: Atul Jain	PART NO.	

Item	Qty	Name	Part #
9	1	Gear Z20	S-025
8	1	Gear Box	S-024
7	1	Screw Insertion Motor	S-023
6	1	Rotating Rod	P-064
5	2	Washer 3mm	P-063
4	1	Brass Bush 8mm id	P-062
3	1	Gear Box Shifting Rod	P-061
2	1	Gear Box Shifter Arm	P-060
1	1	Gear Box Mtg. Brkt. Assy.	A-012

LOUGHBOROUGH UNIVERSITY	TITLE:	SCREW INSERTION MECHANISM ASSEMBLY	
DEPARTMENT OF MECHANICAL ENGINEERING	SCALE 1:2	QTY. 01	MATERIAL M.S.
			DRWG NO. A-011
Tol. If not mentioned is ±0.1	PROJECTION: THIRD ANGLE	DIMENSION: MM	DRAWN BY: Atul Jain
			PART NO.

9	1	Gear Z20	S-025
8	1	Gear Box	S-024
7	1	Screw Insertion Motor	S-023
6	1	Rotating Rod	P-064
5	2	Washer 3mm	P-063
4	1	Brass Bush 8mm id	P-062
3	1	Gear Box Shifting Rod	P-061
2	1	Gear Box Shifter Arm	P-060
1	1	Gear Box Mtg. Brkt. Assy.	A-012
Item	Qty	Name	Part #

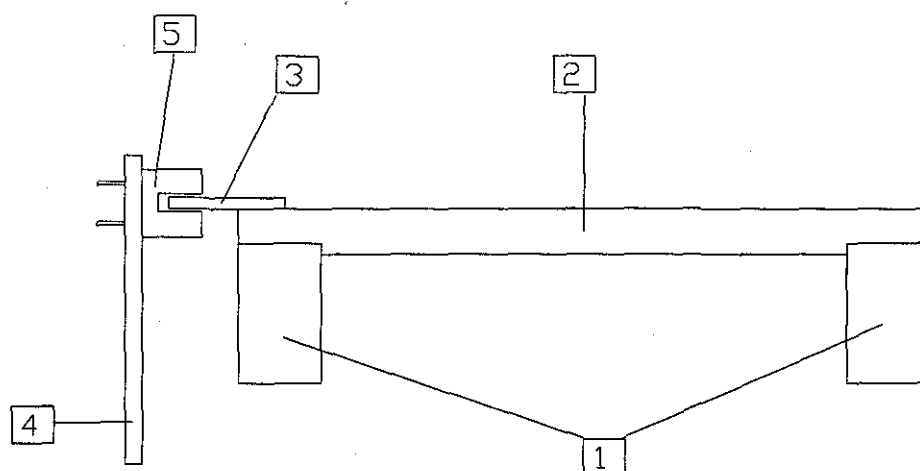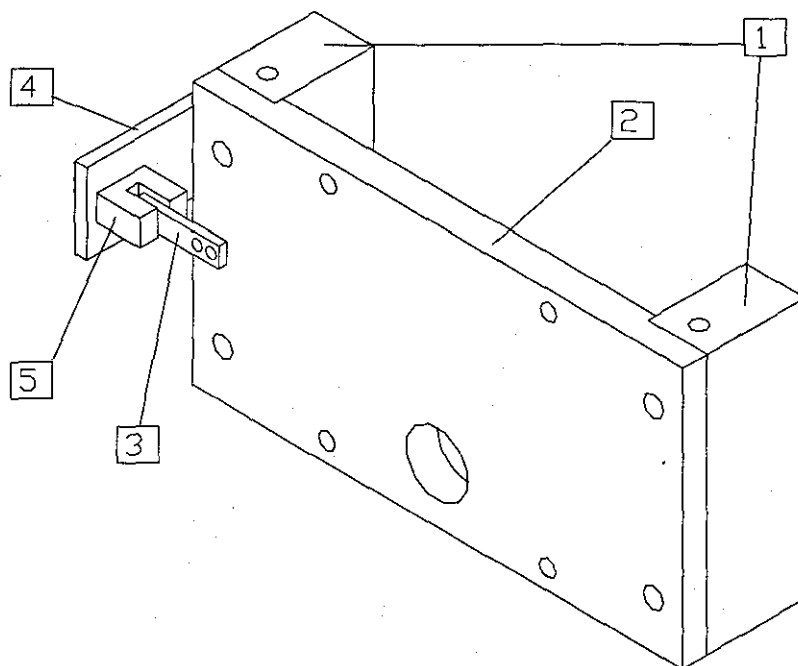| LOUGHBOROUGH UNIVERSITY	TITLE:	SCREW INSERTION MECHANISM ASSEMBLY		
DEPARTMENT OF MECHANICAL ENGINEERING	SCALE 1:2	QTY. 01	MATERIAL M.S.	DRWG NO. A-011
Tol. If not mentioned is ±0.1	PROJECTION: THIRD ANGLE	DIMENSION: MM	DRAWN BY: Atul Jain	PART NO.

5	1	Opto-Switch	S-026
4	1	Opto-Switch Mounting Plate	P-068
3	1	Opto-Switch Actuator	P-067
2	1	Gear Box Mtg. Top Plate	P-066
1	2	Gear Box Mtg. Side Plate	P-065
Item	Qty	Name	Part #

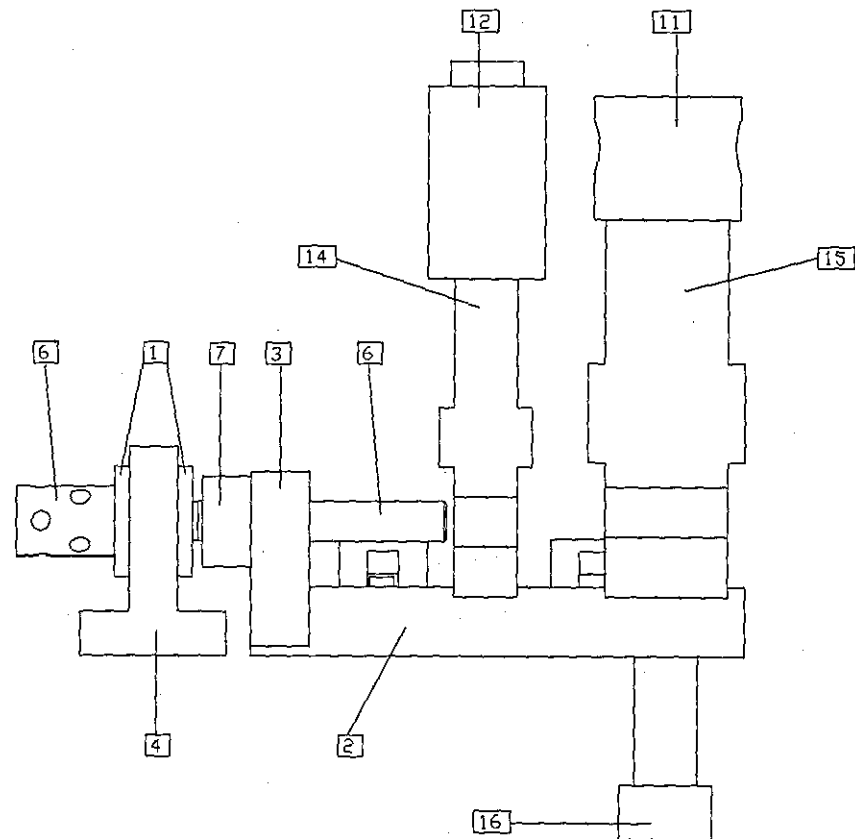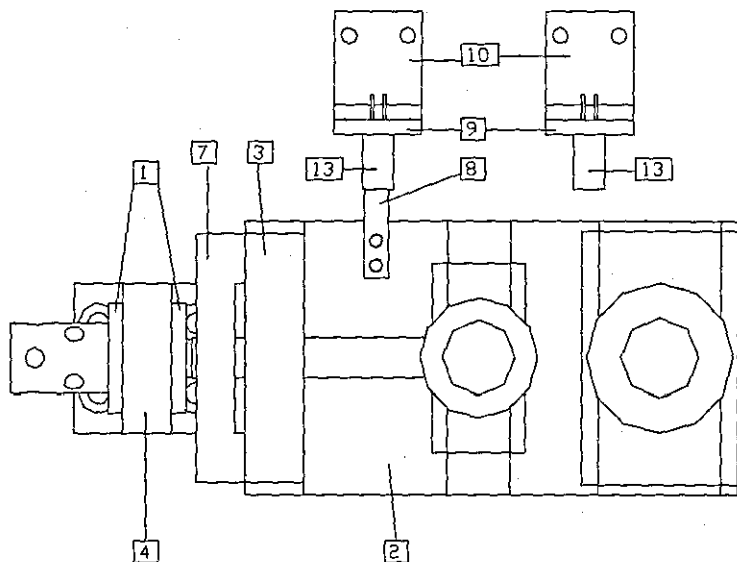| LOUGHBOROUGH UNIVERSITY	TITLE:	Gear Box Mounting Bracket Assembly			
DEPARTMENT OF MECHANICAL ENGINEERING	SCALE As Shown	QTY. 01	MATERIAL M. S.	DRWG NO. A-012	
Tol. If not mentioned is ±0.1	PROJECTION: THIRD ANGLE		DIMENSION: MM	DRAWN BY: Atul Jain	PART NO.

16	1	Bolt	S-029
15	1	Load Cell Screw Pullout	S-028
14	1	Load Cell Drilling	S-027
13	2	Opto-Switch	S-026
12	1	Adaptor Drilling	P-079
11	1	Adaptor Pull Out	P-078
10	2	Mounting Bracket	P-077
9	2	Opto-Switch Mounting Plate LC	P-076
8	1	Opto Switch Actuator LC	P-075
7	1	Load Cell Shifter Arm	P-074
6	1	Shifter Rod	P-073
5	1	Brass Bush 10mm	P-072
4	1	Load Cell Shifting Brkt.	P-071
3	1	Load Cell Mtg. Side Plate	P-070
2	1	Load Cell Mtg. Base Plate	P-069
1	2	Washer 3mm	P-063
Item	Qt	Name	Part

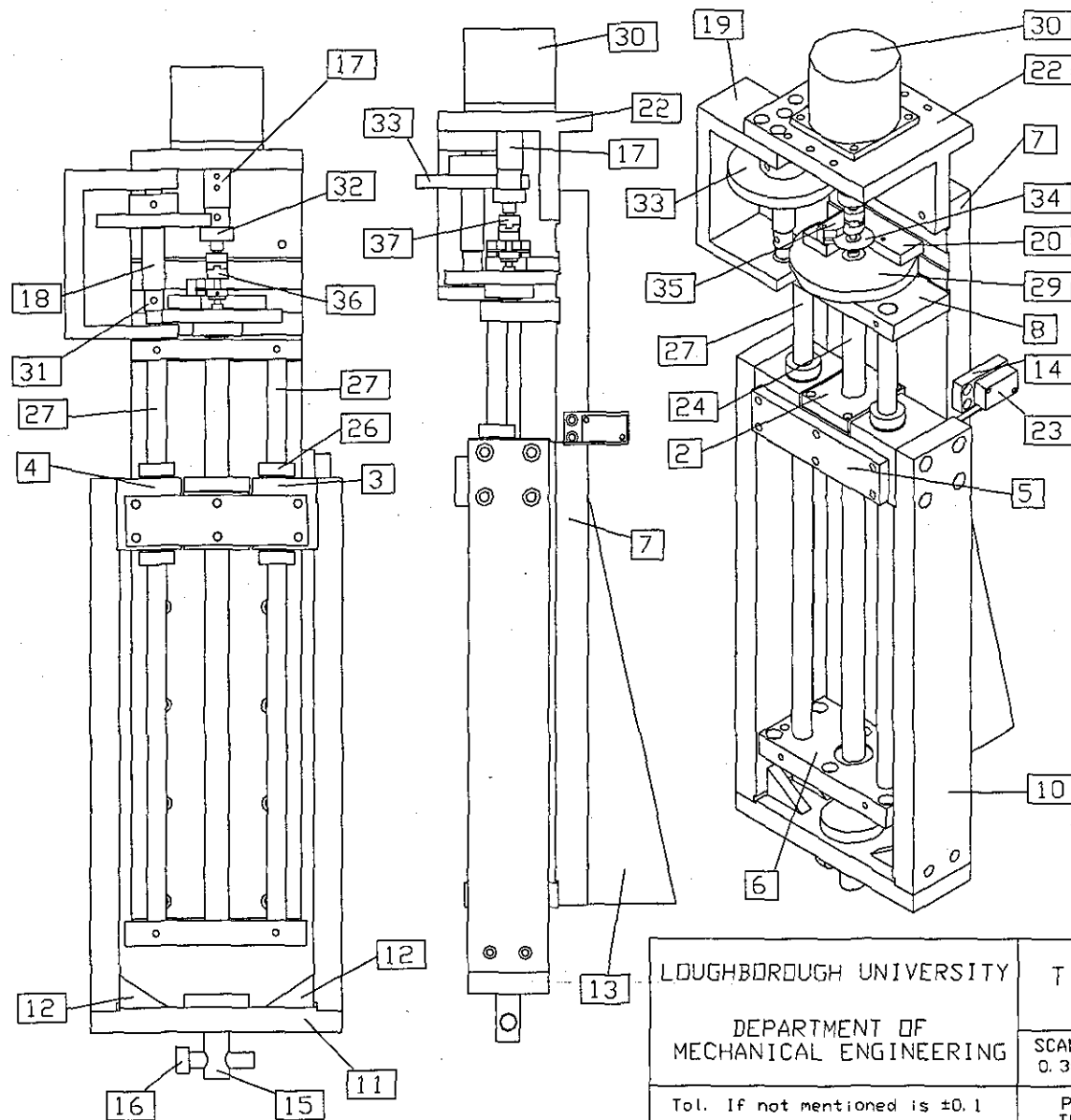| LOUGHBOROUGH UNIVERSITY	TITLE:	LOAD CELL MOUNTING ASSEMBLY		
DEPARTMENT OF MECHANICAL ENGINEERING	SCALE 1: 1.25	QTY. 01	MATERIAL M. S.	DRWG NO. A-013
Tol. If not mentioned is ±0.1	PROJECTION: THIRD ANGLE	DIMENSION: MM	DRAWN BY: Atul Jain	PART NO.

Item	Qty	Name	Part #
40	1	Bearing 4mm	S-046
39	1	Bearing 8mm	S-045
38	1	Coupling Coupler	S-044
37	1	coupling 5mm hub	S-043
36	1	coupling 4mm hub	S-042
35	1	Encoder Reader	S-041
34	1	Encoder wheel	S-040
33	1	Gear Z70	S-039
32	1	Gear Z20	S-038
31	1	Gear Z9	S-037
30	1	Stepper Motor	S-036
29	1	Gear Z80	S-035
28	2	Bearing 9mm	S-034
27	2	Linear Brg. Shaft	S-033
26	2	Linear Bearing	S-032
25	1	Lead Screw Nut	S-031
24	1	Lead Screw	S-030
23	1	Limit Switch (L.S.)	S-002
22	1	Motor Mtg. Bracket	P-101
21	1	Washer	P-100
20	1	Encoder Mtg. Plate	P-099
19	1	Bearing housing Z9	P-098
18	1	Shaft Z70 Z9	P-097
17	1	Bush Gear Z20	P-096
16	1	Locking Pin	P-095
15	1	Load Cell Adaptor	P-094
14	1	L.S. Mtg. Plate	P-093
13	2	Rib Lead Screw	P-092
12	4	Rib Lead Screw Arm	P-091
11	1	Actuator Load Plate	P-090
10	2	Actuator Arm	P-089
9	1	Bush Gear Z80	P-088
8	1	Bracket Motor Side	P-087
7	1	Base Plate	P-086
6	1	Base Side Bracket	P-085
5	1	Connecting Plate	P-084
4	1	Brg. Housing Left	P-083
3	1	Brg. Housing Right	P-082
2	1	Nut Holder Cover	P-081
1	1	Nut Holder	P-080
Item	Qty	Name	Part #

LOUGHBOROUGH UNIVERSITY	TITLE: LEAD SCREW ASSEMBLY			
DEPARTMENT OF MECHANICAL ENGINEERING	SCALE 0.3:1	QTY. 01	MATERIAL M.S.	DRWG NO. A-014
Tol. If not mentioned is ±0.1	PROJECTION: THIRD ANGLE	DIMENSION: MM	DRAWN BY: Atul Jain	PART NO.

2	1	Rope	S-048
1	1	Hook	S-047
Item	Qty	Name	Part #

LOUGHBOROUGH UNIVERSITY	TITLE: Wire Rope Assembly				
DEPARTMENT OF MECHANICAL ENGINEERING	SCALE As Shown	QTY. 01	MATERIAL M. S.	DRWG NO. A-015	
Tol. If not mentioned is ±0.1	PROJECTION: THIRD ANGLE	DIMENSION: MM	DRAWN BY: Atul Jain	PART NO.	
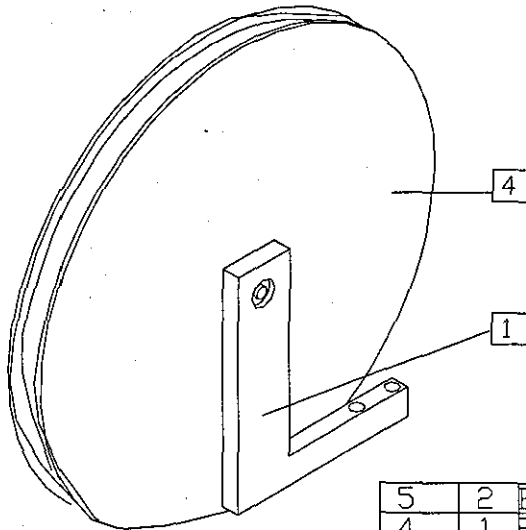
5	2	Bearing 8mm	S-050
4	1	Pulley	S-049
3	1	Shaft Pulley	P-104
2	1	Pulley Housing Right	P-103
1	1	Pulley Housinfg Left	P-102
Item	Qty	Name	Part #

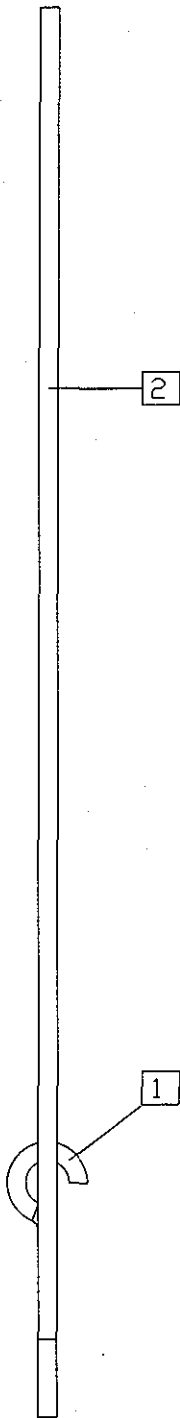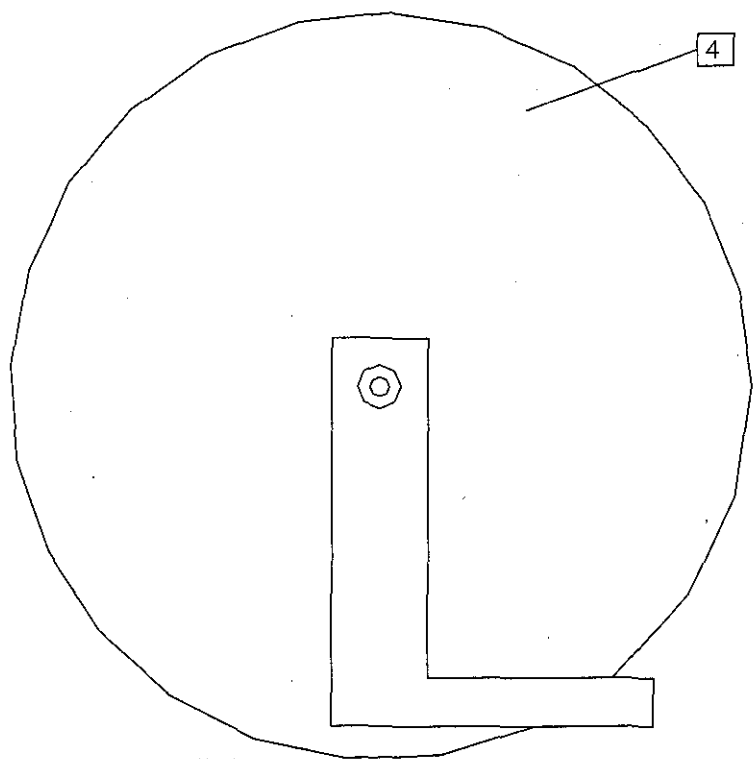| LOUGHBOROUGH UNIVERSITY	TITLE: Right Pulley Housing Assembly			
DEPARTMENT OF MECHANICAL ENGINEERING	SCALE 0. 4: 1	QTY. 01	MATERIAL M. S.	DRWG NO. A-016
Tol. If not mentioned is ±0. 1	PROJECTION: THIRD ANGLE	DIMENSION: MM	DRAWN BY: Atul Jain	PART NO.
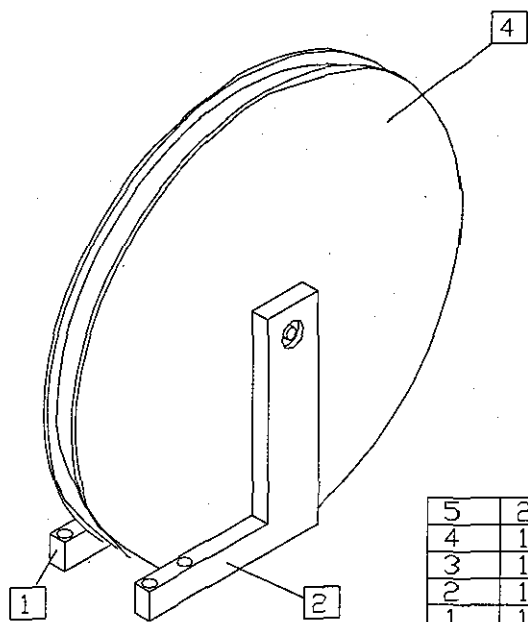
5	2	Bearing 8mm	S-050
4	1	Pulley	S-049
3	1	Shaft Pulley	P-104
2	1	Pulley Housing Right	P-103
1	1	Pulley Housing Left	P-102
Item	Qty	Name	Part #

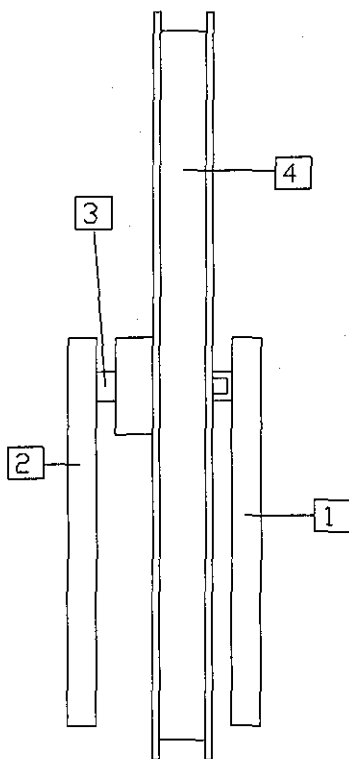| LOUGHBOROUGH UNIVERSITY DEPARTMENT OF MECHANICAL ENGINEERING	TITLE: Pulley Housing Left Assembly				
	SCALE 0.3:1	QTY. 01	MATERIAL M.S.	DRWG NO. A-017	
Tol. If not mentioned is ±0.1	PROJECTION: THIRD ANGLE	DIMENSION: MM	DRAWN BY: Atul Jain	PART NO.	

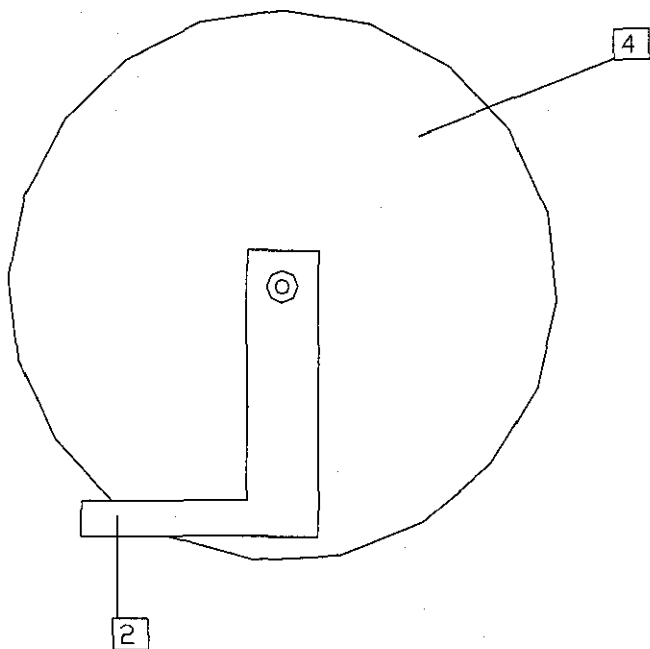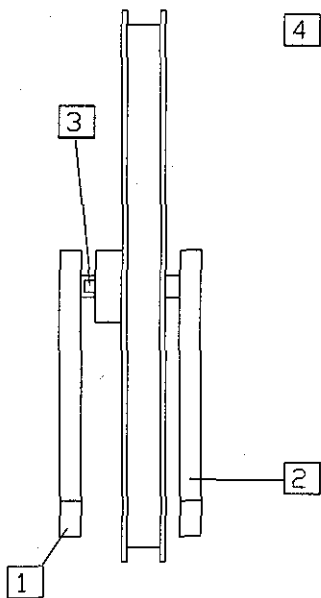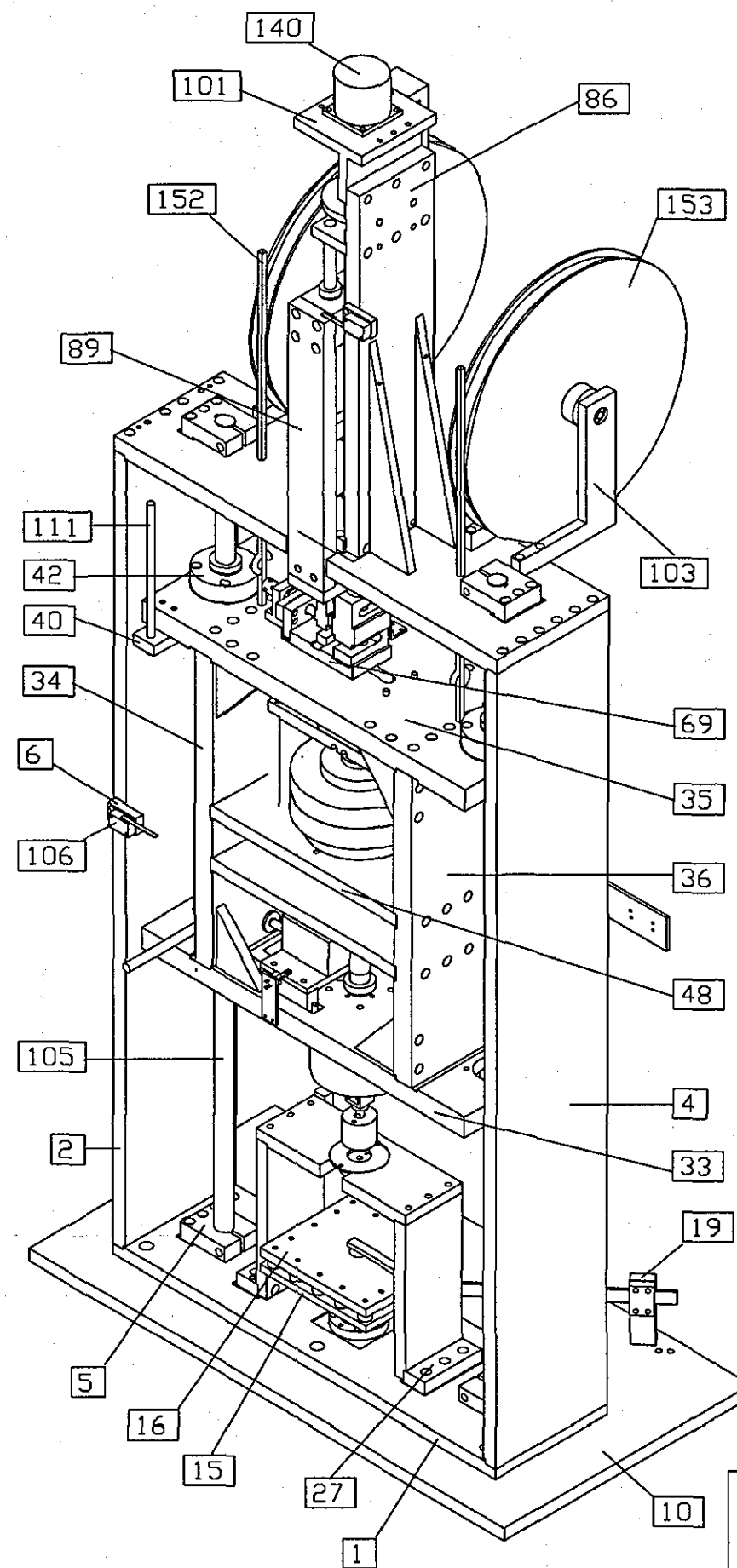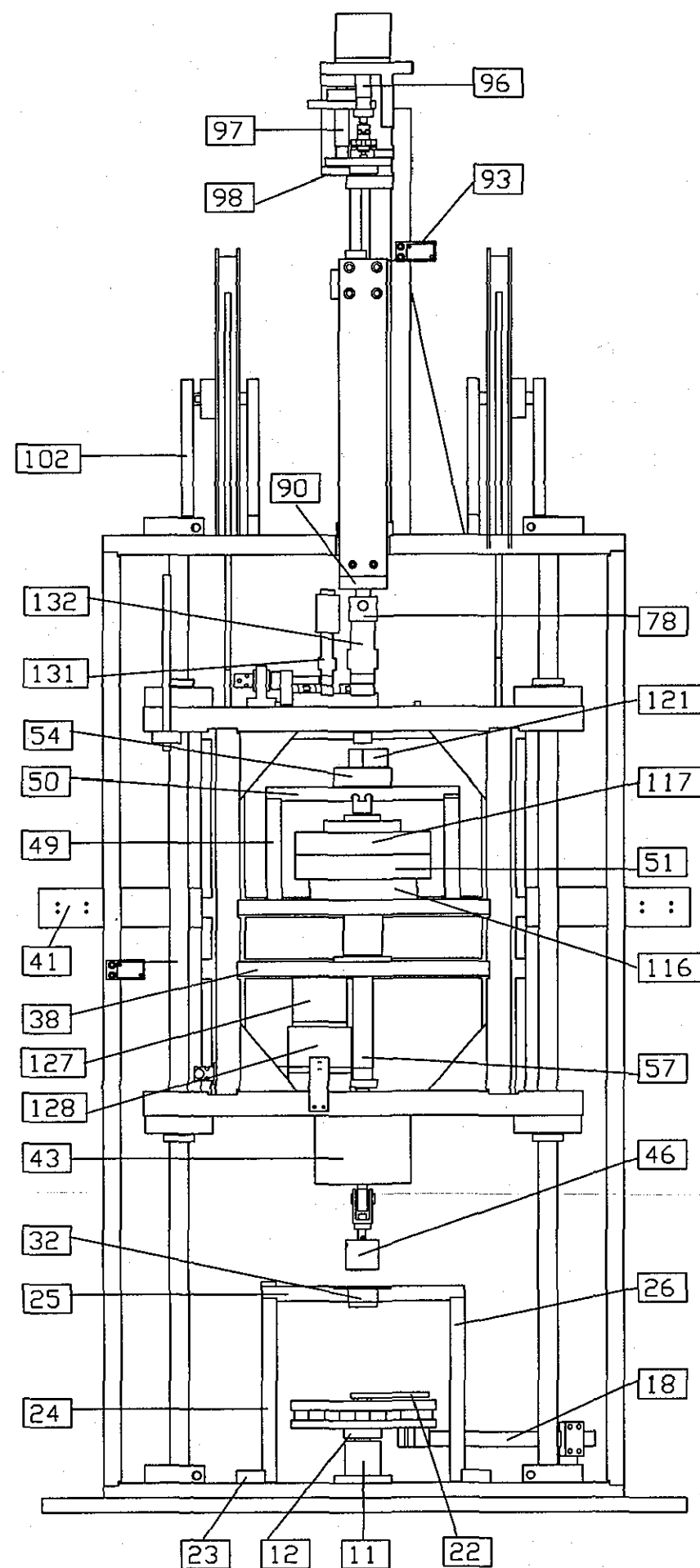| Item	Qty	Name	Part	Item	Qty	Name	Part
154	4	Bearing 8mm	S-050	77	2	Mounting Bracket	P-077
153	2	Pulley	S-049	76	2	Opto-Switch Mtg. Plate	P-076
152	2	Rope	S-048	75	1	Opto Switch Actuator	P-075
151	2	Hook	S-047	74	1	Load Cell Shifter Arm	P-074
150	1	Bearing 4mm	S-046	73	1	Shifter Rod	P-073
149	1	Bearing 8mm	S-045	72	1	Brass Bush 10mm	P-072
148	1	Coupling Coupler	S-044	71	1	Load Cell Shifting Brkt.	P-071
147	1	Coupling 5mm hub	S-043	70	1	Load Cell Mtg. Side Plate	P-070
146	1	Coupling 4mm hub	S-042	69	1	Load Cell Mtg. Base Plate	P-069
145	1	Encoder Reader	S-041	68	1	Opto-Switch Mtg. Plate	P-068
144	1	Encoder wheel	S-040	67	1	Opto-Switch Actuator	P-067
143	1	Gear Z70	S-039	66	1	Gear Box Mtg. Top Plate	P-066
142	1	Gear Z20	S-038	65	2	Gear Box Mtg. Side Plate	P-065
141	1	Gear Z9	S-037	64	1	Rotating Rod	P-064
140	1	Stepper Motor	S-036	63	4	Washer 3mm	P-063
139	1	Gear Z80	S-035	62	1	Brass Bush 8mm id	P-062
138	2	Bearing 9mm	S-034	61	1	Gear Box Shifting Rod	P-061
137	2	Linear Brg. Shaft	S-033	60	1	Gear Box Shifter Arm	P-060
136	2	Linear Bearing	S-032	59	1	Bearing Cover 10 mm	P-059
135	1	Lead Screw Nut	S-031	58	1	Bearing Cover 15 mm	P-058
134	1	Lead Screw	S-030	57	1	Main Shaft	P-057
133	1	Bolt	S-029	56	1	Locking Plate-Top	P-056
132	1	Load Cell Sc. Pullout	S-028	55	1	Locking Plate-Bottom	P-055
131	1	Load Cell Drilling	S-027	54	1	Bearing Housing	P-054
130	3	Opto-Switch	S-026	53	1	Encoder Shaft	P-053
129	1	Gear Z20	S-025	52	1	Encoder Mtg. Coupling	P-052
128	1	Gear Box	S-024	51	1	Tacho Mounting plate	P-051
127	1	Sc. Insertion Motor	S-023	50	1	Encoder Mtg. Horz. Plate	P-050
126	1	Chuck	S-022	49	2	Encoder Mtg. Vert. Plate	P-049
125	1	Bearing 10 mm	S-021	48	1	Drilling Motor Mtg. Plate	P-048
124	1	Gear Z32	S-020	47	1	Screw Pullout Bush	P-047
123	1	Bearing 15 mm	S-019	46	1	Screw Pullout Attachment	P-046
122	1	Coupling	S-018	45	1	Screw Pullout Rod	P-045
121	1	Encoder Drilling Motor	S-017	44	1	Screw Pullout Nut	P-044
120	1	Bearing 4 mm	S-016	43	1	Screw Pullout Nut Adapter	P-043
119	1	Bearing 6mm	S-015	42	4	Linear Brg. Housing	P-042
118	1	Coupling 6mm	S-014	41	1	Drag Chain Mtg. Plate	P-041
117	1	Tachometer	S-013	40	1	Plate	P-040
116	1	Drilling Motor	S-012	39	8	Ribs Inner Frame	P-039
115	1	Sc. Pullout Locking Pin	S-011	38	1	Mtg. Bkt. 15mm Brg.	P-038
114	1	Screw Pullout Fork	S-010	37	1	Inner Frame Plate-Back	P-037
113	1	Screw Pullout Ball Joint	S-009	36	1	Inner Frame Plate-Right	P-036
112	4	Linear Bearing	S-008	35	1	Inner Frame Plate-Top	P-035
111	1	Screw Rod	S-007	34	1	Inner Frame Plate-Left	P-034
110	1	Drill Bush	S-006	33	1	Inner Frame Plate-Bottom	P-033
109	1	Bearing 12mm Special	S-005	32	1	Bush Nut Housing	P-032
108	1	Bearing 12mm Reg.	S-004	31	1	Locking Nut	P-031
107	1	Nut M12	S-003	30	1	Bush Nut	P-030
106	2	Limit Switch (L.S.)	S-002	29	1	Aligning Plate Top	P-029
105	2	Linear Bearing Shaft	S-001	28	1	Alingning Plate Bottom	P-028
104	2	Shaft Pulley	P-104	27	1	Base Bkt.-Bottom Right	P-027
103	2	Pulley Housing Right	P-103	26	1	Base Bkt.-Right	P-026
102	2	Pulley Housing Left	P-102	25	1	Base Bkt.-Top	P-025
101	1	Motor Mtg. Bracket	P-101	24	1	Base Bkt.-Left Side	P-024
100	1	Washer	P-100	23	1	Base Bkt.-Bottom Left	P-023
99	1	Encoder Mtg. Plate	P-099	22	1	Locking Pin	P-022
98	1	Bearing housing Z9	P-098	21	1	Breakthrough Bush	P-021
97	1	Shaft Z70 Z9	P-097	20	1	Beam Clamp	P-020
96	1	Bush Gear Z20	P-096	19	1	Beam Mounting	P-019
95	1	Locking Pin	P-095	18	1	Torque Sensing Beam	P-018
94	1	Load Cell Adaptor	P-094	17	16	Spacer Sp. Mtg.	P-017
93	1	Mtg. Plate	P-093	16	1	Sp. Mtg. Top Plate	P-016
92	2	Rib Lead Screw	P-092	15	1	Sp. Mtg. Bottom Plate	P-015
91	4	Rib Lead Screw Arm	P-091	14	1	Washer	P-014
90	1	Actuator Load Plate	P-090	13	1	Spacer	P-013
89	2	Actuator Arm	P-089	12	1	Clamp Shaft	P-012
88	1	Bush Gear Z80	P-088	11	1	Bearing Housing	P-011
87	1	Bracket Motor Side	P-087	10	1	Base Plate	P-010
86	1	Base Plate	P-086	9	8	Dowel Pin 6mm	P-009
85	1	Base Side Bracket	P-085	8	4	Dowel Pin 6mm	P-008
84	1	Connecting Plate	P-084	7	2	Dowel Pin 6mm	P-007
83	1	Brg. Housing Left	P-083	6	1	Lower Limit Switch Mtg.	P-006
82	1	Brg. Housing Right	P-082	5	4	Linear Brg. Shaft Clamp	P-005
81	1	Nut Holder Cover	P-081	4	1	Outer Fr. Plate-Right	P-004
80	1	Nut Holder	P-080	3	1	Outer Frame Plate-Top	P-003
79	1	Adaptor Drilling	P-079	2	1	Outer Fr. Plate-Left	P-002
78	1	Adaptor Pull Out	P-078	1	1	Outer Fr. Plate-Bottom	P-001
Item	Qty	Name	Part	Item	Qty	Name	Part

LOUGHBOROUGH UNIVERSITY

DEPARTMENT OF MECHANICAL ENGINEERING

TITLE: TEST RIG ASSEMBLY

SCALE 0.18:1	QTY. 01	MATERIAL	DRWG NO A-100
PROJECTION: THIRD ANGLE	DIMENSION: MM	DRAWN BY: Atul Jain	